Coordination Chemistry Reviews 253 (2009) 1099–1201

Contents lists available at ScienceDirect

Coordination Chemistry Reviews

journal homepage: www.elsevier.com/locate/ccr

Review

The evolution of β-diketone or β-diketophenol ligands and related complexes

P. Alessandro Vigato, Valentina Peruzzo, Sergio Tamburini*

Istituto di Chimica Inorganica e delle Superfici, CNR, Area della Ricerca Corso Stati Uniti 4, 35127 Padova, Italy

Contents

ARTICLE INFO

Article history:
Received 28 April 2008
Accepted 19 July 2008
Available online 30 July 2008

Keywords:
Homo-polynuclear complexes

ABSTRACT

The design and properties of the most relevant and illustrative examples of β-diketones or β-ketophenols and related complexes, together with their evolution into more sophisticated linear or tridimensional polymeric systems, are reviewed. The introduction of different functionalities at the periphery of the coordinating moiety of β-diketones and the physico-chemical properties arising from the related complexes are considered also in correlation with their potential in the preparation of probes and devices, where molecular components are essential. The role of the different metal ions in directing the preparation pathways and tuning peculiar properties to the resulting systems is discussed.

* Corresponding author. Tel.: +39 049 8295963; fax: +39 049 8702911.
E-mail address: sergio.tamburini@icis.cnr.it (S. Tamburini).

0010-8545/$ – see front matter
doi:10.1016/j.ccr.2008.07.013

Hetero-polynuclear complexes
β-Diketones
β-Diketophenols
Poly-β-diketones
Poly-β-diketophenols
Photophysical properties

The synthetic procedures aimed at introducing a progressively increasing number of carbonyl groups inside the coordination moiety or at further inserting phenol groups at the end of or between the polyketone moiety and the formation of the related homo- and heteropolynuclear complexes are reported together with the stereochemical, magnetic and optical properties arising from these aggregations. The ability of poly-β-diketones in the selective separation of specific metal ions across liquid membranes is also evaluated. Furthermore, the development of the resulting complexes into the third direction, via coordination of appropriate bridging groups, with the formation of discrete or polymeric systems is illustrated in detail. Finally, the insertion of additional donor groups at the periphery or between the β-diketonato moieties was taken into consideration, together with the role of specific spacers with or without additional donors in determining peculiar architectures and properties of the resulting complexes.

1. Introduction

Classical β-diketones and related ligands have been studied for more than a century and their ability to give rise to a rich and interesting coordination chemistry is well documented [1–13]. They act under appropriate conditions as uninegative O_2-chelating donors, capable of stabilizing mononuclear or polynuclear complexes. In particular, their keto-enol tautomerism (Scheme 1) was studied in solution by IR and NMR spectroscopy and in the solid state by X-ray single crystal diffraction [9–13]. Two excellent reviews appeared while our paper was in preparation or under referees evaluation [12,13].

A special class is represented by the α-diketone 2-hydroxy-2,4,6-cycloheptanetrione (tropolone), its substituted derivatives and the related α-hydroxyketones, which form quite stable complexes with d- and f-metal ions, where up to four or five ligands are firmly coordinated to the metal ion to complete the coordination requirements [14,15].

There is a growing amount of literature which especially deals with the possible applications of these complexes as components of molecular devices or as precursors in the formation of new materials. Phosphors for lighting and high efficiency electroluminescent devices for light-emitting diodes, contrast agents for medical magnetic resonance imaging, NMR shift reagents, transport carriers of alkali metal ions across biological membranes, luminescent probes for proteins and amino acids, light-emitting sensors in fluoroimmunoassays, tags for time-resolved luminescent microscopy, magnetically addressable liquid crystals, magnetic alloys for refrigeration, superconducting materials, specific redox reagents for chemical transformation or molecular-based information, acid catalysts for sophisticated organic transformations or for the cleavage of phosphodiester bridges in RNA, fully justify the efforts made to control the metallic sites and to selectively introduce specific metal ions into organized assemblies [16–31].

The photophysical characterization both in solution and in the solid state of complexes and polymers containing d- and/or 4f-metal ions is relevant in determining the complexes with the best performance for their successful application as emitting layers in light-emitting diodes for display applications. However, the architecture of the device is also of major importance, to allow for good charge transport and recombination and thus obtain pure colours and high emission quantum efficiency. The usually broad emission from organic molecules and transition metal complexes, which occurs either from singlet or from LMCT states, requires the use of filters to obtain monochromatic colors. Further, tuning of device parameters can lead to changes in colour. Organometallic iridium(III) and lanthanide(III) phosphorescent compounds have been widely studied and applied as emitters in high efficient organic light-emitting diodes [32,33].

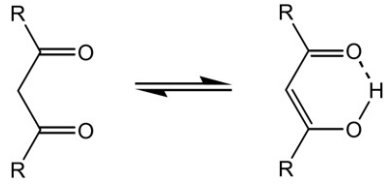

Scheme 1. Keto-enol tautomerism in β-diketones.

Considerable interest has been recently shown in the preparation and photophysical characterisation of heterometallic d, f-complexes, in which the strong absorption of light by MLCT transitions associated with d-block fragments, typically ruthenium(II), osmium(II), rhenium (I) or platinum(II) is used to sensitise luminescence from lanthanide(III) ions with low-energy f–f excited states. This allows near-infrared emission from lanthanide(III) ions to be generated by energy-transfer from the strongly-absorbing d-block antenna group. In the lanthanide(III) ions the emission comes from f–f transitions. Due to the core nature of the 4f electrons, which are shielded from the coordination environment by the $5s^2 5p^6$ electrons, little vibrational coupling with the environment is seen, and the emission bands are narrow and ion-specific, leading to pure colours and potentially high emission efficiencies.

The fields of application of the emitting lanthanide(III) complexes depend on the emission wavelength. Ions with transitions in the visible range of the spectrum are utilized for television screens and LEDs, in liquid crystals, as well as in fluoroimmunoassays and in biophysical applications. The ions which emit in the near-IR have found application in lasers and could also be useful for telecommunications and optical amplifiers. Although these complexes were successfully utilized as emitting layers in LEDs, it is more efficient to incorporate the organometallic or coordination complexes into polymers, which can additionally function as charge-transport layers to facilitate the formation and confinement of excitons. More recently, efforts were started in the utilization of polymers with covalently attached emitting complexes, to avoid phase separation during operation and consequent loss of the emitting layer. In addition, polymers have the advantage of displaying higher flexibility and mechanical stability, as well as ease in processability and device integration [32,33].

The functionalization of these complexes at the periphery of the coordination moiety or their grafting on suitable platforms gives rise to supramolecular structures capable of originating organized systems with peculiar chemical and/or physical properties. Thus, the insertion of additional donor atoms at the periphery of the chelating moiety gives rise to a series of quite interesting self-organizing systems, containing similar or dissimilar metal ions, which form planar or tridimensional metal organic frameworks with defined porosity.

Furthermore, the increasing of carbonyl groups with the consequent formation of tri- or tetraketones and bis-β-diketones or bis-β-triketones (Scheme 2) allowed for the formation of well defined homo- and/or hetero-polynuclear complexes with

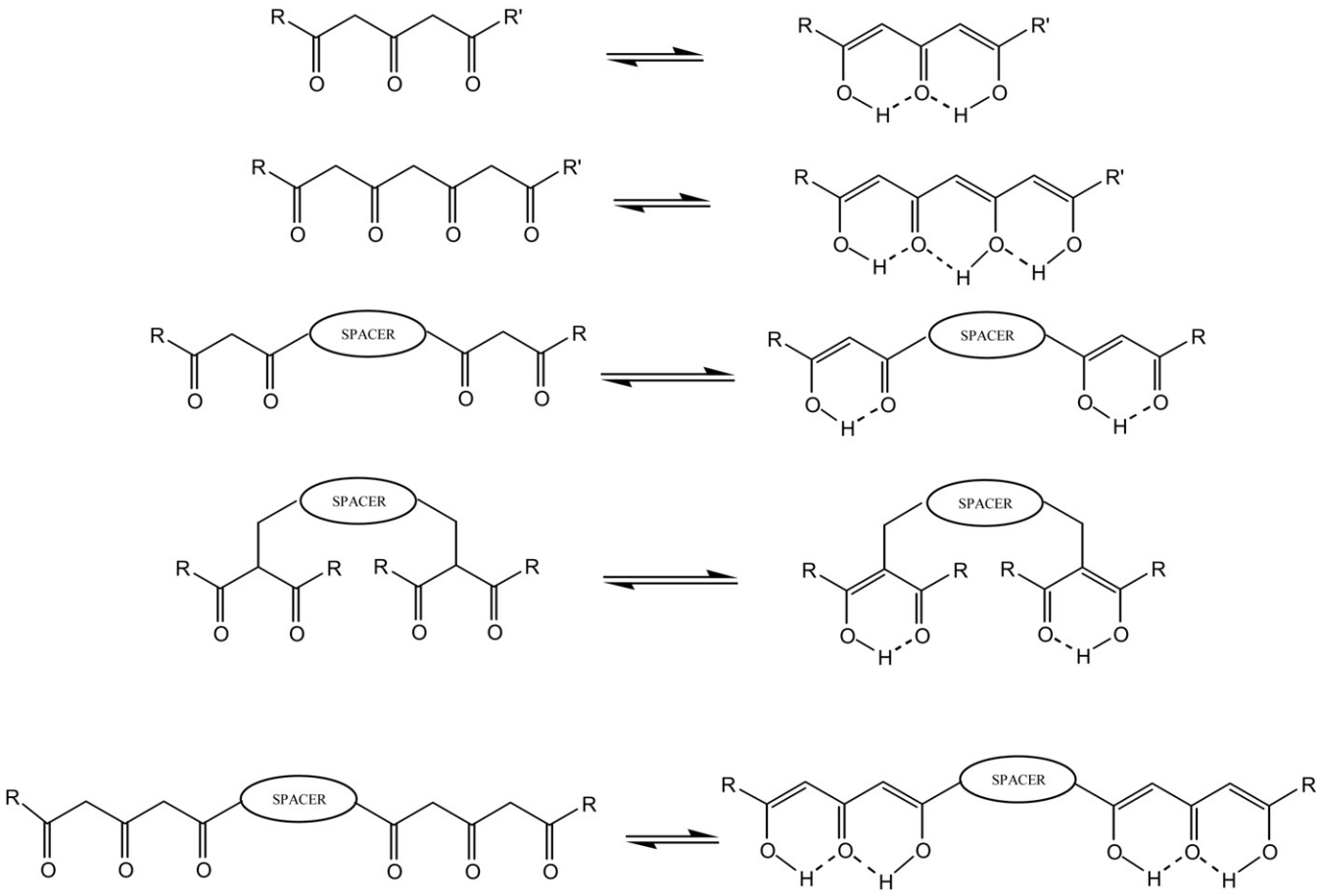

Scheme 2. Poly-β-diketones with or without a spacer and their keto-enol tautomerism.

peculiar physico-chemical properties, arising from the coordination of equal or different metal ions, in close connection and interacting with each other through the carbonyl bridges. Moreover, these ligands generally coordinate in the equatorial plane of metal ions as copper(II), nickel(II), cobalt(II), giving rise to quite flat complexes which can contain coordinating solvents or monodentate ligands in the axial positions. These axial ligands can be exchanged by stronger coordinating ligands which, when potentially bridging linkers as 4,4′-bipyridine, pyrazine, 4,4′-*trans*-azopyridine, 2,2′-dipyridylamine, 1,4-diazabicyclo[2,2,2]octane, 4,4′-dipyridyl sulfide, 2,2′-bipyrimidine, self-organize into oligo- or polymeric-species with quite sophisticated architectures and new functionalities and properties.

Also, the introduction of a suitable spacer with or without additional donor groups between the β-diketonate moieties was successfully carried out. Thanks to the template ability of specific metal ions, such as nickel(II), copper(II), cobalt(II), manganese(II), zinc(II), cadmium(II), vanadyl(IV) or uranyl(IV), two bis-β-diketonates can be ordered in such a way as to offer two, not immediately adjacent, O_2O_2 compartments for the recognition of equal or different metal ions through one or sequential specific recognition processes. Of course, when iron(III), manganese(III), gallium(III) or lanthanide(III) ions are employed as templating agents, three bis-β-diketones can be accommodated in the appropriate coordination environment of these metal ions giving rise to two tridimensional $O_2O_2O_2$ chambers, with the consequent formation of helicate structures. The further presence of donor groups between the two β-diketonate moieties gives rise, upon complexation, to three adjacent compartments, two external O_2O_2 or $O_2O_2O_2$ and one inner $O_2X_{2n}O_2$ or $O_2O_2X_{3n}O_2O_2$ (X = N, O, S; n = 1,2) with the easy formation of homo- or heterotrinuclear complexes and/or homodinuclear complexes which can selective encapsulate into the free coordination chamber alkali or alkaline metal ions, whose additional presence favours the evolution of discrete complexes into polymeric ones.

Finally, the insertion of phenol groups at the end or between the carbonyl moieties generates an interesting series of β-ketophenolate systems (Scheme 3), capable of securing up to eight metal ions in close proximity, the metal ion assembly being mainly governed by the presence or the release of the phenol protons.

All these typologies of β-diketonate or β-diketophenolate systems offer a wide chance to study the properties of the related complexes and to set up the best synthetic procedures for directing the chemical reactions toward discrete, bidimensional or tridimensional systems, varying the metal ion and/or its oxidation state, the number of carbonyl or phenol groups engaged in coordination, the additional donating groups of the ligands and/or the type of bridging ligand.

2. Aim of the review

The review is aimed at giving an overview of the well known β-diketones and β-ketophenols and related complexes (the α-diketones and related derivatives are also inserted for completeness) and their evolution into more sophisticated systems through functionalization or insertion of progressively increasing number of donor groups (i.e. carbonyl and phenol groups, spacers with or without donor atoms) for obtaining quite com-

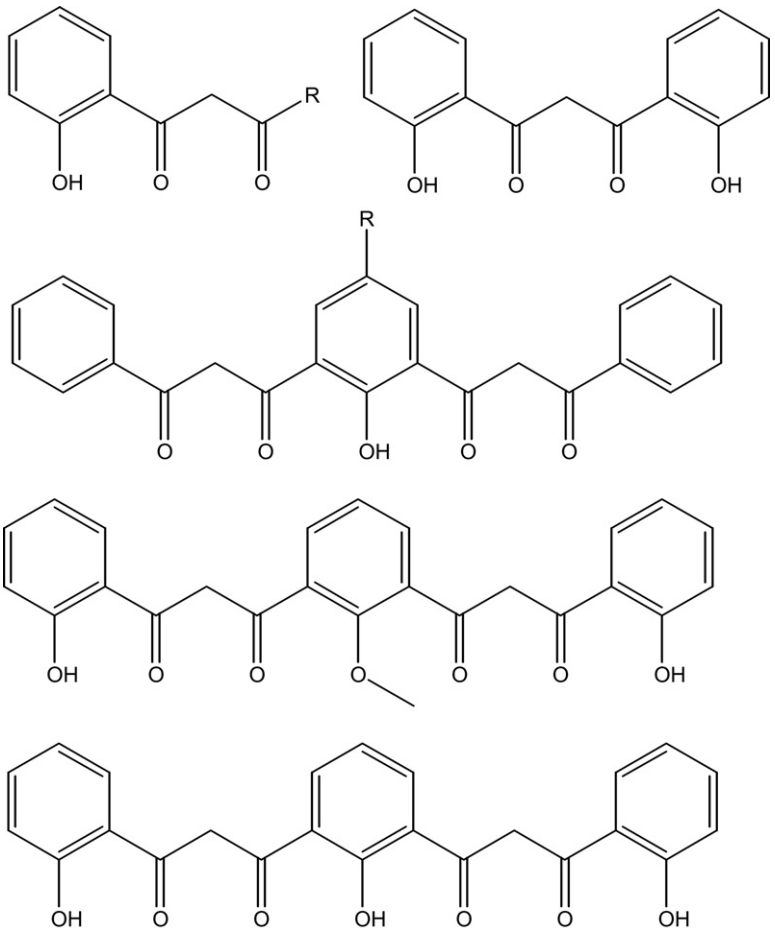

Scheme 3. Keto-phenol derivatives.

plex systems with peculiar and interesting properties to be applied in basic and applied chemistry and technology. The role of these systems as molecular components or precursors in the design of new materials, devices or probes is another goal of the paper.

The formation of discrete, oligomeric or polymeric complexes via the insertion of additional appropriate bridging groups and the stereochemical and physico-chemical (especially, magnetic optical and electrochemical) properties arising from these supramolecular architectures, together with the role of the different metal ions (especially d-and 4f-metal ion) in determining stereochemistry and properties of the resulting complexes represent relevant aspects, considered in the present review.

3. α-Diketonato complexes and related derivatives

Tropolone (2-hydroxy-2,4,6-cycloheptanetrione) and its substituted derivatives (H–**1a**···H–**1d**) can be classified as α-diketones, capable of acting in consequence of deprotonation as strong bidentate oxygen donor chelators of metal ions. Thus, α-diketones and β-diketones share many common features: both ligands are bidentate and both bond through delocalized chelate rings formed through two oxygen atoms. The smaller bite distance and angle and the increased delocalization over the larger tropolonato aromatic system give rise to an increased coordination number at the metal center and change in the physico-chemical properties and reactivity [34,35].

In the past H–**1a** was successfully used for the preparation, by its reaction with a wide variety of metal(II) salts, of [M(**1a**)$_2$] (M = Cu^{II}, Ni^{II}, Co^{II}, Pd^{II}, Zn^{II}, Pb^{II}, Fe^{II}, Mn^{II}, Hg^{II}, Sn^{II}, Be^{II}, Mg^{II}, Ca^{II}, Sr^{II}, Ba^{II}) which are volatile enough to be purified by sublimation without decomposition, except [Fe(**1a**)$_2$] where a partial oxidation to [Fe(**1a**)$_3$] occurs [35].

[Cu(**1a**)$_2$] exists as a sandwich-type dimer: two square planar monomers are stacked face-to-face. The related mesomorphic substituted tropolonato complexes [Cu(**1b**)$_2$] are also square planar with a rod-like calamitic structure, while the packing in the crystals shows a similar arrangement to that in the smectic C phase. There is no Cu···Cu interaction, the closest Cu···Cu approach being at 6.413 Å. The nickel(II) and oxovanadium(IV) complexes of H–**1b**, despite having melting points (50 and 90 °C, respectively) lower than the related copper(II) analogues, do not display any mesophase. An octahedral environment about the nickel(II) ion was proposed [36].

[Cu(**L**)(tmeda)][B(C$_6$H$_5$)$_4$] (H–**L** = H–**1a**, H–**1c**), prepared by CuCl$_2$·2H$_2$O, *N*,*N*,*N*′,*N*′-tetramethylethylenediamine (tmeda) and H–**1a** or H–**1c**, crystallizes as [Cu(**L**)(tmeda)(ClCH$_2$CH$_2$Cl)][B(C$_6$H$_5$)$_4$] and [Cu(**L**)(tmeda)(CH$_3$COCH$_3$)][B(C$_6$H$_5$)$_4$] with the copper(II) ion coordinated by two tropolone oxygen atoms and two diamine nitrogen atoms. The axial interaction with a dichloroethane molecule is weak whereas the axial acetone molecule is firmly coordinated to the copper(II) ion, giving rise to a square pyramidal coordination. These complexes, fairly soluble and remarkably solvatochromic in a large variety of solvents, are useful as Lewis basicity indicators in solution because their d–d bands continuously shift to red with increasing donor number of solvent. The addition of various anions to these solvatochromic systems leads to a quantitative view of the competition between

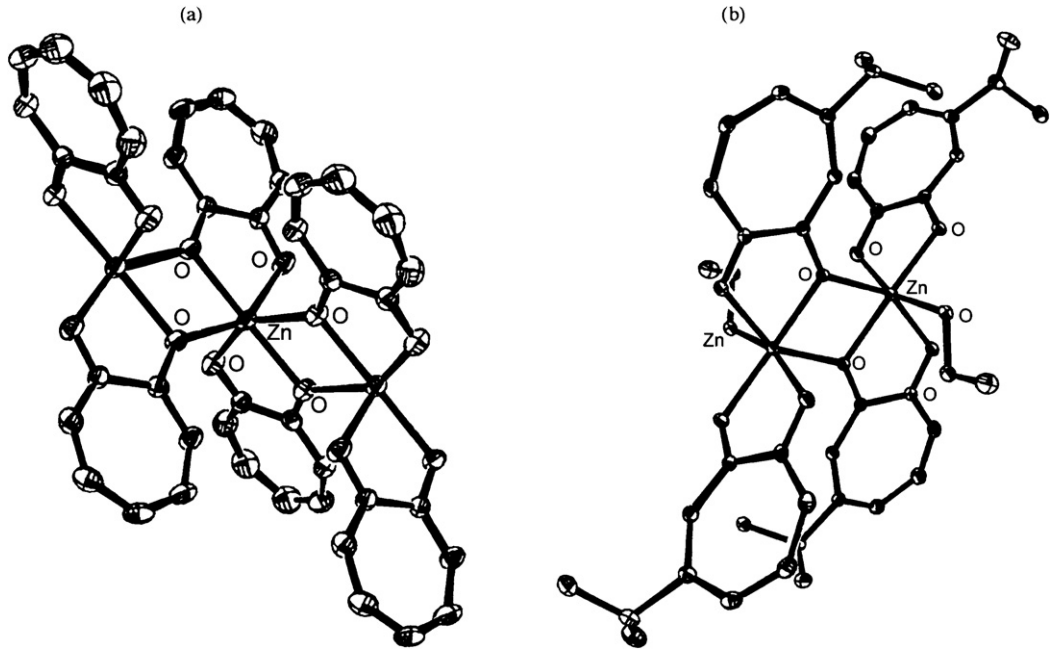

Fig. 1. Structure of $[Zn(\mathbf{1a})_2]_n$ (a) and $[Zn(\mathbf{1c})_2(C_2H_5OH)]_2$ (b) [39].

solvent and anion molecules for coordination to the metal(II) center [37].

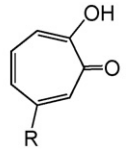

	R
H-**1a**	H
H-**1b**	$(CH_2)_nCH_3$ (n= 8, 10, 12, 14)
H-**1c**	$CH(CH_3)_2$
H-**1d**	CH_3

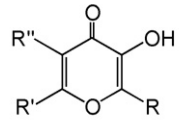

	R	R'	R''
H-**2a**	CH_3	H	H
H-**2b**	C_2H_5	H	H
H-**2c**	H	CH_2OH	H
H-**2d**	CH_3	H	Br

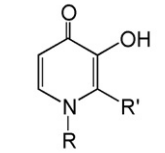

	R	R'
H-**3a**	CH_3	CH_3
H-**3b**	C_2H_5	H
H-**3c**	H	CH_3

The related α-hydroxyketones 3-hydroxy-2,6-disubstituted-4-pyranone (H–**2a**···H–**2c**) and 3-hydroxy-1,2-disubstituted-4-pyridinone (H–**3a**···H–**3c**) form the similar complexes $[M(\mathbf{L})_2]\cdot nH_2O$ when reacted with the appropriate transition or non-transition metal(II) ion [38–40]. The structure of $[Zn(\mathbf{2a})_2]\cdot 1.5H_2O$ can be viewed as layers of ···ABA···ABA··· sandwiches with layers A consisting of five coordinate, square pyramidal complexes, and layers B of six coordinate octahedral complexes. A five coordination is also adopted by $[Sn(\mathbf{3a})_2]$, where the coordination environment is very similar to that of $[Sn(\mathbf{1a})_2]$ [39]. In $[Zn(\mathbf{3a})_2]$ the zinc(II) ion is five coordinate in a distorted square pyramidal geometry while in $[Pb(\mathbf{3a})_2]$ each lead(II) ion is in a O_5 environment, two oxygen atoms acting as bridging groups to give a dimeric structure [38]. Finally, $SnCl_4$ and H_2–**3a** afford $[Sn(\mathbf{3a})_2(Cl)_2]$, which contains two *cis* chloride anions [40].

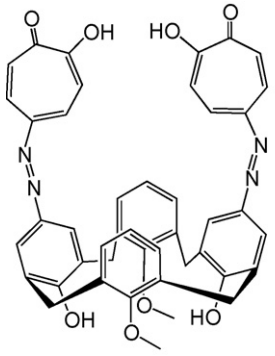

H_2-**4**

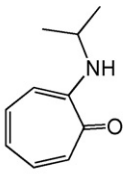

H-**4a**

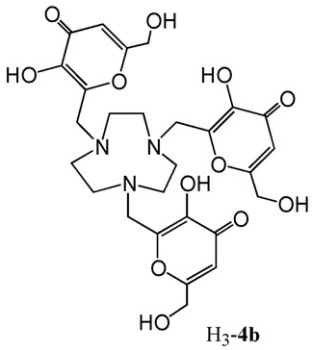

H_3-**4b**

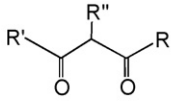

	R	R'	R''
H-**5**	CH_3	CH_3	H
H-**6**	C_6H_5	C_6H_5	H
H-**6a**	p-$CH_3C_6H_5$	p-$CH_3C_6H_5$	H
H-**7**	$C(CH_3)_3$	$C(CH_3)_3$	H
H-**7a**	$C(CH_3)_3$	$CH_2CH(CH_3)_2$	H
H-**7b**	CH_3	$CH_2CH(CH_3)_2$	H
H-**8**	$CF_3CF_2CF_2$	$C(CH_3)_3$	H
H-**9**	C_6F_5	C_6F_5	H
H-**10**	CF_3	CF_3	H
H-**11**	CF_3	$C(CH_3)_3$	H
H-**11a**	CF_3	CH_3	H
H-**12**	C_6H_5	CH_3	H
H-**13**	allyl	CH_3	H
H-**14**	CH_3	CH_3	Br
H-**17**	C_4H_3S	CF_3	H
H-**18**	C_6H_5	CF_3	H
H-**18a**	p-$N(CH_3)_2C_6H_4$	p-$NO_2C_6H_4$	H
H-**18b**	$C_{12}H_{25}O$	$C_{33}H_{16}O$	H
H-**18c**	p-$CN(C_6H_4)_2O(CH_2)_6OC_6H_4$	$C_6H_4O(CH_2)_6O(C_6H_4)_2$-pCN	H

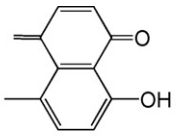

H-**15**

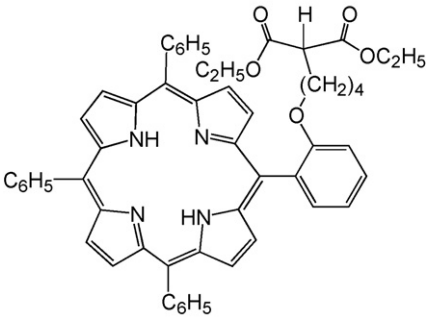

H_3-**16**

The complexes [M(**1a**)$_2$] (M = Ni^{II}, Co^{II}) appear to be oligomeric while in [Zn(**1a**)$_2$] each tropolonato ligand chelates to the zinc(II) ion and, in addition, bridges an adjacent zinc(II) ion giving rise to coordination polymer in which Zn_2O_2 rhomboids are linked in a orthogonally alternating manner and each metal ion is distorted octahedral (Fig. 1a). [Zn(**1c**)$_2$] in ethanol affords [Zn(**1c**)$_2$(C_2H_5OH)]$_2$ whose structure was described as an ethanol-capped dimeric fragment of the polymer adopted by [Zn(**1a**)$_2$]. The two [**1c**]$^-$ ligands chelate the zinc(II) ion; one has also a bridging role. The remaining coordination site of each octahedral zinc(II) ion is occupied by an ethanol oxygen (Fig. 1b) [39].

[Sn(**1a**)$_2$] adopts a pseudo-five coordinate SnO_4E (E = lone pair) severely distorted trigonal bipyramidal structure with one equatorial site occupied by a stereochemically active lone pair (Fig. 2a) [39].

In the six coordinate tin(IV) complexes [Sn(**L**)$_2$(X)$_2$] (H–**L** = H–**1a**, H–**1c**; X = Cl, Br, I), prepared by reaction of SnX_4 and H–**L**, the two halogenide anions are *cis* to each other, as ascertained for [Sn(**1a**)$_2$(Cl)$_2$] (Fig. 2b) [40]. Furthermore, $SnCl_4$ and H–**1b** (in a 1:2 molar ratio) in benzene/methanol afford [Sn(**1b**)$_2$(Cl)$_2$] which evolves into [Sn(**1b**)$_3$(Cl)] in the presence of [Na(**1b**)] [34,40]. A mixture of [Sn(CH_3)$_3$(Cl)] and [NH_4(**1a**)] gives rise to [Sn(**1a**)(CH_3)$_3$], where the tin(IV) geometry is intermediate between square pyramidal and trigonal bipyramidal as occurs also in [Sn(**1a**)(C_6H_5)$_3$]. Both in the solid state and in solution [Sn(**1a**)(CH_3)$_3$] demethylates to [Sn(**1a**)$_2$(CH_3)$_2$], where the octahedral tin(IV) ion is surrounded by the two [**1a**]$^-$ chelating ligands and two *cis*-methyl groups [41].

Heating $IrCl_3$ with an excess of H–**1a** and sodium acetate in water forms [Ir(**1a**)$_3$] together with a polymeric red-black solid which, by addition of [Zn(CH_3)$_3$] in tetrahydrofuran/pyridine, affords [Ir(**1a**)$_2$(CH_3)(py)]. The octahedral iridium(III) ion is equatorially coordinated by two chelating [**1a**]$^-$ ligands and axially by a methyl group trans to a pyridine molecule. At high temperature the methyl group can be substituted by various solvents (cyclohexane, mesitylene, benzene, acetone, etc.) proving the ability of this complex to activate the C—H bond of these molecules with an activation capability higher than that of the related acetylacetonate complex [42].

[M(**1a**)$_4$] or [M(**1c**)$_4$] occur for M = Pb^{IV}, Sn^{IV}, Th^{IV}, U^{IV}, Pa^{IV}, Np^{IV}, Pu^{IV}. NMR studies of the contact and pseudocontact shifts of the eight coordinate complex [U(**1c**)$_4$], using [Th(**1c**)$_4$] as the diamagnetic analogue, indicate that the uranium(IV) complex has bis-disphenoid structure in $CHCl_3$ and a D_4 square antiprism structure in dimethylsulfoxide [43].

$AnCl_4$ (An = Th^{IV}, Pa^{IV}, U^{IV}, Np^{IV}, Pu^{IV}) and [Li(**1a**)] afford in oxygen-free dichloroethane [An(**1a**)$_4$] which, with the exception of the neptunium(IV) and plutonium(IV) complexes, form [An(**1a**)$_4$(DMF)] by recrystallization from oxygen-free dimethylformamide, as confirmed by the X-ray structure of [Th(**1a**)$_4$(DMF)], where the monocapped square antiprismatic nine coordination about the thorium(IV) ion is formed by eight oxygen atoms from four bidentate [**1a**]$^-$ ligands and one dimethylformamide oxygen (Fig. 3). The complexes [An(**1a**)$_4$] evolve into Li[An(**1a**)$_5$] when reacted with [Li(**1a**)] in oxygen-free DMF. Furthermore, [Pa(**1a**)$_4$(X)] (X = Cl^-, Br^-), prepared by $PaCl_5$ and H–**1a** in CH_2Cl_2, reacts with [Li(**1a**)] in ethanol at 60 °C to form [Pa(**1a**)$_4$(C_2H_5O)], which turns into [Pa (**1a**)$_4$(ClO_4)] by the addition of $HClO_4$ in acetone. Finally, [Pa(**1a**)$_4$(Cl)] in DMSO/CH_2Cl_2 forms [Pa(**1a**)$_4$(Cl)(DMSO)] [44].

Because of their similar charge to ionic radius ratios, the cerium(IV) ion is a generally accepted structural analog for the plutonium(IV) ion, and thus the complexes [Ce(**L**)$_4$] (H–**L** = H–**2a**, H–**2d**) have been employed as structural models for the corresponding [Pu(**L**)$_4$] structures. The expectation of structural correlation between the plutonium(IV) and cerium(IV) complexes was met in the near identical [M(**2a**)$_4$] crystal structures, which exhibit a tetragonal dodecahedral coordination geometry. However, substitution of [**2a**]$^-$ for [**2d**]$^-$ led to a dramatic change in the coordination polyhedron about the cerium(IV) ion, particularly the ligand orientation about the metal ion, a result that was surprisingly absent in the analogous plutonium(IV) structure [45].

[Mo_2O_4(**1a**)$_2$(OC_2H_5)$_2$], prepared by H–**1a** and [Mo_2O_4]$^{2+}$ which derives from $Na_2MoO_4{\cdot}2H_2O$ and hydrazinium dichloride in HCl, shows a [MoO(μ-O)$_2$MoO]$^{2+}$ core in a *syn* configuration, with a Mo···Mo distance of 2.564 Å. The distorted octahedral coordination geometry of each molybdenum ion is completed by a tropolonato and an ethanol ligand (Fig. 4a) [46].

H_2–**4**, containing two molybdenocene-tropolonato groups appended to the upper ring of a calix-[**4**]-arene platform via photoactive azo spacers in order to change the properties of the resulting calixarene in response to light, was prepared by reaction of calix-[**4**]-arene with methyl-*p*-toluensulfonate in the presence of K_2CO_3 followed by treatment of the resulting 1,3-dimethoxy-calix-[**4**]-arene with an excess of tropolone-diazonium salt. Complexation of [Mo_2(C_5H_4)$_4$(OH)$_2$] (CF_3SO_3)$_2$ with H_2–**4** forms the air stable complex [Mo_2(**4**)(C_5H_4)$_4$(OH)$_2$] (CF_3SO_3)$_2$, resulting in a large change in the UV–vis spectrum due to the

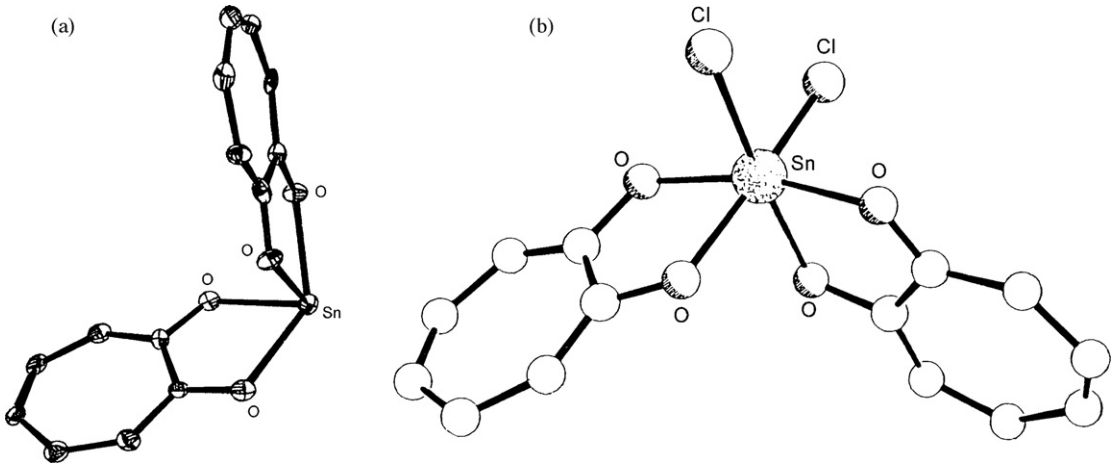

Fig. 2. Structures of [Sn(**1a**)$_2$] (a) [39] and [Sn(**1a**)$_2$(Cl)$_2$] (b) [40].

equilibrium, strongly dependent from the solvent, between the hydrazonic form and the diiminic form of [**4**]$^-$ which takes place in pyridine but not in methanol where [**4**]$^-$ is exclusively in the hydrazone form [47].

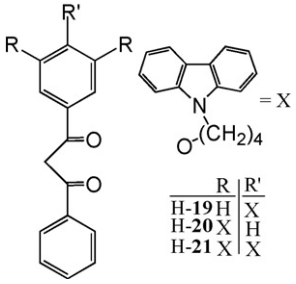

Photodeposition experiments demonstrate that the uranyl(VI) complexes [UO_2(**L**)$_2$(S)] (H–**L** = tropolone, *iso*-amyltropolone, *tert*-octyltropolone, *tert*-amyltropolone, *n*-hexyltropolone, *n*-octyltropolone; S = solvent) are excellent precursors for the preparation of thin films of uranium oxides to be used as patterns in X-ray masks. The H_2–**L** ligands derived by alkylation of sodium cyclopentadienyl with an alkyl halide, followed by cycloaddition with dichloroketene and further hydrolysis of the cycloadduct [48].

In [UO_2(**1a**)$_2$(L)] (L = C_2H_5OH, C_5H_5N), prepared from $UO_2(NO_3)_2{\cdot}6H_2O$ and H–**1a** in ethanol or pyridine, the equatorial coordination about an almost perpendicular O–U–O group consists of four oxygen atoms from two [**1a**]$^-$ ligands and one ethanol oxygen or one pyridine nitrogen (Fig. 4b) [49].

In the past [Ln(**1a**)$_3$] and M[Ln(**1a**)$_4$] (M = NH_4^+, K^+) were synthesized for the whole series of the lanthanide(III) ions [34]; the recently solved structure of {K[Ln(**1a**)$_4$]·DMF}$_\infty$ (Ln = Tb^{III}, Dy^{III}, Ho^{III}, Er^{III}, Tm^{III}, Yb^{III}, Lu^{III}), proves that the lanthanide(III) ion is coordinated by the eight oxygen atoms of four [**1a**]$^-$ ligands. The potassium cation bridges two {Ln(**1a**)$_4$}$^-$ units and has a coordination number of seven through interactions with six oxygen atoms from two {Ln(**1a**)$_4$}$^-$ units and one oxygen atom from a dimethylformamide molecule. These lanthanide complexes are isostructural, except the terbium(III) one, whose structure differs about the relative position of the potassium ion with respect to the lanthanide(III) ion. In all cases, a distorted dodecahedron around the lanthanide cation occurs (Fig. 5a) [50].

Spectrophotometric titrations show that H–**1a** reacts with all the lanthanide cations to form [M(**1a**)]$^{2+}$, [M(**1a**)$_2$]$^+$, [M(**1a**)$_3$], and [M(**1a**)$_4$]$^-$, successively. The calculated formation constants of [M(**1a**)$_3$] and [M(**1a**)$_4$]$^-$, K_3 and K_4 respectively, show different trends that depend on the size of lanthanide cations: $\log K_3$ increases as the size of the lanthanide decreases, as usually observed for lanthanide cations where no steric hindrance is present between ligands upon complex formation, as the interaction between lanthanide cations and the ligand is mainly electrostatic. The strength of this interaction increases with the

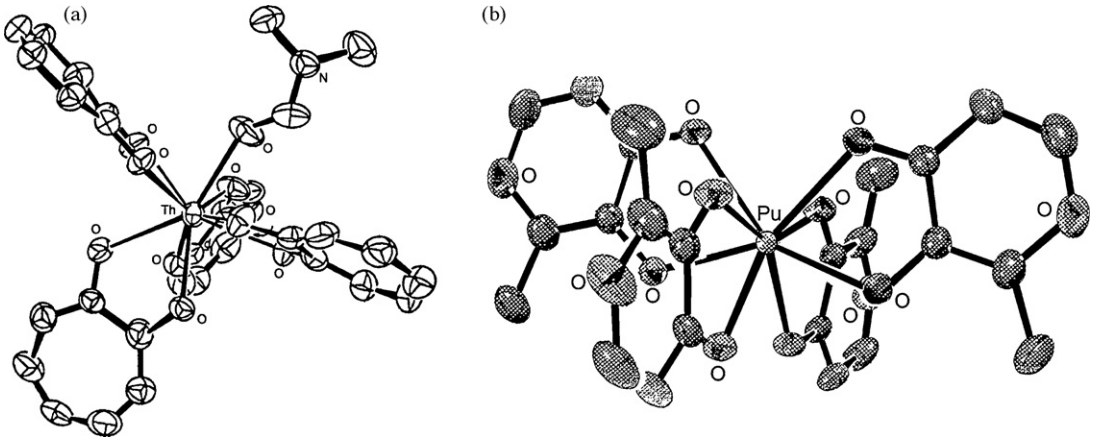

Fig. 3. Structure of [Th(**1a**)$_4$(DMF)] (a) [44] and [Pu(**2a**)$_4$] (b) [45].

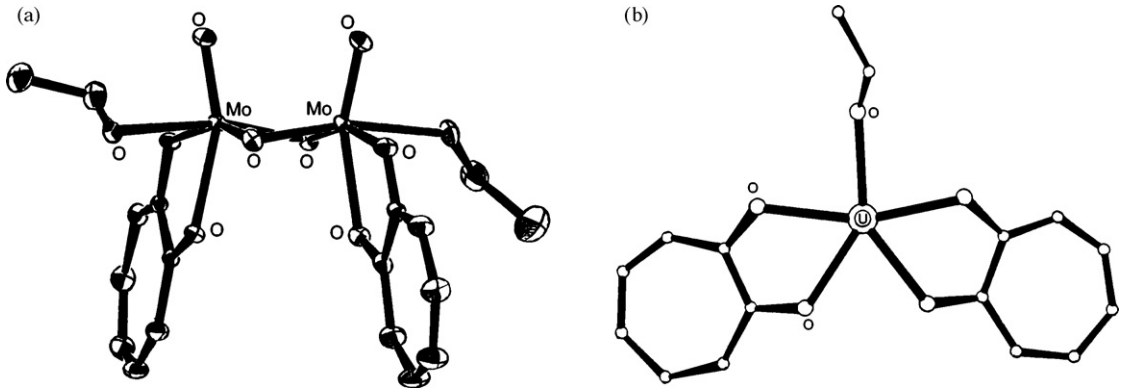

Fig. 4. Structures of $[Mo_2O_4(\mathbf{1a})_2(OC_2H_5)_2]$ (a) [46] and $[UO_2(\mathbf{1a})_2(C_2H_5OH)]$ (b) [49].

atomic number of the lanthanide. As the atomic number increases, the charge density on the lanthanide cation increases, leading to larger log K_3 values. The log K_4 values steadily decreases as the size of the lanthanide cation decreases, owing to the increasing steric hindrance between the four ligands in $[M(\mathbf{1a})_4]^-$ with the smaller lanthanide cations: the ligands must be located at closer proximity when the effective radii of the lanthanide(III) cations decrease [50].

Luminescence lifetimes of the ytterbium(III) complex in H_2O/D_2O and CH_3OH/CD_3OD-d_4 provide evidence of one coordinated water or methanol molecule, indicating that the coordination geometry around the lanthanide(III) cation in $[M(\mathbf{1a})_4]^-$ in solution is different than that in the solid state, where no solvent molecule is bound to the lanthanide cation. Nevertheless, $[\mathbf{1a}]^-$ is able to sensitize several lanthanide cations that emit in the near-infrared domain with quantum yields comparable to the highest quantum yields reported for other lanthanide complexes that emit in the NIR domain in organic solvents. For all the complexes $[Ln(\mathbf{1a})_4]$, however, a significant residual ligand emission persists owing to an incomplete energy transfer from the ligand to the lanthanide ion [50].

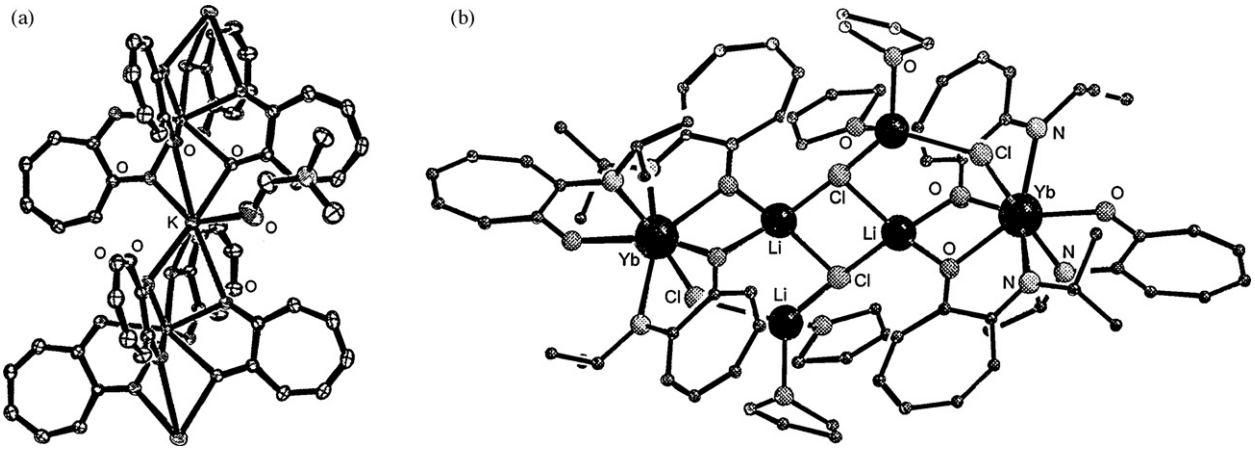

Fig. 5. Structure of $\{K[Yb(\mathbf{1a})_4]\cdot DMF\}_\infty$ (a) [50] and $[Yb_2Li_4(\mathbf{4a})_6(Cl)_4]$ (b) [52].

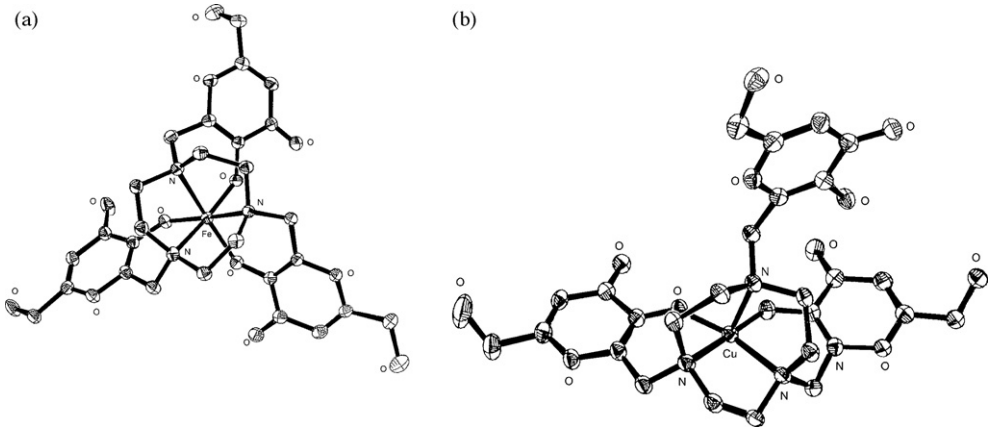

Fig. 6. Structure of $[M(\mathbf{4b})]$ ($M = Fe^{III}, Ga^{III}$) (a) and $[Cu(H\text{-}\mathbf{4b})]$ (b) [53].

The air stable complexes [Ln(**1c**)$_3$] (Ln = Eu, Er, Yb), derived from H–**1c**, NaOH and the appropriate $LnCl_3 \cdot 6H_2O$, contain only traces of water or methanol although recovered from a water/methanol solution; they have been supposed to be dimeric or trimeric in order to complete the high coordination number required by the lanthanide(III) ions. The NMR spectra of [Eu(**1c**)$_3$]$_n$ in $(CD_3)_2SO$ show a double pattern of [**1c**]$^-$ ligands, indicating the different role of the oxygen atoms bridging the europium(III) ions. The lack of quenching in the fluorescence of these complexes is an additional proof of the absence of water in the coordination environment of the lanthanide(III) ion. These oligomeric complexes easily turn into the monomeric ones [Ln(**1c**)$_3$(phen)] in the presence of 1,10-phenanthroline. [Er(**1c**)$_3$(phen)]·H_2O is soluble in a variety of solvents and appears to be monomeric with the metal ion in an eight coordinate environment. Thermogravimetric analyses indicate the loss of one non-coordinated water molecule. Again the presence of water only in the crystalline framework and not directly bonded to the central metal ion is proved by the photophysical behaviour [51].

A functionalization at the periphery of the chelating nitrogen-containing ligands was introduced in order to allow them to serve as dinucleating ligands towards equal or different lanthanide(III) ions. 1,10-Phenanthroline-5,6-dione (pdon) is a ditopic ligand which contains two well separated coordinating sites, one containing two nitrogen atoms and one containing two oxygen atoms, both suitable for lanthanide(III) complexation. Thus, the reaction of [Er(**1c**)$_3$]$_n$ with pdon in anhydrous methanol in a 1:1 molar ratio under reflux affords [Er(**1c**)$_3$(pdon)]·0.2H_2O with the lanthanide(III) ion coordinated to the two nitrogen atoms of the functionalized phenanthroline. This mononuclear complex reacts an equimolar amount of [Er(**1c**)$_3$]$_n$ in anhydrous hot methanol to produce [Er$_2$(**1c**)$_6$(pdon)]·H_2O, as proved by ESI–MS spectrometry and IR and NMR spectroscopy. The erbium(III) complexes show efficient NIR emissions at about 1550 nm upon excitation at 355 nm in the UV ligand absorption band, emerging as possible candidates as active materials of plastic amplifiers for telecommunication. In particular [Er(**1c**)$_3$]$_n$, [Er(**1c**)$_3$(phen)], [Er(**1c**)$_3$(pdon)], and [{Er(**1c**)$_3$}$_2$(pdon)] show photoluminescent efficiency values at 1550 nm larger than that for [Er(Q)$_3$] (H–Q = 8-hydroxyquinoline), normally assumed as a reference material [51].

H–**1a** easily affords 2-(tosyloxytropone), which gives rise to H–**4a** in the presence of an excess of isopropylamine. [Li(**4a**)]$_6$, resulting from the treatment of H–**4a** with an excess of *n*-butyllithium in toluene, contains an hexameric core of two Li_3O_3 rings each showing a chair conformation. The aminotroponate moieties bridge both six-membered rings. Each lithium(I) ion is tetracoordinate. H–**4a** and KH afford [K(**4a**)] which reacts with $LnCl_3$ (Ln = Y, Lu) to form [Ln(**4a**)$_3$] whose structure was not reported yet. On the contrary, a 2:1 mixture of [Li(**4a**)]$_6$ and $YbCl_3$ produces [Yb_2Li_4(**4a**)$_6$(Cl)$_4$], where two {Yb(**4a**)$_3$} units are bridged by four {LiCl} units. Each heptacoordinate ytterbium(III) ion is surrounded by three [**4a**]$^-$ ligands and one chloride ion. The center of the complex contain a {Li–Cl–Li–Cl} square with two square planar lithium(I) ion surrounded by two chloride and two the oxygen atoms of the [**4a**]$^-$ ligands, while the other two tetracoordinate lithium(I) ions are coordinated by two chloride anions and two tetrahydrofuran oxygen atoms (Fig. 5b) [52].

The amide derivative [Ca(L)$_2$(THF)$_2$] (H–L = [N{Si(CH$_3$)$_2$}]$^-$) reacts with H–**4a** in tetrahydrofuran or H–**4a** and *N*-isopropyl-2-(isopropylamino)troponeimine (H–L′) in toluene to afford the dinuclear complexes [Ca(**4a**)$_2$(L)$_2$(THF)$_2$] and [Ca(**4a**)$_2$(L′)$_2$], respectively. In the former complex, each metal ion is asymmetrically bridged by the oxygen atoms of the [**4a**]$^-$ ligands, the coordination environment being completed by two amide nitrogen atoms, one from [**4a**]$^-$ and the other from [L]$^-$, and by one tetrahydrofuran oxygen. In the latter complex the two five coordinate metal ion are symmetrically bridged by the oxygen atoms of the [**4a**]$^-$ ligands. The distorted trigonal bipyramidal environment about each calcium(II) center is completed by the amide nitrogen of a [**4a**]$^-$ chelate and the two nitrogen atoms of one [L′]$^-$ ligand [52].

One equivalent of 1,4,7-triazacyclononane, 3 equiv. of 5-hydroxy-2-hydroxymethyl-4H-4-pyranone and an excess formaldehyde give H_3–**4b**, which in the presence of appropriate metal salt, forms the isostructural [M(**4b**)] (M = Fe^{III}, Ga^{III}, In^{III}) or [Cu(H-**4b**)]·3H_2O. In [M(**4b**)], the coordination about the metal(III) ion is a distorted octahedron with three amine nitrogen atoms occupying one face and the opposite face being occupied by three enolate–oxygen atoms (Fig. 6a). In [Cu(H-**4b**)]·3H_2O the copper(II) ion is square pyramidal with [H-**4b**]$^{2-}$ acting as a pentadentate ligand through the three tertiary amine nitrogen and two enolate oxygen atoms. One of the three 3-hydroxy-4-pyrone chelating arms remains free and protonated (Fig. 6b). The cyclic voltammogram of [Fe(**4b**)] exhibits a quasi-reversible redox wave at $E_{1/2} = -0.53$ mV (reference electrode Ag/AgCl) from the {Fe^{III}(**4b**)}/{Fe^{II}(**4b**)}$^-$ couple, whereas [Cu(H-**4b**)] shows an irreversible one-electron reduction of [Cu^{II}(H-**4b**)]/[Cu^{I}(H-4a)]$^-$ at $E_{pc} = -0.87$ V. These low redox potentials indicate that the iron(III) ion in [Fe(**4a**)] and the copper(II) ion in [Cu(H-**4b**)] are preferentially stabilized by the macrocyclic ligand. Variable temperature ^{1}H NMR spectra show that [Ga(**4b**)] is more rigid than [In(**4b**)] [53].

4. β-Diketonato complexes with oxygen donor ligands

4.1. Complexes with d-transition and non transition metal ions

β-Diketones react with stoichometric amounts of the appropriate metal(II) ion to form [M(β-dike)$_2$]$_n$ (n = 1–4) and [M(β-dike)$_2$(S)$_n$] (n = 1, 2) in non coordinating and coordinating solvents, respectively. On gentle heating, the solvent molecules can be removed from [M(β-dike)$_2$(S)$_n$] with the consequent formation of the mononuclear complexes [M(β-dike)$_2$] which, in the absence of additional coordinating ligands, quite often turn into the di- or -polynuclear ones by oligomerization through the bridging oxygen atoms, as observed in [Ni$_3$(**5**)$_6$] [54] and [Co$_4$(**5**)$_8$] [55]. The structure of [Ni$_3$(**5**)$_6$] shows that the three nearly octahedral nickel(II) ions are in the linear trimeric array, resulting from the sharing of triangular faces of adjacent octahedral. A [**5**]$^-$ oxygen is at each apex of linear triad of fused octahedra. The intramolecular Ni···Ni distances are 2.882 and 2.896 Å. The closest intermolecular Ni···Ni distance is ∼8 Å. A similar octahedral coordination about each metal(II) ion was found also in [Co$_4$(**5**)$_8$]. Ferromagnetic coupling between adjacent ions and a smaller antiferromagnetic interaction between the terminal ions occurs in [Ni$_3$(**5**)$_6$]. The addition of an excess of β-diketone to [M(β-dike)$_2$]$_n$ avoids oligomerization forming [M(β-like)$_3$]$^-$ as found for [Co(**5**)$_3$]$^-$ [54,56].

[M(**6**)$_2$(H$_2$O)$_2$] (M = Ni^{II}, Zn^{II}, Cd^{II}), prepared from H–**6** and the appropriate metal salt in ethanol, gives rise to [M(**6**)$_2$(py)$_2$] in pyridine, with the nickel(II) ion in a *trans*-configuration and the zinc(II) and cadmium(II) ones in a *cis*-configuration. [M(**6**)$_2$(H$_2$O)$_2$] evolves into [M(**6**)$_2$], when heated at 100 °C in non coordinating solvents. When heated at 215 °C for 30 min or in benzene at 70 °C for several days, [Ni(**6**)$_2$] forms [Ni$_3$(**6**)$_6$] and [Ni$_3$(**6**)$_6$]·2C_6H_6, respectively. Furthermore, [Zn$_2$(**6**)$_4$] results from evaporation at 70 °C of a benzene solution of [Zn(**6**)$_2$] [57].

The structure of [Ni(**6**)$_2$], similar to that of the copper(II) and palladium(II) analogues, contains a square planar metal(II) ion surrounded by four oxygen atoms from two chelating [**6**]$^-$ ligands. On

the contrary, in [Zn(**6**)$_2$] a very distorted tetrahedral coordination about the metal ion occurs [57].

[Ni$_3$(**6**)$_6$] has a linear Ni$_3$ cluster (Ni···Ni distances of 2.811 Å) surrounded by chelating and bridging [**6**]$^-$ ligands. Each nickel(II) ion is in an O$_6$ distorted octahedral environment of six oxygen atoms from the [**6**]$^-$ ligands (Fig. 7a). [Ni$_3$(**6**)$_6$]·2C$_6$H$_6$ has a very similar structure with the benzene guests filling up the cavity spaces [58].

In [Zn$_2$(**6**)$_4$] two [**6**]$^-$ ligands chelate to each zinc(II) ion by four oxygen atoms, while one oxygen atom also bridges to the neighbouring zinc(II) center. The coordination environment of the zinc(II) ions is intermediate between trigonal bipyramidal and square pyramidal (Fig. 7b) [57].

In [Pb(**5**)$_2$], obtained by refluxing an acetylacetone/toluene mixture over the lead foil, the lead(II) ion is chelated by two [**5**]$^-$ ligands, giving rise to a distorted square pyramidal PbO$_4$ geometry. Short contacts among neighbouring molecules give rise to zigzag chains [58].

[Pb(**6**)$_2$] contains polymeric chains of the dimeric {Pb$_2$(**6**)$_4$} units, linked through hexa–hapto-interactions of the lead(II) ions with phenyl groups from adjacent units. Each lead ion also appears to be involved in intraunit dihapto–aromatic interactions, thus attaining a total hapticity of 13. Thus, rather than an highly unusual PbO$_5$ coordination sphere, the complex has been considered to contain a tridecahapto PbO$_5$C$_8$ center with an irregular but "holodirected" coordination sphere. [Sn(**6**)$_2$] strongly resembles the lead(II) analogue with the SnO$_5$ unit "hemidirected" and where both η^2- and η^6-interaction with ligand phenyl groups occur through the face remote from the oxygen donors. The interactions, giving rise to a polymeric form in the solid, are stronger for the lead(II) than for the tin(II) complex [59].

[Pb(**7**)$_2$], obtained from equivalent amounts of Pb(CH$_3$COO)$_2$ and [Na(**7**)] in water at room temperature, contains a four coordinate lead(II) ion, chelated by the oxygen atoms of the two [**7**]$^-$ ligands; the coordination sphere around the lead ion can be described as a square pyramid with four oxygen atoms forming the square plane and the lone pair of electrons at the axial position. The structure of [Pb(**8**)$_2$], obtained from Pb(CH$_3$COO)$_2$ and [Na(**8**)], is similar to those of [Cu(**7**)$_2$] and [Ni(**7**)$_2$] but differs from that of [Pb(**7**)$_2$] as it is based on a dinuclear {Pb$_2$(**8**)$_4$} unit, where each lead ion can be viewed as seven coordinate, chelated by the oxygen atoms of two diketonate ligands, the coordination environment being completed by one fluorine and two further bridging oxygen atoms [60].

The family of butterfly-type tetrametallic vanadium alkoxide clusters [V$_2^{III}$(V^{IV}O)$_2$(**5**)$_4$(OCH$_3$)$_6$], [(V^{IV}O)$_4$(**5**)$_2$(H-tea)$_2$(OCH$_3$)$_2$] and [(V^{IV}O)$_4$(**5**)$_2$(L)$_2$(OCH$_3$)$_2$] (H$_3$-tea = triethanolamine; H$_2$–L = *N*,*N*′-bis-(2-hydroxyethyl)-*N*′-(2-pirrolylmethylidene)ethylenediamine), was recently enlarged to [V$_2$(VO)$_2$(**5**)$_4${RC(CH$_2$O)$_3$}$_2$], [V$_2$(VO)$_2$(**5**)$_2$(C$_6$H$_5$COO)$_2${CH$_3$C(CH$_2$O)$_3$}$_2$], [V$_4$Cl$_2$(**6**)$_4${RC(CH$_2$O)$_3$}$_2$] (R = CH$_3$, C$_2$H$_5$, CH$_2$OH), and [V$_4$Cl$_2$(**6**)$_4$(CH$_3$O)$_6$]. In particular, the V$_2^{III}$V$_2^{IV}$ complexes [V$_2$(VO)$_2$(**5**)$_4${RC(CH$_2$O)$_3$}$_2$] are prepared by heating equimolar amounts of [V(**5**)$_3$], [VO(**5**)$_2$] and RC(CH$_2$OH)$_3$ in CH$_3$CN under reflux for 12 h; the same products are also isolated, but in much lower yields, when [VO(**5**)$_2$] is omitted from the reaction. Their similar structure (Fig. 8a) contains four coplanar metal ions at the corners of a rhombus bound by two triply deprotonated, μ_2,μ_2,μ_3-[R(CH$_2$O)$_3$]$^{3-}$ ligands. The two vanadyl(IV) ions are easily detectable as they have the characteristic V=O group, whereas the other two vanadium(III) ions are in a regular octahedral geometry. Each μ_2-arm of the tris-alkoxides bridges an edge of the rhombus. The μ_3-arms of the two tris-alkoxides bridge three adjacent vanadium ions, forming a butterfly core. A chelating diketonate completes the six-coordination at each metal ion. The structures of these complexes are closely related to the tetrametallic mixed-valence V$_2^{III}$V$_2^{IV}$ cluster [V$_2$(VO)$_2$(**5**)$_4$(OCH$_3$)$_6$] where six methoxides take the place of the two [CH$_3$C(CH$_2$O)$_3$]$^{3-}$ groups in these complexes. The V$_4^{III}$ clusters [V$_4$(**6**)$_4$(Cl)$_2$ {RC(CH$_2$O)$_3$}$_2$] (R = CH$_3$, C$_2$H$_5$, CH$_2$OH) have been isolated from the reaction at 15 °C for 16 h of [VCl$_3$(THF)$_3$], RC(CH$_2$OH)$_3$ and [Na(**6**)] in tetrahydrofuran or acetonitrile under anaerobic conditions. In these complexes, each vanadium(III) ion has a chelating [**6**] ligand; also two vanadium(III) ions have a terminal chloride (Fig. 8b). The similar reaction in methanol and in the absence of the triol yields [V$_4$(**6**)$_4$(Cl)$_2$ (OCH$_3$)$_6$], where six methoxides replace the six arms of the two tris-alkoxides of [V$_4$(**6**)$_4$(Cl)$_2$ {RC(CH$_2$O)$_3$}$_2$] (R = C$_2$H$_5$, CH$_2$OH) (Fig. 8c). All these clusters are dominated by antiferromagnetic interactions [61].

A simple method for obtaining heterotrinuclear complexes was recently reported for [Pt$_2$Co(**5**)$_2$(μ-CH$_3$COO)$_4$], prepared from [Pt(**5**)$_2$] and Co(CH$_3$COO)$_2$·4H$_2$O in air and in acetic acid at 110 °C. The central, slight distorted tetrahedral cobalt(II) ion is coordinated to four oxygen atoms of two bridging acetates which connect it to each square planar platinum(II) ion whose coordination sphere is completed by the two oxygen atoms of a [**5**]$^-$ chelate (Fig. 9). The synthesis requires air oxygen, while no reaction between [Pt(**5**)$_2$] and Co(CH$_3$COO)$_2$·4H$_2$O occurs in argon. A rather complicated pathway was proposed where the intermediate cobalt (III) species, formed in the oxidative Co^{II}/O$_2$ system, remove [**5**]$^-$ (e.g., by its free radical oxidation to CH$_3$COOH) from the platinum(II) coordination sphere, facilitating the entry of cobalt (II) acetate into the coordination vacancies thus formed. Noticeably, zinc(II) acetate, where the metal ion is not oxidizable, does not react with [Pt(**5**)$_2$] [62].

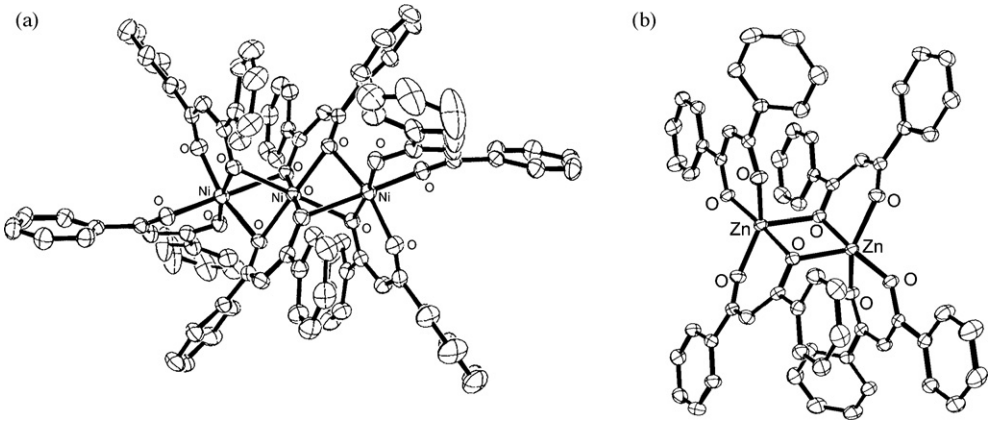

Fig. 7. Structure of [Ni$_3$(**6**)$_6$] (a) [58] and [Zn$_2$(**6**)$_4$] (b) [57].

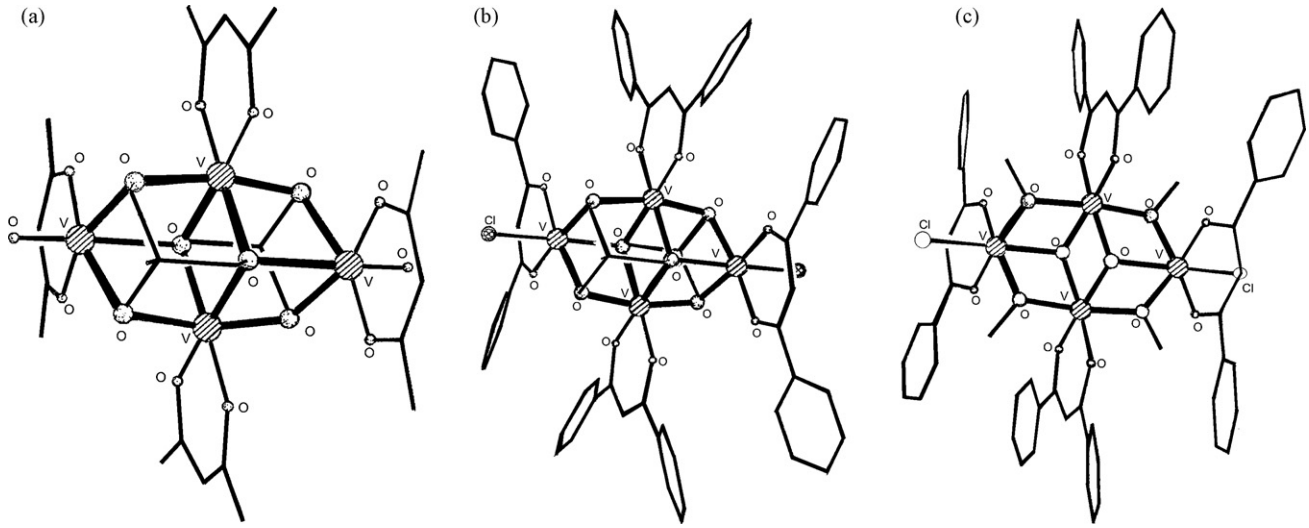

Fig. 8. Structure of $[V_2(VO)_2(\mathbf{5})_4\{CH_3C(CH_2O)_3\}_2]$ (a), $[V_4(\mathbf{6})_4(Cl)_2\{CH_3C(CH_2O)_3\}_2]$ (b) and $[V_4(\mathbf{6})_4(Cl)_2(OCH_3)_6]$ (c) [61].

The stacked homo- and heterodinuclear complexes $\{[M(\mathbf{6})_2][Cu(\mathbf{9})_2]\}$, (M = Cu^{II}, Pt^{II}, Pd^{II}), are achieved by mixing equimolar CH_2Cl_2 solutions of $[M(\mathbf{6})_2]$ and $[Cu(\mathbf{9})_2]$. $\{[Cu(\mathbf{6})_2][Cu(\mathbf{9})_2]\}_n$ contains two approximately planar copper(II) centers; the two complexes are alternately aligned as columnar stacks, with an average phenyl-pentafluorophenyl distance of 3.610 Å (Fig. 10). Synchrotron radiation X-ray powder experiments indicate that the same alignment was achieved through similar arene-perfluoroarene interactions in all these complexes. The M···M distance at 100K was estimated to be 3.611 Å (Cu···Cu), 3.605 Å (Cu···Pd) and 3.592 Å (Cu···Pt). The formation of $\{[M(\mathbf{6})_2][Cu(\mathbf{9})_2]\}$ does not depend on the starting ratios of $[M(\mathbf{6})_2]$ and $[Cu(\mathbf{9})_2]$. When equimolar amounts of $[Cu(\mathbf{6})_2]$, $[Pd(\mathbf{6})_2]$ and $[Cu(\mathbf{9})_2]$ are mixed together, $\{[Pd(\mathbf{6})_2][Cu(\mathbf{9})_2]\}$ exclusively forms. Similarly, $[Cu(\mathbf{6})_2]$, $[Pt(\mathbf{6})_2]$ and $[Cu(\mathbf{9})_2]$ in a 1:1:1 molar ratio give $\{[Pt(\mathbf{6})_2][Cu(\mathbf{9})_2]\}$, while $[Pd(\mathbf{6})_2]$, $[Pt(\mathbf{6})_2]$ and $[Cu(\mathbf{9})_2]$ in a 1:1:1 molar ratio produces a mixture (≈1:2) of $\{[Pd(\mathbf{6})_2][Cu(\mathbf{9})_2]\}$ and $\{[Pt(\mathbf{6})_2][Cu(\mathbf{9})_2]\}$ [63]. Non-radiative decay occurs in solid-state luminescence and UV–vis spectroscopy of the CuPt complex, while $[Pt(\mathbf{6})_2]$ shows luminescence around 540 nm (irradiation at 440 nm), suggesting an energy transfer between the closely arranged platinum(II) and copper(II) complexes [63].

4.2. Lanthanide and actinide complexes

The larger lanthanide(III) or actinide(III) ions afford mononuclear complexes where the coordination insaturation of the complexes $[M(\beta\text{-dike})_3]$ is filled by coordinating solvent molecules (generally water) or by an additional β-diketonate ligand as occurs for the isostructural complexes $Cs[M(\mathbf{10})_4]$ (M = Y^{III}, Eu^{III}, Am^{III}), where the metal(III) ion is dodecahedrally coordinated to the eight, essentially equivalent, oxygen atoms of the four chelating $[\mathbf{10}]^-$ ligands [64]. Furthermore, the actinide ions, showing a wider range of oxidation states (III–VII), form a larger variety of β-diketonato complexes, the most studied being $[An(\beta\text{-dike})_4]$, with the eight coordinate actinide(IV) ion in a dodecahedral or square antiprismatic environment, often isostructural with the cerium(IV)

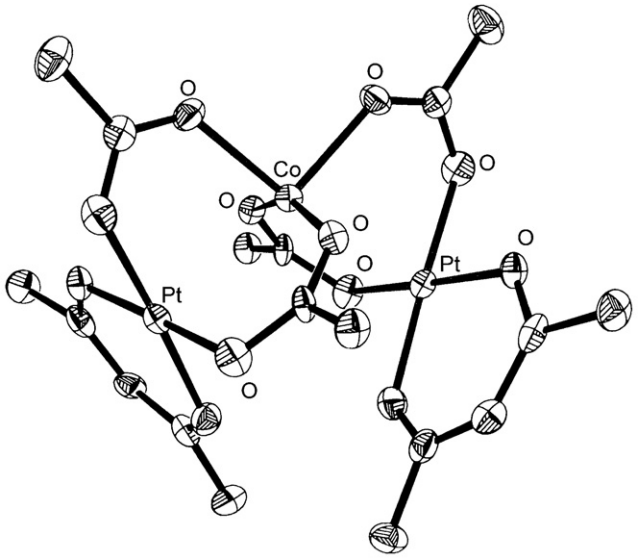

Fig. 9. Structure of $[Pt_2Co(\mathbf{5})_2(\mu\text{-}CH_3COO)_4]$ [62].

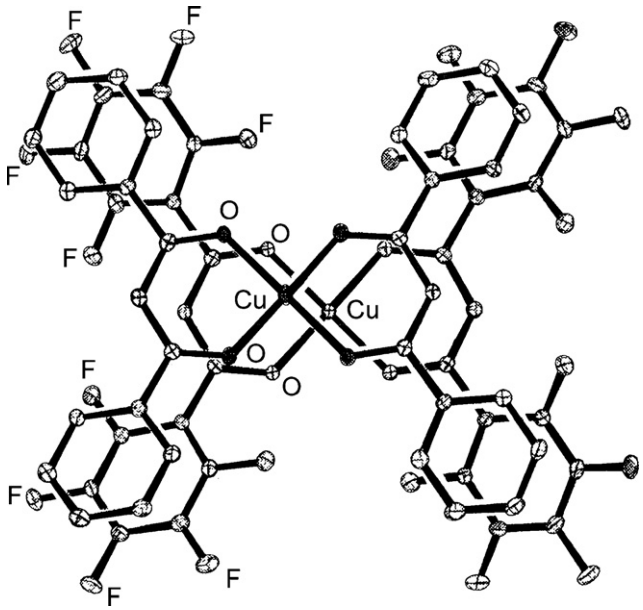

Fig. 10. Structure of $\{[Cu(\mathbf{6})_2][Cu(\mathbf{9})_2]\}$ [63].

analogues, and $[UO_2(\beta\text{-dike})_2(L)]$ where L is a neutral monodentate ligand with the uranium(VI) ion in a pentagonal bipyramidal environment. Their structure and properties were exhaustively reviewed in the past [6].

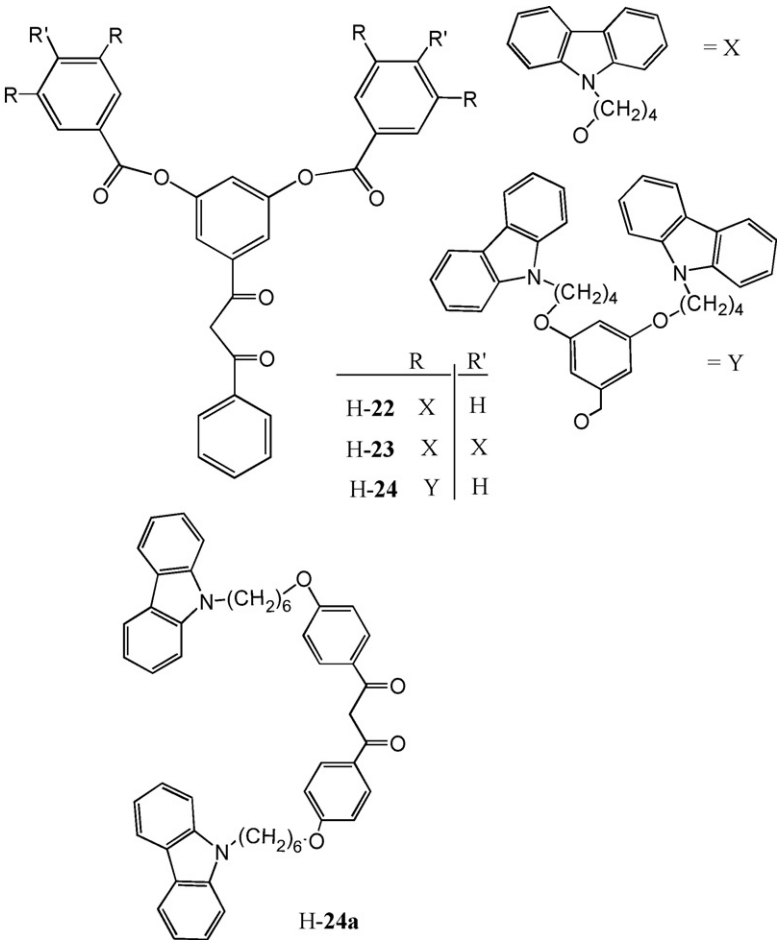

The same behaviour was observed with the whole series of lanthanide(III) salts and variously substituted β-diketones. The cerium(III) salts, however, can give rise to additional complexes, as found in $[Ce(\mathbf{5})_3(H\text{-}\mathbf{5})_2]$, obtained from H–**5**, neutralized with NH_3, and $Ce(NO_3)_3{\cdot}6H_2O$, where the distorted square antiprismatic cerium(III) ion is coordinated by eight oxygen atoms of three bidentate $[\mathbf{5}]^-$ ligands and two unidentate H–**5** ligands. Intra- and intermolecular H-bonds through the neutral enol H–**5** unidentate ligands, result in the formation of a cyclic dimer with a Ce···Ce distance of 7.976 Å (Fig. 11a) [65]. Furthermore, $[Ce^{IV}(\mathbf{11})_4]$ and $M[Ce^{III}(\mathbf{11})_4]$, ($M = Na^+$, NH_4^+) were obtained by mixing an aqueous solution of $CeCl_3{\cdot}7H_2O$ with an ethanol solution of H–**11** and NaOH or NH_4OH: an excess of H–**11** forms $M[Ce(\mathbf{11})_4]$ whereas an excess of $CeCl_3{\cdot}7H_2O$ causes oxidation to cerium(IV) with formation of $[Ce(\mathbf{11})_4]$. Sublimation at reduced pressure was successful for $[Ce(\mathbf{11})_4]$ and $Na[Ce(\mathbf{11})_4]$ while $[NH_4][Ce(\mathbf{11})_4]$ decomposes to $[NH_4](\mathbf{11})$ and $[Ce(\mathbf{11})_3]$. $[Ce(\mathbf{11})_4]$ contains an O_8 eight coordinate, square antiprismatic cerium(IV) ion, coordinated by four bidentate $[\mathbf{11}]^-$ ligands (Fig. 11b). The molecules are totally enveloped by the $C(CH_3)_3$ and CF_3 groups and this explains the high volatility. The molecules in $[NH_4][Ce(\mathbf{11})_4]$, where the coordination of $[\mathbf{11}]^-$ to the metal centers is similar to that of $[Ce(\mathbf{11})_4]$, form helices by hydrogen bridges causing the non-volatility nature of the complex [66].

$CeCl_3{\cdot}7H_2O$ or $Ce(NO_3)_3{\cdot}6H_2O$ and $[M(\mathbf{5})]$ ($M = Na^+$, NH_4^+) in aqueous solution at 21 and 45 °C yield $[Ce(\mathbf{5})_3(H_2O)_2]{\cdot}H_2O$ or $[Ce(\mathbf{5})_3(H_2O)_2]$, respectively, whereas similar treatment of $(NH_4)_2[Ce(NO_3)_6]$ gives only the former complex at both temperatures. Desiccation of the hydrate complexes over silica gel turns the former into $[Ce(\mathbf{5})_3(H_2O)_2]$, whereas the latter $[Ce(\mathbf{5})_3(H_2O)_2]{\cdot}H_2O$ undergoes decomposition rather than dehydration. Aerial oxidation of $[Ce(\mathbf{5})_3(H_2O)_2]$ in dichloromethane/toluene affords α-$[Ce(\mathbf{5})_4]$ and β-$[Ce(\mathbf{5})_4]$, respectively. Careful treatment of an aqueous solution of $(NH_4)_4[Ce(SO_4)_4]$ and H–**5** in aqueous ammonia at pH 5 gives the unstable, light-sensitive $[Ce(\mathbf{5})_4]{\cdot}10H_2O$ whose structure contains layers of $[Ce(\mathbf{5})_4]$ sandwiched between extensive hydrogen-bonded layers of water molecules which do not interact with the metal ion. Electrochemical experiments show the unstable nature of $[Ce(\mathbf{5})_3(H_2O)_2]$, while the reduction of $[Ce(\mathbf{5})_4]$ yields well-defined cyclic voltammograms in acetonitrile or acetone, corresponding to a quasi-reversible process. For the $[Ce^{IV}(\mathbf{5})_4]/[Ce^{III}(\mathbf{5})_4]^-$ redox couple, a reversible potential of 0.22 V versus SHE was obtained in acetone or acetonitrile at both gold and glassy carbon electrodes, consistent with the ease of both oxidation and reduction of the cerium acetylacetonate complexes as found in the synthetic studies [67].

The complexes $[Ce(\beta\text{-dike})_4]$ have been employed as precursors in metal organic chemical vapour deposition (MOCVD) and atomic layer epitaxy (ALE) or as dopants in SrS and $CaGa_2S_2$ thin films, owing to their ability to produce blue-green or green electroluminescent phosphors. $[Ce(\mathbf{10})_4]$, reported as an explanatory example of these complexes, derives from the reaction of $[NH_4]_4[Ce(SO_4)_4]{\cdot}2H_2O$ in H_2O and H–**10** in toluene in a 1:4 molar ratio; its structure exhibits an eight coordinate cerium(IV) ion in a distorted square antiprism [68].

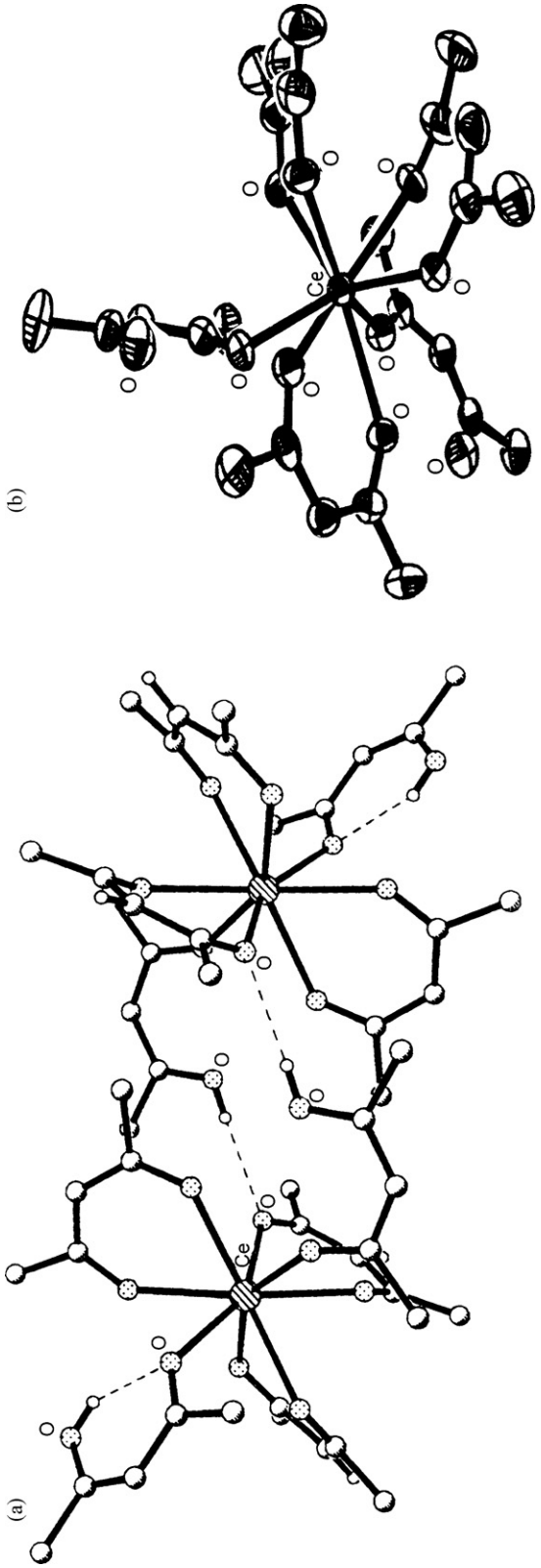

Fig. 11. Structures of $[Ce(\mathbf{5})_3(H\text{-}\mathbf{5})_2]$ (a) [65] and $[Ce(\mathbf{11})_4]$ (b) [66].

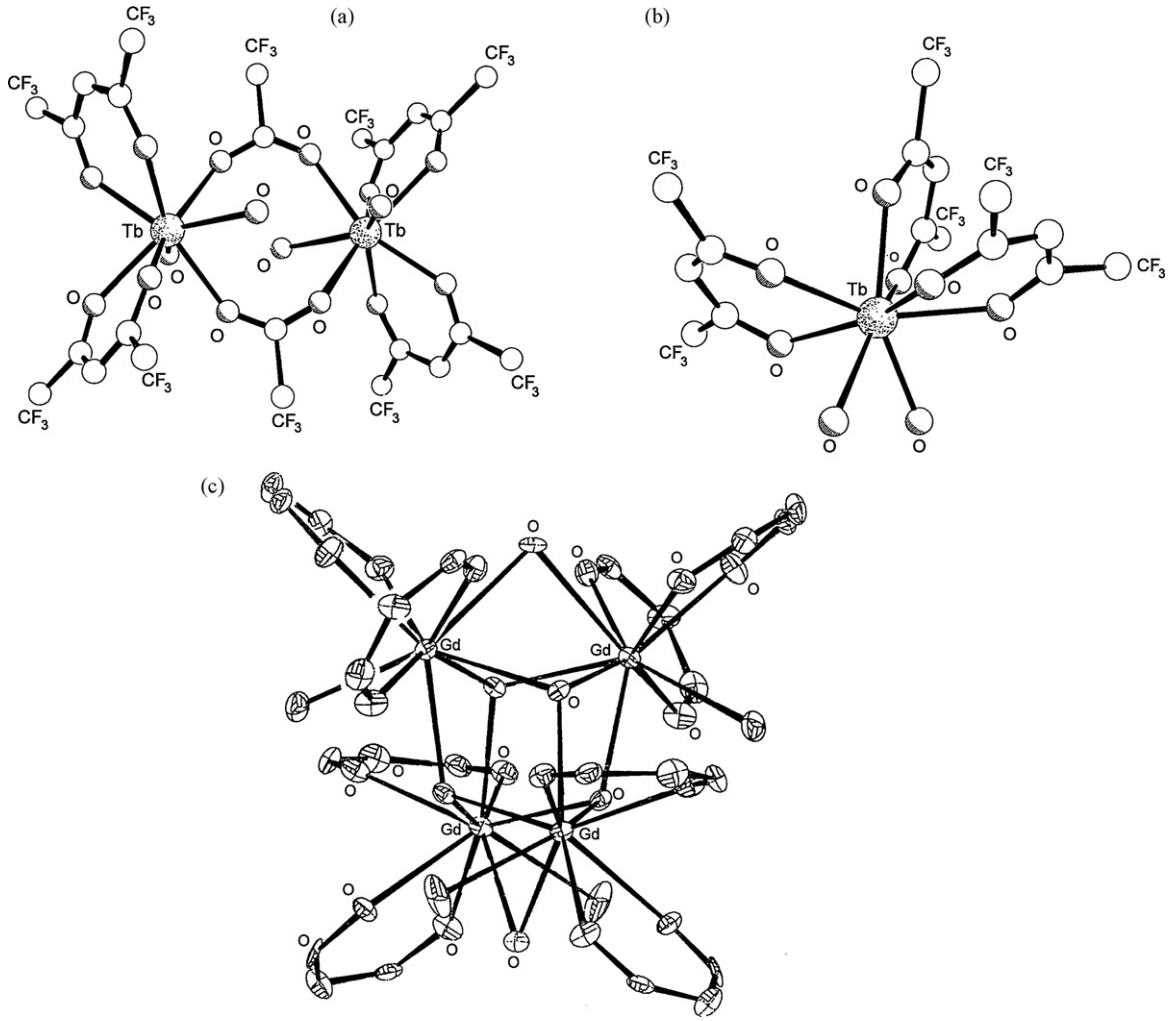

Fig. 12. Structures of $[Tb_2(\mathbf{10})_4(CF_3COO)_2(H_2O)_4]$ (a) [72] $[Tb(\mathbf{10})_3(H_2O)_2]$ (b) [72] and $[Gd_4(\mathbf{10})_8(OH)_4(H_2O)_6]$ (c) [73].

The sodium salts of H–**7**, H–**7a** and H–**7b** react with $Sc(NO_3)_3{\cdot}nH_2O$ to form $[Sc(\mathbf{L})_3]$, whose structure indicates an octahedral coordination about the scandium(III) ion. Crystals of $[Sc(\mathbf{7a})_3]$ contains both facial and meridional isomers in a 2:1 ratio. $[Sc(\mathbf{7a})_3]$ and $[Sc(\mathbf{7b})_3]$, which have a lower melting point and a higher volatility than $[Sc(\mathbf{7})_3]$, deposit thin films of Sc_2O_3 over a wide temperature range (400–600 °C) [69].

$[Ln(\beta\text{-dike})_3(H_2O)_n]$, derived from $LnCl_3{\cdot}nH_2O$ and [Na(β-dike)] in water/ethanol and in a 1:3 molar ratio, can exist as the only one or together with dimeric or oligomeric species [70]. $[Y(\mathbf{12})_3(H_2O)]$ contains a seven coordinate yttrium(III) ion in an O_7 distorted monocapped octahedron formed by six oxygen atoms of three β-diketonates and the oxygen of a water molecule [70] while in the isostructural complexes $[Ln(\mathbf{5})_3(H_2O)_2]$ (Ln = La, Pr, Nd, Sm) each metal(III) ion is surrounded by eight oxygen atoms, contributed by three bidentate $[\mathbf{5}]^-$ groups and two water molecules arranged at the vertices of a distorted square antiprism [71].

Similar experimental conditions form $[Tb_2(\mathbf{10})_4(CF_3COO)_2(H_2O)_4][Tb(\mathbf{10})_3(H_2O)_2]_2$, where the CF_3COO^- bridging ligands originate from the reaction of the β-diketone with unreacted NaOH

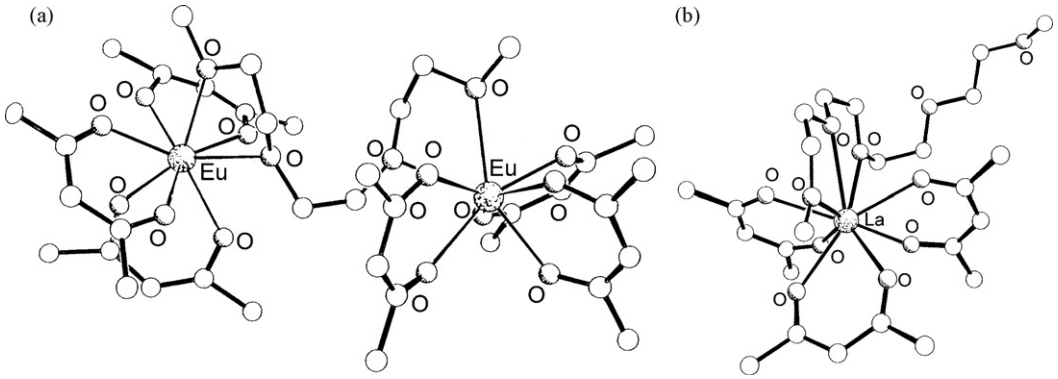

Fig. 13. Structures of $[Eu_2(\mathbf{7})_6(triglyme)]$ (a) and $[La(\mathbf{7})_3(tetraglyme)]$ (b) [74].

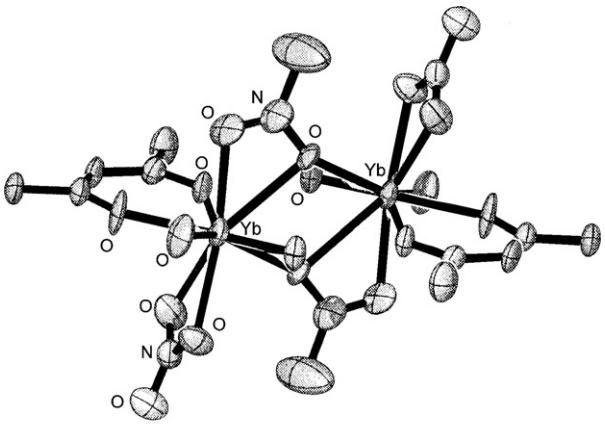

Fig. 14. Structure of $[Yb_2(\mathbf{5})_2(\mu\text{-}NO_3)_2(NO_3)_2(H_2O)_4]$ [75].

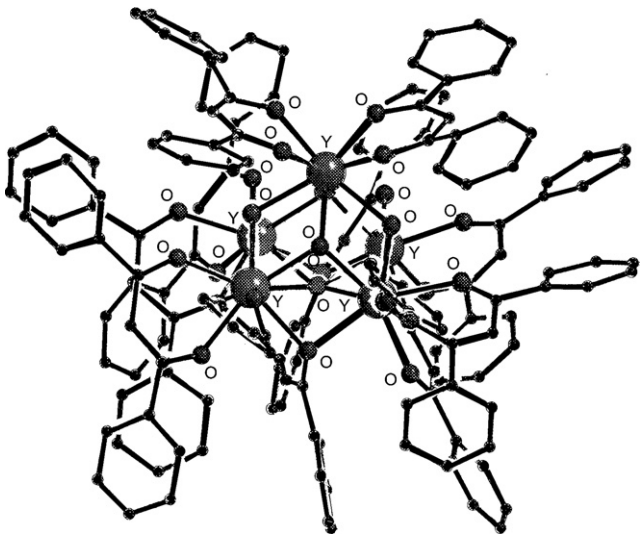

Fig. 15. Structure of $[Y_5(\mu\text{-}\mathbf{6})_4(\mathbf{6})_6(\mu_4\text{-}O)(\mu_3\text{-}O)_4]^{5-}$ [81].

in water/methanol. Each eight coordinate monomeric terbium unit comprises three chelating $[\mathbf{10}]^-$ ligands and two water molecules arranged in a distorted square antiprismatic geometry. The dimeric unit consists of two distorted antiprismatic terbium(III) centers bridged by two trifluoroacetate molecules; each of these is coordinated to two $[\mathbf{11}]^-$ ligands and two water molecules (Fig. 12a and b) [72].

$GdCl_3{\cdot}6H_2O$ and $[Na(\mathbf{10})]$ give $[Gd_4(\mathbf{10})_8(OH)_4(H_2O)_6]$ in water/ethanol and $[Gd(\mathbf{10})_3(CH_3COCH_3)(H_2O)]$ in acetone. The tetramer has a distorted dicapped cubane structure, containing four gadolinium(III) ions and four triply bridging hydroxy ligands. Each tricapped trigonal prismatic gadolinium ion is bonded to three μ_3-hydroxo ligands, one μ_2- and one terminal aqua ligand and two asymmetrically chelated $[\mathbf{10}]^-$ ligands (Fig. 12c). In $[Gd(\mathbf{10})_3(CH_3COCH_3)(H_2O)]$, two $[\mathbf{10}]^-$ ligands are symmetrically chelated to the eight coordinate square antiprismatic gadolinium(III) ion while the third $[\mathbf{10}]^-$ ligands is asymmetric owing to a strong intermolecular hydrogen bonding with the coordinated water [73].

The reaction of $[Ln(\mathbf{7})_3(H_2O)_2]$ with 2,5,8,11-tetraoxadodecane (triglyme) in hexane yields $[Ln_2(\mathbf{7})_6(\text{triglyme})]$ (Ln = Eu, Tb), where two $\{Ln(\mathbf{7})_3\}$ moieties are linked by a triglyme molecule. Both metal centres are eight coordinate in a square antiprismatic geometry (Fig. 13a). In contrast, $[La(\mathbf{7})_3(H_2O)_2]$ and 2,5,8,11,14-pentaoxapentadecane (tetraglyme) in hexane form $[La(\mathbf{7})_3(\text{tetraglyme})]$ where the nine coordinate lanthanum(III) ion binds to all three bidentate $[\mathbf{7}]^-$ ligands and only to three of the five possible oxygen atoms of the tetraglyme ligand. The metal ion adopts a square monocapped antiprismatic geometry with an oxygen atom capping one of the square faces (Fig. 13b). These air- and moisture-stable complexes have good volatility and thermal stability [74].

$Ln(NO_3)_3{\cdot}6H_2O$ (Ln = La, Pr, Nd, Sm) and H_2–acacen, derived from the [2 + 1] condensation of H–**5** and ethylendiamine, form in tetrahydrofuran/cyclohexane $\{[Ln(H_2\text{-acacen})_2(NO_3)_3]{\cdot}C_6H_{12}\}_n$, where the 10 coordinate metal(III) ion is linked by three bidentate nitrate anions and four oxygen atoms from two H_2–acacen ligands, one acting as chelate through an unusual [14]-membered ring and the other acting as a bridging ligand. The heavier lanthanide(III) nitrates decompose H_2–acacen in water and to a lower extent in tetrahydrofuran, giving rise to $[Ln_2(\mathbf{5})_2(\mu\text{-}NO_3)_2(NO_3)_2(H_2O)_4]$ as proved for the ytterbium(III) complex, where the nine coordinate lanthanide(III) ion contains two water molecules, two bidentate nitrate anions one of which bridges the two metal centres via one oxygen atom (Fig. 14) [75].

The synthesis and structural characterisation of lanthanide oxo/hydroxyl clusters attract considerable attention since they have proved to be useful for a variety of applications ranging from luminescent and magnetic materials to their use in homogeneous catalysis and in developing synthetic nucleases for hydrolysis of phosphate diester bonds, including those present in nucleic acids. Recent developments have successfully revealed the formation mechanism of these finite sized molecular entities. When lanthanide salts, usually LnX_3 ($X = Cl^-$, I^-, NO_3^-, $CF_3SO_2^-$, ClO_4^-), are hydrolysed in the presence of a base, they tend to form polynuclear oxo/hydroxo aggregates on the condition that the extent of hydrolysis is carefully controlled. These clusters can be formed from the lanthanide salt alone or in presence of a ligand (i.e. carboxylates, β-diketonates, alkoxides, phenoxides), in which case the term ligand controlled hydrolysis is used. However, the molecular structure of the final compound often remains unpredictable and unexpected and unusual assemblies have been isolated and characterised. Recently, a reliable method for the synthesis of hydroxo-bridged lanthanide cages has been developed, whose synthetic pathway involves the reaction of $LnCl_3{\cdot}6H_2O$ and a β-diketone in the presence of triethylamine as a base. In general, the dimensions of the cage depend on the size of both lanthanide(III) and the ligand: more bulky substituents (as phenyl groups) at the periphery of the ligand give rise to smaller metal aggregation [76–79].

$[Ln_5(\mu\text{-}\mathbf{6})_4(\mathbf{6})_6(\mu_4\text{-}OH)(\mu_3\text{-}OH)_4]$ (Ln = Eu^{III}, Dy^{III}) and $H_5[Y_5(\mu\text{-}\mathbf{6})_4(\mathbf{6})_6(\mu_4\text{-}O)(\mu_3\text{-}O)_4]$, prepared by reaction of the appropriate $LnCl_3{\cdot}6H_2O$ with H–**6** in a 1:2 molar ratio and in the presence of $N(C_2H_5)_3$ [80,81], show a similar structure with a square pyramidal core of five metal ions surrounded by 10 peripheral $[\mathbf{6}]^-$ ligands. Each square antiprismatic lanthanide ion is coordinated by eight oxygen atoms. In the yttrium complex each triangular face of the square pyramid is capped by one μ_3-O moiety, as occurs in $[Ln_9(\mathbf{12})_{16}(O)_2(OH)_8]^-$ (Ln = Sm, Eu, Gd, Dy, Er) [82] or $[Na(C_2H_5OH)_6][Y_9(\mathbf{13})_{16}(\mu_4\text{-}O)_2(\mu_3\text{-}OH)_8]^-$ [83]. In the square base, four yttrium(III) ions are linked by one μ_4-O atom. Six $[\mathbf{6}]^-$ ligands are terminal chelates and four are bridging chelates bonding to two metal ions that belong to the base of the polyhedra. The apical yttrium(III) ion is bonded to two chelate ligands (Fig. 15). This complex acts as homogeneous catalyst in the oxidation by air of aliphatic aldehydes, but not the aromatic ones, to the corresponding acids. For $[Dy_5(\mu\text{-}\mathbf{6})(\mathbf{6})_6(\mu_4\text{-}OH)(\mu_3\text{-}OH)_4]$ the appearance of slow relaxation of the magnetization below 3K is typical of single molecular magnets [81].

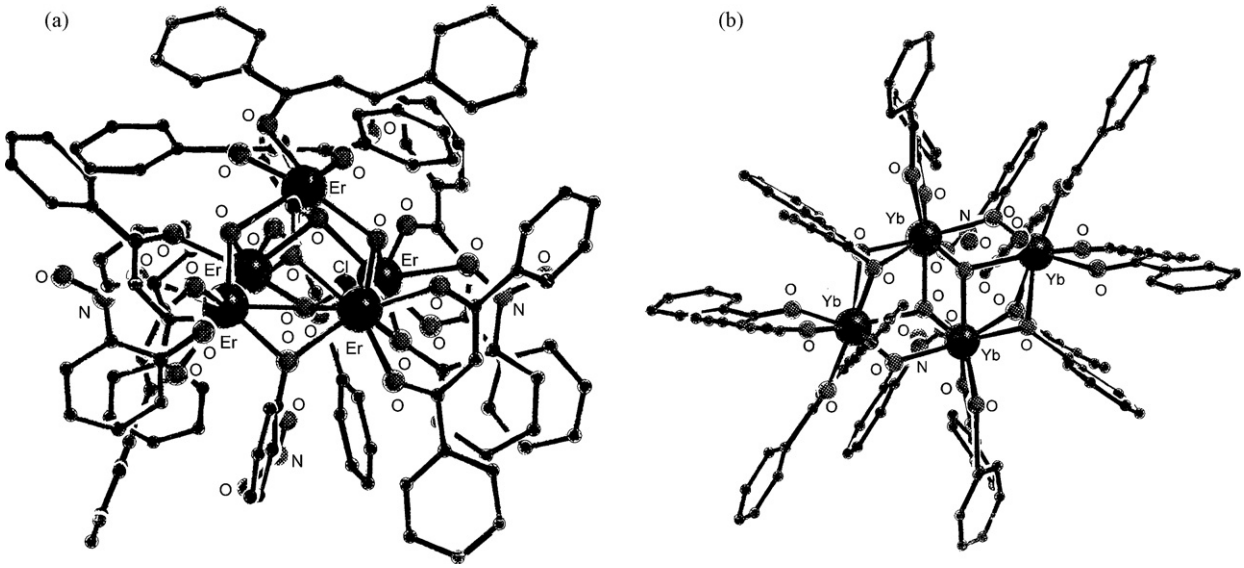

Fig. 16. Structures of $[Er_5(\mathbf{6})_7(\mu_3\text{-}OH)_4(\mu_4\text{-}OH)_7(o\text{-}NO_2C_6H_4O)_3(Cl)]^-$ (a) and $[Yb_4(\mathbf{6})_8(\mu_3\text{-}OH)_2(o\text{-}NO_2C_6H_4O)_2]$ (b) [84].

$LnCl_3{\cdot}6H_2O$ (Ln = Er, Tm), H–**6** and *o*-nitrophenol (H–L) in methanol and in the presence of $N(C_2H_5)_3$, yield the isomorphous clusters $[NH(C_2H_5)_3][Ln_5(\mathbf{6})_7(\mu_3\text{-}OH)_4(\mu_4\text{-}OH)_7(L)_3(Cl)]$, containing a pentanuclear square pyramidal core of lanthanide ions surrounded by 10 peripheral ligands and a chloride anion. Each triangular face of the square pyramid is capped by one μ_3-O moiety. In the square base, four lanthanide atoms are linked by one μ_4-O atom. Differently from $[Eu_5(\mathbf{6})_{10}(OH)_5]$, where six ligands are terminal chelates and four are bridging chelates bonding to two metal ions that belong to the base of the polyhedron, in these complexes three of the four bridging $[\mathbf{6}]^-$ ligands are formally substituted by *o*-nitrophenolato ligands. The phenolate oxygen atoms always bridge two lanthanide ions. Two of the three *o*-nitrophenolato ligands also bind a lanthanide ion through one oxygen atom of the NO_2 group, whereas the NO_2 group of the third *o*-nitrophenolato ligand, located between two lanthanide(III) ions is turned away from the cluster core. This generates a free coordination site on one lanthanide (III) ion, which is occupied by a chlorine atom, and results in a negatively charged cluster core (Fig. 16a). The formation of the hydroxido bridges can be explained by the presence of water in the reaction mixture which can be deprotonated by the addition of base [84].

Under the same reaction conditions, $LnCl_3{\cdot}6H_2O$ (Ln = Yb, Lu) affords $[Ln_4(\mathbf{6})_8(\mu_3\text{-}OH)_2(L)_2]$ (H–L = *o*-nitrophenol) (Fig. 16b). A comparable Ln_4 core was observed also in the $[Nd_4(\mu_2\text{-},\mu_1\text{-}\mathbf{5})_6(\mathbf{5})_4(\mu_3\text{-}OH)_2]$ and $[Ln_4(\mathbf{6})_{10}(\mu_3\text{-}OH)_2]$ (Ln = Pr, Nd, Sm). Two types of coordination modes are observed for the ligation of $[\mathbf{6}]^-$ to the ytterbium(III) and lutetium(III) centers in the tetranuclear clusters. Of the eight $[\mathbf{6}]^-$ ligands, six chelate the metal centers in η^2-fashion, and two more both chelate and bridge two metal centers. The *o*-nitrophenolato ligands chelate one metal ion and bridge another metal ion through one oxygen atom, thus they are (μ-O)-η^2-coordinating. The tetranuclear core of $[Ln_4(\mathbf{6})_{10}(\mu_3\text{-}OH)_2]$ (Ln = Pr, Nd, Sm) is similar to that in $[Ln_4(\mathbf{6})_8(\mu_3\text{-}OH)_2(L)_2]$ with the $[\mathbf{6}]^-$ ligands coordinating in a chelating and bridging fashion. The only difference between these complexes derives from the presence of the two *o*-nitrophenolato ligands. In $[Ln_4(\mathbf{6})_{10}(\mu_3\text{-}OH)_2]$, the positions of the *o*-nitrophenolato ligands are formally replaced by two more $[\mathbf{6}]^-$ ligands, which bind in the same coordinating and bridging arrangement. A significant difference arises with respect to the ionic radius of the center metal ion: whereas the cluster size decreases from $[Ln_5(\mathbf{6})_{10}(OH)_5]$ or $[Ln_4(\mathbf{6})_{10}(\mu_3\text{-}OH)_2]$ by increasing the ionic radius, the opposite trend is observed for $[NH(C_2H_5)_3][Ln_5(\mathbf{6})_7(\mu_3\text{-}OH)_4(\mu_4\text{-}OH)(L)_3(Cl)]$, and $[Ln_4(\mathbf{6})_8(\mu_3\text{-}OH)_2(L)_2]$ where the two μ_3-oxygen atoms in the core of the cluster are parts of hydroxy groups. Each metal ion is coordinated to eight oxygen atoms in a square antiprismatic arrangement [84].

Furthermore, the isomorphous oxo-clusters $[NH(C_2H_5)_3][Ln_9(\mu\text{-}\mathbf{12})_8(\mathbf{12})_8(\mu_4\text{-}O)_2(\mu_3\text{-}OH)_8]{\cdot}2CH_3OH{\cdot}CHCl_3$ (Ln = Sm, Eu, Gd, Dy, Er) were obtained by mixing $LnCl_3{\cdot}nH_2O$ and H–**12** in a 9:16 molar ratio in methanol and subsequent addition of an excess of $N(C_2H_5)_3$, which ready produces oxo and hydroxo groups capable to bridge the lanthanide ions making up a $\{Ln_9(\mu_4\text{-}O)_2(\mu_3\text{-}OH)_8\}$ core and 16 peripheral $[\mathbf{12}]^-$ ligands, eight acting as chelating and eight as bridging and chelating groups. By similar procedures $[Eu_8(\mathbf{7})_{12}(\mu_4\text{-}O)(\mu_3\text{-}OH)_{12}]$ was synthesised. In the $\{Ln_9(\mu_4\text{-}O)_2(\mu_3\text{-}OH)_8\}$ core the metal skeleton has been considered to be formed by two square pyramidal pentanuclear units assembled via an apical lanthanide(III) ion. Each triangular face of the square pyramids is capped by one μ_3-OH group, so that the central square antiprismatic lanthanide(III) ion is surrounded by eight μ_3-OH groups. Four lanthanide(III) metal ions in each square base are linked by one μ_4-O. Each lanthanide(III) ion, at the corner of the square bases, is chelated by one terminal $[\mathbf{6}]^-$ chelate and further coordinated by two bridging and chelating $[\mathbf{6}]^-$ ligands, which link the metal ion with two neighbour metal ions at the corners. Thus, each lanthanide(III) ion is eight coordinate in a distorted bicapped trigonal prismatic geometry (Fig. 17a) [83].

Methanolic solutions of $LaCl_3$, H–**6** and an excess of $N(C_2H_5)_3$ result in the formation of $[La_{12}(\mathbf{6})_{18}(OH)_{12}(Phgly)_2(CO_3)_2]$, where $[Phgly]^-$ is the unexpected phenylglyoxylate anion bonded in a μ_2-η^1:η^2-fashion and each lanthanum(III) ion is coordinated by nine oxygen atoms. In the cage, 12 oxygen atoms act as μ_3- and four as μ_2- bridging groups. Two CO_3^{2-} anions, most likely due to CO_2 fixation from the atmosphere, are trapped in the middle of the cage, each carbonate binding to six different metal centres with a chelating and bridging configuration. Overall a μ_6-η^1: η^1: η^1: η^1: η^1: η^2-coordination mode occurs. Repeating the preparation and the subsequent crystallisation of the product under nitrogen and in the complete absence of CO_2, and adding different sources of carbonate to the reaction mixture (K_2CO_3, $(NH_4)_2CO_3$) failed to yield the templated dodecanuclear lanthanum(III) cluster. The two phenylglyoxylate ligands can plausibly originate during the formation and

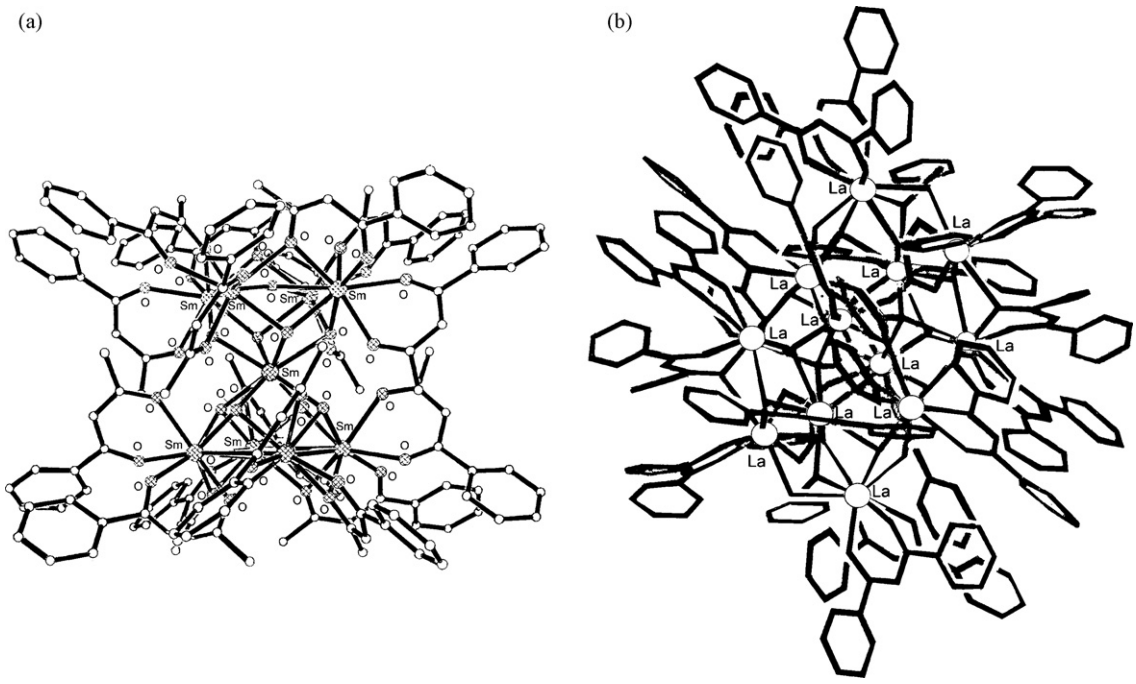

Fig. 17. Structures of $[Sm_9(\mu\text{-}\mathbf{12})_8(\mathbf{12})_8\ (\mu_3\text{-}O)_2(OH)_8]^-$ (a) [83] and $[La_{12}(\mathbf{6})_{18}(OH)_{12}(Phgly)_2(CO_3)_2]$ (b) [85].

growth of the La_{12} hydroxyl cage which acts as catalyst in the oxidation reaction of $[\mathbf{6}]^-$ to phenylglyoxylate by the atmospheric oxygen (Fig. 17b) [85].

The coordinated β-diketonate can be partially (or totally) substituted by other ligands: equimolar amounts of $[Ce(\mathbf{5})_4]$ or $[Ce(\mathbf{10})_4]$ and the calix-4-arene (H_2–L) in boiling toluene give $[Ce(\mathbf{5})_2(L)]$ or $[Ce(\mathbf{10})_2(L)]$. The further reaction of $[Ce(\mathbf{5})_2(L)_2]$ with bromine in a 1:2 ratio in diethyl ether resulted in bromination of $[\mathbf{5}]^-$ in the 3-position with formation of $[Ce(\mathbf{14})_2(L)_2]$. The same bromination by N-bromosuccinimide occurs also in $[Ce(\mathbf{5})_4]$ to form $[Ce(\mathbf{14})_4]$. These complexes show the typical cone geometry of the calixarene ligand with the methoxy groups bound to the eight coordinate square antiprismatic cerium(IV) ion. The four donor atoms of the calixarene in these complexes define a mean O_4 plane with the cerium(IV) ion above this plane (Fig. 18) [68].

In $[Eu(\mathbf{15})_3(H_2O)(DMF)]$, prepared by reaction in ethanol of $EuCl_3{\cdot}6H_2O$ with 3 equiv. of H–**15** deprotected with an aqueous solution of ammonia, followed by recrystallization of the resulting precipitate from dimethylformamide, the square antiprismatic europium(III) ion is coordinated by the three chelating $[\mathbf{15}]^-$ ligands, one dimethylformamide and a water molecule which forms strong hydrogen bonds to the oxygen atoms of two ligands of a second $\{Eu(\mathbf{15})_3\}$ moiety, giving rise to a dimeric array (Fig. 19). Remarkably, the europium(III) ion can be sensitized by visible light (up to 475 nm). To circumvent the coordination of solvent molecules to the lanthanide ions, $[NH(C_2H_5)_4][Eu(\mathbf{15})_4]$ was tested; it shows a better shielding while solubility and visible light excitation remain similar [86].

5. β-Diketonato complexes with nitrogen donors ligands

5.1. Lanthanide complexes

The reaction of *meso*-tetraphenylporphyrin (H_2-TPP) with $[Eu(\mathbf{5})_3(H_2O)_2]$ in refluxing 1,2,4-trichlorobenzene affords $[Eu(\mathbf{5})(TPP)]$. The reaction is general and proceeds with several different β-diketonato complexes of the entire lanthanide series. Attempts to obtain single crystals, suitable for X-ray diffraction analysis, of $[Ln(\mathbf{5})(TPP)]$ (Ln = Gd, Sm) have failed so far; thus, extended X-ray absorption fine structure spectroscopy (EXAFS) was used to elucidate the structure of $[Ln(\mathbf{5})(TPP)]$ in the solid state. In $[Gd(\mathbf{5})(TPP)]$ the gadolinium(III) ion was found to be coordinated by four monoporphyrin nitrogen atoms and three or four oxygen atoms from a $[\mathbf{5}]^-$ anion and one or two water molecules. The presence of the second water molecule in the coordination sphere was barely discernible by EXAFS analysis, also supported by molecular modelling and Monte Carlo simulations which display slight distortions in the lanthanide coordination geometry (Fig. 20) [87].

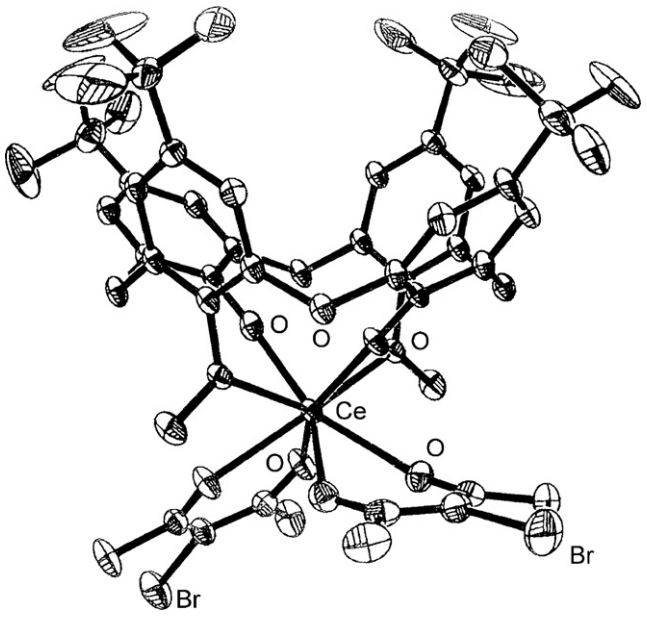

Fig. 18. Structure of $[Ce(\mathbf{14})_2(L)_2]$ [68].

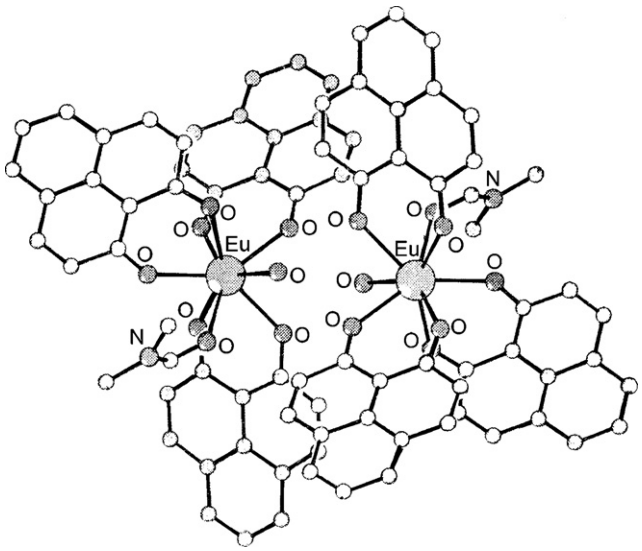

Fig. 19. Structure of [Eu(**15**)$_3$(H$_2$O)(DMF)] [86].

A quite interesting approach was proposed, based on the reaction of appended β-diketonate to the appropriate position of the porphyrin ring through an alkali chain (H$_3$–**16**) and subsequent lanthanide(III) coordination with an excess of [Ln{N(Si(CH$_3$)$_3$)$_2$}$_3$]·[Li(Cl)(THF)$_3$] (Ln = Nd, Eu, Yb) in refluxing bis(2-methoxyethyl)ether, to afford the complexes [Ln(**16**)(H$_2$O)], similar to each other according to their mass spectra. H$_3$–**16** derives from the condensation of *o*-hydroxybenzaldehyde, benzaldehyde and pyrrole in a molar ratio of 3:1:4 in propionic acid. Treatment of the resulting phenol containing porphyrin with an excess of 1,4-dibromobutane in dry dimethylformamide and in the presence of anhydrous K$_2$CO$_3$ forms 5-(2-(4-bromobutyl)-phenyl)-10,15,20-triphenylporphyrin, which gives H$_3$–**16** by the addition of diethyl malonate and a slight excess of sodium methoxide in dry dimethylformamide. Spectroscopic evidence suggests that the structures of [Ln(**16**)(H$_2$O)] contain one [**16**]$^{3-}$ ligand coordinated to the metal ion with four nitrogen atoms of the porphyrinate and three oxygen atoms, two from the appended diethyl malonate anion and one from water. Photoluminescence studies indicate that the porphyrin ring could act as an antenna for the near-infrared emission of lanthanide ions [88].

In order to obtain suitable photophysical properties, the water molecule in [Ln(β-dike)$_3$(H$_2$O)$_n$] must be substituted by donating ligands capable of enhancing the luminescence efficiency, like the neutral monodentate nitrogen donor ligands (L), which form [Ln(β-dike)$_3$(L)$_2$] as found in [Eu(**10**)$_3$(py)$_2$] or [Ho(**10**)$_3$(4-pic)$_2$] where the metal ion is in a square antiprismatic environment (Fig. 21) [89], and especially the neutral bidentate nitrogen donors ligands, i.e. phenanthroline (phen) or bipyridine (bipy), which form

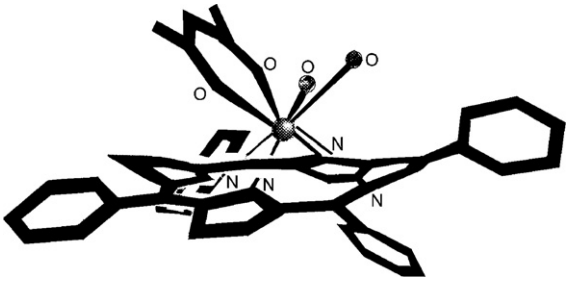

Fig. 20. Proposed structure of [Gd(**5**)(TPP)] [87].

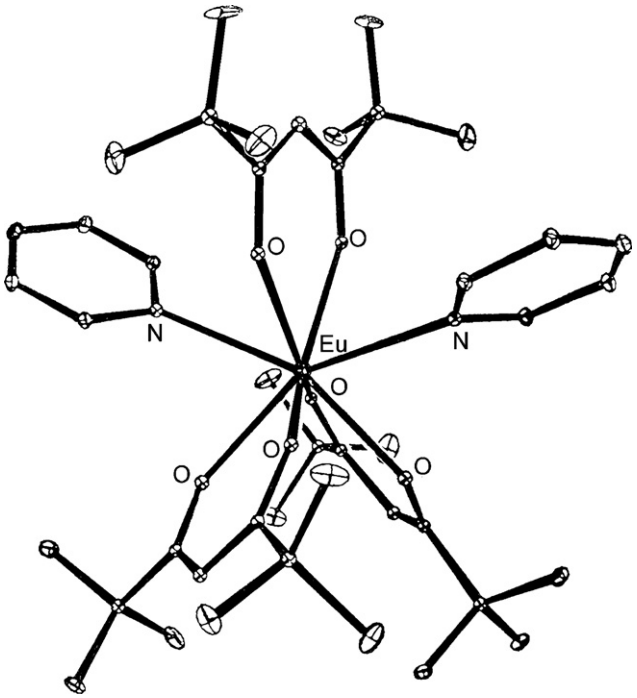

Fig. 21. Structure of [Eu(**10**)$_3$(py)$_2$] [89].

[Ln(**10**)$_3$(phen)$_n$] or [Ln(**10**)$_3$(bipy)$_n$] where the coordination chemistry depends on the size of the lanthanide(III) ions and on the solvent. The lanthanide(III) complexes derive from the reaction of Ln(CF$_3$SO$_3$)$_3$ with H–**10**, CsOH and either bipy or phen in a 1:3:3:1 ratio in methanol; for the analogous erbium(III) complexes acetonitrile was used [90]. With the heavier lanthanide ions the eight coordinate complexes [Ln(**10**)$_3$(bipy)] (Ln = Er, Dy, Ho, Yb) or [Ln(**10**)$_3$(phen)] (Ln = Tb, Ho, Yb) were isolated whereas with the early lanthanide ions the 10 coordinate complexes [Ln(**10**)$_3$(bipy)$_2$] (for Ln = La, Sm) and [Ln(**10**)$_3$(phen)$_2$] (Ln = La, Ce, Pr, Nd) were isolated; [Sm(**10**)$_3$(bpy)$_2$] and [Sm(**10**)$_3$(bpy)(H$_2$O)]·(bpy) have been synthesized in dry or in regular methanol, respectively [90].

In [Er(**10**)$_3$(phen)] the square antiprismatic environment about the eight coordinate erbium(III) ion is reached by six oxygen atoms from three [**10**]$^-$ ligands and two phenanthroline nitrogen atoms (Fig. 22a). In [Sm(**10**)$_3$(bipy)(H$_2$O)]·bipy the nine coordination around the samarium(III) ion consists of seven oxygen atoms from three [**10**]$^-$ ligands and one water molecule and two bipyridine nitrogen atoms (Fig. 22b). On the contrary, in [La(**10**)$_3$(bipy)$_2$] both bipy ligands are bound to the O$_6$N$_4$ 10 coordinate lanthanum(III) ion together with three chelating [**10**]$^-$ ligands (Fig. 22c) [90].

Also, 4,7-diethyldicarboxylate-1,10-phenanthroline or 4,4′-dimethoxy-2,2′-bipyridine (L), reacting in toluene for 15 days with [Ln(**5**)$_3$(H$_2$O)$_2$], form [Ln(**5**)$_3$(L)] (Ln = Eu, Er, Yb, Tb), with the eight coordinate lanthanide(III) ion in a slightly distorted square antiprism formed by six oxygen atoms of the three bidentate [**5**]$^-$ ligands and the two nitrogen atoms of the neutral chelating ligand. Attempts to prepare the analogous lanthanide complexes of the 2,2′-bipyridine-4,4′-diethyldicarboxylate under similar conditions were unfruitful [91].

Remarkable electronic effects of the substituents on the basicity of the nitrogen atoms have been found in bipyridine systems: with electron-attracting groups, such as in 2,2′-bipyridine-4,4′-diethyldicarboxylate, no coordination to any lanthanide ions was observed while an enhanced basicity of the coordinating nitrogen atoms, deriving by the replacing the substituents with the two electron-donating OCH$_3$ groups, allows the isolation of the

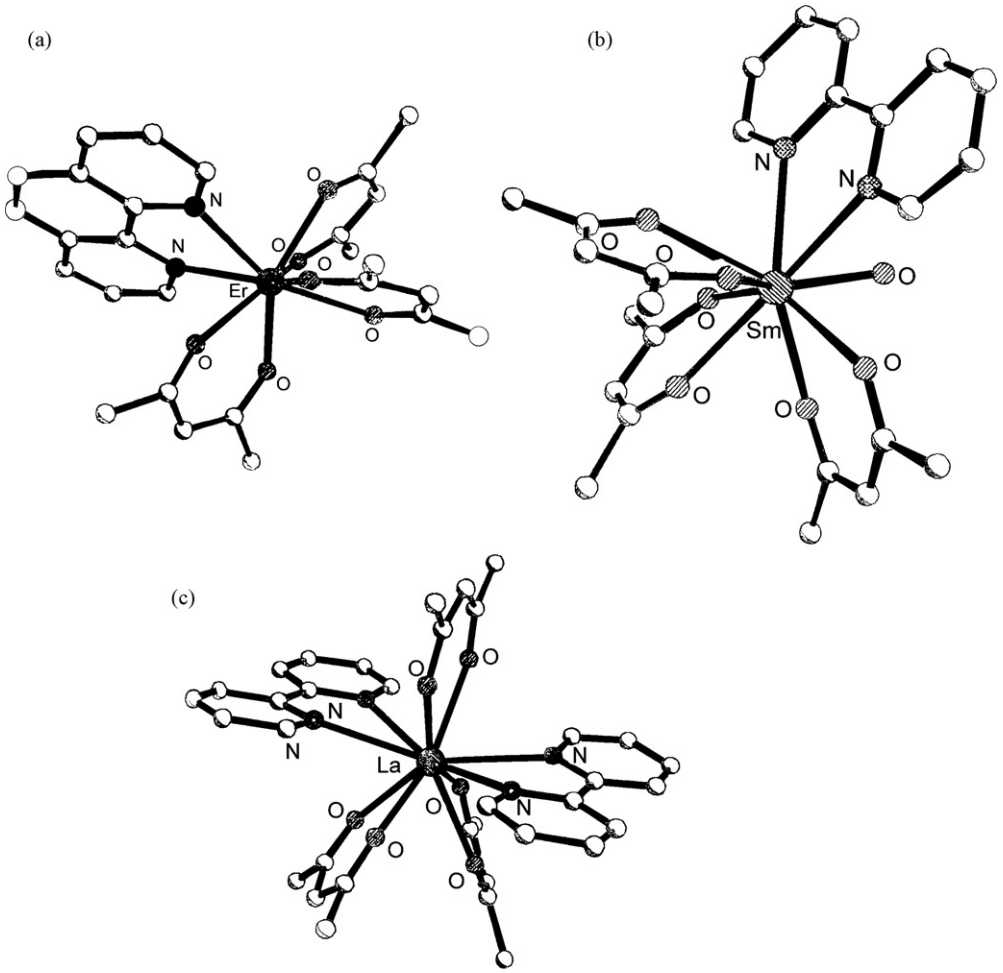

Fig. 22. Structures of [Er(**10**)$_3$(phen)] (a), [Sm(**10**)$_3$(bipy)(H$_2$O)] (b) and [La(**10**)$_3$(bipy)] (c) [90].

lanthanide(II) complexes. On the other hand, the presence of two carboxyethyl groups on the 4, 7 positions of the phenanthroline ligand does not prevent coordination to these lanthanide(III) ions, although a lengthening, of the Ln–N bond distance was measured especially for the europium(III) complex. The lengthening of the Eu–N bond distances observed in the solid state became a strong instability once in solution and the loss of the aromatic ligand, monitored by UV–vis analysis, causes a progressively lowering of the emission properties of the complex. On the other hand, a slight change in size of the lanthanide(III) ion, moving from europium(III) to terbium(III), produced an increase in stability such that it was possible to perform the UV–vis spectra in solution in the case of the terbium(III) complex with 1,10-phenanthroline-4,7-diethyldicarboxylate and observe the expected metal-centered luminescence. While the erbium(III) and ytterbium(III) complexes with 4,4′-dimethoxy-2,2′-bipyridine show no sensitized emission in the UV–vis range, the europium(III) and terbium(III) derivatives perform an appreciable energy transfer from the ligand to the metal ion. In particular, [Tb(**5**)$_3$(L)] shows a complete transfer, and the emission quantum yield is almost the same as its ligand 4,4′-dimethoxy-2,2′-bipyridine. Moreover, the use of relatively long alkoxy chains (OC$_8$H$_{17}$) as 4,7-substituents on 1,10-phenanthroline led to the formation of the related pro-mesogenic europium(III) complex [91].

Furthermore, the aqua ligands of [Eu(**L**)$_3$ (H$_2$O)$_2$] (H–**L** = H–**10**, H–**17**, H–**18**) can be replaced by 4,4′-dimethoxy-2,2′-bipyridine (dmbipy) and 4,7-dimethyl-1,10-phenanthroline (dmphen). The metal ion coordination is influenced by the nature of the β-diketonate ligand, which can be rationalized by considering the enhanced electron-withdrawing power of the hexafluorinated [**10**]$^-$ ligand versus the trifluorinated [**17**]$^-$ and [**18**]$^-$ ones; coordinating ability of the oxygen atom in the former is weaker due to the presence of an additional electron-withdrawing CF$_3$ group in the former. A larger ligand-metal separation releases more of the steric congestion around the lanthanide ion for the complexes with [**10**]$^-$ when compared to those with [**17**]$^-$ or [**18**]$^-$, making facile the accommodation of the neutral ligand and, possibly, a larger number of coordinated ligands resulting in a different metal coordination. Complexes of [**10**]$^-$ feature a nonacoordinate distorted square antiprismatic monocapped metal center with a coordinated water in [Eu(**10**)$_3$(dmbipy)(H$_2$O)] or ethanol in [Eu(**10**)$_3$(dmphen)(C$_2$H$_5$OH)]. The use of [**17**]$^-$ and [**18**]$^-$ affords eight coordinate, distorted square antiprismatic complexes [92].

Photoluminescence studies show that excitation of the complexes is ligand based and that the emission is characteristic of the europium(III) ion. The higher overall quantum yields of [Eu(**10**)$_3$(dmbipy)(H$_2$O)] and [Eu(**10**)$_3$(dmphen)(C$_2$H$_5$OH)] is due to the high efficiencies of ligand-to-metal energy transfer processes prior to lanthanide-centered luminescence, indicated by the sensitization efficiencies [92].

Appropriate fuctionalization at the periphery of 2-(2-pyridyl)benzimidazole (PB) was introduced according to Scheme 6c in order to modify the photophysical properties of the resulting lan-

thanide(III) complexes. Thus, the ligand L^A, containing a chelating 2-(2-pyridyl)benzimidazole unit with a pendant anthacenyl group (An) connected via a methylene spacer, was used to prepare the eight coordinate lanthanide(III) complexes $[Ln(\mathbf{10})_3(L^A)]$ (Ln = Nd, Gd, Er, Yb) by slow evaporation of a 1:1 mixture of $[Ln(\mathbf{10})_3(H_2O)_2]$ in dichloromethane/heptane. All the complexes have a square antiprismatic N_2O_6 coordination geometry. In $[Yb(\mathbf{10})_3(L^A)]$ the anthracene unit is folded back towards the chelating PB unit, with the centroid of the anthracene unit being 3.8 Å from the centroid of the pyridyl ring [93].

Whereas the free ligand L^A displays typical anthracene-based fluorescence, this fluorescence is completely quenched in its complexes. The An group in L^A acts as an antenna unit: in the complexes $[Ln(10)_3(L^A)]$ (Ln = Nd, Er, Yb) selective excitation of the anthracene results in sensitised near-infrared luminescence from the lanthanide centres with concomitant quenching of An fluorescence. The anthracene fluorescence is also quenched even in the gadolinium(III) complex. The quenching of anthracene fluorescence in coordinated L^A was proposed to be due to intraligand photoinduced electron-transfer from the excited anthracene chromophore $^1An^*$ to the coordinated PB unit generating a short-lived charge-separated state $[An^{\bullet+}–PB^{\bullet-}]$ which collapses by back electron-transfer to give $^3An^*$. This electron-transfer step is only possible upon coordination of L^A to the metal centre, which strongly increases the electron acceptor capability of the PB unit, such that $^1An^* \rightarrow$ PB PET is endoergonic in free L^A but exergonic in its complexes. It was proposed that the sensitization mechanism includes $^1An^* \rightarrow$ PB photoinduced electron transfer to generate charge-separated $[An^{\bullet+}–PB^{\bullet-}]$, then back electron-transfer to generate $^3An^*$ which finally sensitises the lanthanide(III) centre via energy transfer. The presence of $^3An^*$ in L^A and its complexes is confirmed by nanosecond transient absorption studies, which have also shown that the $^3An^*$ lifetime in the neodymium(III) complex matches the rise time of Nd-centered near-infrared emission, confirming that the final step of the sequence is $^3An^* \rightarrow$ Ln(III) energy-transfer [93].

Furthermore, when the dendritic ligands L^B–L^D of Scheme 6c are treated with $[Eu(\mathbf{6})_3(H_2O)_2]$ under conventional conditions, only the zeroth-generation europium complex $[Eu(\mathbf{6})_3(L)]$ is obtained; the superior homologues do not form europium(III) complexes [93].

Conjugated 1,10-phenanthrolines, where the 3,8-substituents are $-C{\equiv}C_6H_4R$ (R = H, CH_3, OCH_3, $N(CH_3)_2$) were synthesized as tunable fluorophores by cross-coupling reactions of 3,8-dibromo-1,10-phenanthroline with substituted phenylacetylenes or by cross-coupling reactions of 3,8-diethynyl-1,10-phenanthroline with substituted haloarenes. Both approaches are applicable to most derivatives; however, when an unstable or highly volatile alkyne is required for the former route, the latter one is preferred. These conjugated phenanthrolines show a red shift in acetonitrile of the major electronic transitions, high fluorescence quantum efficiencies in various solvents and short excited. State lifetime, suggesting that the emitting excited state is a singlet π–π^* state. The weak emission of 1,10-phenanthroline is blue-shifted upon increasing solvent polarity. This behaviour was attributed to a close proximity of the π–π^* and n–π^* singlet excited states, with the latter becoming more contributing in nonpolar solvents. This may explain the low fluorescence quantum efficiency of 1,10-phenanthroline, since n–π^* excited states often decay by non-radiative pathways [93].

Emission colour changes from purple to bright blue is attained by the addition of metal ions (i.e. zinc(II) ions) into an acetonitrile solution of the phenylethynyl (R=H) or the tolyl derivative ($R{=}CH_3$). A bright yellow fluorescence is observed when zinc(II) ions are added to a solution of the 4-methoxyphenylethynyl derivative ($R{=}OCH_3$) in acetonitrile. More relevant shifts are observed when strong acids are added to protonate the conjugated ligands. While the parent derivative (R=H) exhibits a bright purple emission, addition of methanesulfonic acid to its solution in acetonitrile causes an intense yellow-green emission. A slightly smaller shift to longer wavelengths is observed in dichloromethane, as expected for a less polar solvent. A relatively small drop in fluorescence quantum efficiency is observed upon protonation [93].

A simple approach for red shifting the absorption spectrum of the β-diketonato ligands by incorporating both an electron donor and an electron acceptor ligands was successfully tested [94]. H–**18a**, derived from 4-(dimethylamino)acetophenone and methyl-4-nitrobenzoate, reacts with $LnCH_3{\cdot}nH_2O$ in methanol and in the presence of NaOH to form $[Ln(\mathbf{18a})_3(phen)$ [(Ln = Nd, Er, Yb) with a structure similar to those above reported for the other $[Ln(\beta\text{-dike})_3(phen)]$ complexes. They display an intense intra-ligand charge-transfer absorption transition in the visible region of the spectrum at 400–550 nm which was utilized to achieve visible-light excitation of metal centred infrared luminescence of the lanthanide(III) ions. Indeed, the complexes $[Ln(\mathbf{18a})_3(phen)]$ (Ln = Nd, Er, Yb), displaying a characteristic infrared emission due to f–f transition upon excitation in ligand absorption bands, both in the solid state and in dimethylsulfoxide are suitable for visible-light excitation of NIR-emitting lanthanide ions. The main advantage of $[\mathbf{18a}]^-$ is its lowest energy absorption transition which extends into the visible range and allows excitation of lanthanide luminescence with wavelengths up to 550 nm [94].

The standard synthetic procedure affords $[Ln(\mathbf{18b})_3(phen)]$ (Ln = La, Nd, Eu, Gd, Dy, Er, Yb). No liquid crystal phases are observed for the light lanthanides complexes (Ln = La, Nd), whereas the heavy lanthanide complexes exhibit a monotropic smectic A phase with the molecules arranged in layers with interdigitation of the molten aliphatic chains. The modification of the dibenzoylmethanate ligand by addition of long alkyl chains to obtain liquid crystal phases has no influence on the excellent luminescent properties of these materials. As luminescent materials, these lanthanide(III) β-diketonate complexes offer an alternative to the luminescent liquid crystal that are obtained by doping luminescent non-mesomorphic lanthanide(III) β-diketonate complexes in a liquid crystalline host matrix [94].

When 2,2′-bipyrimidine (bpm) is used as chelating ligand, dinuclear or polynuclear lanthanide(III) complexes have been synthesized. A H–**L**:$LnCl_3{\cdot}6H_2O$:bpm = 6:2:1 molar ratio affords $[Ln_2(\mathbf{L})_6(bpm)]$ ($Ln = Eu^{III}$, Tb^{III}, Er^{III} for H–**L** = H–**17**; $Ln = Eu^{III}$ for H–**L** = H–**6**), where bpm acts as a bridging ligand. $[Eu_2(\mathbf{6})_6(bpm)]$ has two eight coordinate distorted square antiprismatic europium(III) sites, 7.011 Å apart and symmetrically related by an inversion center lying on the planar bpm moiety (Fig. 23a). Although the Eu···Eu, Eu–O, and Eu–N distances are similar to those in $[Eu_2(\mathbf{6})_6(bpm)]$, the coordination sphere of each metal(III) ion in $[Eu_2(\mathbf{17})_6(bpm)]$ is a square bicapped trigonal prism (Fig. 23b). Both structures show strong intermolecular π–π interactions that may be responsible for their high melting points. The analysis of the absorption, excitation, and emission spectra of the dinuclear complexes along with a comparison with analogous mononuclear complexes containing the same β-diketone ligands and 1,10-phenanthroline suggests that the dinuclear complexes follow the luminescence mechanism of general lanthanide(III) complexes. An electroluminescent device with the structure ITO/PEDOT/PVK + PBD + $[Eu_2(\mathbf{6})_6(bpm)]$ 10 wt.%/LiF/Al shows pure red emission with an efficiency similar to those of mononuclear complexes (PVK = poly(9-vinylcarbazole), PBD = 2-(4-biphenylyl)-5-(4-*tert*-butylphenyl)-1,3,4-oxadiazole, PEDOT = poly(styrenesulfonate)-doped poly(3,4-ethylenedioxythiophene)). It seems that in solution the photoluminescence efficiency depends more

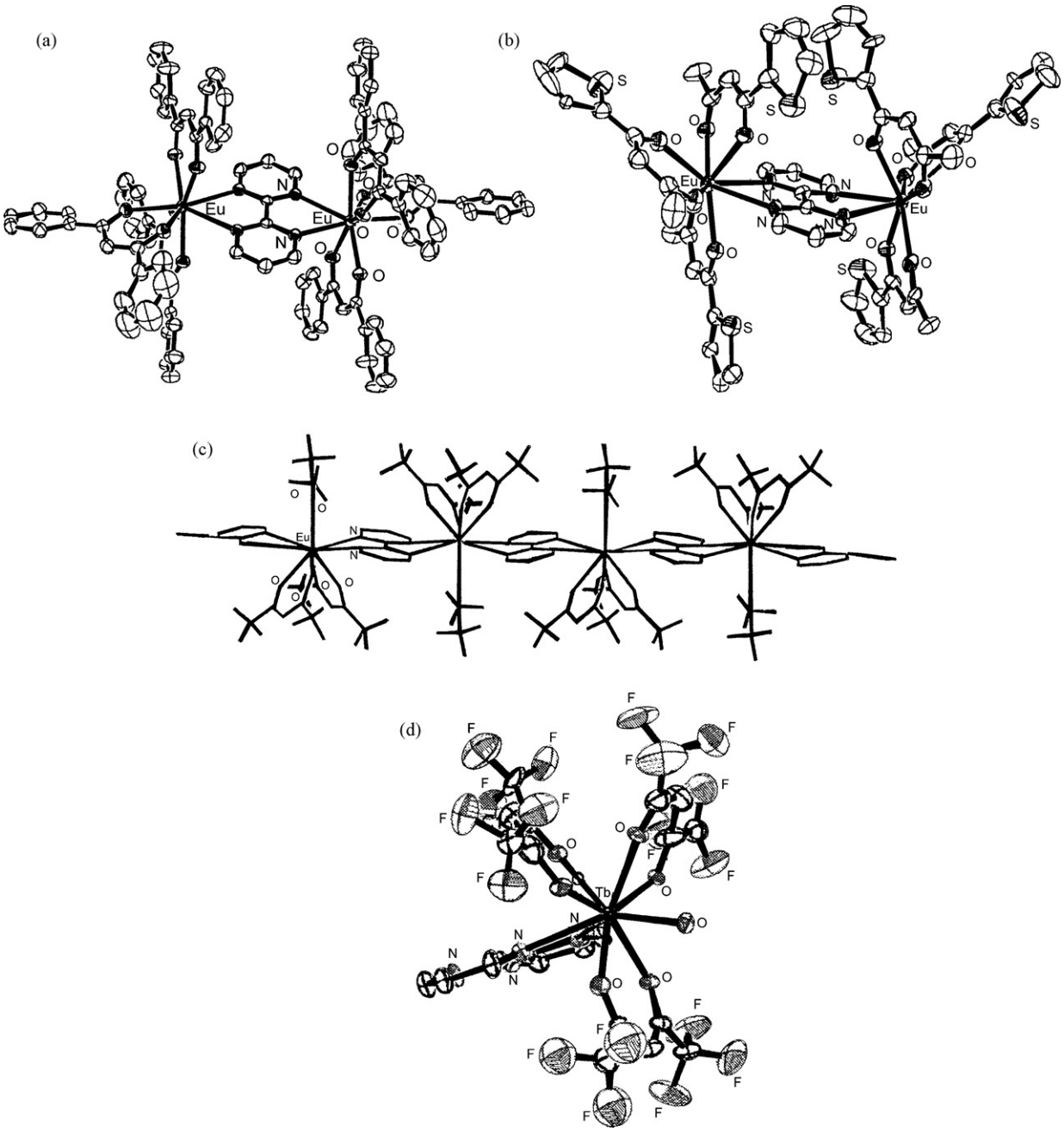

Fig. 23. Structures of $[Eu_2(\mathbf{6})_2(bpm)]$ (a), $[Eu_2(\mathbf{17})_2(bpm)]$ (b), $[Eu(\mathbf{10})_3(bpm)]_n$ (c) and $[Tb(\mathbf{10})_3(bpm)(H_2O)]$ (d) [95].

on the β-diketone sensitizing ligand than the nuclearity or the bridging ligand. The dinuclear compounds are also considered to follow the luminescence mechanism adopted in mononuclear lanthanide complexes. $[Eu_2(dbm)_6(bpm)]$ readily forms a polymer electroluminescent (EL) device ITO/PEDOT (30 nm)/PVK + PBD + Eu complex (≈80 nm)/LiF(1 nm)/Al(100 nm) that produces pure red EL. Overall, the dinuclear system shows similar thermal stability, improved EL colour purity, and comparable EL efficiency with respect to the corresponding mononuclear system [95].

Attempts to synthesize homodinuclear complexes using the larger lanthanum(III), praseodymium(III) or neodymium(III) ions by this method result in the mononuclear complexes $[Ln(\mathbf{17})_3(bpm)]$, even in the presence of excess lanthanide salt and excess $[\mathbf{17}]^-$ ligand. By the same procedure H–**10** affords $[Ln(\mathbf{10})_3(bpm)]$ ($Ln = Nd^{III}$, Eu^{III}, Gd^{III}), where an unusual one-dimensional array occurs in which each lanthanide(III) complex is connected to another through bpm bridging units. Each 10 coordinate lanthanide(III) ion is coordinated by six oxygen atoms from three β-diketonate ligands and four nitrogen atoms from two bpm ligands (Fig. 23c). Under similar conditions $TbCl_3{\cdot}5H_2O$, produces $[Tb(\mathbf{10})_3(bpm)(H_2O)]$, where the terbium(III) ion is nine coordinate with six oxygen atoms coming from the three $[\mathbf{10}]^-$ ligands, two nitrogen atoms coming from the bpm ligand, and one covalently bonded water molecule (Fig. 23d) [95].

Luminescent studies show that the neodymium(III) complex undergoes non-radiative relaxation through solvent vibrational deactivation, while the lowest excited state of the gadolinium complex, $^6P_{7/2}$, is higher in energy than the T_1 state of the $[\mathbf{10}]^-$ ligand,

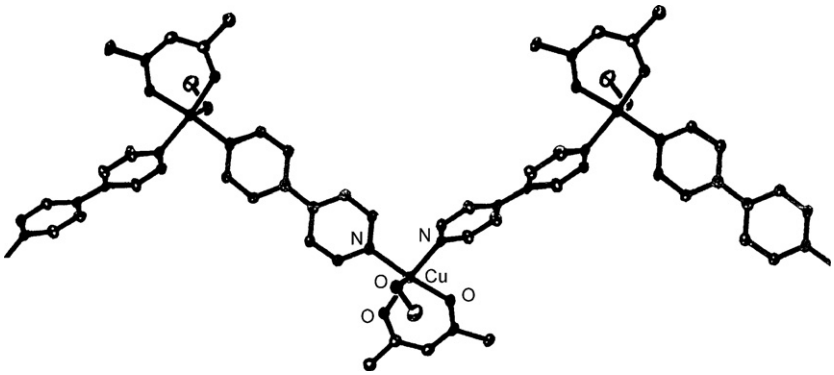

Fig. 24. Structures of $\{[Cu(\mathbf{5})(\mu\text{-}4,4'\text{-bipy})(CH_3OH)]^+\}_n$ [96].

making luminescence improbable for both of these complexes. In contrast, the terbium(III) complex emits in the visible region of the spectrum when solutions of the complex are excited at 304 nm associated with the π–π^* transition of the $[\mathbf{10}]^-$ ligand. Emission lines corresponding to transitions from the $^5D_4$ state to the ^7F_J manifold of the terbium(III) are observed. The intensity of these emissions decreases as temperature is increased. Lifetime measurements of the terbium complex fit to a monoexponential with the lifetime decreasing as the temperature is increased [95].

β-Diketonato complexes can derive from hydrolysis of the related ketoimine derivatives. For instance, 6-amino-3-methyl-1-phenyl-4-azahex-2-en-1-one or 6-amino-3,6-dimethyl-1-phenyl-4-azahex-2-en-1-one (H–L) react with $Cu(ClO_4)_2{\cdot}6H_2O$ in the presence of $N(C_2H_5)_3$ to yield $[Cu_3(L)_3(\mu_3\text{-}OH)](ClO_4)_2$, whereas 7-amino-3-methyl-1-phenyl-4-azahept-2-en-1-one undergoes hydrolysis under the same reaction conditions, forming [Cu(**12**)(pn)ClO_4] (pn = 1,3-propandiamine). Furthermore, $Cu(BF_4)_2{\cdot}6H_2O$ and the tridentate Schiff base 7-amino-4-methyl-5-aza-3-hepten-2-one (H-L), prepared by the [1 + 1] condensation of 1,2-diaminoethane and H-**5**, gives rise to $[Cu_2(L)_2(\mu\text{-}4,4'\text{-bipy})](BF_4)_2$ which hydrolyses to the linear polymeric compound $[Cu(\mathbf{5})_2(\mu\text{-}4,4'\text{-bipy})]_n$, where each copper ion is in an elongated octahedron. When $Cu(ClO_4)_2{\cdot}6H_2O$ is employed, $\{[Cu(\mathbf{5})(\mu\text{-}4,4'\text{-bipy})(CH_3OH)](ClO_4)\}_n$ occurs, where the five coordinate metal centers, bridged via 4,4′-bipyridyl units, are in a square pyramidal environment with a methanol oxygen in the axial position. The equatorial plane consists of two *cis*-coordinated 4,4′-bipyridine ligands and two oxygen atoms of the $[\mathbf{5}]^-$ moiety. Each 4,4′-bipyridine ligand links adjacent $\{Cu(\mathbf{5})(CH_3OH)\}^+$ units giving rise to the 1D zigzag chain (Fig. 24) [96].

The 1D flexible zigzag coordination polymer, $\{[Zn(\mathbf{12})_2(bpp)]{\cdot}1.5H_2O\}_n$ (bpp = 1,3-bis(4-pyridyl)-propane), synthesized by ambient evaporation of mixed solutions of $Zn(NO_3)_2{\cdot}6H_2O$, H–**12** and bpp, each distorted octahedral zinc(II) ion is surrounded by four equatorial oxygen atoms from two $[\mathbf{12}]^-$ ligands and two axial nitrogen donors from two bpp ligands. The notable feature of this material is the flexible zigzag chains running in two nearly perpendicular directions, which enables them to interweave, generating 2D entangled network [97].

β-Diketone functionalization at the periphery of the coordinating moiety was primarily carried out in order to maintain their coordination properties toward appropriate 3d- or 4f-metal ions, enhancing their physico-chemical properties, especially the optical ones. The same strategy was used also in the design and synthesis of the emitting complexes $[Ln(\beta\text{-dike})_3(L)]$ varying in the neutral antenna L, mainly substituted phenanthroline or bipyridine.

Lanthanide(III)-based LEDs have become increasingly common. The appeal of these emitting ions lies within the pure emission colour as well as the possibility of attaining near unity photoluminescence quantum yields as well as electroluminescence efficiencies higher than for organic and transition metal-based devices. While several examples exist of materials containing these f elements, the field is wide open. The synthesis and characterization of new precursors will allow the determination of which ligand architectures lead to the more promising charge transport and recombination properties, as well as better matching with the common hole and electron transport layers. Further, new ligands will also allow for incorporation of the complexes into polymer hosts and thus taking advantage of the processability and long-term stability of polymer-based emitting layers.

Incorporation of these complexes into polymers has been carried out through two different strategies: (i) formation of blended compounds, i.e. incorporation of complexes into the polymers and (ii) formation of polymers based on methylmethacrylate and acrylic acid with the emitting complex covalently attached to the polymer backbone.

The f–f transitions which are responsible for the lanthanide(III) luminescence are parity and, in some cases, spin forbidden. As such, the most efficient mechanism of excitation involves excitation of a coordinated ligand, leading to population of its singlet state which subsequently decays through intersystem crossing (ISC) to a triplet state. The triplet state, finally, through a dipole–dipole exchange mechanism, leads to the population of the emissive f excited state. More recently, Ln(III)-based emitting complexes have been described in which the sensitization occurs through LMCT states of transition metal complex moieties present in the lanthanide ion edifice [33].

Dentritic β-diketones represent an interesting class of chelating ligands with different functionalizations at the periphery of the coordinating moiety in order to tune adequately the physico-chemical properties of the resulting complexes to make them suitable for different applications, ranging from laser materials, to organic light-emitting diodes and fluorescent probes [98,99].

Several dendritic β-diketonates and corresponding europium complexes were designed and synthesized based on the following consideration: (i) high light-harvesting capability and efficient energy transfer to the focal ion in virtue of high extinction coefficient of the terminated carbazole units; (ii) dendron functionalization to incorporate carbazole units to realize the carrier-injection adjustment; (iii) avoiding core luminescence quenching by the means of the dendron to enhance core luminescence. The dendritic β-diketonate ligands contains diben-

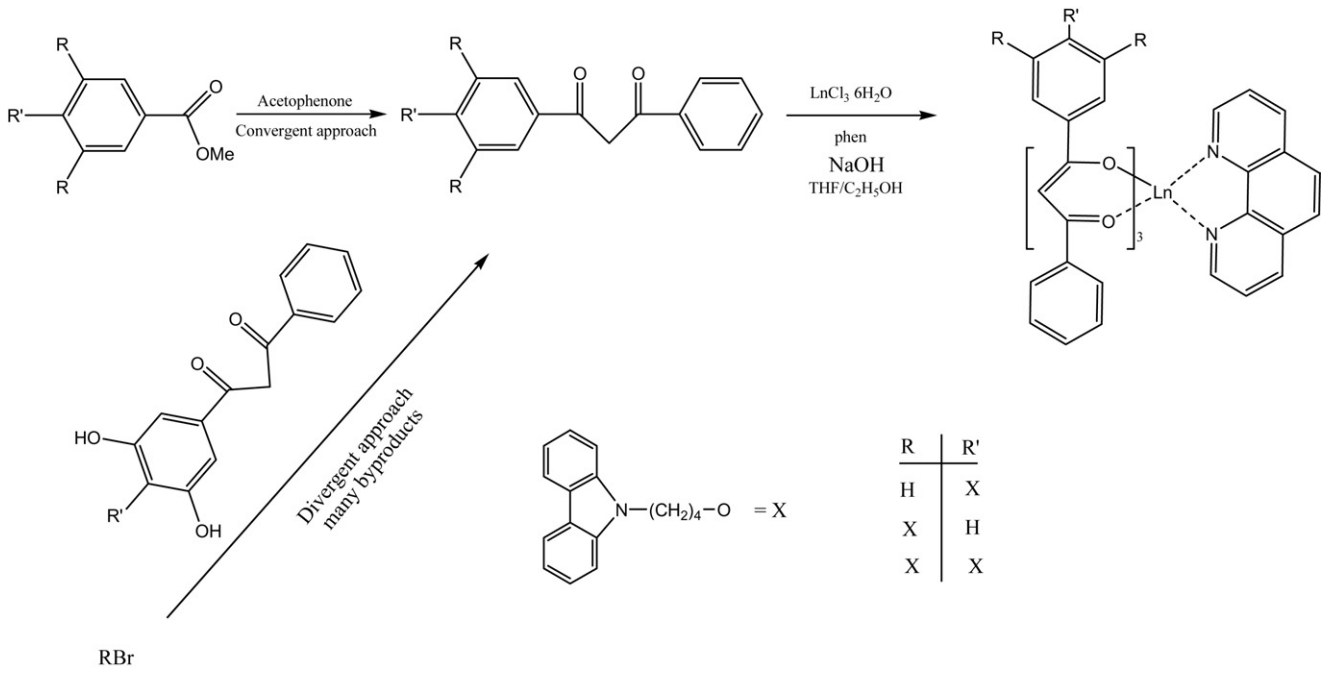

Scheme 4. Procedure for designing the first generation dendritic ligands and the related lanthanide(III) complexes.

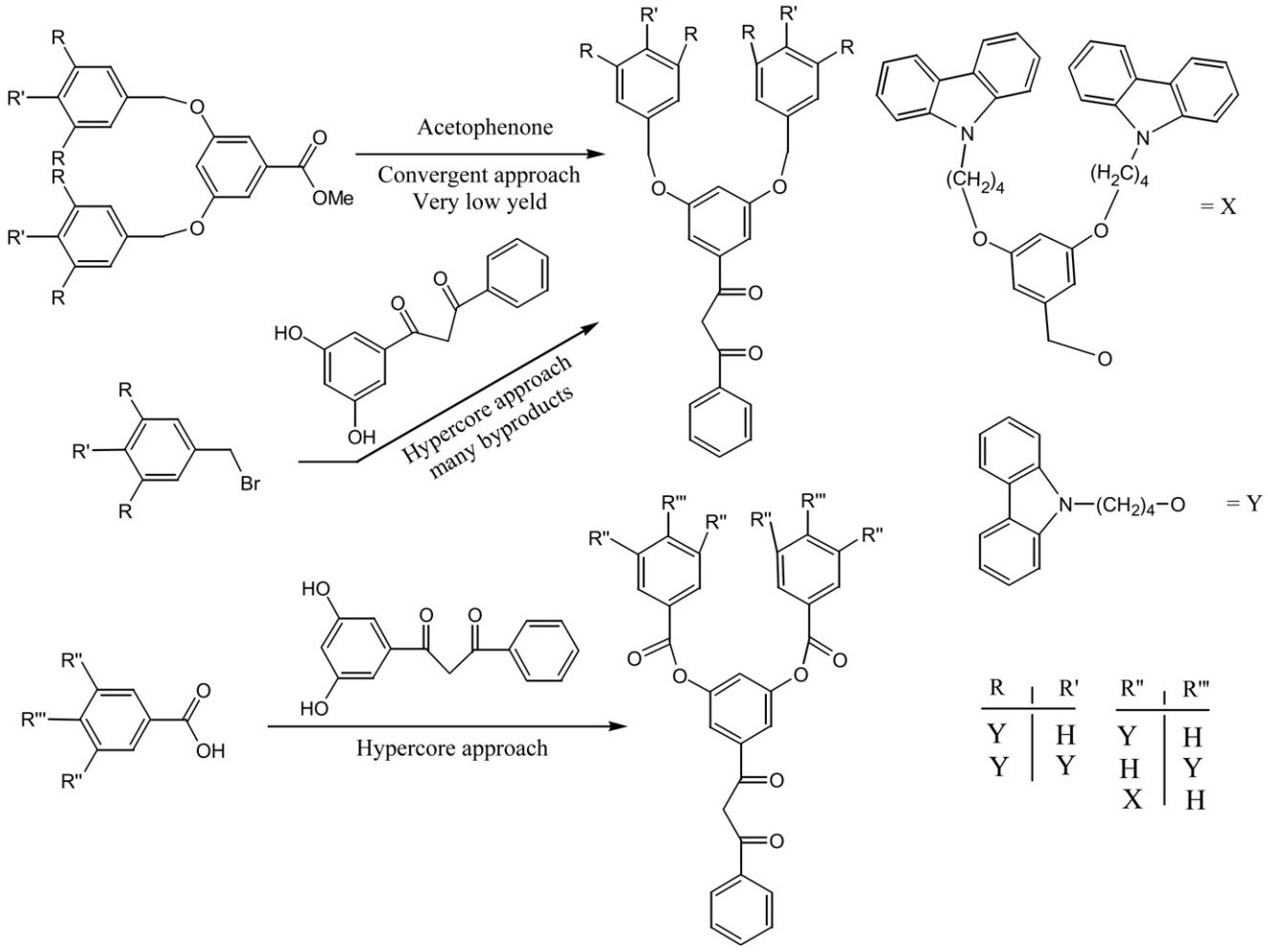

Scheme 5. Procedure for designing the second and third generation dendritic ligands.

zoylmethane cores, poly(arylether) dendrons, and the grafted carbazole peripheral functional groups. Due to the acceptable yield of Claisen condensation, convergent synthetic approach through etheral connectivity was utilized to achieve the first generation europium complexes. For the second and third generation dendrons, a hyperbranch core synthetic approach containing the advantages of convergent and divergent approaches was introduced. In particular, a first generation branched dibenzoylmethane derivatives and the related europium(III) complexes [Eu(**L**)$_3$(phen)] (H–**L** = H–**19**, H–**20** and H–**21**) were synthesized, according the approach of Scheme 4 [99]. The second and third generation dendrons and the related europium(III) complexes [Eu(**L**)$_3$(phen)] (H–**L** = H–**22**, H–**23** and H–**24**) were obtained by the hypercore approaches of Scheme 5. These systems have been characterized by NMR and MALDI-TOF spectra which gave fully support to the proposed structure of the ligands and the related europium(III) complexes. The dendron-functionalized carbazole units not only tune the carrier-transporting capability, but also exhibit strong light-harvesting potential, resulting in a strong intense emission from the central europium(III) ion via sensitization [100].

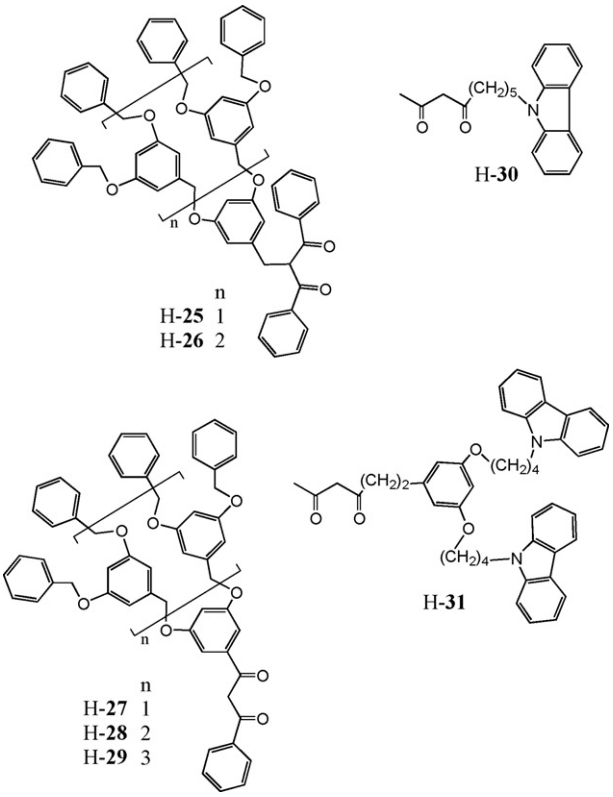

Furthermore, the bis-substituted dibenzylmethane H–**24a**, prepared by condensation under strong basic conditions (NaH) of the related ester- and keto-derivatives both containing appended carbazole units, reacts with $EuCl_3{\cdot}6H_2O$ and 1,10-phenantholine or 4,7-phenyl-1,10-phenantholine (L), to form [Eu(**24a**)$_3$(L)], whose photoluminescence properties in dichloromethane and in solid matrix show the carbazole moiety to be a better sensitizer for the metal-centered emitting states of the europium(III) ion compared to the dibenzoylmethane and phenanthroline units. Thus an efficient population of the europium(III) emitting states by energy transfer occurs from the carbazole units. Notably, in both cases, a strong enhancement in the metal centered luminescent intensity was detected in solid matrix, which provides evidence for the limited action of the vibrational quenchers under these conditions [98]. Transporting properties of the carbazole moieties appear to be appealing when integrated into the emitting units [100].

Moreover, attachment of the dendritic bromides to the 2-position of dibenzoylmethane was achieved from the corresponding dendritic bromides and dibenzoylmethane in tetrahydrofuran and in the presence of NaH as a strong base (Scheme 6a), while the dendritic dibenzoylmethane derivatives with the polyether dendron attached to the phenyl group of the β-diketones were synthesized by condensation of the appropriate dendritic ester with acetophenone in the presence of NaH (Scheme 6b). The structure of the systems were inferred by NMR and mass spectra [100].

The dendritic β-diketonato ligands H–**25**, H–**26**, H–**27**, H–**28** and H–**29**, which contain a dibenzoylmethane core and poly(arylether) dendron, have been synthesized by a convergent strategy. The attachment point of the dendron to dibenzoylmethane plays an important role in the preparation of europium(III) complexes. Reaction of the β-diketonato ligands H–**27**, H–**28** and H–**29**, which bear a dendron substituted on the phenyl group of dibenzoylmethane, with $EuCl_3{\cdot}6H_2O$ gives the first- to third-generation dendritic europium(III) complexes in good yields, while europium(III) complexes could not be formed with β-diketonato ligands H–**25** and H–**26**, which have dendrons attached to the 2-position of dibenzoylmethane. The resulting dendritic europium(III) complexes [Eu(**L**)$_3$] (H–**L** = H–**25**···H–**29**) were characterized by MALDI-TOF mass spectrometry, and further confirmed by luminescence measurements. Incorporation of 1,10-phenanthroline as the second ligand in these dendritic (β-diketonato)europium(III) complexes gives new dendritic europium(III) complexes with enhanced luminescence intensity [101].

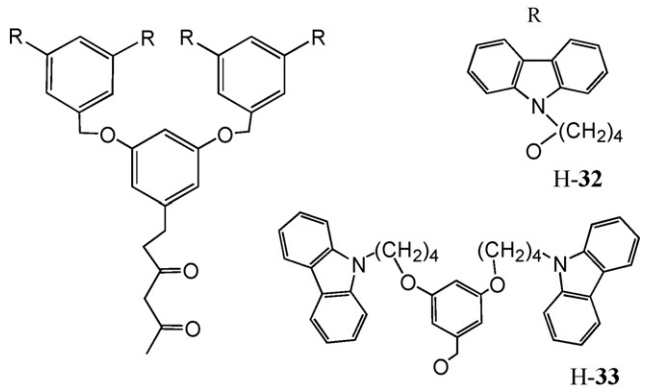

5.2. Iridium(III) complexes

A family of cyclometalated iridium(III) complexes successfully used as molecular components for organic light-emitting oxides (OLED), was prepared by reaction of $IrCl_3{\cdot}nH_2O$ with an excess of the desired pyridine containing ligand L (Scheme 7) to give a chloride-bridged dimer [Ir$_2$(L-H)$_4$(μ-Cl)$_2$], subsequently converted into the emissive, stable iridium(III) complexes [Ir(β-dike)(L–H)$_2$] by replacing the bridging chloride ions with a β-diketonate ligand, i.e. H–**5**, H–**6**, H–**7** and H–**12**. In these complexes, which are stable and sublimable in vacuum without decomposition, the iridium(III) ion is octahedrally coordinated by the three chelating ligands, with the cyclometalating groups in a trans disposition, and the two carbon in a *cis*-disposition as found in [Ir(**5**)(ppy-H)$_2$] and [Ir(**5**)(tpy-H)$_2$] (Fig. 25a), reported as explanatory examples, where close intermolecular contacts in both the complexes lead to significantly red shifted emission spectra for crystalline samples relative to their solution spectra [102].

The majority of the [Ir(**5**)(L–H)$_2$] complexes phosphoresce with high quantum efficiencies, resulting form spin–orbit coupling of the iridium(III) center. The lowest energy (emissive) excited state in these complexes is a mixture of ^{3}MLCT and $^3(\pi-\pi^*)$ states. By choosing the appropriate [L–H]$^-$ ligand, the related [Ir(**5**) (L–H)$_2$] complexes can be prepared which emit in any colour from green to red. Simple, systematic changes in the [L–H]$^-$ ligands, which lead to bathochromic shifts of the free ligands, lead to similar bathochromic shifts in the iridium(III) complexes of the same ligands, consistent with {Ir(L–H)} centered emission [102].

[Ir(**5**)(pba-H)], prepared by reaction of $IrCl_3{\cdot}3H_2O$ with 4-(2-pyridyl)benzaldehyde (pba) in 2-ethoxyethanol/water, is an excellent homocysteine-selective sensor. The addition of homocysteine (Hcy), $HS(CH_2)_2CH(NH_2)COOH$, to [Ir(**5**)(pba-H)] in CH_2Cl_2/CH_3OH causes a colour change from orange to yellow and a luminescent variation from deep red to green, attributed to the formation of a thiazinone group by selective reaction of the aldehyde group of the coordinated [pba-H]$^-$ with homocysteine with the consequent formation of a complex formulable as [Ir(**5**)(pba = cy-H)$_2$]. Remarkably, [Ir(**5**)(pba-H)$_2$] shows uniquely luminescent recognition of Hcy over other amino acids (including cysteine) and thiol-related peptides (reduced glutathione), in agreement with the higher luminescent quantum yield of the adduct of [Ir(**5**)(pba-H)$_2$] with Hcy compared with that of the adduct with Cys. A photoinduced electron-transfer process might be responsible for the high specificity of [Ir(**5**)(pba-H)$_2$] toward Hcy over Cys [102].

[Ir(**5**)(ppy-H)$_2$], [Ir(**5**)(bt-H)$_2$], [Ir(**5**)(btp-H)$_2$], doped into the emissive region of multilayer, vapor-deposited organic light-emitting diodes, give green, yellow, and red electroluminescence, respectively, with very similar current–voltage characteristics. These systems give high external quantum efficiencies, the {Ir(**5**)(ppy-H)$_2$}dopant giving the highest one. The {Ir(**5**)(btp-H)$_2$} based device gives saturated red emission with a quantum efficiency of 6.5% and a luminance efficiency of 2.2 Im/W. These {Ir(**5**)(L–H)$_2$} doped OLEDs show some of the highest efficiencies reported for organic light-emitting diodes. The high efficiencies result from efficient trapping and radiative relaxation of the singles and triplet excitons formed in the electroluminescent process [102].

The convergent synthetic approach, involving the reaction of the corresponding dendritic bromide and acetylacetonate

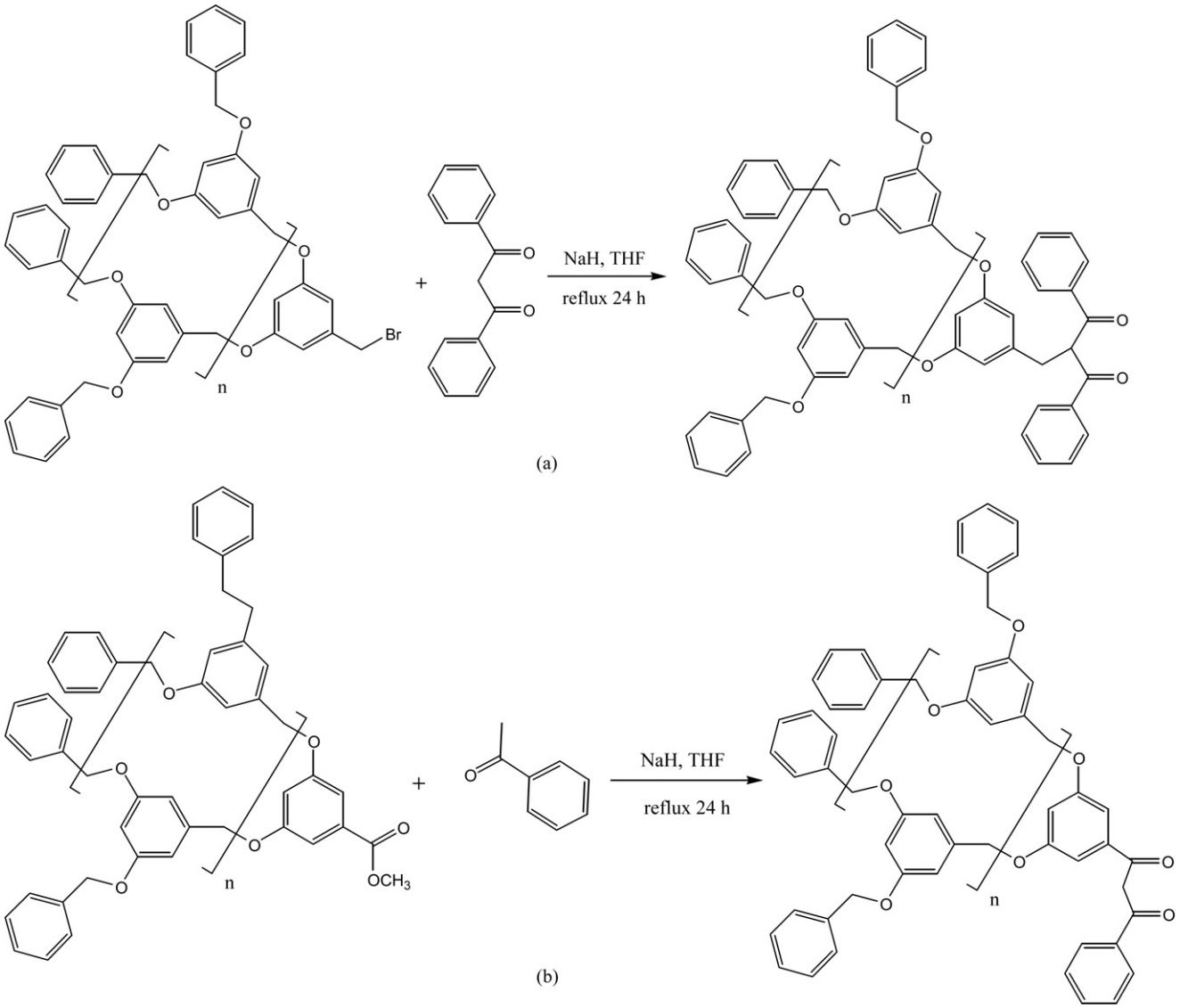

Scheme 6. Syntheses of polyarylether-containing dendrons.

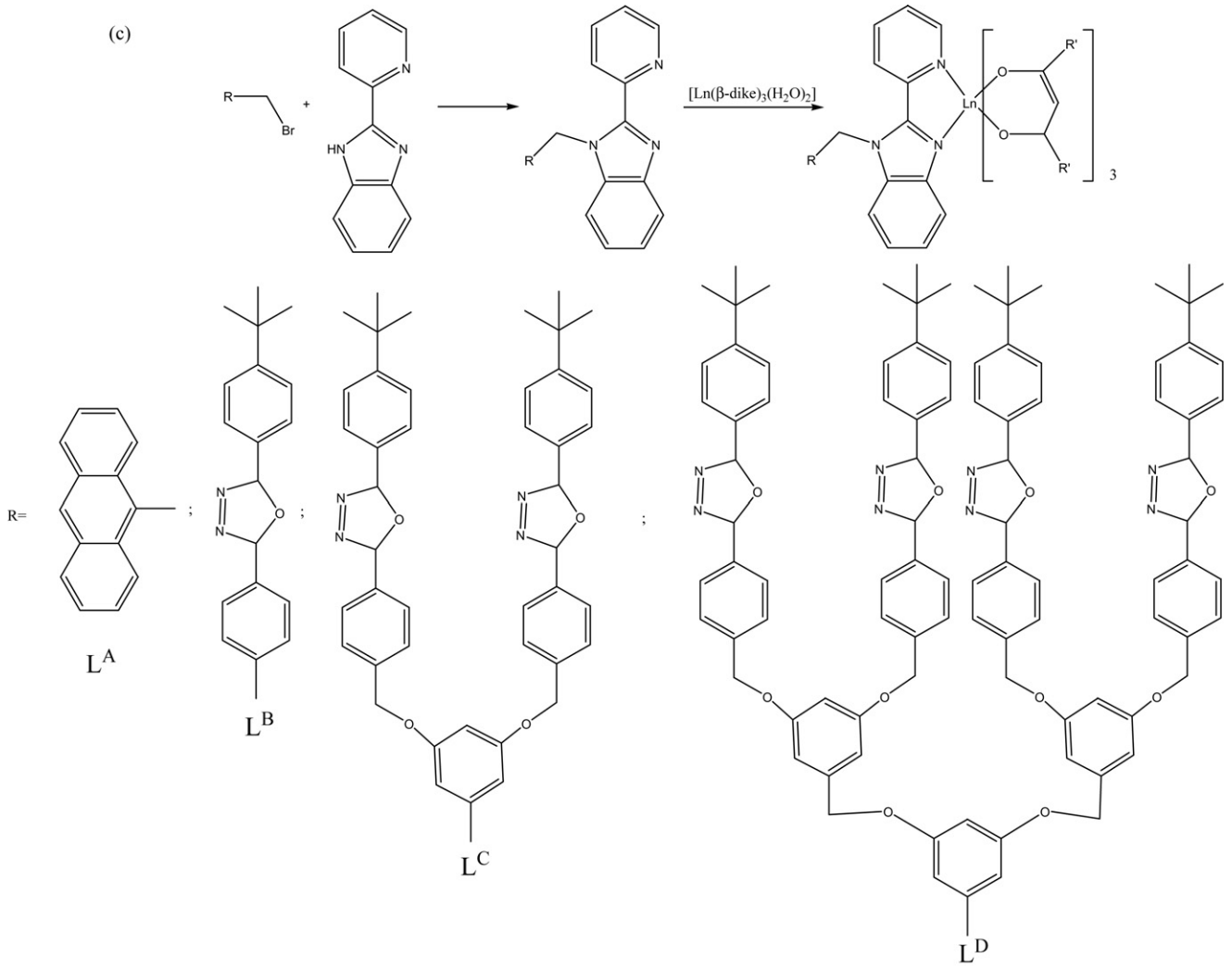

Scheme 6. (*Continued*).

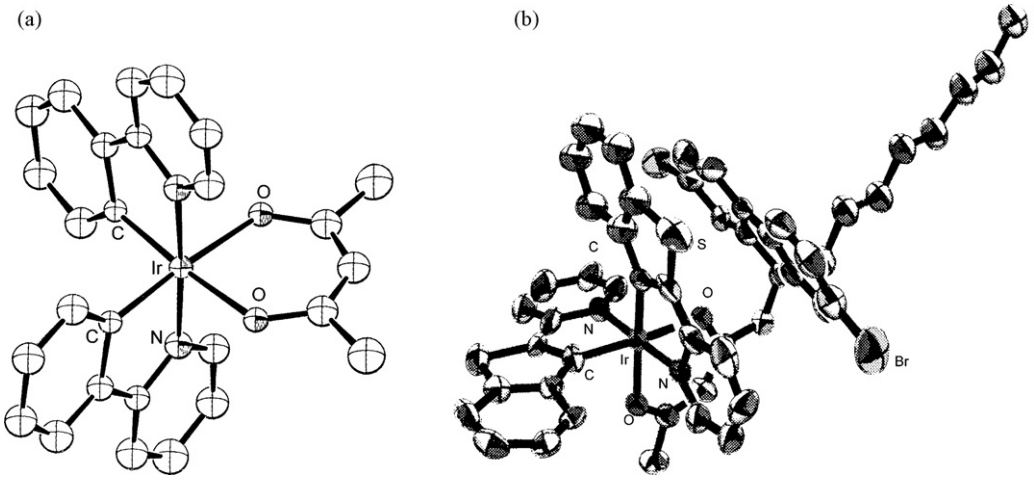

Fig. 25. Structures of [Ir(**5**)(ppy-H)$_2$] (a) [102] and [Ir(**5**)(btp-H)$_2$] (b) [105].

in the presence of NaH, has been developed also for the synthesis of carbazole peripherally functionalized β-diketonato dendrons H–**30**···H–**33**, which smoothly give the green emitters [Ir(**L**)(ppy-H)$_2$] when mixed with [Ir$_2$(μ-Cl)$_2$(ppy-H)$_4$], derived from IrCl$_3$·nH$_2$O and 2-phenylpyridine (ppy) in the presence of Na$_2$CO$_3$ in 2-ethoxyethanol [103].

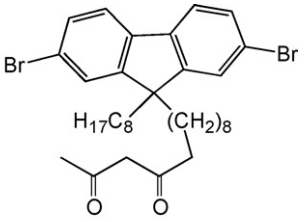

H-**34a**

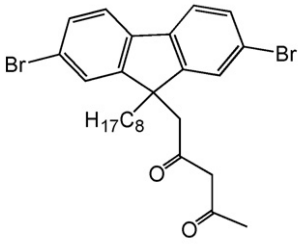

H-**34b**

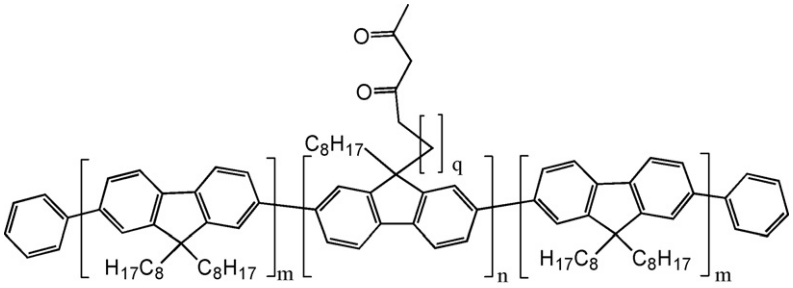

	q	m	n
H-**35a**	0	9.6	0.06
H-**35b**	0	8.5	0.18
H-**35c**	8	9.6	0.08
H-**35d**	8	9.3	0.30

Notably, in the cases of the second- and third-generation dendrons, the reactions proceeded slowly, probably owing to the large space hindrance and low solubility of the high-generation dendritic ligands. Another advantage of this approach is the possibility of easily tuning the color of emission with the same kind of β-diketonato dendrons by using different cyclometallating ligands instead of ppy. Following the same two-step procedure, the blue-green-emitting and red-emitting iridium(III)-cored dendrimers, [Ir(**32**)(dfp-H)$_2$] and [Ir(**32**)(btp-H)$_2$], were obtained in a pure form by neutral alumina column chromatography. All these dendritic iridium complexes are soluble in common organic solvents, such as dichloromethane, trichloromethane, tetrahydrofuran and toluene. Their photoluminescent properties both in solution and in the solid state were tested. It was found that all the dendrimers retained the photophysical properties of the corresponding small analogues with high emission quantum yields (0.06–0.30). Efficient energy transfer from the carbazole units to the iridium core has been observed. These dendrimeric functionalized carbazole units exhibited distinct light-harvesting potential, resulting in a strong intense emission from the iridium core of the dendrimers [103].

The blended and covalently bonded β-diketonate synthetic strategies, above described for the lanthanide(III) complexes, have been used to obtain polymers containing iridium(III) phosphor dopings. In the first strategy conjugated polymers as poly(phenylenevinylenes), polyfluorenes, and poly(*p*-phenylenes) or non nonconjugated polymers as polyvinylcarbozole have been used to prepare OLEDs. The devices obtained, however, have relatively low efficiency [104].

Several routes to obtain electroluminescent polymers by grafting high-efficiency phosphorescent organometallic complexes as dopants and charge transport moieties onto alkyl side chains of fully conjugated polymers for polymer light-emitting diodes (PLED) with single layer/single polymers have been studied. The polymer system investigated involves polyfluorene as the base conjugated polymer, carbazole as the charge transport moiety and a source for green emission by forming an electroplex with the PF main chain, and cyclometalated iridium complexes as phosphorescent dopants. The devices prepared therewith can emit red light with the high efficiency 2.8 cd/A at 7 V and 65 cd/m^2, comparable to that of the same iridium(III) complex-based OLED, and can emit the light with broad band containing blue, green, and red peaks (2.16 cd/A at 9 V) [105].

Red-emitting phosphorescent iridium complexes based on [Ir(**5**)(btp-H)$_2$] (btp = 2-(2′-benzo[b]thienylpyridine)) have been attached either directly (spacerless) or through a –(CH$_2$)$_8$– chain (octamethylene–tethered) at the 9-position of a 9-octylfluorene host. The resulting dibromo-functionalized spacerless complex [Ir(**34a**)(btp-H)$_2$] or octamethylene–tethered complex [Ir(**34b**)(btp-H)$_2$] were chain extended by Suzuki polycondensations using the appropriate bis(boronate)-terminated fluorine macromonomers in the presence of end-capping chlorobenzene solvent to produce the statistical spacerless H–**38** and octamethylene–tethered copolymers H–**35a**, H–**35b**, H–**35c** and H–**35d**, (where *m* and *n* as referred in the related formula have been estimated by ^{1}HNMR spectra) containing an even dispersion of the pendant phosphorescent fragments.

The structure of the spacerless monomer complex [Ir(**34b**)(btp-H)$_2$], which resembles that of the non-functionalized phosphorescent iridium(III) complex [Ir(**5**)(btp-H)$_2$] adopts a face-to-face conformation of the iridium complex and fluorenyl group in the crystalline state (Fig. 25b). This conformation, with a separation of only 3.6 Å between cyclometalating ligand and fluorenyl group at the closest point, is expected to facilitate π–π interactions between these parts of the spacerless monomer. Such orbital interactions are know to be the key requirement for triplet energy transfer [105].

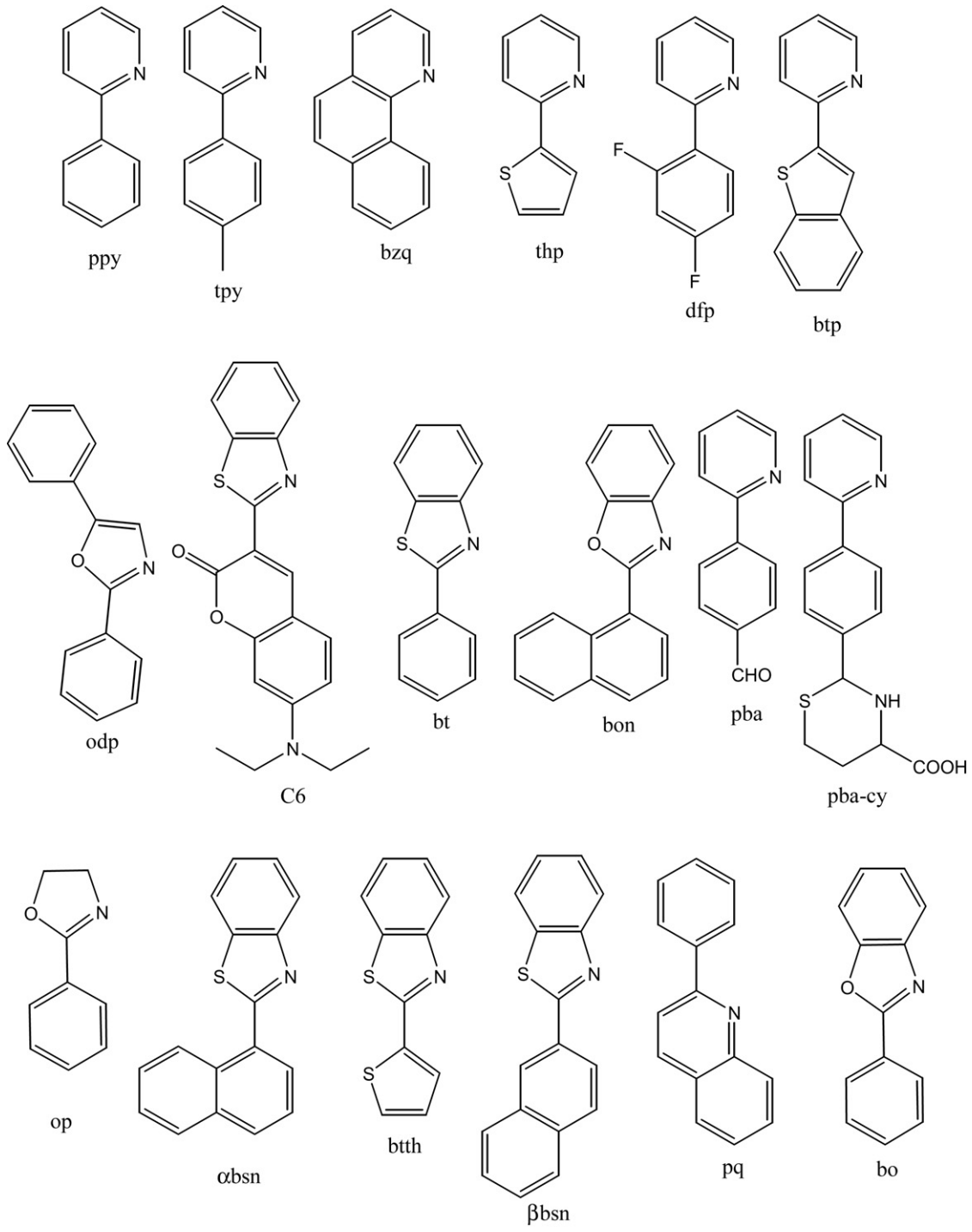

Scheme 7. Pyridine containing ligands (L) employed in the preparation of [Ir(β-dike)(L–H)$_2$].

The photo- and electroluminescence efficiencies of the octamethylene-tethered copolymers [Ir(**35a**)(btp-H)$_2$] and [Ir(**35b**)(btp-H)$_2$] are double those of the spacerless copolymers [Ir(**35c**)(btp-H)$_2$] and [Ir(**35d**)(btp-H)$_2$], and this is consistent with suppression of the back transfer of triplets from the red phosphorescent iridium complex to the polyfluorene backbone in [Ir(**35c**)(btp-H)$_2$] and [Ir(**35d**)(btp-H)$_2$]. The incorporation of a –$(CH_2)_8$– chain between the polymer host and phosphorescent guest is thus an important design principle for achieving higher efficiencies in those electrophosphorescent organic light-emitting diodes for which the triplet energy levels of the host and guest are similar.

The lower photo- and electroluminescence efficiencies of the spacerless copolymers [Ir(**35a**)(btp-H)$_2$] and [Ir(**35b**)(btp-H)$_2$] are consistent with greater triplet energy transfer in the spacerless systems and with triplet energy back transfer reducing the triplet population at the iridium complexes. In thin films, triplet energy back transfer is inhibited in the octamethylene–tethered copolymers [Ir(**35c**)(btp-H)$_2$] and [Ir(**35d**)(btp-H)$_2$]by the distance imposed through the tether. It was concluded that the incorpora-

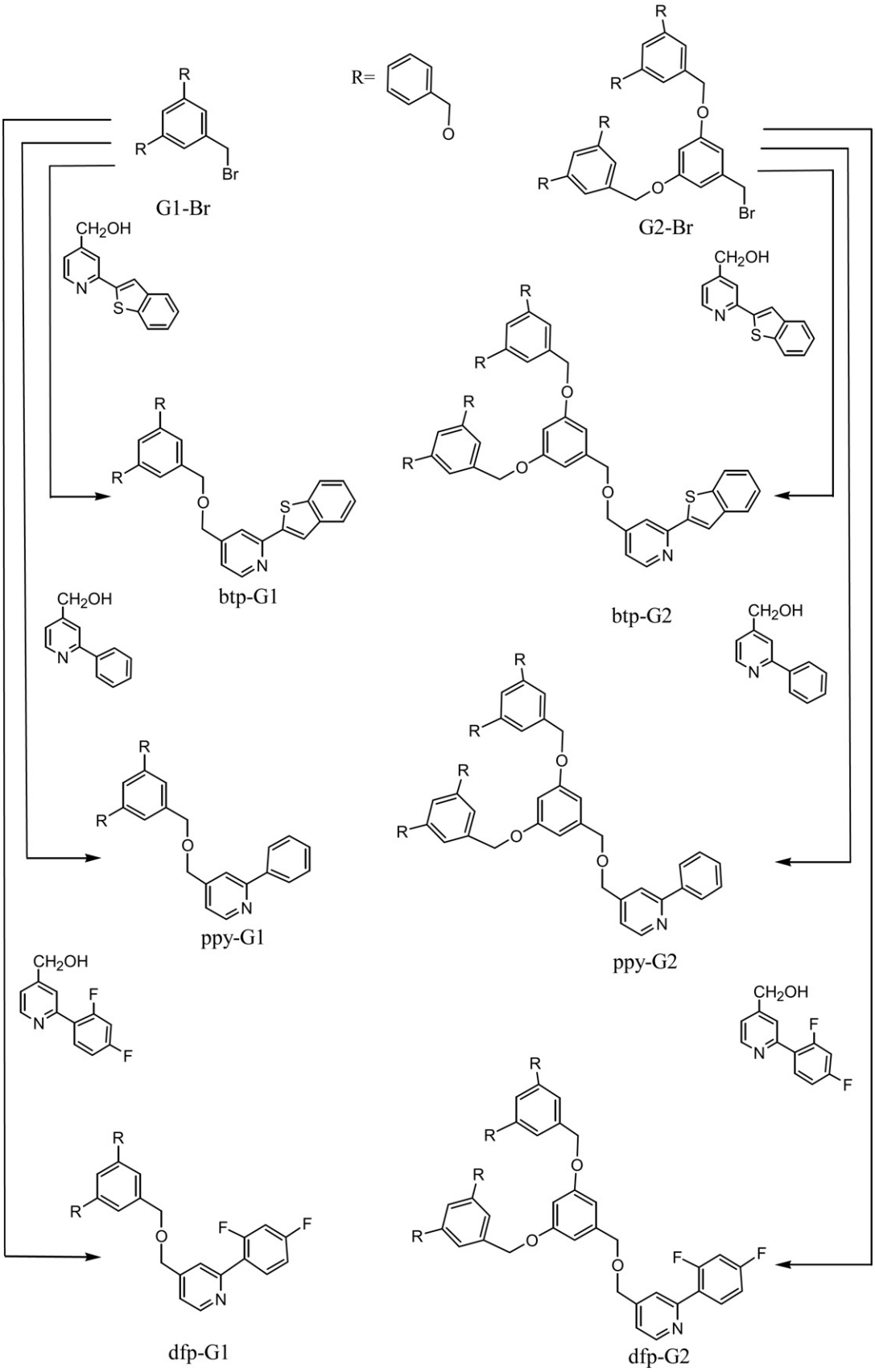

Scheme 8. Preparation of dendritic pyridine-based ligands.

tion of a spacer between polymer host and phosphorescent guest is an important design principle for achieving higher efficiencies in those electrophosphorescent OLEDs for which the triplet energy levels of the host and guest are similar. Furthermore, it was demonstrated that covalently linking the guest through a tether rather than by conjugative linkage is an important improvement in the design of solution processible electrophosphorescent polymers [103,105].

Also a simple synthetic route was developed for the dendritic iridium(III) complexes [Ir(**5**)(L–H)] (L = dfp-G1, dfp-G2, ppy-G1, ppy-G2, btp-G1, btp-G2) based on the tunable pyridine-based ligands of Scheme 8. [Ir(**5**)(L–H)] (L = ppy, dfp, btp) were used as the cores of these dendrimers to tune the phosphorescent emission from blue to red. These dendritic iridium(III) complexes exhibit tunable photoluminescence from blue to red. The photoluminescence quantum yields of these dendritic complexes in neat films increased with the increasing generation number of dendritic CN̂ chelating ligands. These iridium complexes were used as dopants for fabricating polymer-based electrophosphorescent light-emitting diodes with the highest external quantum efficiency of 12.8% [105].

The condensation of 2-acetyl-1,10-phenanthroline with 2,2,3,3,3-pentafluoro-propanate in the presence of Na in benzene affords H-**36**, which reacts with $[Ir_2(\mu\text{-}Cl)_2(dfp\text{-}H)_4]$ to form $[Ir(\mathbf{36})(dfp\text{-}H)_2]$, where the iridium(III) ion is six coordinated by two carbon atoms and four nitrogen atoms from the two cyclometalated $[dfp\text{-}H]^-$ ligands and two nitrogen atoms from $[\mathbf{36}]^-$. The two carbonyl groups in the β-diketone fragment of $[\mathbf{36}]^-$ are in the *trans* form and uncoordinated (Fig. 26a) [106].

$[Ir(\mathbf{36})(dfp\text{-}H)_2]$ and $LnCl_3{\cdot}6H_2O$ (Ln = Eu, Gd) or $[Eu(\mathbf{11a})_3(H_2O)_2]$ give $[LnIr_3(\mathbf{36})_3(dfp\text{-}H)_6(Cl)](Cl)_2$ or $[EuIr(\mathbf{36})(\mathbf{11a})(dfp\text{-}H)_2]$, respectively. In the tetranuclear $EuIr_3$ complex (Fig. 26b) each iridium(III) ion maintains the same configuration of $[Ir(\mathbf{36})(dfp\text{-}H)_2]$ while the seven coordinate europium(III) ion is linked by six oxygen atoms of the three $[\mathbf{36}]^-$ ligands and one chloride anion coming from the starting $EuCl_3{\cdot}6H_2O$. The Eu···Ir distances, 6.028, 5.907, and 6.100 Å, are suitable for effective energy transfer in the donor–bridge–acceptor system. Photophysical studies indicate that the high efficient red luminescence from the europium(III) ion is sensitized by the ^{3}MLCT (metal-to-ligand-charge transfer) energy based on the $\{Ir^{III}(\mathbf{36})(dfp\text{-}H)_2\}$ unit. The excitation window for the $EuIr_3$ complex extends up to 530 nm (1×10^{-3} M in ethanol), indicating that it can emit red light under the irradiation of sunlight. Furthermore, when the dinuclear EuIr are complex excited at 480 nm, a bright red emission centered at 613 nm is observed, again sensitized by the ^{3}MLCT energy of the Ir-based chromophore $\{Ir(\mathbf{36})(dfp\text{-}H)_2\}$. Moreover, the high quantum efficiencies of the these complexes implies not only that the d → f energy transfer occurs between the iridium(III) center and the europium(III) center but also that the energy transfer is very efficient [106].

6. β-Diketonato complexes containing redox groups

6.1. Ferrocene containing complexes

Multiferrocene assemblies have received attention owing to the redox active properties associated with the ferrocene units. These organometallic assemblies are useful in a huge range of applications from designing electron reservoirs, recognition of anionic species like $H_2PO_4^-$ to enzyme sensors and model compounds for fixation of organometallic species on suitable surfaces. Ferrocene containing β-diketones belong to this class of compounds. They derive from benzoylation or acylation of the methyl ketone groups of acetylferrocene or bisacetylferrocene and have been used in metal ion

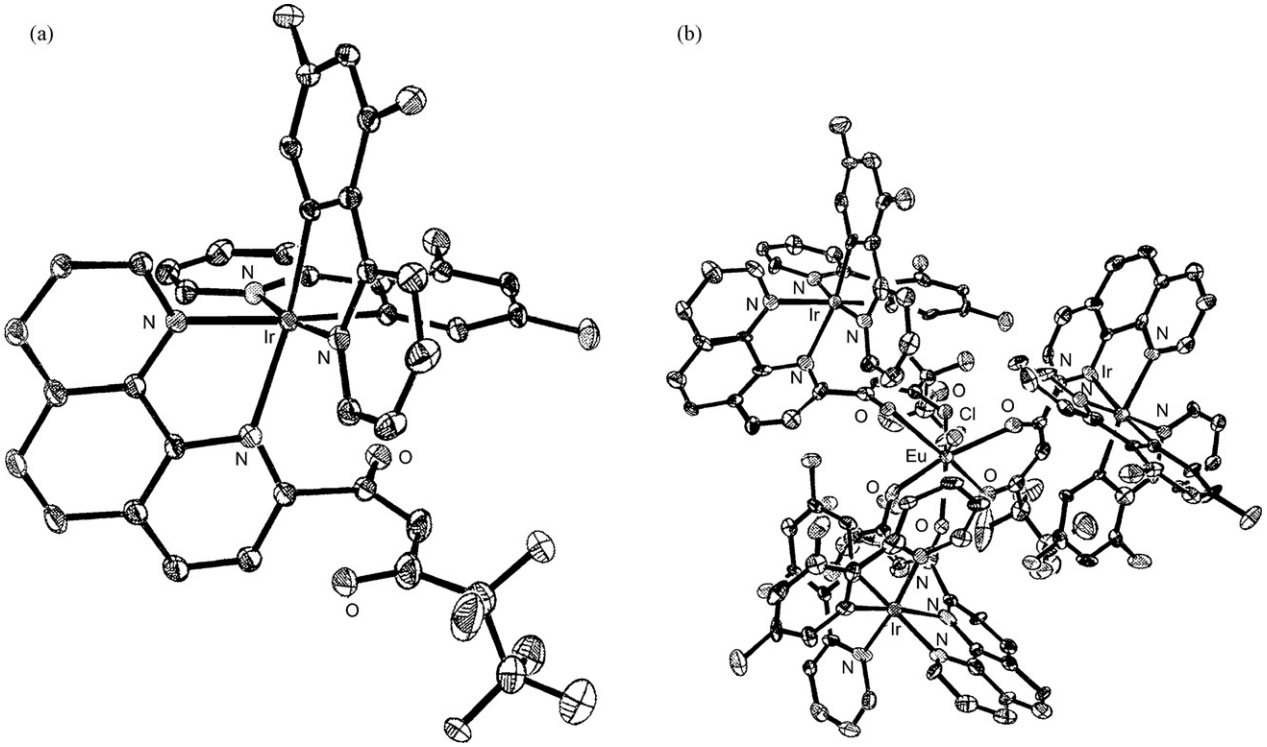

Fig. 26. Structures of $[Ir(\mathbf{36})(dfp\text{-}H)_2]$ (a) and $[EuIr_3(\mathbf{36})_3(dfp\text{-}H)_6(Cl)]^{2+}$ (b) [106].

complexation [107].

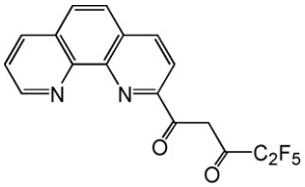

H-**36**

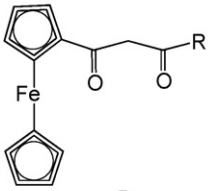

	R
H-**37**	CH_3
H-**38**	$C_5H_5FeC_5H_4$
H-**39**	CF_3
H-**40**	C_6H_5
H-**41**	CH_3

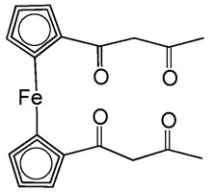

H_2-**37a**

H–**37** or H–**38** and copper(II) acetate afford [Cu(**37**)$_2$], or [Cu(**38**)$_2$] with a four coordinate square planar copper(II) ion bound to two bidentate [**37**]$^-$ or [**38**]$^-$ ligands, respectively. The ferrocene substituents in [Cu(**37**)$_2$] are in an *anti* arrangement. The pairs of ferrocene substituents on each ligand in [Cu(**38**)$_2$] are *syn* and adopt an *anti* arrangement with respect to the pair on the other diketonate ligand (Fig. 27a and b) [108].

[M(**37**)$_3$] (M = Al^{III}, Cr^{III}, Mn^{III}, Fe^{III}) and [M(**37**)]$_2$ (M = Co^{II}, Ni^{II}, Cu^{II}), prepared by a similar procedure, undergo reversible one-electron oxidation at potential values essentially overlapping each other. This means that the central metal ion prevents any electronic communication between the two or three ferrocene fragments. In addition to these reversible ferrocene-centered oxidations, there are reversible one-electron reductions at the metal(III) ion for [Mn(**37**)$_3$] and [Fe(**37**)$_3$] (but nor for [Cr(**37**)$_3$] or [A1(**37**)$_3$]. The metal-centre reductions of [M(**37**)$_2$] are irreversible owing to further reactions following reduction [108].

A mixture of H–**37**, tris(2-aminoethyl)amine (tren) and cobalt(II) chloride do not give the related tripodal ketoimine complex but [Co(**37**)(tren)](BPh$_4$)·CH$_3$COCH$_3$, where the slightly distorted octahedral cobalt(II) ion is coordinated by the four nitrogen atoms of tren and the two oxygen atoms of [**37**]$^-$ [109].

1,2-Bis(4-pyridyl)ethane (bpe), Zn(CH$_3$COO)$_2$·2H$_2$O and H–**37** afford in methanol and in the dark the one-dimensional complex chain {[Zn(**37**)$_2$(bpe)]·2H$_2$O}$_n$, consisting of six coordinate zinc(II) centers, bridging 1,2-bis(4-pyridyl)ethane and chelating [**37**]$^-$ ligands. Each zinc(II) ion is in a distorted octahedral environment with four oxygen atoms from two [**37**]$^-$ ligands in the equatorial plane, and two nitrogen atoms from the bridging bpe ligands in the axial positions. The intrachain Zn···Zn distance is 13.806 Å (Fig. 28) [109].

The corresponding reaction of H_2–**37a** with copper(II) acetate yields the square planar complex [Cu(**37a**)]. Furthermore, H_2–**37** or H_2–**37a** and UO$_2$(NO$_3$)·6H$_2$O afford [UO$_2$(**37**)$_2$(S)] or [UO$_2$(**37a**)(S)], where the equatorial five coordination about the uranyl(VI) ion is reached by two β-diketonato moieties and one solvent molecule [110].

1-Ferrocenylbutane-1,3-dione (H–**37**), 1,3-diferrocenylpropane-1,3-dione (H–**38**), 1-ferrocenyl-3-phenylpropane-1,3-dione (H–**39**), 1-ferrocene-4,4,4-trifluorobutane-1,3-dione (H–**40**) and 4,4,4-trichloro-1-ferrocenylbutane-1,3-dione (H–**41**), prepared by Claisen condensation of acetylferrocene with the appropriate ester in the presence of sodium amide, sodium ethoxide or lithium diisopropylamide, form [Rh(**L**)(cod)] when treated with [Rh$_2$(Cl)$_2$(cod)$_2$] and [Cu(**L**)$_2$] with copper(II) acetate just as readily [111].

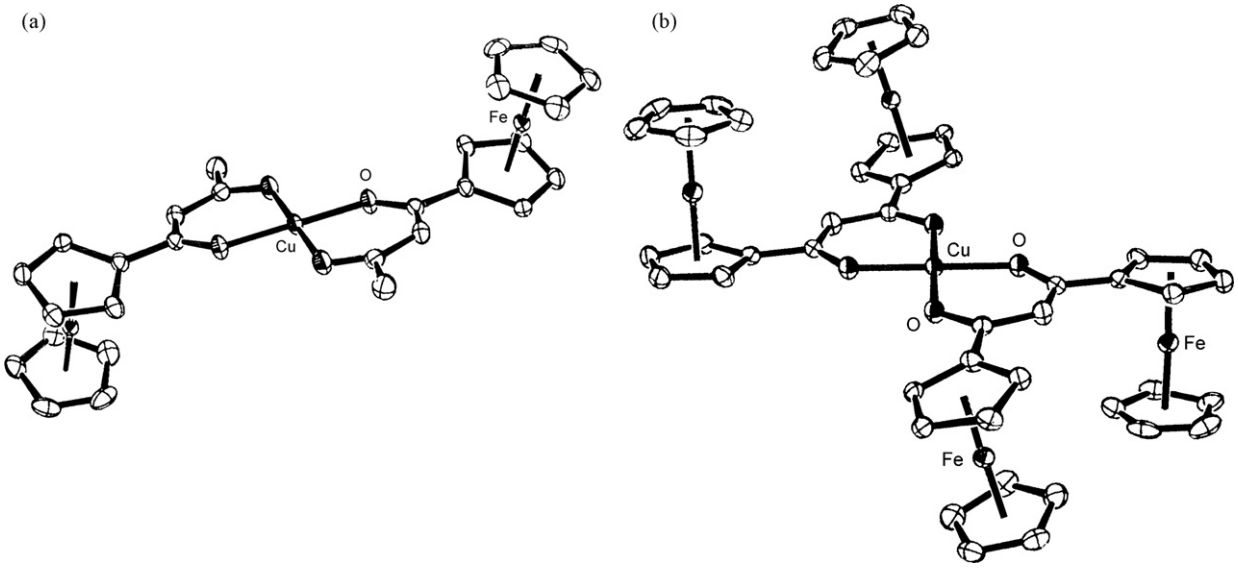

Fig. 27. Structures of [Cu(**37**)$_2$] (a) and [Cu(**38**)$_2$] (b) [108].

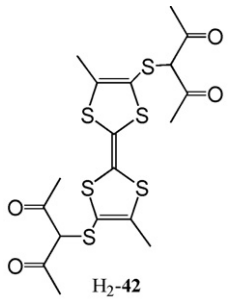

H_2-**42**

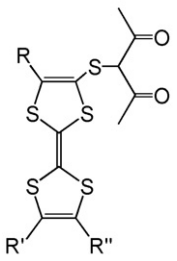

	R	R'	R''
H-**43**	CH_3	SCH_3	CH_3
H-**44**	CH_3	CH_3	CH_3
H-**45**	SCH_3	SCH_3	SCH_3
H-**46**	SCH_3	SCH_3	SC_2H_5
H-**47**	SCH_3	SC_4H_9	SC_4H_9

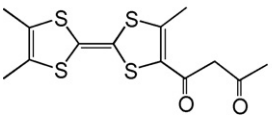

H-**48**

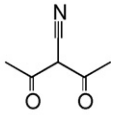

H-**49**

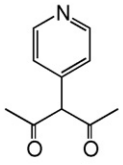

H-**50**

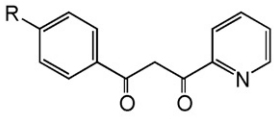

	R
H-**51a**	CH_3
H-**51b**	H

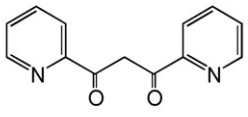

H-**51c**

Treatment of [Rh(**L**)(cod)] with CO affords [Rh(**L**)$(CO)_2$] (H–**L** = H–**37**, H–**38**, H–**40**) in a better yield than the treatment of [Rh(Cl)$(CO)_2$] with H–**L**. In [Rh(**40**)$(CO)_2$] the rhodium(I) ion is square planar with two *cis* CO ligands. The further reaction with PPh_3 affords [Rh(**40**)$(PPh_3)(CO)_2$]. The formal reduction potential for the electrochemically reversible one electron oxidation of the ferrocenyl group varies between 0.304 V (for the complex with [**40**]$^-$) and 0.172 V (for the complex with [**38**]$^-$) versus Fc^+/Fc in a manner that could be directly traced to the electronegativities of the R groups of the β-diketonato ligands, as well as to the pK_a' values of the free β-diketones. Anodic peak potentials for the dominant cyclic voltammetry peak associated with rhodium(I) oxidation are between 0.718 V (for the complex with [**39**]$^-$) and 1.022 V (for the complex with [**37**]$^-$) versus Fc/Fc^+. Coulombmetric experiments implicate a second, much less pronounced anodic wave for the apparent two-electron rhodium(I) oxidation that overlaps with the ferrocenyl anodic wave and that the redox processes associated with these two rhodium(I) oxidation waves are in slow equilibrium with each other [112].

$LnCl_3{\cdot}6H_2O$ (Ln = Yb, Lu) and 2 equiv.of H–**39** in methanol in the presence of $N(C_2H_5)_3$ hydrolyse to [Ln_4(**39**)$_8$(μ-OH)$_4$], made up of a distorted Ln_4O_4 cubane core consisting of four μ_3-oxygen atoms while the eight [**39**]$^-$ ligands build up the peripheral part of the cluster making them lipophilic and enabling the clusters to dissolve in a huge range of organic solvents like chloroform, dichloromethane and toluene. The oxygen atoms of the clusters core are μ_3-coordinated, these oxygen atoms being part of hydroxyl groups. The [**39**]$^-$ ligands are uniformly η^2-coordinated to each metal centre (Fig. 29) [113,114].

In [Ln(**39**)$_3$(phen)] (Ln = La, Nd, Eu, Yb), obtained by addition of 1,10-phenanthroline to [Ln(**39**)$_3(H_2O)_2$] in 1,2-dichloroethane, the eight coordinate lanthanide(III) ion is bound by the oxygen atoms of three [**39**]$^-$ ligands and two nitrogen atoms of the phenanthroline ligand as found in the [Nd(**39**)$_3$(phen)] (Fig. 30a) [113].

3,8-Bis(ferrocenyl-ethynyl)-1,10-phenanthroline (Fc_2phen) was used with the aim to improve the solubility in organic solvents of the related complexes [Ln(**L**)$_3$(Fc_2phen)] (Ln = La, Nd, Eu, Yb; H–**L** = H–**6**, H–**17**, H–**37**), obtained by mixing equimolar amounts of Fc_2phen and [Ln(**L**)$_3(H_2O)_2$] in dichloroethane, and to expand the π-system of the phenanthroline ring in order to produce a red shift of the excitation wavelength. The ligand was prepared by reacting under argon 3,8-dibromo-1,10-phenanthroline, ferrocenylacetylide, [Pd$(PPh_3)_2(Cl)_2$], CuI and diisopropylimide followed by the addition of dry *N*,*N*-dimethylformamide and after 2 days of an aqueous solution of potassium cyanide, separation of the organic phase and purification of the resulting product by chromatography on a silica column. In [Nd(**17**)$_3$(Fc_2phen)] three [**17**]$^-$ ligands and one 3,8-bis(ferrocenyl-ethynyl)-1,10-phenanthroline ligand coordinate to the distorted dodecahedral neodymium(III) ion. The two ferrocene moieties are oriented opposed to each other with respect to the axis along the ethynyl bridges (Fig. 30b). The best luminescence properties were found for [Ln(**6**)$_3$(Fc_2phen)] where visible light with a wavelength up to 420 nm (blue light) could be used for excitation of the europium(III), neodymium(III) and ytterbium(III) ions. The presence of the ferrocene moieties shifts the ligand absorption bands of the rare-earth complexes to longer wavelengths so that the complexes can be excited not only by ultraviolet radiation but also by visible light of wavelengths up to 420 nm. Red photoluminescence is observed for the europium(III) complexes and near-infrared photoluminescence for the neodymium(III) and ytterbium(III) complexes [114].

6.2. Tetrathiafulvalene containing complexes

Various redox-active ligands, where the electroactive lead is played by the tetrathiafulvalene (TTF) moiety, have been prepared with the aim of forming via their coordination to a metal ion hybrid organic–inorganic building blocks. Depending on the coordination function and on the number of free coordination sites, modulation of the molecular architectures and electronic properties can be envisioned in regard to the preparation of multifunctional materials.

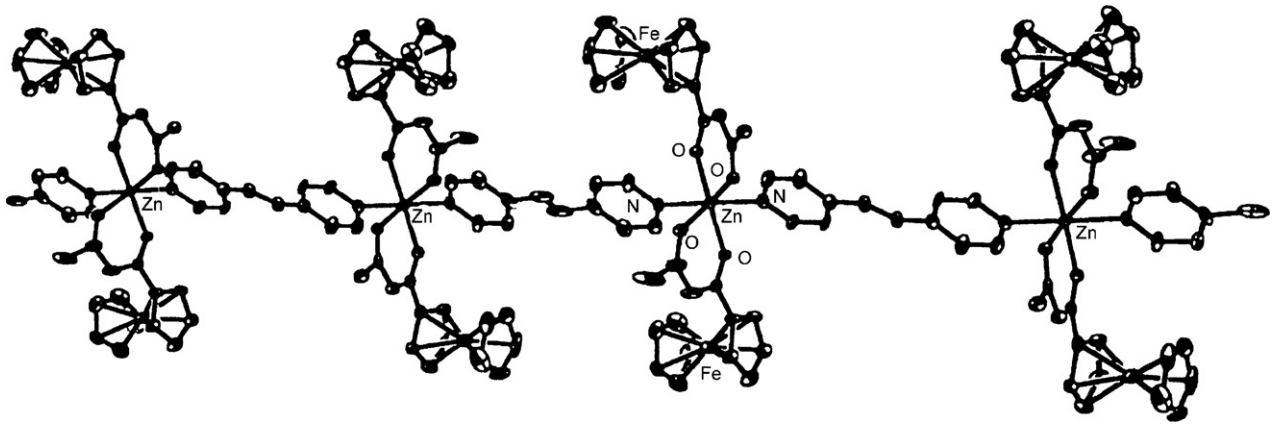

Fig. 28. Structure of $\{[Zn(\mathbf{37})_2(bpe)]\cdot 2H_2O\}_\infty$ [109].

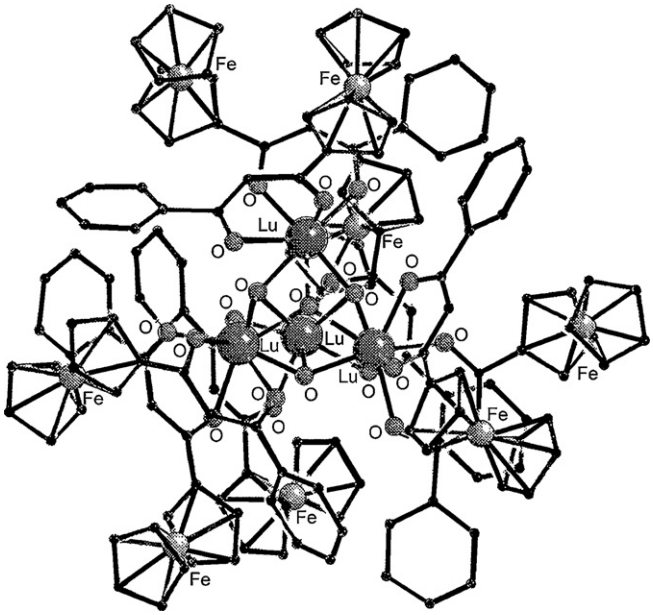

Fig. 29. Structure of $[Lu_4(\mathbf{39})_8(\mu\text{-}OH)_4]$ [113].

H_2–**42**, H–**43** and H–**44**, prepared according to Scheme 9a, form the related nickel(II), cobalt(II) and manganese(II) complexes, whose insolubility precludes any further electrochemical investigation or the use of these building blocks to prepare redox-active materials. On the contrary, the similarly prepared ligands H–**45**, H–**46** and H–**47**, which are in the enol form in solution and in the solid state as confirmed by X-ray structural determinations [115,116], form the soluble complexes $[M(\mathbf{L})_2]$ ($M = Zn^{II}$, Ni^{II}), when reacted with the appropriate metal(II) acetate at 0 °C in tetrahydrofuran/methanol. The complexes $[M(\mathbf{L})(py)_2]$, obtained by dissolving $[M(\mathbf{L})_2]$ in pyridine, contain an octahedral metal(II) ion is chelated in the equatorial plane by two $[\mathbf{L}]^-$ ligands and by two axial pyridine molecules (Fig. 31a) [116].

Moreover H–**48**, prepared according Scheme 9b, when treated with the appropriate metal(II) acetate in tetrahydrofuran gives rise to $[M(\mathbf{48})_2(H_2O)_2]$ ($M = Cu^{II}$, Ni^{II}, Zn^{II}), which turns into $[M(\mathbf{48})_2(S)_2]$ (S = pyridine, dimethylsulfoxide) in coordinating solvents, as proved by the X-ray structure of $[Zn(\mathbf{48})_2(DMSO)_2]$ where the six coordinate zinc(II) ion is chelated by two $[\mathbf{48}]^-$ ligands in the equatorial plane with the axial position occupied by two dimethylsulfoxide molecules (Fig. 31b) [117].

The complexes $[M(\mathbf{45})_2(py)_2]$ ($M = Ni^{II}$, Zn^{II}) exhibit two main reversible systems, the first one being broader (+0.00 V for the zinc(II) complex and +0.00/+0.08 V for the nickel(II) complex vs. Fc^+/Fc) than the second one (+0.33 V for the zinc(II) complex and +0.37 V for the nickel(II) complex vs. Fc^+/Fc). Thin-layer cyclic voltammetry shows that each system involves the exchange of two electrons. The first oxidation wave was deconvoluted into two peaks corresponding to a one-electron process for each with a well-defined separation for the $[Zn(\mathbf{45})_2(py)_2]$. The second oxidation wave is a two-electron process. The splitting of the first system indicates that the two TTF cores in one complex oxidize successively into cation radical species, which subsequently oxi-

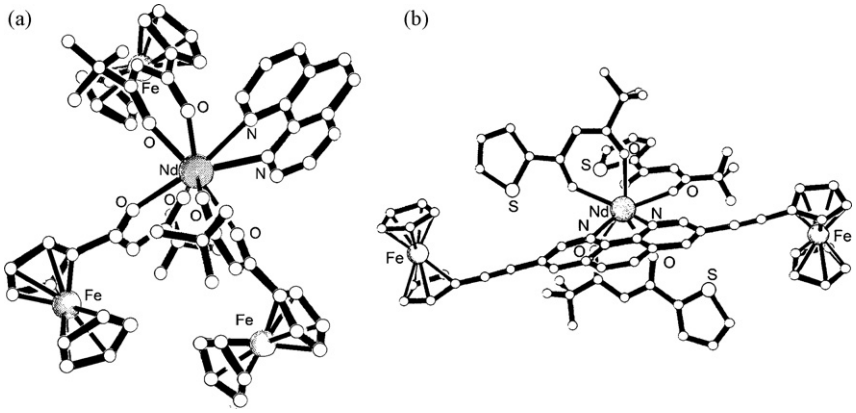

Fig. 30. Structures of $[Nd(\mathbf{39})_3(phen)]$ (a) [113] and $[Nd(\mathbf{17})_3(Fc_2phen)]$ (b) [114].

dize simultaneously into the dication species, accordingly to the sequence described in scheme. This splitting, independent of the concentration, shows the existence of intramolecular electronic interactions between the two TTF cores within the zinc(II) and the nickel(II) complexes, also confirmed by the UV–vis-near IR investigation carried out after the chemical oxidation of $[M(\mathbf{45})_2(py)_2]$ by a successive aliquot addition of $NOSbF_6$. In both cases, chemical oxidation with 1 equiv. of $NOSbF_6$ leads to the appearance

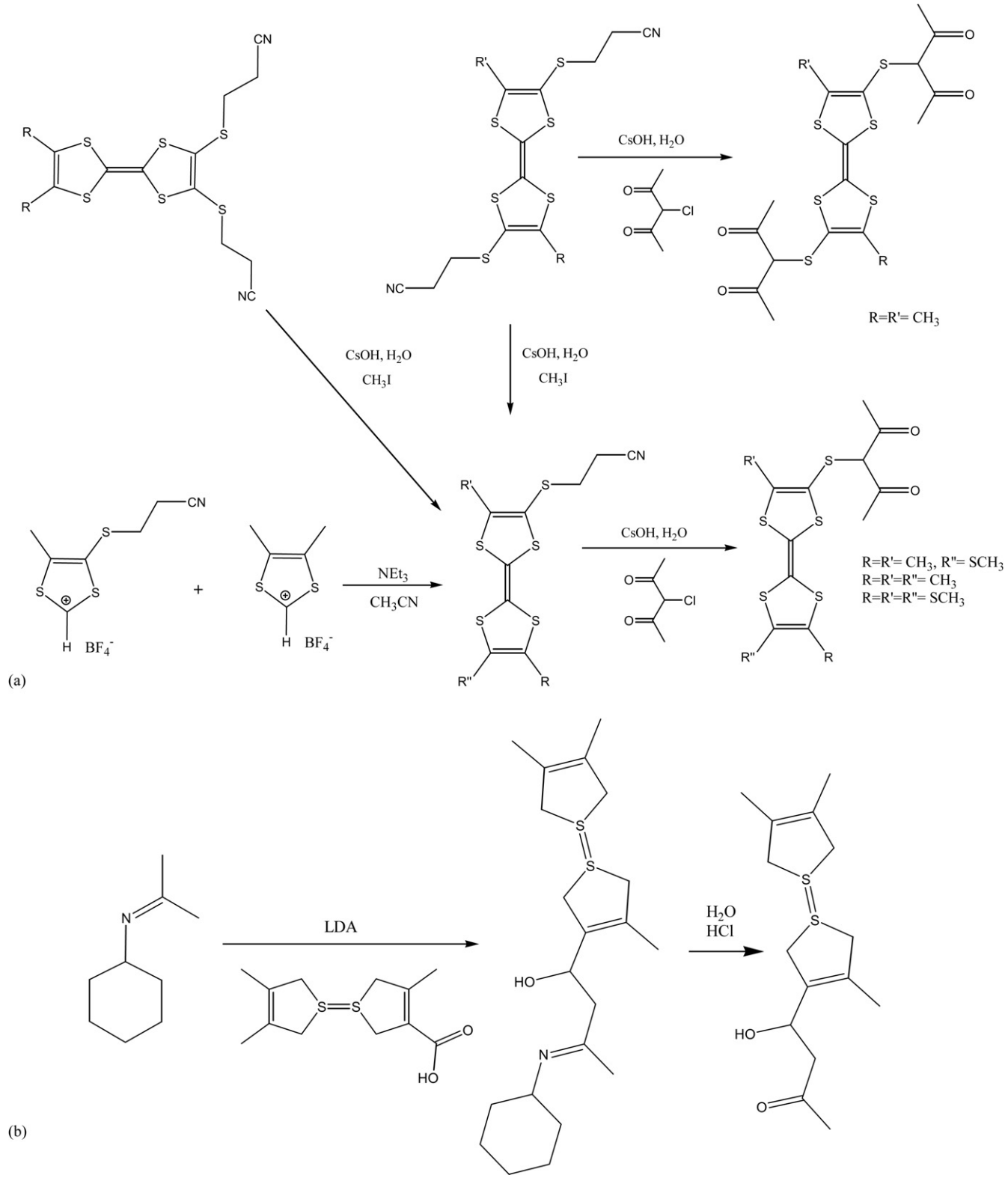

Scheme 9. Preparation of electroactive tetrafulvalene-containing ligands.

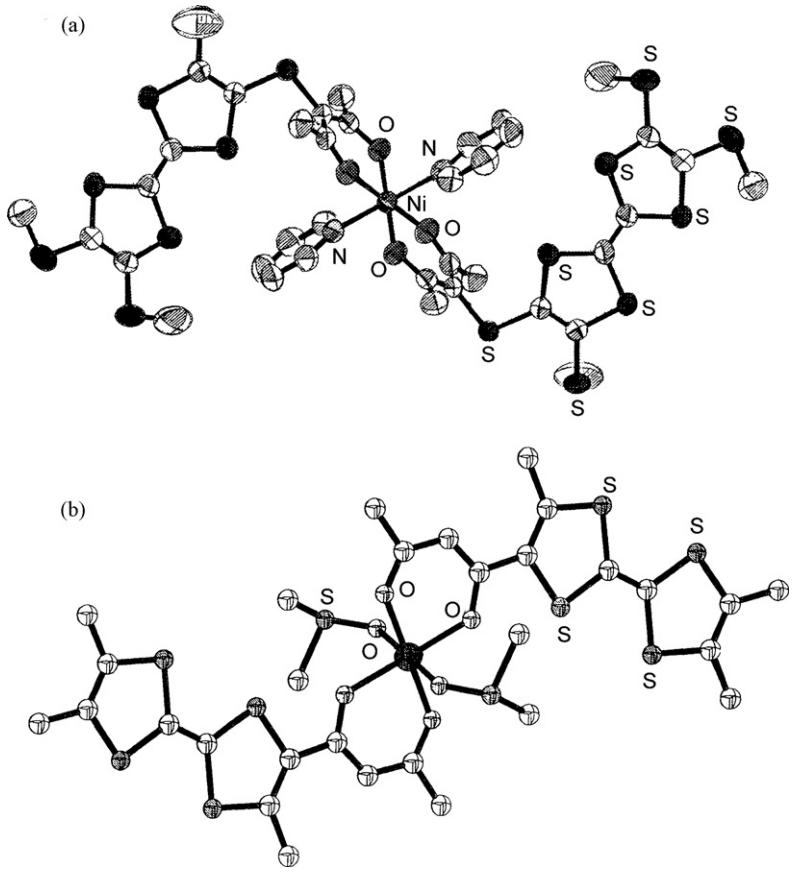

Fig. 31. Structures of $[Ni(\mathbf{45})_2(py)_2]$ (a) [116] and $[Zn(\mathbf{48})_2(DMSO)_2]$ (b) [117].

of new bands, diagnostic of the formation of the cation radical species. As expected, the maximum absorption for the two former bands is obtained with 2 equiv. of the oxidizing agent. Interestingly, a weaker and broader band is also observed at 2200 nm, which reaches its maximum with 1 equiv. of the oxidizing agent and disappears upon the addition of another equivalent of $NOSbF_6$. This band, more intense for the nickel(II) complex than for the zinc(II) one and independent of the concentration in CH_2Cl_2, is observed at low concentration in a mixture of CH_3CN/CH_2Cl_2, suggesting the formation of an intramolecular mixed-valence species during the addition of 1 equiv. of $NOSbF_6$ [117].

A similar cyclic voltammetry behaviour was found for $[Zn(\mathbf{48})_2(L)_2]$ (L = pyridine, dimethylsulfoxide) or $[Ni(\mathbf{47})_2(py)_2]$ in CH_2Cl_2 and for $[M(\mathbf{48})_2(H_2O)_2]$ (M = Zn, Ni, Cu) in tetrahydrofuran. It was verified also that tuning of the redox properties of the TFF can be achieved by changing the apical ligand of the six coordinated metal complexes from water to dimethylsulfoxide or pyridine [117].

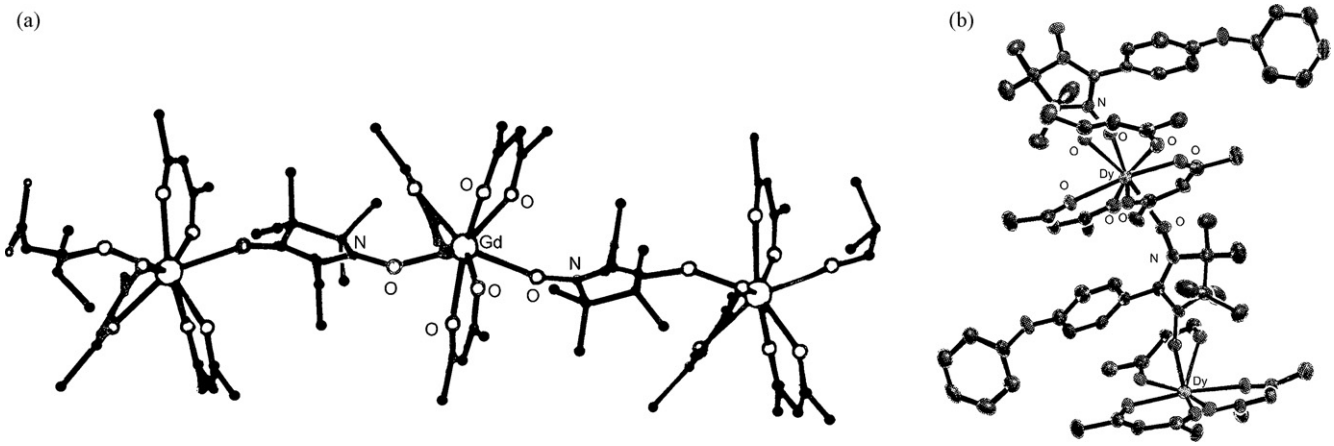

Fig. 32. Structures of $[Gd(\mathbf{10})_3(NIT\text{-}C_2H_5)]_\infty$ (a) [122] and $[Dy(\mathbf{10})_3(NIT\text{-}C_6H_4OC_6H_5)]_\infty$ (b) [123].

6.3. Redox and photoactive complexes

H–**6a**, prepared from 4-methyl-benzoyl acid-methyl ester and tolyl acetone in the presence of NaH, reacts with $RuCl_3$ to form [Ru(**6a**)$_3$] which by subsequent reduction with Zn–Hg amalgam in acetonitrile and water, produces *cis*-[Ru(**6a**)$_2$(CH_3CN)$_2$]. The final addition of the Schiff base 1-(4-hydroxy-5-[(pyridin-2-ylmethylene)-amino]-methyl-tetrahydro-furan-2-yl)-5-methyl-1*H*-pyrimidine-2,4-dione (L), prepared by refluxing 5′-amino-5′-deoxy-thymidine and 2-pyridinecarboxaldehyde in anhydrous ethanol, gives a diastereomeric mixture of [Ru(**6a**)$_2$(L)], separated by chromatography [118]. [Ru(**6a**)$_2$(L)] belongs to the class of redox- and photoactive transition-metal complexes that function as spectroscopic probes for photophysical studies in nucleic acids. These complexes have been used to study long-range electron transfer and energy transfer in DNA, DNA hybridization, and the development of biosensors. Modification of the 5′ position of thymidine by covalent attachment of iminopyridine allows access to both metal complexes and does not complicate the phosphoramidation at the 3′ position, which is necessary for the incorporation of metal nucleosides into DNA [119–121]. Electrochemical ($E_{1/2}$ = 0.265 V vs. NHE) and electronic (λ_{max} = 600, 486 nm) data indicate that [Ru(**6a**)$_2$(L)] is a suitable probe for DNA-mediated ground-state electron-transfer studies [118].

7. β-Diketonato complexes containing radicals as ligands

The linear chain lanthanide(III) β-diketonate complexes with nitronyl-nitroxide radicals [Ln(**10**)$_3$(NIT-R)]$_\infty$ have been prepared by mixing [Ln(**10**)$_3$(H_2O)$_2$] (Ln = Gd, Dy, Tb, Eu, Ho, Tm) with the appropriate nytronyl-nitroxide radical NIT-R (NIT-R = 2-(4′-R)-4,4′,5,5′-tetramethylimidazoline-1-oxyl-3-oxide; R = C_2H_5, $CH_2CH(CH_3)_2$, $C_6H_4OC_6H_5$) in non-coordinating solvents. In these complexes the nytronyl-nitroxide radicals bridge two different lanthanide(III) ions, giving rise to a 1D-linear chain molecular framework. The metal ions are eight coordinate, their dodecahedral environment being completed by three chelating [**10**]$^-$ ligands (Fig. 32a and b) [122,123].

The magnetism of this type of lanthanide-radical chain is characterized by the presence of nearest neighbour (NN) ferromagnetic metal–radical and next-nearest neighbour (NNN) antiferromagnetic metal–metal or radical–radical magnetic coupling (J_{Mr}, J_{MM}, and J_{rr}, respectively). The overall behaviour at low temperature depends on the ratio between ferro- and antiferromagnetic interactions. The low-temperature powder data suggest that ferromagnetic interactions dominate [121–123].

Furthermore, [Dy(**10**)$_3$(NIT$C_6H_4OC_6H_5$)] represents a successful preparation of a single chain magnet from a material known to undergo 3D magnetic ordering. The chains exhibit all the features of a slowly relaxing system, including a crossover between two Arrhenius regimes, and a hysteresis loop opens below 3 K. The observation of such a crossover in [Dy(**10**)$_3$(NIT$C_6H_4OC_6H_5$)], if due to finite-size effects, would suggest a significant contribution to the barrier coming from the anisotropic building blocks, as the barrier is not exactly halved. This allows one to investigate the effect of the dynamics of rare-earth single-ion units when arranged in chains. These dynamic features are accompanied by a very rich static behaviour that could be due to the interplay of NN and NNN interactions, with the presence of several low-energy states [122].

[Tm(**10**)$_3$(NIT$C_6H_4OC_6H_5$)]$_\infty$ belongs to the family of single chain magnets. Both static and dynamic magnetic measurements and a dependence of the out-of-phase signal on the frequency, observed below 3 K, indicate Ising magnetic anisotropy. Comparison of the extracted parameters with those of other isostructural lanthanide compounds confirms a trend along the lanthanide series [123].

Very little data are available on the magnetic anisotropy of thulium(III) which often is EPR-silent. Magnetic measurements confirm a sizeable magnetic anisotropy. In particular dc measurements confirm the trend observed in the position and in the with of unusual steps in magnetization curves, which is characteristic of the anisotropic lanthanide(III) ions. They also give access to a value of the intra-chain exchange interaction. Dynamic measurements agree with a trend on the blocking temperature of the family, with the thulium(III) compound fitting between holmium(III) and erbium(III) derivatives. It confirms the importance of the single-ion anisotropy in building one-dimensional lanthanide-based magnets, showing that fine tuning of the behaviour of these isostructural magnets can be achieved by choosing the appropriate lanthanide(III) ion [123].

Also, the 1D-magnetic chains [M(**10**)$_2$(NITC_6H_4OR)]$_\infty$ (M = Mn^{II}, Co^{II}, Cu^{II}; R = H, CH_3) have been obtained; again the radicals act as bridging building block in the formation of 1D-magnetic chains, showing slow relaxation of the magnetization and hysteresis effect. In particular [Co(**10**)$_2$(NIT$C_6H_4OCH_3$)]$_\infty$ consists of alternating {Co(**11**)$_2$} and radical moieties arranged in 1D arrays with a helical structure arising from the trigonal crystallographic lattice. Similar structures have been reported for the manganese analogue (Fig. 33a) [124,125].

The temperature dependence of χT of the cobalt(II) complex indicates 1D ferrimagnetic behaviour. The rapid increase of χT below 100 K suggests strong intrachain interactions as observed in 1D ferro- and ferrimagnets. Antiferromagnetic coupling between cobalt(II) and the NIT$C_6H_4OCH_3$ radical is suggested by the temperature dependence of the magnetic susceptibility of the mononuclear complex [Co(**10**)$_2$(NIT$C_6H_4OCH_3$)$_2$], where the coordination of the central cobalt(II) ion is essentially the same as in the chain compound. The unique feature of [Co(**10**)$_2$(NIT$C_6H_4OCH_3$)]$_\infty$ its highly one-dimensional nature, allowed to record the slow relaxation of the magnetization in the paramagnetic phase of a 1D compound. The different magnetic behaviour of the manganese(II) derivative, which orders ferrimagnetically at 4.6 K is because of the almost negligible anisotropy of the manganese(II) centers. The anisotropy of the cobalt–radical exchange interaction in the chain gives a barrier for the reorientation of the magnetization. This, combined with the smaller spin of cobalt(II) compared to manganese(II) centers, determines slow relaxation of the magnetization before the weak interchain dipolar interaction can induce three-dimensional magnetic order [124,125].

1D magnetic systems are well known to be able to show long-range order only at 0 K. The research in molecular magnetism of the last two decades therefore has been characterized by strong efforts to efficiently connect magnetic chains in 3D networks to observe bulk magnetism. It was shown that magnetic bistability and the related memory effect can indeed be observed in a 1D material without requiring any interchain interaction. These results may open new perspectives including that of storing information in a single magnetic polymer as well as in the novel class of 1D materials where ionic structures are obtained inside carbon nanotubes [124,125].

In [Mn(**10**)$_2$(L)]$_n$, resulting from the coordination of [Mn(**10**)$_2$] with the biradical ligand L obtained by grafting two nitronyl nitroxide radicals in the 5 and 5′ protons of a 2,2′bipyridine ligand, the bipyridine moiety acts as a chelate toward one {Mn(**10**)$_2$} unit, while the pendent nitronyl nitroxide radicals are symmetrically bound in *trans* configuration to additional {Mn(**10**)$_2$} units, giving rise to an infinite chain with a biradical bridging {Mn(**10**)$_2$} units and pending {Mn(**10**)$_2$(bipyridine)}cores (Fig. 33b) [126].

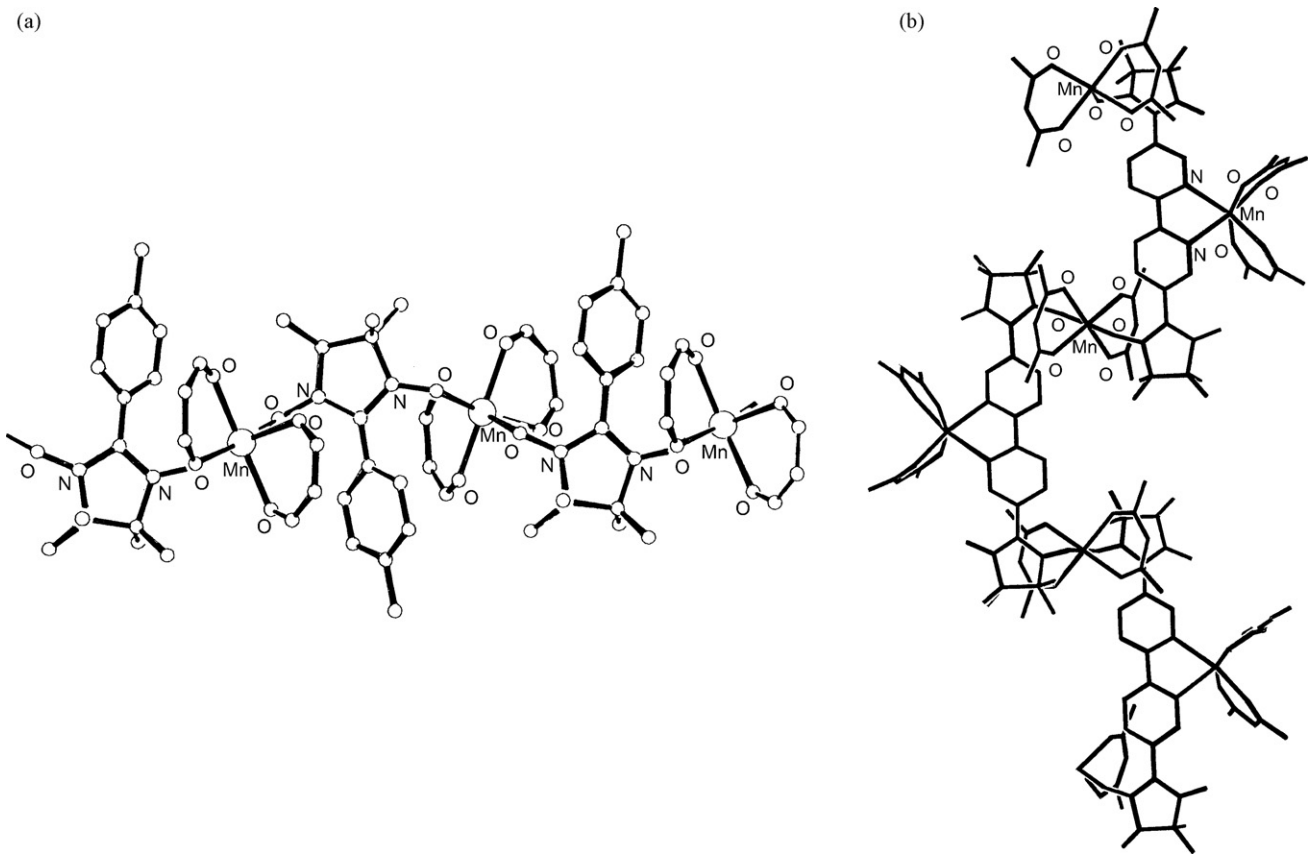

Fig. 33. Structure of $[Mn(\mathbf{10})_2(NIT\text{-}C_6H_4OCH_3)]_\infty$ (a) [124,125] and $[Mn(\mathbf{10})_2(L)]_\infty$ (L = 5,5′-nitronylnitroxide-2,2′-bipyridine) (b) [126].

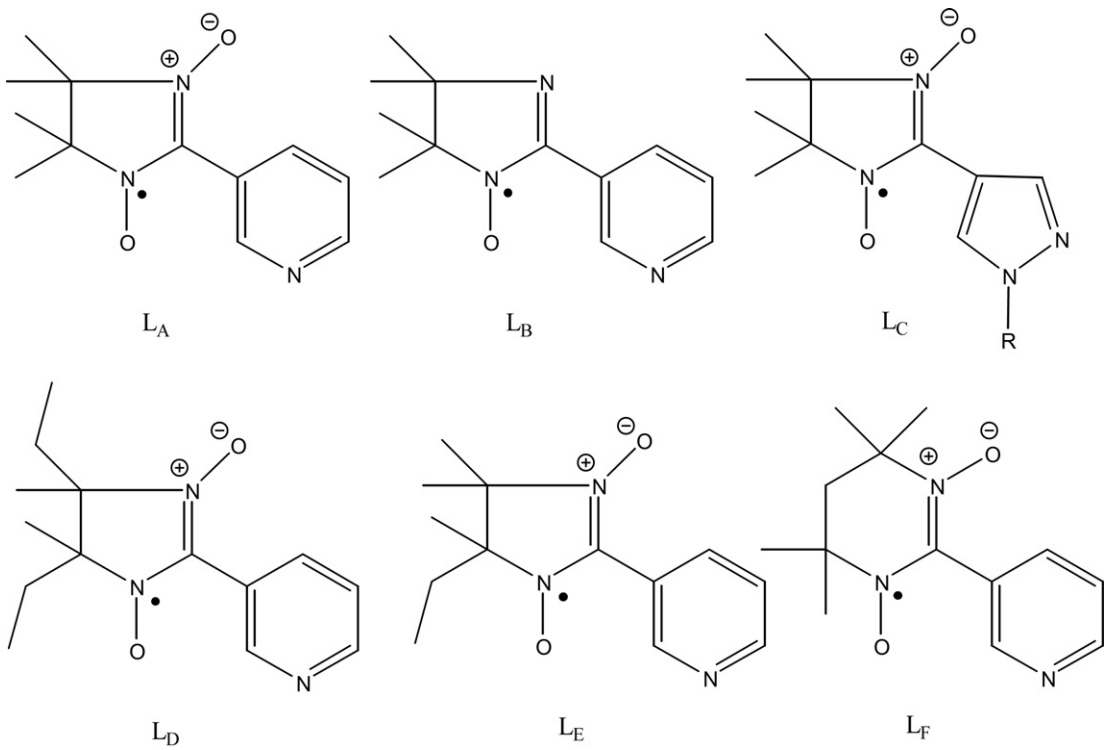

Scheme 10. Nitroxide ligands used in the design of spin-transition-like copper(II) complexes.

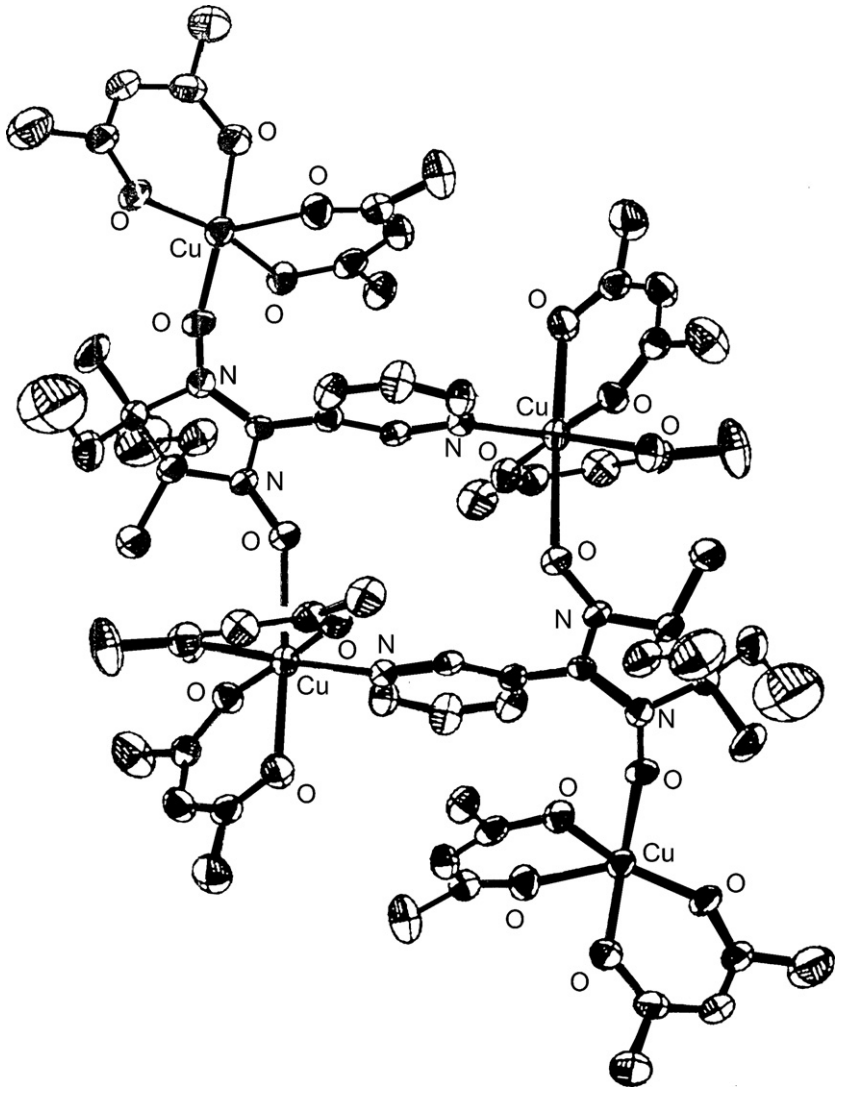

Fig. 34. Structure of $[Cu_4(\mathbf{10})_8(L^D)_2]$ [127].

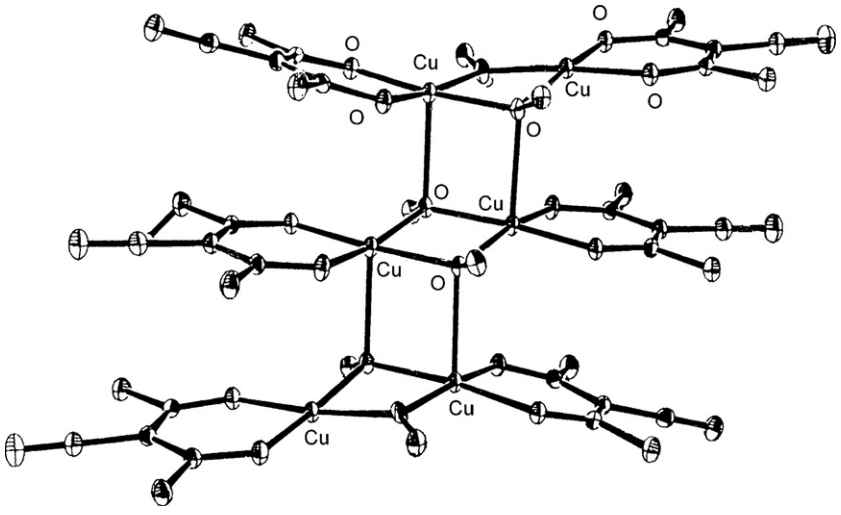

Fig. 35. Structure of $[Cu_6(\mathbf{49})_6(\mu_3\text{-}OCH_3)_4(\mu\text{-}OCH_3)_2]$ [128].

The magnetic behaviour of this complex is dominated by the strong antiferromagnetic interactions ($J = -203\,cm^{-1}$) due to the radical centers directly bound to manganese(II) ions while a second antiferromagnetic interaction ($J' = -0.62\,cm^{-1}$) results from the coupling of the peripherical nitronyl nitroxide radicals with the central manganese(II) ions coordinated to the bipyridine moiety. Qualitatively, the minimum found in the susceptibility measurements closely matches the value expected for a ground spin state $S = 3/2$ added to a spin $S = 5/2$ imported by the additional manganese center. The susceptibility increase found at cryogenic temperature was viewed as the result of fictive ferromagnetic coupling related to the true antiferromagnetic coupling J_1 between the pseudospin $S = 3/2$ and spin $S = 5/2$ of the additional manganese ion [126].

Mononuclear, dinuclear and tetranuclear copper(II)-nitroxide complexes have been prepared with the nitroxide ligands L_A–L_F of Scheme 10. In the mononuclear complexes [Cu(**10**)$_2$(L)$_2$], prepared by reaction of [Cu(**10**)$_2$] and the appropriate ligand L in a 1:2 molar ratio in heptane, two radical ligands coordinate to the copper(II) ion by their pyridyl nitrogen while the oxyl groups are not coordinated. In these complexes the magnetic metal–ligand interaction is weak. Changing the [Cu(**10**)$_2$]:L ratio the dinuclear [Cu$_2$(**10**)$_4$(L)$_2$] and the tetranuclear [Cu$_4$(**10**)$_8$(L)$_2$] complexes occur, where L includes *meso*, chiral, and *racemic* 2-(3-pyridyl)-nitronyl nitroxides differently substituted in positions 4 and/or 5 by ethyl groups and pyrimidyl nitroxides, exhibiting a spin-transition-like behaviour have been prepared and characterized. Depending on the stoichiometry of the reaction, tetranuclear and binuclear complexes were obtained whose structures are cyclic. The tetranuclear species, which include two intracyclic and two exocyclic metal sites, are similar to the previously reported complex of the tetramethylated analogue, while the binuclear complexes involve only endocyclic metal ions and have uncoordinated N-oxyl groups. The tetranuclear complexes exist as two isomers depending on the crystallization temperature: at room temperature, N-oxyl ligand coordination is axial–axial, while it is axial–equatorial at low temperature (Fig. 34). This isomerism concerns N-oxyl bonding to the exocyclic metal centers for the derivatives of 4,5-diethyl-substituted ligands while it involves the endocyclic metal site in the complex of the monoethylated ligand, which converts reversibly from a high-spin state to a low-spin state, as observed for the complex of the tetramethylated ligand. Binuclear complexes are diamagnetic at room temperature but convert to a paramagnetic state on warming (90–110 °C); the transition is irreversible and sharp [127].

8. β-Diketonato complexes with additional donor groups at the periphery of the coordinating moiety

The introduction of additional donor groups at the periphery of the coordinating moiety of β-diketones can give rise, via molecular assembly, to quite sophisticated supramolecular architectures.

A first example is represented by H–**49**, which reacts with $CuCl_2{\cdot}2H_2O$ in methanol and in the presence of $N(C_2H_5)_3$ to afford [Cu(**49**)$_2$]. The use of $Cu(NO_3)_2{\cdot}3H_2O$ instead of $CuCl_2{\cdot}2H_2O$ produces [Cu$_6$(**49**)$_6$(μ_3-OCH$_3$)$_4$(μ-OCH$_3$)$_2$], where two of the three independent copper ions are square pyramidal, coordinated to two oxygen atoms from a [**49**]$^-$ ligand and three methoxy ligands, though for one copper(II) ion the methoxy ligands all have μ_3-coordination whereas for the other copper(II) ion one of them bridges between only two copper centres. The third copper(II) ion is square planar, coordinated to two oxygen atoms from a [**49**]$^-$ ligand, one μ_2-methoxy ligand and one μ_3-methoxy ligand. The two outer {Cu$_2$(μ-OCH$_3$)$_2$(**49**)$_2$} units in the hexacopper complex are markedly curved, with the [**49**]$^-$ ligands bent away from the central {Cu$_2$(μ-OCH$_3$)$_2$} unit (Fig. 35) [128].

[Cu(**49**)$_2$] and $AgNO_3$ in dimethylformamide/methanol give [CuAg(**49**)$_2$(NO$_3$)]$_\infty$, where the copper(II) ion adopts a distorted square pyramidal geometry with the equatorial positions occupied by four oxygen atoms from two [**49**]$^-$ ligands and the axial position occupied by an oxygen atom of the nitrate anion. The silver ion adopts a distorted T-shaped geometry, being coordinated to two cyanide groups and also to the coordinated oxygen atom of the nitrate ion. Coordination to the two cyanide groups to the silver(I) ion links the {Cu(**49**)$_2$} units into one-dimensional polymeric chains. The bridging nitrate ligands interlink pairs of chains to form a ladder structure (Fig. 36) [128].

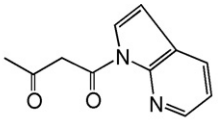

H-**52**

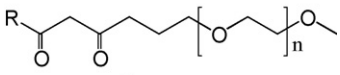

	R	n
H-**53a**	CH_3	1
H-**53b**	C_6H_5	1
H-**53c**	C_4H_9	1
H-**53d**	2,4,6-$(CH_3)_3C_6H_2$	1
H-**53e**	CH_3	2

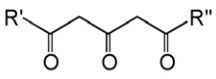

	R'	R''
H_2-**54a**	CH_3	CH_3
H_2-**54b**	C_6H_5	C_6H_5
H_2-**54c**	$C(CH_3)_3$	$C(CH_3)_3$
H_2-**54d**	$CH_3OC_6H_4$	$CH_3OC_6H_4$
H_2-**54e**	CF_3	CF_3
H_2-**54f**	$C(CH_3)_3$	CH_3
H_2-**54g**	C_6H_5	CH_3

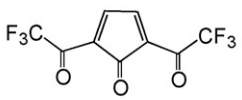

H-**55**

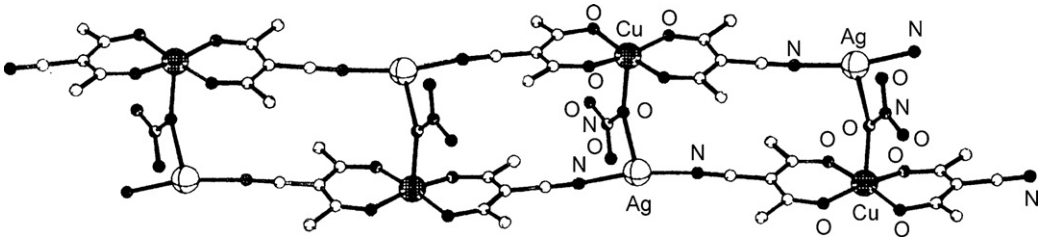

Fig. 36. Structure of [CuAg(**49**)$_2$(NO$_3$)]$_\infty$ [128].

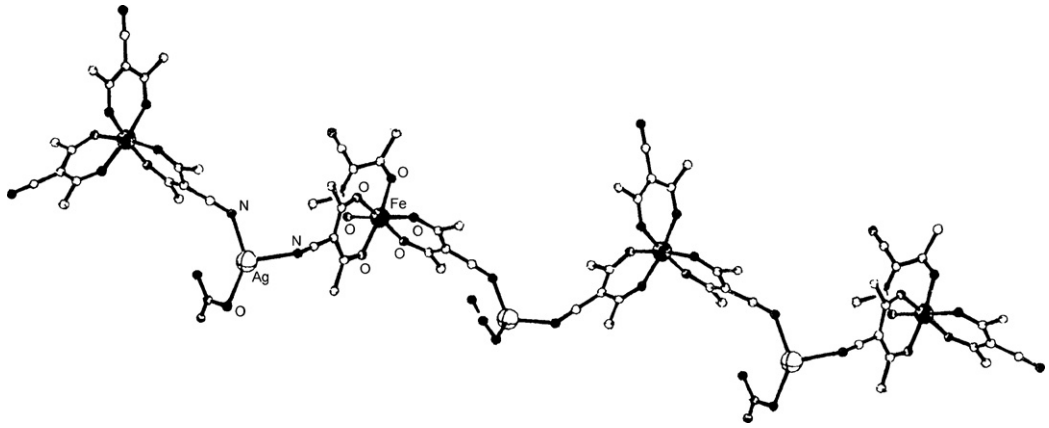

Fig. 37. Structure of $[FeAg(\mathbf{49})_3(NO_3)]_\infty$ [128].

In $[Fe(\mathbf{49})_3]$, synthesised from $Fe(NO_3)_3{\cdot}9H_2O$ and 3 equiv. of H–**49** in methanol in the presence of $N(C_2H_5)_3$, the distorted octahedral iron(III) ion is coordinated by six oxygen atoms from three $[\mathbf{49}]^-$ ligands. $[Fe(\mathbf{49})_3]$ and $AgNO_3$ in acetone/methanol give after two weeks a mixture of $\{[Fe_2Ag_2(\mathbf{49})_4(\mu\text{-}OCH_3)_2(NO_3)_2]{\cdot}CH_3COCH_3\}_\infty$ and $[Fe_2Ag(\mathbf{49})_4(\mu\text{-}OCH_3)_2(NO_3)]_\infty$, the former being the major product, and $[FeAg(\mathbf{49})_3NO_3]_\infty$ when left for longer periods.

In $[FeAg(\mathbf{49})_3(NO_3)]_\infty$ the iron(III) ion has the same coordination geometry as in $[Fe(\mathbf{49})_3]$, while the distorted trigonal planar silver ion is coordinated to two cyanide groups and to an oxygen atom from the nitrate ion; this enables the $\{AgNO\}_3$ units to bridge between $\{Fe(\mathbf{49})_3\}$ moieties and to link the iron complexes into one-dimensional chains (Fig. 37). One of the three cyanide groups present on each $\{Fe(\mathbf{49})_3\}$ moiety is uncoordinated and this prevents cross-linking of the chains into layers [128].

Each distorted octahedral iron centre of $\{[Fe_2Ag_2(\mathbf{49})_4(\mu\text{-}OCH_3)_2(NO_3)_2]{\cdot}CH_3COCH_3\}_\infty$ is coordinated to two bidentate $[\mathbf{49}]^-$ ligands and two methoxides which bridge two iron centres, leading to the formation of $\{Fe_2(\mathbf{49})_4(\mu\text{-}OCH_3)_2\}$ dimers. One four coordinate, flattened tetrahedral silver ion is linked to two cyanide groups and two nitrate groups; the other is three coordinate, and bound to two cyanide groups and one nitrate ion. One nitrate ion bridges the silver centres while the cyanide groups link the $\{Fe_2(\mathbf{49})_4(\mu\text{-}OCH_3)_2\}$ dimers into tapes. Each cyanide group of the dimer is coordinated and two silver centres link each dimer to its neighbour, generating [28]-membered rings. The bridging nitrate interlinks these tapes into a layer structure. The layers are connected into the gross structure by short Ag···Ag contacts (3.323 Å) (Fig. 38a). Also in $[Fe_2Ag(\mathbf{49})_4(\mu\text{-}OCH_3)_2(NO_3)]_\infty$, each iron centre is coordinated to two bidentate $[\mathbf{49}]^-$ ligands, while the bridging methoxide ligands lead to the formation of $\{Fe_2(\mathbf{49})_4(\mu\text{-}OCH_3)_2\}$ dimers. The distorted tetrahedral silver centre is surrounded by three nitriles and one oxygen atom of a nitrate anion. This coordination links the $\{Fe_2(\mathbf{49})_4(\mu\text{-}OCH_3)_2\}$ dimers into a one-dimensional tape structure. One of the nitriles on each dimer is uncoordinated, and as a consequence there are no coordination links between neighbouring tapes (Fig. 38b) [128].

$[Fe(\mathbf{49})_3]$ and $AgNO_3$ in methanol afford $[FeAg(\mathbf{49})_3(NO_3)]_\infty$ and $[Fe_2Ag_2(\mathbf{49})_4(\mu\text{-}OCH_3)_2(NO_3)_2]$ as major products, together with small quantities of $\{[Fe_2Ag(\mathbf{49})_4(\mu\text{-}OCH_3)_2](OH){\cdot}0.4H_2O\}_\infty$. In this complex the distorted octahedral iron centre is coordinated to two bidentate $[\mathbf{49}]^-$ ligands and two bridging methoxides, giving rise to $\{Fe_2(\mathbf{49})_4(\mu\text{-}OCH_3)_2\}$ dimers. The distorted tetrahedral silver centre is coordinated to four cyanide groups. Furthermore, all of the cyanide groups are coordinated to silver centres, giving rise to a three-dimensional network (Fig. 38c) [128].

$[Al(\mathbf{49})_3]{\cdot}6H_2O$, derived from equimolar methanolic solutions of $Al(NO_3)_3{\cdot}9H_2O$ and H–**49** in the presence of $NaHCO_3$, transmetalates when reacted with $AgNO_3$ in dimethylformamide/methanol affording $[Ag(\mathbf{49})]_\infty$. The silver(I) ion in a distorted T-shaped coordination mode is bound to two oxygen atoms from different $[\mathbf{49}]^-$ ligands and the nitrogen atom of a cyanide group. This coordination leads to the formation of a two-dimensional sheet structure containing both [12]- and [24]-membered rings. The *anti* conformation adopted by the $[\mathbf{49}]^-$ ligand prevents chelation of the oxygen atoms (Fig. 38d) [128].

H–**50**, prepared by the reaction of 4-methylpyridine with CH_3COCl in $CHCl_3$ at 20 °C followed by purification of the resulting residue by extraction with toluene and chromatography using hexane/ethylacetate as eluant [129], forms the square planar $[Cu(\mathbf{50})_2]$, the tetrahedral $[Be(\mathbf{50})_2]$, and the octahedral complexes $[M(\mathbf{50})_3]$ ($M = Al^{III}$, Fe^{III}) capable to act as building blocks in the formation of a group of metal organic frameworks (MOFs) by reaction with appropriate metal salts [130]. In particular, H–**50** and $Cu(NO_3)_2{\cdot}2.5H_2O$ in methanol/water/tetrahydrofuran and in the presence of $NaHCO_3$ form $[Cu(\mathbf{50})_2]{\cdot}2.5H_2O{\cdot}0.5THF$, where the copper(II) ion is in a slightly distorted square planar O_4 environment and the pyridyl rings are aligned approximately perpendicular to the coordinating moiety [131]. Furthermore, $Cu(CH_3COO)_2{\cdot}H_2O$ and H–**50** in ethanol/water at room temperature produces $[Cu(\mathbf{50})_2]{\cdot}0.5C_2H_5OH.3H_2O$, which turns into $[Cu(\mathbf{50})_2]$ by removal of solvate molecules under vacuum. Crystallization of $[Cu(\mathbf{50})_2]$ in a variety of solvents affords the related solvate complexes. The coordination about the copper(II) ion always is square planar, however the molecules self assemble in a two-dimensional square grid or a three-dimensional framework according to the solvent used. The major of the prepared complexes are two-dimensional square grid frameworks, while two solvate complexes are three-dimensional doubly interpenetrated frameworks. In these complexes one DMSO, one C_6H_6, one C_5H_5N or two CH_3CN guest molecules per square-grid unit are enclathrated between the square-grid $[Cu(\mathbf{50})_2]$ layers, respectively, with interlayer Cu···Cu separations of 7.65, 7.56, 7.42, and 7.43 Å. $[Cu(\mathbf{50})_2]{\cdot}4DMF$ and $[Cu(\mathbf{50})_2]{\cdot}4THF$ have very similar square-grid structures, but with larger numbers of solvent molecules and correspondingly larger Cu···Cu separations, 8.92 and 9.30 Å, respectively. In $[Cu(\mathbf{50})_2]{\cdot}0.5C_2H_5OH{\cdot}3H_2O$ and $[Cu(\mathbf{50})_2]{\cdot}0.1THF{\cdot}2.25H_2O$, two identical slightly distorted NbO three-dimensional frameworks are interpenetrated with each other. Despite this interpenetration, these compounds retain one dimensional pores of about 7 Å diameter which are filled with solvent molecules. In the 2D square grid frameworks, the solvent guest molecules have no specific interactions with one another (Fig. 39a); while in the 3D NbO frame-

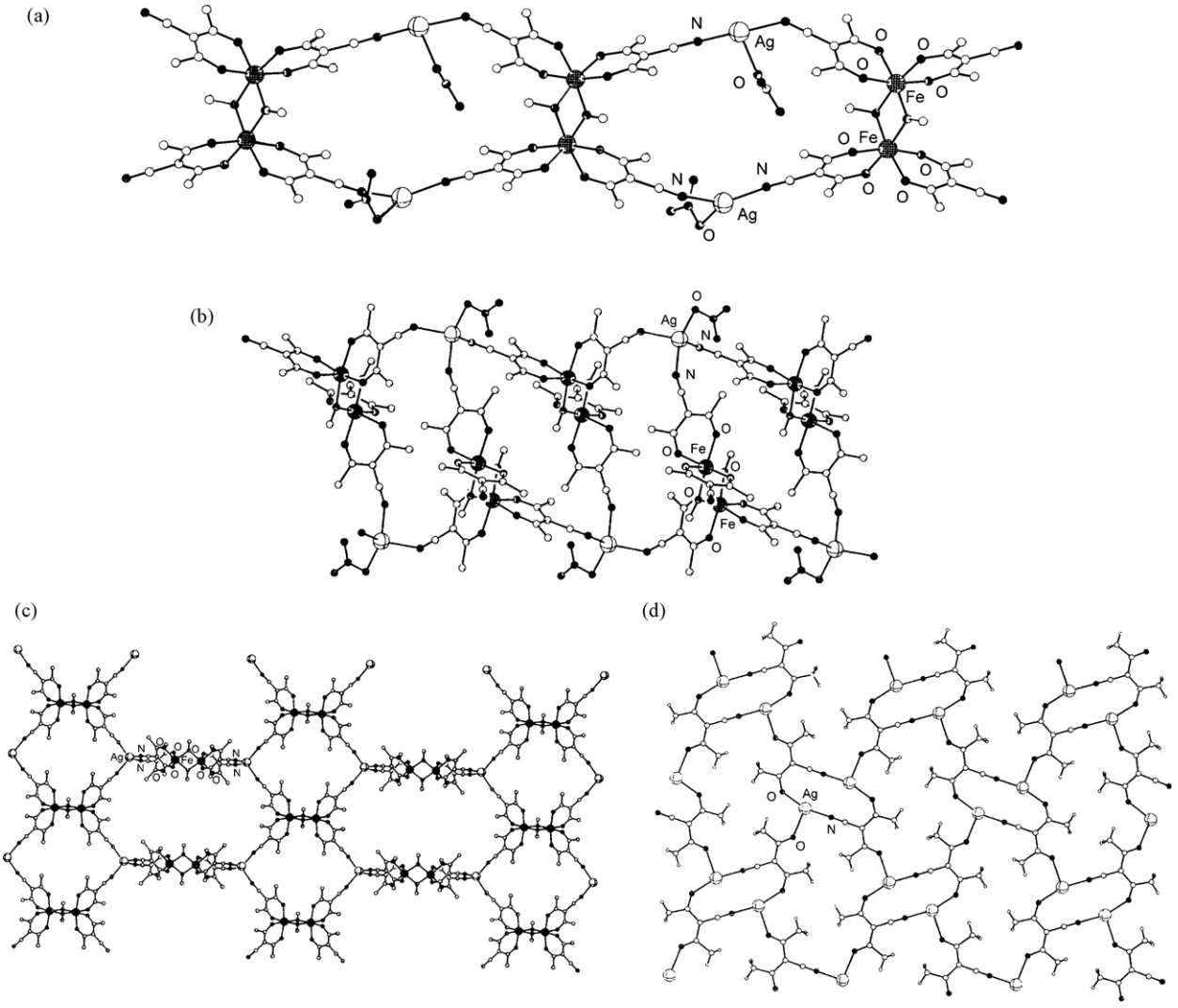

Fig. 38. Structures of $[Fe_2Ag_2(\mathbf{49})_4(\mu\text{-}OCH_3)_2(NO_3)_2]_\infty$ (a), $[Fe_2Ag(\mathbf{49})_4(\mu\text{-}OCH_3)_2(NO_3)]_\infty$ (b), $\{[Fe_2Ag(\mathbf{49})_4(\mu\text{-}OCH_3)_2](OH)\cdot 0.4H_2O\}_\infty$ (c) and $[Ag(\mathbf{49})]_\infty$ (d) [128].

works, the solvent guest molecules of $[Cu(\mathbf{50})_2]\cdot 0.5C_2H_5OH\cdot 3H_2O$ and $[Cu(\mathbf{50})_2]\cdot 0.1THF\cdot 2.25H_2O$ form hydrogen-bonded aggregates which support the interconnected one-dimensional pores in the 3D NbO $[Cu(\mathbf{50})_2]$ frameworks (Fig. 39b) [131].

$[Cu_3Cd(\mathbf{50})_6(NO_3)_2]\cdot 3CH_3OH\cdot 1.5THF$ and $[Cu_2Cd(\mathbf{50})_4(Cl)_2]\cdot 5H_2O.THF$ have been obtained over a period of two days by layering a methanol solution of $Cd(NO_3)_2\cdot 4H_2O$ or a water solution of $CdCl_2\cdot 2.5H_2O$, respectively, onto a tetrahydrofuran solution of $[Cu(\mathbf{50})_2]$. The Cu_3Cd complex is an example of a 1D non-interpenetrating ladder structure, with the 1D ladders stacked together in ABCABC packing. The pores in one 1D ladder are close to those in adjacent layers and b crystallographic directions, giving

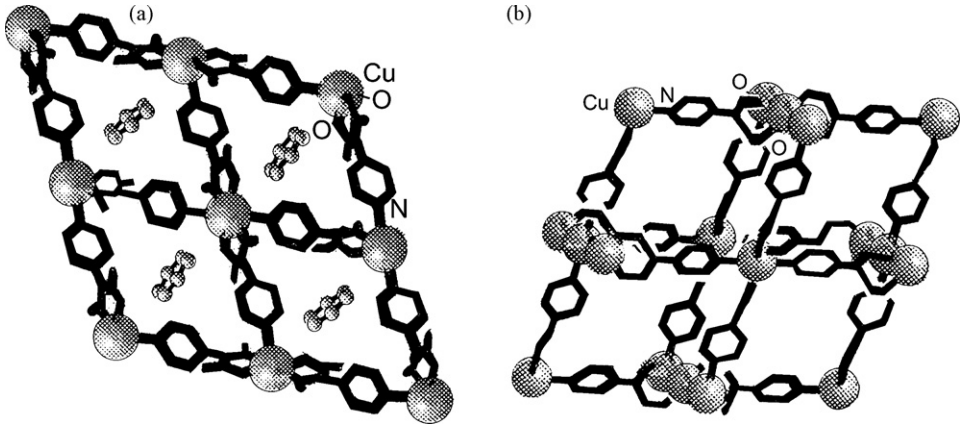

Fig. 39. The two-dimensional square grid framework of $[Cu(\mathbf{50})_2]\cdot C_6H_6$ (a) and the three-dimensional doubly interpenetrated framework of $[Cu(\mathbf{50})_2]\cdot 0.5C_2H_5OH.3H_2O$ (b), where the methyl groups and the solvent molecules are omitted for clarity [131].

rise to a 2D network of interconnected channels. The resulting pores occupy about 60% of the crystal volume. The Cu_2Cd complex has a 2D square-grid structure in which $\{Cd(Cl)_2\}$ units are bridged by $\{Cu(\mathbf{50})_2\}$ building blocks with a Cd···Cd and Cu···Cu distance of 19.718 Å. The 2D square-grid layers are stacked so as to repeat every six layers (ABCDEF... packing). The porosity of the Cu_2Cd complex is about 63% [132].

The copper sites in these two porous Cu_3Cd and Cu_2Cd M′MOFs are accessible for host–guest interactions. Encapsulation of solvent molecules to the copper sites occurs in the crystal structures of both the Cu_3Cd and Cu_2Cd complexes which turn opaque in air; the desolvated frameworks are stable up to about 220 and 210 °C, respectively, and then decompose [132].

In $[Be(\mathbf{50})_2]\cdot CH_3OH$, prepared from H–**50**, beryllium sulfate in aqueous pyridine solution followed by recrystallization of the precipitate from methanol/water, the tetrahedral beryllium(II) ion is coordinated by two β-diketonate moieties. $[Be(\mathbf{50})_2]$ is an extended connector for the generation of $[Be_2Co(\mathbf{50})_2(Cl)_2]\cdot H_2O$, $[Be_2Co(\mathbf{50})_2(SO_4)(CH_3OH)_2]\cdot H_2O\cdot CH_3OH$, $[Be_2Cu_2(\mathbf{50})_4(Cl)_3]$, $[Cu_2Be_2(\mathbf{50})_4(Br)_2]\cdot 5.33CHCl_3$ or $[Be_2Cu_2(\mathbf{50})_4(Br)_3]$ by reaction with the appropriate metal(II) salt in ethanol/chloroform [133].

$[Be_2Co(\mathbf{50})_2(Cl)_2]\cdot H_2O$ exists as a discrete molecular complex where two $\{Be(\mathbf{50})_2\}$ units act as monodentate ligands toward a central four coordinate cobalt(II) ion which is further linked by two chloride ions (Fig. 40a). Also in $[Be_2Co(\mathbf{50})_2(SO_4)(CH_3OH)_2]\cdot H_2O$ the two $\{Be(\mathbf{50})_2\}$ units connect two cobalt(II) ions, 18.41 Å apart, with the generation of a mixed-metal-organic chain. The coordination environment of the cobalt ion is completed with two *trans* oxygen atoms of the bridging sulfate anions, which give rise to Co···Co distance 5.39 Å and two methanol molecules (Fig. 40b). The isomorphous complexes $[Be_2Cu_2(\mathbf{50})_4(X)_3]$ (X = Cl, Br) are the mixed-valence species with copper–halogenide linkages closely related to molecular diamonds. The Cu_2X_2 ring involves both copper(I) and copper(II) ions, the latter coordinating an additional halogenide ion and thus making the valence state of the two copper centres easily distinguishable. The complexes adopt a one-dimensional structure and exist as double chains (Fig. 40c). In $[Be_2Cu_2(\mathbf{50})_4(Br)_2]\cdot 5.33CHCl_3$ an open 2D structure was observed, involving the square-like $\{Cu_2Br_2\}$ unit which serves as a four-connected point for the 2D regular square-grid networks where the two $\{Be(\mathbf{50})_2\}$ ligands bridge pairs of tetrahedral copper(I) ions at distances of 18.1–18.5 Å, and the successive layers are separated by only 4.1 Å. The structure is very open and enclathrates a set of guest molecules (Fig. 40d). Unfortunately, removal of the accumulated chloroform molecules leads to disintegration of the network and a loss of crystallinity [133].

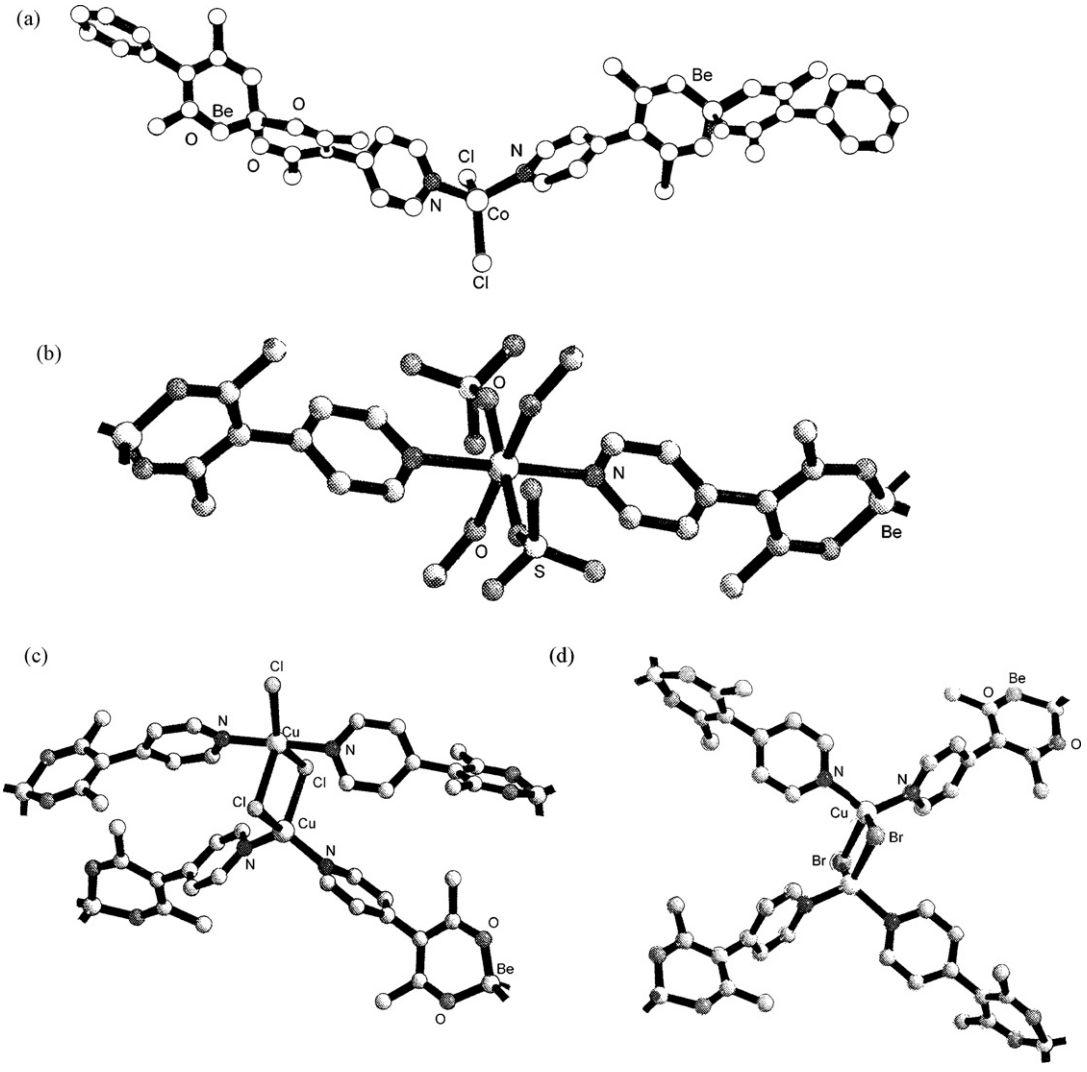

Fig. 40. Structures of $[Be_2Co(\mathbf{50})_2(Cl)_2]$ (a), $[Be_2Co(\mathbf{50})_2(SO_4)(CH_3OH)_2]_n$ (b), $[Be_2Cu_2(\mathbf{50})_4(Cl)_3]_n$ (c) and $[BeCu_2(\mathbf{50})_4(Br)_2]_n$ (d) [133].

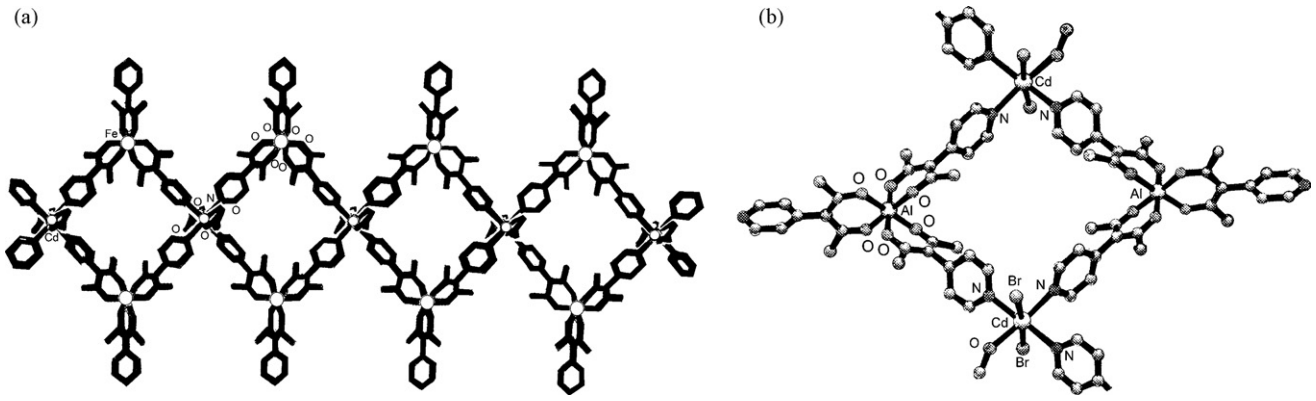

Fig. 41. Structures of $[Fe_2Cd\ (\mathbf{50})_6(NO_3)_2]_n$ (a) and $[AlCd(\mathbf{50})_3(Br)_2(CH_3OH)]_n$ (b) [133].

The distorted octahedral complexes $[M(\mathbf{50})_3]$ ($M = Al^{III}$, Fe^{III}), prepared by addition of $M(NO_3)_3{\cdot}nH_2O$ in water to a methanol solution of H–**50** neutralized with $NaHCO_3$, have structural features suitable to be used as triangular building blocks for the synthesis of heteropolynuclear polymers via complexation with the appropriate metal salts. Thus, $Cd(NO_3)_2{\cdot}4H_2O$ and $[Fe(\mathbf{50})_3]$ in methanol afford $\{[Fe_2Cd(\mathbf{50})_6(NO_3)_2]{\cdot}2H_2O\}_n$. Similarly, slow diffusion of $CoCl_2{\cdot}6H_2O$ into a methanol/chloroform solution of $[Al(\mathbf{50})_3]$ leads to $[Al_2Co(\mathbf{50})_6(Cl)_2]{\cdot}4CHCl_3{\cdot}2CH_3OH$. $[AlCo(\mathbf{50})_3(X)_2(CH_3OH)]$ ($X = NO_3^-$, Cl^-), containing a different amount of solvate molecules were synthesized in a similar way. These Al_2Co or AlCo complexes readily lose incorporated solvent molecules with disintegration of the structure. They are also unstable under the mother solution since the initially formed crystals lose crystallinity and dissolve in a period of 15–20 days. It was not possible to obtain crystals by the same method using $[Fe(\mathbf{50})_3]$: but only the isomorphous complexes $[M(\mathbf{50})_2(H_2O)_2]{\cdot}3H_2O$ ($M = Cd^{II}$, Co^{II}) [133].

$\{[Fe_2Cd(\mathbf{50})_6(NO_3)_2]{\cdot}2H_2O\}_n$, containing alternating cadmium(III) and iron(III) centres, exemplifies a 1D array of heterobimetallic squares sharing opposite vertices (Fig. 41a). The $\{Fe(\mathbf{50})_3\}$ units serve as angular bidentate connectors and the organic ligands bridge pairs of iron and cadmium ions at 10.0 Å. The six coordination of the cadmium ions includes the pyridyl nitrogen atoms of four $\{Fe(\mathbf{50})_3\}$ molecules and two *trans*-situated nitrate groups. The same structure was observed for $\{[Al_2Co(\mathbf{50})_6(Cl)_2]{\cdot}4CHCl_3{\cdot}2CH_3OH$. The chloride ions, which are *trans*-coordinated to cobalt(II) centres, have a smaller size than the nitrate groups in the Fe_2Cd complex: the liberated crystal volume is occupied by guest chloroform molecules, four per cobalt ion [133].

A 2D network takes place in $[AlCd(\mathbf{50})_3(NO_3)_2(CH_3OH)]{\cdot}2CHCl_3$ and $[AlCd(\mathbf{50})_3(Br)_2(CH_3OH)]{\cdot}2CHCl_3{\cdot}2CH_3OH$, where all the available side functionalities of $[Al(\mathbf{50})_3]$ are employed for binding with cadmium ions, resulting in the generation of a polymer. In the former complexes the cadmium ions adopt a distorted seven coordination including three pyridyl nitrogen atoms and oxygen atoms of monodentate and asymmetric-bidentate nitrate groups and a methanol molecule. In the latter complex, the six coordination of the cadmium ions is retained with two *trans*-situated bromide anions and also with three equatorial pyridyl nitrogen-donors and a methanol molecule. Thus, both the aluminum and cadmium ions provide three-connected vertices for the polymeric structure. The resulting coordination network is very open and consists of two kinds of equal regions, i.e. dense molecular squares and very open octagons, these last providing large enough voids for hosting the guest molecules (Fig. 41b) [133].

$\{[FeAg(\mathbf{50})_3(NO_3)]{\cdot}2CH_3CN{\cdot}2(1,2\text{-}C_6H_4Cl_2)\}_n$ or $\{[Fe_2Ag_3(\mathbf{50})_6(NO_3)_3]{\cdot}5.5(1,2\text{-}C_6H_4Cl_2)\}_n$ were obtained by the reaction of $[Fe(\mathbf{50})_3]$ in $1,2\text{-}C_6H_4Cl_2$ and a lower and a larger concentration of $AgNO_3$ in CH_3CN, respectively. Crystals of the FeAg complex, which has a 2D trigonal grid structure with approximately hexagonal (11.7 Å × 16.0 Å) pores filled by solvent molecules, became opaque when immersed in other solvents, showing that the lattice is not stable under solvent exchange.

The framework of Fe_2Ag_3 complex is much more stable, as it can encapsulate a variety of guest solvent molecules which can be interconverted in single crystal to single crystal transformations. In the crystal structure $AgNO_3$ nodes are bridged by tridentate $\{[Fe(\mathbf{50})_3]\}$ building blocks to form a 1D porous ladder with Fe···Fe distances of 19.50 Å (across the "rungs" of the ladder) and 18.35 and 19.01 Å (along the "uprights"). This framework encloses two crystallographically independent, centrosymmetric pores, the larger one accomodating six guest molecules and the smaller one five. These 1D ladders are further interconnected by weak Ag···Ag interactions (3.29 Å) and accompanying bridging nitrate anions to form infinite 2D sheets separated by ca. 5.9 Å. Also, the "rung" Ag atoms in adjacent 2D layers are linked by nitrate ions to produce an overall 3D network. $\{[Fe_2Ag_3(\mathbf{50})_6(NO_3)_3]{\cdot}6C_6H_5Br\}_\infty$, occurring when the above reaction is carried out dissolving $[Fe(\mathbf{50})_3]$ in C_6H_5Br, has the same structure of the above Fe_2Ag_3 complex except that all pores have the same dimensions and contain six bromobenzene guest molecules. The two Fe_2Ag_3 crystals can be inetrconverted each other by treatment with the appropriate solvent, maintaining the framework connectivity despite the fact that the different guests lead to noticeable changes in the pore geometry and symmetry, Fe···Fe and Ag···Ag distances, and interlayer separations [134].

Polynuclear manganese clusters often exhibit large, sometimes abnormally large spin values in the ground state. This large spin value, combined with a large magnetic anisotropy, has led some of these species to be single molecule magnets (SMMs), attracting extensive attention because they represent nanoscale magnetic particles of a well-defined size. They display sluggish magnetization relaxation phenomena such as magnetization hysteresis loops and frequency-dependent out-of-phase alternating current magnetic susceptibility. The remarkable magnetic properties of a SMM arise from its high-spin ground state split by a large negative axial zero-field splitting. A number of SMMs containing different metal ions have been reported and the development of rational syntheses of multinuclear metal complexes, especially from building blocks possessing high spin ground states, is a stimulating goal of coordination chemists [135–145].

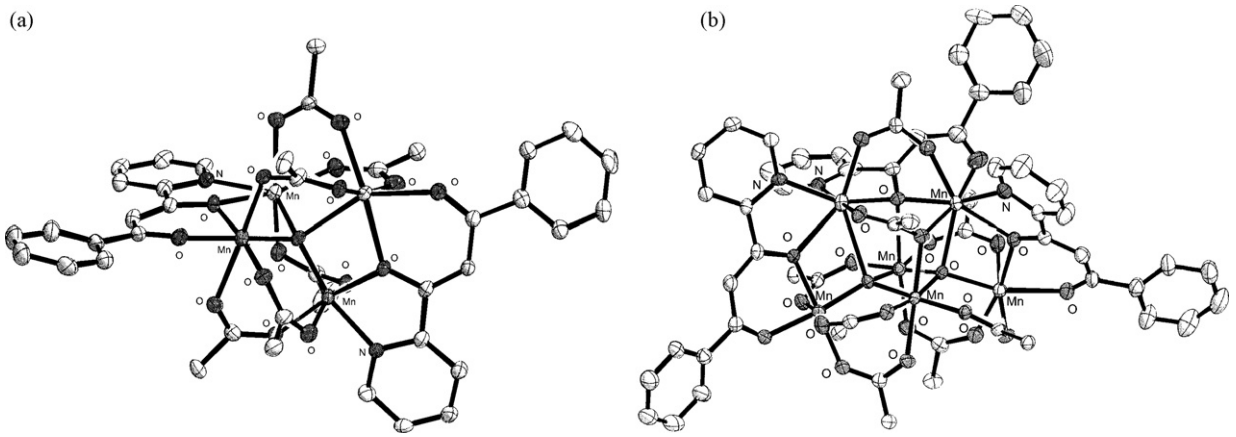

Fig. 42. Structure of $[Mn_2^{II}Mn_2^{III}(\mathbf{51b})_2(O)(Cl_3CCOO)_6]$ (a) and $[Mn_3^{II}Mn_3^{III}(\mathbf{51a})_3(O)_2(C_6H_5COO)_8]$ (b) [146].

The pyridine-containing β-diketone ligands H–**51a** and H–**51b**, prepared by Claisen condensation of ethyl picolinate with *p*-methylacetophenone or acetophenone and sodium ethoxide in a 1:1:1 molar ratio in anhydrous ether, react with $[Mn_3(O)(Cl_3CCOO)(H_2O)_3]$ in a 1.5:1 molar ratio and in CH_2Cl_2/Et_2O to give $[Mn_4(\mathbf{L})_2(O)(CH_3CCOO)_6]$. When $[Mn_3(O)(C_6H_5COO)(py)_2(H_2O)]$ was employed as manganese source, the above reactions afford $[Mn_6(O)_2(\mathbf{L})_3(C_6H_5COO)_6]$ [146].

In $[Mn_4(\mathbf{51b})_2(O)(Cl_3CCOO)_6]$ the central $[Mn_4(\mu_4\text{-}O)]^{8+}$ core contains a distorted Mn_4 tetrahedron with two octahedral manganese(III) and two octahedral manganese(II) ions. A μ_4-O atom bridges the four manganese ions. The Mn···Mn distances fall in the range 3.214···3.674 Å with the shortest one being between $Mn^{III}\cdots Mn^{II}$ ions, which are bridged through the μ_4-O atom and an oxygen of the diketonate group, and the longest one being between the $Mn^{II}\cdots Mn^{III}$ ions, which are bridged only by the μ_4-O atom and two bidentate chelate carboxylato ligands. The peripheral ligations are provided by six bridging trichloroacetate anions and two bridging diketonate groups which behave as $\eta^1{:}\eta^2{:}\eta^1{:}\mu_2$-ligands, bridging one manganese(III) and one manganese(III) ion; each ligand chelates one metal ion through its nitrogen atoms and connects this metal ion with a second one through bridging oxygen atoms. The six bridging trifluoroacetate anions can be separated into three classes: the groups bridging two manganese(III) ions, the groups bearing bridging two manganese(II) ions and the groups bridging one manganese(II) and one manganese(III) ion. The structure of the tetramanganese complex with $[\mathbf{51b}]^-$ is very similar to that of $[\mathbf{51a}]^-$ except that one of six Cl_3CCOO^- groups is bridging two manganese ions in a $\eta^2{:}\eta^1{:}\mu_2$-binding mode, completing a distorted pentagonal bipyramid coordination environment around one manganese(II) ion (Fig. 42a) [146].

H–**51a** and H–**51b** and $\{Mn_3O(C_6H_5COO)_6(H_2O)(py)\}$ in CH_2Cl_2 afford the isostructural complexes $[Mn_6(\mathbf{L})_3(O)_2(C_6H_5COO)_8]$ with a $\{Mn^{II}{}_3Mn^{III}{}_3(\mu_4\text{-}O)_2\}^{11+}$ core and peripheral ligations provided by eight benzoate groups and three $[\mathbf{L}]^-$ ligands. Seven of the eight $C_6H_5COO^-$ groups are bridging two manganese ions and are in a *syn,syn*- $\eta^1{:}\eta^1{:}\mu_2$ binding mode. The remaining $C_6H_5COO^-$ group is in a $\eta^1{:}\eta^2{:}\mu_3$ mode, one oxygen atom being terminal to one manganese ion and the other one bridging other two manganese ions. Two $[\mathbf{L}]^-$ ligands behave as $\eta^1{:}\eta^2{:}\eta^1{:}\mu_2$ ligands, where each ligand chelates one metal ion through its nitrogen atom and connects this metal ion with a second one through a bridging oxygen atom and a terminal oxygen atom; and the third $[\mathbf{L}]^-$ ligand chelates as a $\eta^1{:}\eta^3{:}\eta^1{:}\mu_3$-bridging group; the coordination of this ligand is similar to the other two β-diketonates by connecting to the metal ion terminally though the nitrogen and one oxygen atoms, but bridging three manganese ions by the other oxygen atom. Four manganese ions are six coordinate with slight distorted octahedral geometry while the other two are seven coordinate with distorted pentagonal bipyramidal geometry (Fig. 42b) [146].

Both the complexes $[Mn_4(\mathbf{L})_2(O)(Cl_3CCOO)_6]$ are trapped valence tetranuclear $Mn^{II}{}_2Mn^{III}{}_2$ species where intramolecular antiferromagnetic exchange occur. Variable temperature magnetic susceptibility and magnetization measurements indicate that the $Mn^{II}{}_3Mn^{III}{}_3$ complexes have a ground state spin value of $S = 7/2$ with significant magnetoanisotropy as gauged by the *D*-value of $-0.46\,cm^{-1}$. The frequency dependence of the out-of-phase component in alternating current magnetic susceptibilities indicates the slow magnetic relaxation of a superparamagnetic molecule [146].

An isopropanol solution of H–**51c** and an aqueous solution at pH 3 of $LaCl_3{\cdot}6H_2O$ afford $[La_2(\mathbf{51c})_6]$, where each of the two 10 coordinate lanthanum ions is bound by four terminal diketonate oxygen atoms, four bridging diketonate oxygen atoms and two terminal pyridyl nitrogen atoms. Two of the terminal oxygen atoms arise from solely bidentate diketonates which have non-coordinating pyridyl nitrogen atoms, the other two arising from bidentate diketonates that also bridge to the other lanthanum ion centre through the other oxygen atom. The pyridyl nitrogen of the bridging β-diketonate ligands is coordinated to the other lanthanum ion. Thus, one of the diketonate ligands at each lanthanum ion is bidentate through two oxygen atoms, two are bidentate through a bridging oxygen and a pyridyl nitrogen and the other is bidentate through a bridging and terminal oxygen and overall eight pyridyl nitrogen atoms are unbound by lanthanum. Dimerization via diketonate oxygen atoms is preferred over the coordination of either dangling pyridyl nitrogen atoms or solvent water molecules. The La···La distance is 3.783 Å (Fig. 43a) [147].

The isostructural complexes $[Ln_2(\mu\text{-}\mathbf{52})_2(\mathbf{52})_4]$ (Ln = Tb,Y) were prepared by the reaction of $LnCl_3$ with a slight excess of H–**52** in acetone/water. Attempts to prepare the mononuclear complexes $[Tb(\mathbf{52})_3(L)]$, where L is a chelating ligand such as 2,2′-bipyridine or 1,10-phenanthroline, were not successful [148].

$[Tb_2(\mu\text{-}\mathbf{52})_2(\mathbf{52})_4]$ contains two metal(III) ions, 4.027 Å apart, each chelated by two $[\mathbf{52}]^-$ ligands through the diketonate oxygen atoms. The remaining two $[\mathbf{52}]^-$ ligands display chelating and bridging bonding mode-chelate to one of the terbium(III) ions through the nitrogen atom of the 7-azaindolyl group and one oxygen atom of the diketonate and chelate to the second terbium(III) ion by using two oxygen atoms of the diketonate, giving rise to eight

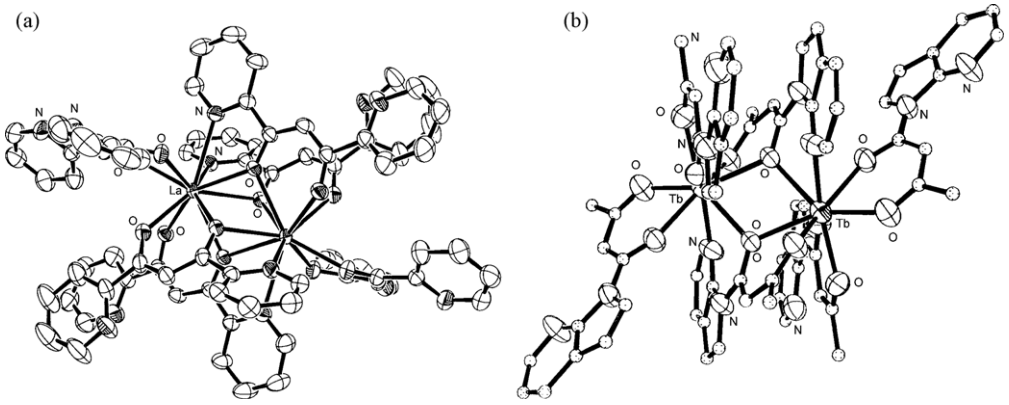

Fig. 43. Structures of $[La_2(\mathbf{51c})_6]$ (a) [147] and $[Tb_2(\mu\text{-}\mathbf{52})_2(\mathbf{52})_4]$ (b) [148].

coordinate terbium(III) ions a distorted square antiprism formed by the four oxygen atoms from the two chelating ligands in one square plane and two oxygen atoms and two nitrogen atoms from the two bridging ligands in another square plane. An extensive π stacking in the crystal lattice occurs (Fig. 43b) [148].

$[Tb_2(\mu\text{-}\mathbf{52})_2(\mathbf{52})_4]$ displays characteristic terbium(III) emission bands while the yttrium(III) analogue displays weak blue luminescence attributable to the ligand. Single-layer and double-layer electroluminescent devices for $[Tb_2(\mu\text{-}\mathbf{52})_2(\mathbf{52})_4]$ were made, where the complex doped poly(vinylcarbazole) (PVK) layer functions as both the emitting layer and the hole transport layer and prebulk deposition (PBD) material (2,4-(diphenyl)-5-(4-*tert*-butylphenyl)-1,3,4-oxadiazole) functions as an electron transport layer (in the double-layer device), demonstrating that $[Tb_2(\mu\text{-}\mathbf{52})_2(\mathbf{52})_4]$ is a green emitter in electroluminescent devices [148].

A range of β-diketones, bearing a side polyether chain, designed with the aim to obtain monomeric, volatile complexes to be used in MOCVD, was prepared by deprotonation of H–**5** or H–**12** with sodium in liquid ammonia in the presence of catalytic amounts of $Fe(NO_3)_3$, followed by treatment with 1 equiv. of $BrCH_2CH_2(OCH_2CH_2)_nOCH_3$ to give, after work-up, the desired functionalized β-diketone H–**53a**···H–**53e**. On reaction with the desired β-diketone in dry toluene, BaH_2 dissolves smoothly to form $[Ba(\mathbf{L})_2]$, proposed to be monomer in solution but polymeric in the solid state. The same behaviour was observed for the copper(II) complexes $[Cu(\mathbf{L})_2]$, derived from the reaction of the same β-diketones with $Cu(NO_3)_2$ in water/ethanol solution containing NH_3. $[Cu(\mathbf{53e})_2]$ is polymeric with each octahedrally distorted, copper ion surrounded by six oxygen atoms: two $[\mathbf{53e}]^-$ ligands are bound in a bidentate manner to each copper(II) ion to give a distorted square planar arrangement, while the two axial coordination sites are taken up by the terminal oxygen atoms of the polyether chain from a β-diketone attached to the neighbouring copper ion (Fig. 44) [149].

9. Heteropolynuclear β-diketonato complexes

The substitution of the coordinated water molecules in $[Ln(\beta\text{-dike})_3(H_2O)_n]$ ($n = 1, 2$) can be achieved by using appropriate metal complexes as ligands. In the resulting heterodi- or heteropolynuclear complexes a quite sophisticated supramolecular array takes place, with peculiar photophysical or magnetic properties originating from the typology of the metal ions interfering each other.

Transition metal complexes containing antenna chromophores have been successfully experimented as lanthanide sensitizers. The d-block containing chromophores afford a series of advantages, including (i) low-energy absorption in the visible region arising from the red-shifted ILCT (intraligand charge transfer) or MLCT (metal-to-ligand charge transfer) transitions, causing a better energy match between d-block donors and lanthanide(III) acceptors and thus less waste in energy, (ii) relatively high triplet quantum yields resulting from the rapid intersystem crossing induced by heavy-metal effect, (iii) relatively long lived triplet excited states that facilitate energy transfer to the adjacent lanthanide(III) centers, (iv) facile detection of both quenching of the d-block chromophores and the sensitized emission from the lanthanide(III) centers.

The tetranuclear Ru_2Ln_2 nature of the complexes $[Ru_2Ln_2(\mathbf{17})_6(bipy)_4(4,4\text{-}bipy)_4(H_2O)](Cl)_4$, prepared by reaction of $[Ru(bipy)_2(4,4'\text{-}bipy)_4](Cl)_2$ with $[Ln(\mathbf{17})_3(H_2O)_2]$ (Ln = Nd, Yb, Gd) in methanol, was inferred by ESI–MS spectra. By exciting the Ru_2Nd_2 complex at 420 nm, strong emission bands originate at

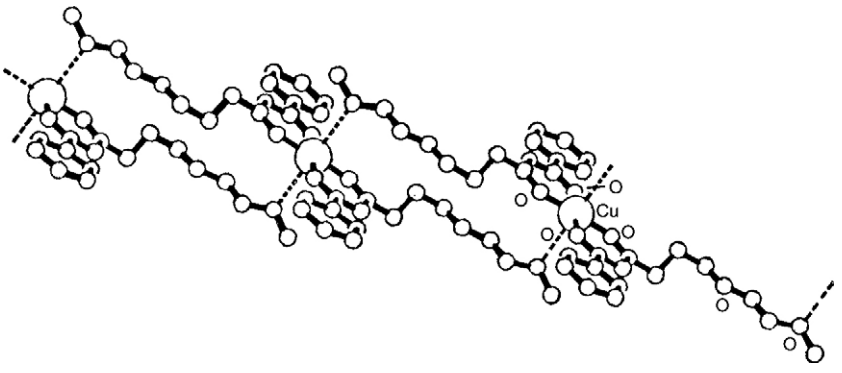

Fig. 44. Structure of $[Cu(\mathbf{53e})_2]_n$ [149].

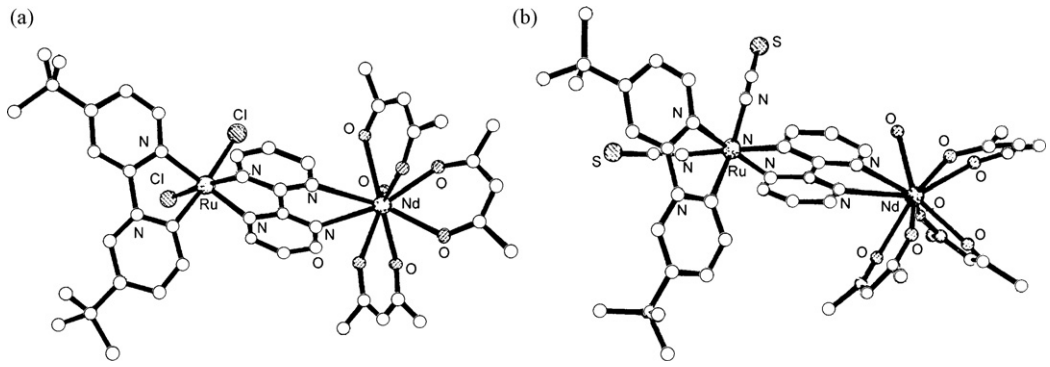

Fig. 45. Structures of [RuNd(**10**)$_3$(Cl)$_2$(*t*-bubipy)$_2$(bpm)] (a) and [RuNd(**10**)$_3$(SCN)$_2$(*t*-bubipy)$_2$(bpm)(H$_2$O)] (b) [151].

900, 1059, and 1333 nm, due to the $^4F_{3/2} \rightarrow {}^4I_{9/2}$, $^4I_{11/2}$, and $^4I_{13/2}$ neodymium(III) transitions, indicating that the neodymium(III) ions are excited by the ^{3}MLCT (metal-to-ligand charge transfer) state of the Ru-bipy sensitizer. In the same way, no emission bands are observed in the near-infrared region for the complexes [Ru(bipy)$_2$(4,4′-bipy)$_2$](Cl)$_2$ and [Nd(**17**)$_3$(H$_2$O)$_2$]. Emission in the near-infrared region of the Ru_2Yb_2 complex was also observed. The energy transfer rates in the Ru_2Nd_2 and the Ru_2Yb_2 complexes are rather high [150].

[Ru(*t*-bubipy)$_2$(bpm)](PF$_6$)$_2$ and [Os(*t*-bubipy)$_2$(bpm)](PF$_6$)$_2$ (*t*-bubipy = 4,4′-*tert*-butyl-2,2′-bipyridine, bpm = 2,2′-bipyrimidine) were prepared by reaction of the appropriate [M(*t*-bubipy)$_2$(Cl)$_2$] with 1 equiv. of bpm, followed by anion metathesis, while the subsequent addition of *t*-bubipy and bpm to [Ru(dmso)$_4$(Cl)$_2$] affords [Ru(*t*-bubipy)(bpm)(Cl)$_2$] whose chloride ions can be replaced with thiocyanates by treatment with 2 equiv. of AgNO$_3$ followed by addition of KNCS. The further reaction of these complexes with [Ln(**10**)$_3$(H$_2$O)$_2$] affords [MLn(**10**)$_3$(*t*-bubipy)$_2$(bpm)](PF$_6$)$_2$, [MLn(**10**)$_3$(SCN)$_2$(*t*-bubipy)$_2$(bpm)(H$_2$O)] or [MLn(**10**)$_3$(Cl)$_2$(*t*-bubipy)$_2$(bpm)] (M = Ru^{II}, Os^{II}; Ln = Nd, Pr, Gd, Yb), where the transition metal ion is octahedral and the lanthanide(III) ion is nine coordinate in the presence of an additional water molecule and eight coordinate when the water molecule is absent (Fig. 45a and b). [Ru(*t*-bubipy)(bpm)(X)$_2$] (X = Cl$^-$, NCS$^-$) and [M(*t*-bubipy)$_2$(bpm)](PF$_6$)$_2$ (M = Ru^{II}, Os^{II}) have a low-energy LUMO arising from the presence of 2,2′-bipyrimidine ligand, and consequently have lower-energy ^{1}MLCT and ^{3}MLCT states than analogous complexes of bipyridine. UV–vis and luminescence studies show that binding of the {Ln(**10**)$_3$} fragment at the second site of the bpym ligand reduces the ^{3}MLCT energy of the ruthenium(II) or osmium(II) fragment still further; consequently in [RuLn(*t*-bubipy)$_2$(bpm)(**10**)$_3$(X)$_2$)] (X = Cl$^-$, NCS$^-$) and [OsLn(*t*-bubipy)$_2$(bpm)(**10**)$_3$](PF$_6$)$_2$ the ^{3}MLCT is too low to sensitize the luminescent f–f states of neodymium(III) or ytterbium(III) ions, but in [RuLn(*t*-bubipy)$_2$(bpm)(**10**)$_3$](PF$_6$)$_2$ the ^{3}MLCT energy allows energy transfer to the neodymium(III) or ytterbium(III) ions resulting in sensitized near-infrared luminescence on the microsecond timescale [151].

Furthermore, d-block chromophores have been converted to the lanthanide luminophore by bifunctional ligands with suitable bonding sites for d- and f-metal ions. Acetylide-functionalized pyridine, bipyridine, phenanthroline and terpyridine have been used for the synthesis of d, f-heterometallic arrays, capable to allow d → f energy transfer to occur from transition metal alkynyl chromophores to f-block luminophores, thus emitting NIR lanthanide luminescence by excitation of the charge transfer absorption in the organometallic energy donors.

The key feature of the molecular design of di- or multinuclear PtLn systems is the grafting of a square planar {Pt(N–N)}, {Pt(N–N–N)} or {Pt(P–P)} unit (N–N = bipyridine, phenanthroline; N–N–N = terpyridile; P–P = diphosphine) onto an ethynyl ligand suitable for lanthanide(III) complexation. The resulting PtLn, $PtLn_2$, Pt_2Ln_2 or $PtLn_4$ complexes exhibit relatively easy synthesis and high stability, strong luminescence of the lanthanide(III) center due to quantitative energy transfer from visible-light irradiation up to 460 nm, a luminescence quantum yield independent of the presence of oxygen and a redox behaviour of the platinum(II) unit insensitive to binding of the lanthanide(III) species.

[Pt(*t*-buterpy)(C≡Cterpy)](BF$_4$), prepared by [Pt(*t*-buterpy)(Cl)](BF$_4$) (*t*-buterpy = 4,4′,4″-*tert*-butyl-2,2′:6′,2″-terpyridine) and 4-ethynil-2,2′:6′,2″-terpyridine (HC≡Cterpy) in dimethylformamide mediated by CuI under anaerobic conditions, reacts with [Eu(**10**)$_3$(H$_2$O)$_2$] in CH_2Cl_2 under argon to afford [PtEu(*t*-buterpy)(C≡Cterpy)(**10**)$_3$](BF$_4$). The flat {Pt(*t*-buterpy)(C≡Cterpy)} core links to the nine coordinated distorted monocapped square antiprismatic europium(III) ion with the three nitrogen atoms of the free terpyridine subunit and six oxygen atoms of the three [**10**]$^-$ ligands (Fig. 46). Irradiation up to 460 nm in the MLCT state of the platinum(II) subunit results in an energy transfer to the europium(III) center, which strongly luminesces in the red with an overall luminescence quantum yields of 38%. The energy transfer process is quantitative and not sensitive to oxygen and the complexation of the europium(III) to the platinum(II) metallosynthon allows the recovery of the energy lost due to triplet-oxygen quenching of the MLCT state observed in the uncomplexed platinum(II) precursor

The Cu^I-catalyzed coupling of *cis*-[Pt(N–N)(Cl)$_2$] (N–N = bipy, *t*-bubipy) with 4-ethynylpyridine (HC≡Cpy) or 3-ethynyl-1,10-phenantroline (HC≡Cphen) affords *cis*-[Pt(N–N)(C≡Cpy)$_2$] or *cis*-[Pt(N–N)(C≡Cphen)$_2$], respectively. *Cis*-[Pt(N–N)(C≡Cpy)$_2$] reacts with [Ln(β-dike)$_3$(H$_2$O)$_2$] ([β-dike]$^-$ = [**10**]$^-$, [**17**]$^-$; Ln = Gd, Pr, Nd, Er, Eu) to give *cis*-[PtLn(N–N)(C≡Cpy)$_2$(β-dike)$_3$]$_\infty$. *Cis*-[PtLn(bipy)(C≡Cpy)$_2$(**17**)$_3$] (Ln = Yb, Er) (Fig. 47a) contains a zigzag chain with a *cis* arrangement of the two 4-pyridyl units at the platinum(II) centres. Each lanthanide(III) centre is eight coordinate square antiprismatic from the three bidentate [**17**]$^-$ ligands and two monodentate pyridyl ligands, each from a different platinum(II) unit. The Pt···Yb distances within the chain are at 9.92 and 9.88 Å. The {Pt(bipy)} units from adjacent chains are stacked together in pairs such that there is a Pt···Pt separation of 3.334 Å in the PtTb and 3.337 Å in the PtEu complexes, approximately perpendicular to the zigzag chain. The Pt···Pt interactions change the photophysical properties of these complexes, with the lowest energy excited state changing from ^{3}MLCT excited state in monomers to ^{3}MMLCT (metal–metal bond to ligand charge-transfer) in stacked dimers or oligomers where a metal–metal bonding interaction takes place [153].

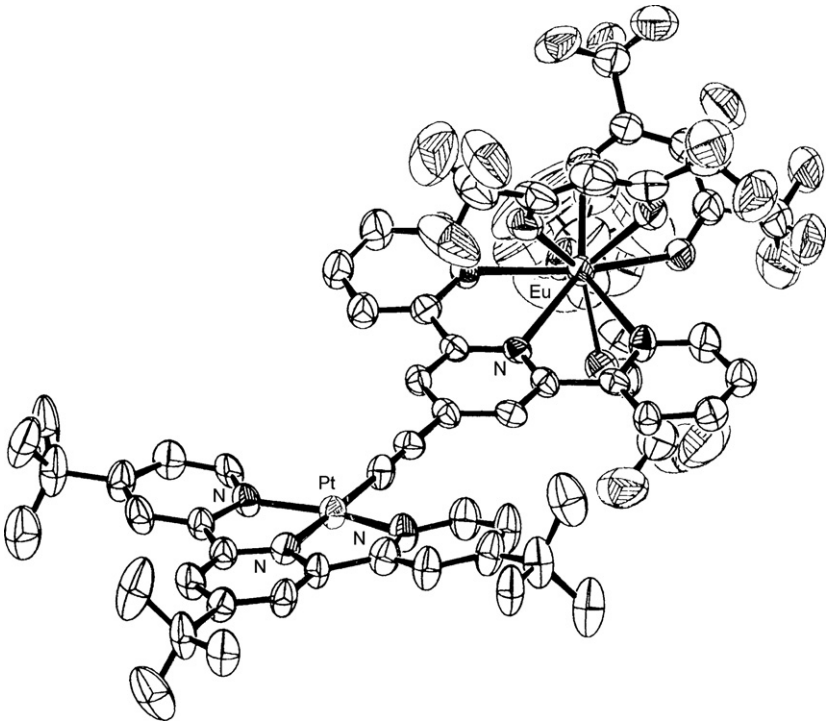

Fig. 46. Structure of [PtEu(*t*-bubipy)(C≡Cterpy)(**10**)$_3$]$^+$ [152].

On the contrary, [PtLn$_2$(*t*-bubipy)(C≡Cphen)$_2$(**10**)$_6$], prepared from a mixture of [Pt(*t*-bubipy)(C≡Cphen)$_2$] and [Ln(**10**)$_3$(H$_2$O)$_2$], forms discrete trinuclear PtLn$_2$ complexes by attachment of a {Ln(**10**)$_3$} fragment at each of the two pendant phenanthroline sites as ascertained by the structure of the PtYb$_2$ complex, where a square planar platinum(II) and two eight coordinate square-antiprismatic ytterbium(III) centres occur (Fig. 47b) [153].

In solution the complexes [Pt(N–N)(C≡CR)$_2$] show platinum(II)-centered ^{3}MLCT luminescence between 508 and 526 nm, which is quenched by the addition of the {Ln(β-dike)$_3$} fragments. For [PtLn$_2$(*t*-bubipy)(C≡Cphen)$_2$(**10**)$_6$] (Ln = Yb, Nd, Er), this quenching

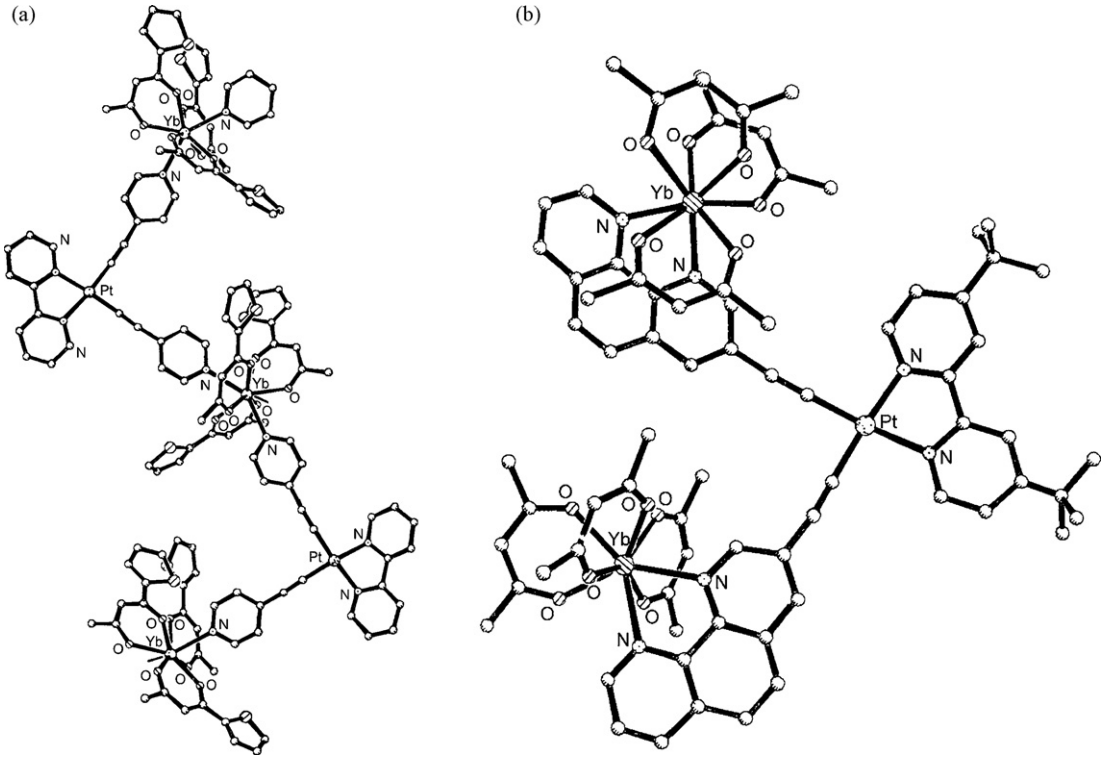

Fig. 47. Structures of *cis*-[PtYb(bipy)(C≡Cpy)$_2$(**17**)$_3$]$_n$ (a) and [PtYb$_2$(*t*-bipy)(C≡Cphen)$_2$(**10**)$_6$] (b) [153].

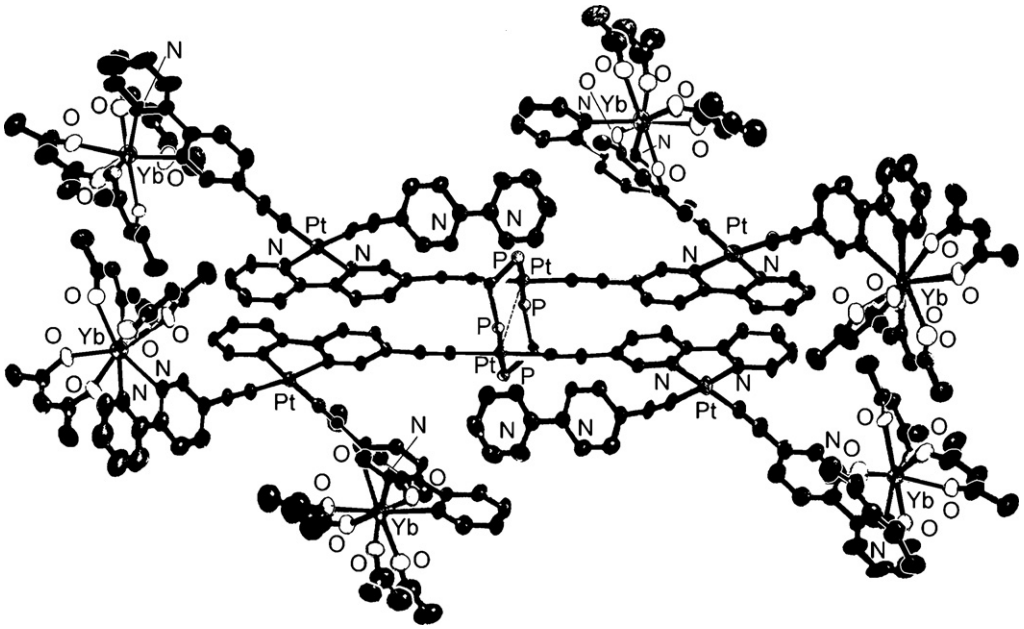

Fig. 48. Structure of $[Pt_6Ln_6(\mu\text{-dppm})_2(C{\equiv}Cbipy)_{12}(\mathbf{10})_{18}]$ [154].

is associated with Pt→Ln energy transfer resulting in sensitised near-infrared luminescence characteristic of these lanthanide(III) ions. For $[PtLn(bipy)(C{\equiv}Cpy)_2(\mathbf{17})_3]_\infty$ in solution, however, the quenching arises from a shift of the platinum(II) based ^{3}MLCT transition to higher energy following coordination of the $\{Ln(\mathbf{17})_3\}$ fragment; this increase in the ^{3}MLCT energy was supposed to bring it energetically close to a higher lying non-radiative excited state which provides an efficient quenching pathway. On the contrary, in the solid state, where the complexes $[Pt_2Ln_2(bipy)_4(C{\equiv}Cpy)_4(\beta\text{-dike})_6]$ occur via aggregation of two monomeric PtLn species, the chromophore has ^{3}MMLCT character rather than ^{3}MLCT character and luminescence at lower energies (ca. 630 nm) than those of the monomeric platinum(II) complexes. In the PtLn adducts (Ln = Yb, Nd, Er, Pr) the platinum(II) based ^{3}MMLCT luminescence is quenched to an extent depending on the ability of the different lanthanide(III) ions to act as energy acceptors, with ytterbium(III) ion providing the least quenching (slowest Pt → Ln energy transfer) and either neodymium(III) or europium(III) ions providing the most quenching (fastest Pt → Ln energy transfer) depending on whether the platinum(II)-based emission comes from an ^{3}MLCT state (better overlap with the absorption spectrum of the europium(III) complex) or a lower energy ^{3}MMLCT state (better overlap with the absorption spectrum of the neodymium(III) complex) [153].

Furthermore, $[Pt\{(CH_3)_3SiC{\equiv}Cbipy\}(C{\equiv}Cbipy)_2]$, prepared by the reaction of $[Pt\{(CH_3)_3Si\ C{\equiv}Cbipy\}(Cl)_2]$ with HC≡Cbipy in the presence of CuI and diisopropylamine, reacts with $[Ln(\mathbf{10})_3(H_2O)_2]$ (Ln = Nd, Yb) to form $[PtLn_2\{(CH_3)_3SiC{\equiv}Cbipy\}(C{\equiv}Cbipy)_2(\mathbf{10})_6]$, while it reacts with *cis*-$[Pt(dppm)(Cl)_2]$ (dppm = $(Ph)_2PCH_2P(Ph)_2$) in the presence of KF and CuI to give $[Pt_6(\mu\text{-dppm})_2(C{\equiv}Cbipy)_{12}]$. Addition of 8.8 equiv. of $[Ln(\mathbf{10})_3(H_2O)_2]$ (Ln = Nd, Gd, Yb) to a suspension of $[Pt_6(\mu\text{-dppm})_2(C{\equiv}Cbipy)_{12}]$ in dichloromethane induces formation of $[Pt_6Ln_6(\mu\text{-dppm})_2(C{\equiv}Cbipy)_{12}(\mathbf{10})_{18}]$, by incorporation of six $\{Ln(\mathbf{10})_3\}$ units through the 2,2′-bipyridyl chelating groups as ascertained in the Pt_6Yb_6 complex by X-ray diffraction. The $\{Pt_6(\mu\text{-dppm})_2(C{\equiv}Cbipy)_{12}\}$ moiety is made up of a $\{Pt_2(\mu\text{-dppm})_2(C{\equiv}Cbipy)_4\}$ unit incorporating four $\{Pt(C{\equiv}Cbipy)_2\}$ units via 2,2′-bipyridyl chelating in the diplatinum unit. The $\{Pt_2(\mu\text{-dppm})_2(C{\equiv}Cbipy)_4\}$ framework displays a face-to-face conformation, with a Pt···Pt distance of 3.221 Å, suggesting that a π–π stacking is operative between face-to-face bipyridyl rings. The {bipyC≡C—Pt—C≡Cbipy} arrays in four $\{Pt(bipy)(C{\equiv}Cbipy)_2\}$ moieties are *cis*-arranged. As observed in $[Pt\{(CH_3)_3SiC{\equiv}Cbipy\}(C{\equiv}Cbipy)_2]$, the four $\{Pt(bipy)(C{\equiv}Cbipy)_2\}$ moieties in $\{Pt_6(\mu\text{-dppm})_2(C{\equiv}Cbipy)_{12}\}$ assembly are characteristic of platinum(II) square planar geometries built by 2,2′-bipyridyl chelating and bis(acetylide) σ-coordination. Of the eight $[C{\equiv}Cbipy]^-$ ligands in the four $\{Pt(bpy)(C{\equiv}Cbipy)_2\}$ moieties, six are bound to $\{Yb(\mathbf{10})_3\}$ units through 2,2′-bipyridyl chelating whereas the other two are not coordinated. The eight coordinate ytterbium(III) centres are in a N_2O_6 distorted square antiprism. The Pt···Pt distances through bridging $[C{\equiv}Cbipy]^-$ moieties are 8.54 and 8.52 Å. The Pt···Yb separations across the bridging $[C{\equiv}Cbipy]^-$ moieties are in the range 8.41–8.80. Other Pt···Yb distances are of 10.48, 16.73, and 16.37 Å, respectively (Fig. 48) [154].

For the $PtLn_2$ (Ln = Nd, Yb) species, the platinum(II) chromophore-based ^{3}MLCT emission in the visible region disappears entirely, indicating unambiguously that the $\{Pt^{II}(bipy)(C{\equiv}CR)_2\}$-based emission is entirely quenched because of rapid and complete energy transfer from the platinum(II)-based energy donors. In contrast, residual emissions due to Pt_6 alkynyl moiety are observed with maxima at 520–650 nm for Pt_6Ln_6 (Ln = Nd, Yb) compounds, revealing incomplete energy transfer from the platinum(II) based antenna donors to the lanthanide(III) centres. As there exist both $\{Pt(bipy)(acetylide)_2\}$ and $\{Pt_2(dppm)_2(acetylide)_2\}$ antenna chromophores in the Pt_6Ln_6 species, sensitized NIR lanthanide(III) luminescence in these Pt_6Ln_6 complexes is likely induced by Pt → Ln energy transfer from both $d(Pt) \rightarrow \pi^*(bpy)$ ^{3}MLCT and $d(Pt_2) \rightarrow \pi^*(C{\equiv}Cbpy)$ ^{3}MMLCT triplet states. As revealed in $PtLn_2$ compounds, the Pt → Ln energy transfer from the $\{Pt(bipy)(acetylide)_2\}$ antenna group to the lanthanide centre is rapid and complete, due to the direct linkage of $\{Pt(bipy)(C{\equiv}CR)_2\}$ chromophores with lanthanide centres, the short Pt···Ln distances (8.4–8.80 Å) as well as the favourable conjugation in the bridging ligand C≡Cbpy. By contrast, Pt → Ln energy transfer from the $\{Pt_2(dppm)_2(acetylide)_2\}$ cluster chromophore is indirect, long-range (Pt···Ln = 10.5, 16.4 and 16.7 Å) and incomplete, inducing some residual platinum(II) based emission in the Pt_6Ln_6 species [154].

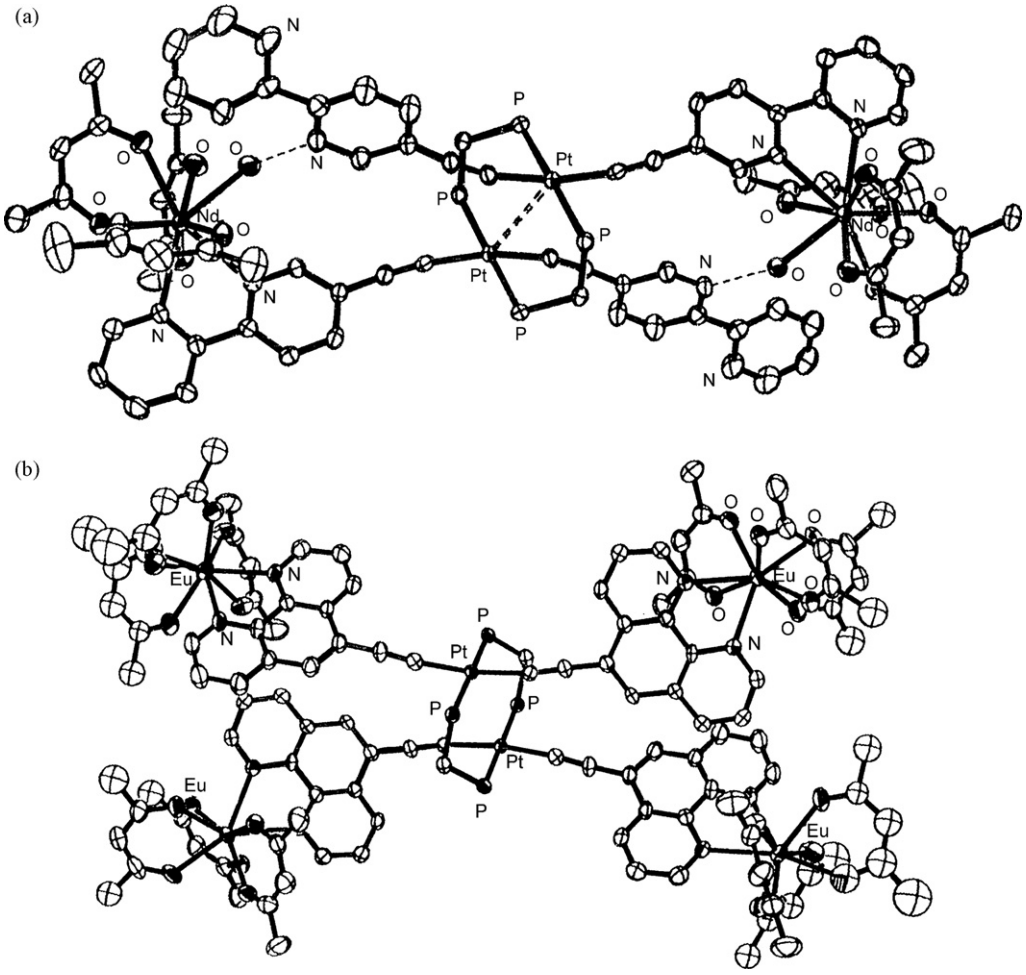

Fig. 49. Structures of $[Pt_2Ln_2(\mu\text{-dppm})_2(C{\equiv}Cbipy)_4(\mathbf{10})_6(H_2O)_2]$ (a) and $[Pt_2Eu_4(\mu\text{-dppm})_2(C{\equiv}Cphen)_4(\mathbf{10})_{12}]$ (b) [154].

$[Pt(dppm)(Cl)_2]$ reacts with 3-$(CH_3)_3SiC{\equiv}$Cbipy in the presence of the desilylation fluoride catalyst KF and CuI or with 5–HC≡Cphen in the presence of CuI to give $[Pt_2(\mu\text{-dppm})_2(C{\equiv}Cbipy)_4]$ or $[Pt_2(\mu\text{-dppm})_2(C{\equiv}Cphen)_4]$, which link$[Ln(\mathbf{10})_3(H_2O)_2]$ (Ln = Nd, Eu, Tb) to afford $[Pt_2Ln_2(\mu\text{-dppm})_2(C{\equiv}Cbipy)_4(\mathbf{10})_6(H_2O)_2]$ or $[Pt_2Ln_4(\mu\text{-dppm})_2(C{\equiv}Cphen)_4(\mathbf{10})_{12}]$, respectively [154].

The Pt_2Ln_2 array is composed of $\{Pt_2(\mu\text{-dppm})_2(C{\equiv}Cbipy)_4\}$ units incorporating $\{Ln(\mathbf{10})_3\}$ groups through 2,2′-bipyridyl chelating, stabilized by strong intramolecular hydrogen bonding interactions between the coordinated water and the free bipyridyl nitrogen atom. The $\{Pt_2(\mu\text{-dppm})_2(C{\equiv}Cbipy)_4\}$ unit displays a face-to-face conformation with a Pt···Pt distance of ca. 3.25 Å, implying the presence of metal···metal contacts. The nine coordinate lanthanide(III) center is in a N_2O_7 distorted capped square antiprism. The platinum(II) center exhibits a square planar geometry built from *trans*-oriented N_2P_2 donors. The intramolecular Pt···Ln separation is ca. 8.8 Å (Fig. 49a) [154].

In the Pt_2Eu_4 complex four $\{Eu(\mathbf{10})_3\}$ units are linked to the $\{Pt_2(\mu\text{-dppm})_2(C{\equiv}Cphen)_4\}$ unit through 1,10-phenantroline chelation. The platinum(II) center exhibits an approximately square planar geometry with *trans*-oriented C_2P_2 donors, whereas the eight coordinated europium(III) center is in a N_2O_6 distorted square antiprism. The Pt···Pt distance (3.298 Å) is a little longer than those in the Pt_2Nd_2 and Pt_2Eu_2 complexes (3.246 and 3.251 Å). The intramolecular Pt···Eu separation is ca. 10.2 Å (Fig. 49b). Upon irradiation of the MLCT absorption of the diplatinum alkynyl moiety at 350–450 nm, all of the Pt_2Ln_2 and Pt_2Ln_4 complexes exhibit characteristic emissions for these lanthanide ions with lifetimes in the microsecond range in both the solid state and in CH_2Cl_2 solution at 298 K. By contrast, MMLCT and ligand-centered emissions from diplatinum alkynyl chromophores disappeared entirely for all of the Pt–Ln complexes in both the solid state and in CH_2Cl_2 solution, indicating that the Pt-based luminescence is completely quenched because of a quite efficient and fast energy transfer occurring from the d-block chromophores to the f-block luminophores. Three emission bands were observed for the PtNd complexes at ca. 865, 1060 and 1330 nm, four for the PtEu complexes at ca. 595, 615, 650 and 695 nm and one for PtYb complexes at ca. 980 nm. For the Pt_2Ln_2 and Pt_2Ln_4 arrays in $[Pt_2Ln_2(\mu\text{-dppm})_2(C{\equiv}Cbipy)_4(\mathbf{10})_6(H_2O)_2]$ or $[Pt_2Ln_4(\mu\text{-dppm})_2(C{\equiv}Cphen)_4(\mathbf{10})_{12}]$ (Ln = Nd, Eu, Yb), the excitation of $d(Pt) \rightarrow \pi^*(R{-}C{\equiv}C)$ MLCT absorption induces sensitisation of lanthanide luminescence through efficient $d \rightarrow f$ energy transfer from platinum(II) alkynyl chromophores [154].

$[Pt(dppm)(Cl)_2]$ reacts with 2.3 equiv. of $HC{\equiv}CC_6H_4$terpy in the presence of CuI and diisopropylamine to form *cis*-$[Pt(dppm)(C{\equiv}CC_6H_4terpy)_2]$. Instead, the reaction of *cis*-$[Pt(dppm)(C{\equiv}CC_6H_4terpy)_2]$ with 1 equiv. of dppm affords trans-$[Pt_2(dppm)_2(C{\equiv}CC_6H_4terpy)_4]$ which is also accessible by reaction of $[Pt(dppm)(Cl)_2]$ with 2.3 equiv. of $HC{\equiv}CC_6H_4$terpy in the presence of 1 equiv. of dppm. The subsequent reaction of *cis*-$[Pt(dppm)(C{\equiv}CC_6H_4terpy)_2]$ or *trans*-$[Pt_2(dppm)_2(C{\equiv}CC_6H_4terpy)_4]$ with an excess of $[Ln(\mathbf{10})_3(H_2O)_2]$ (Ln = Nd, Eu, Gd, Yb) in dichloromethane

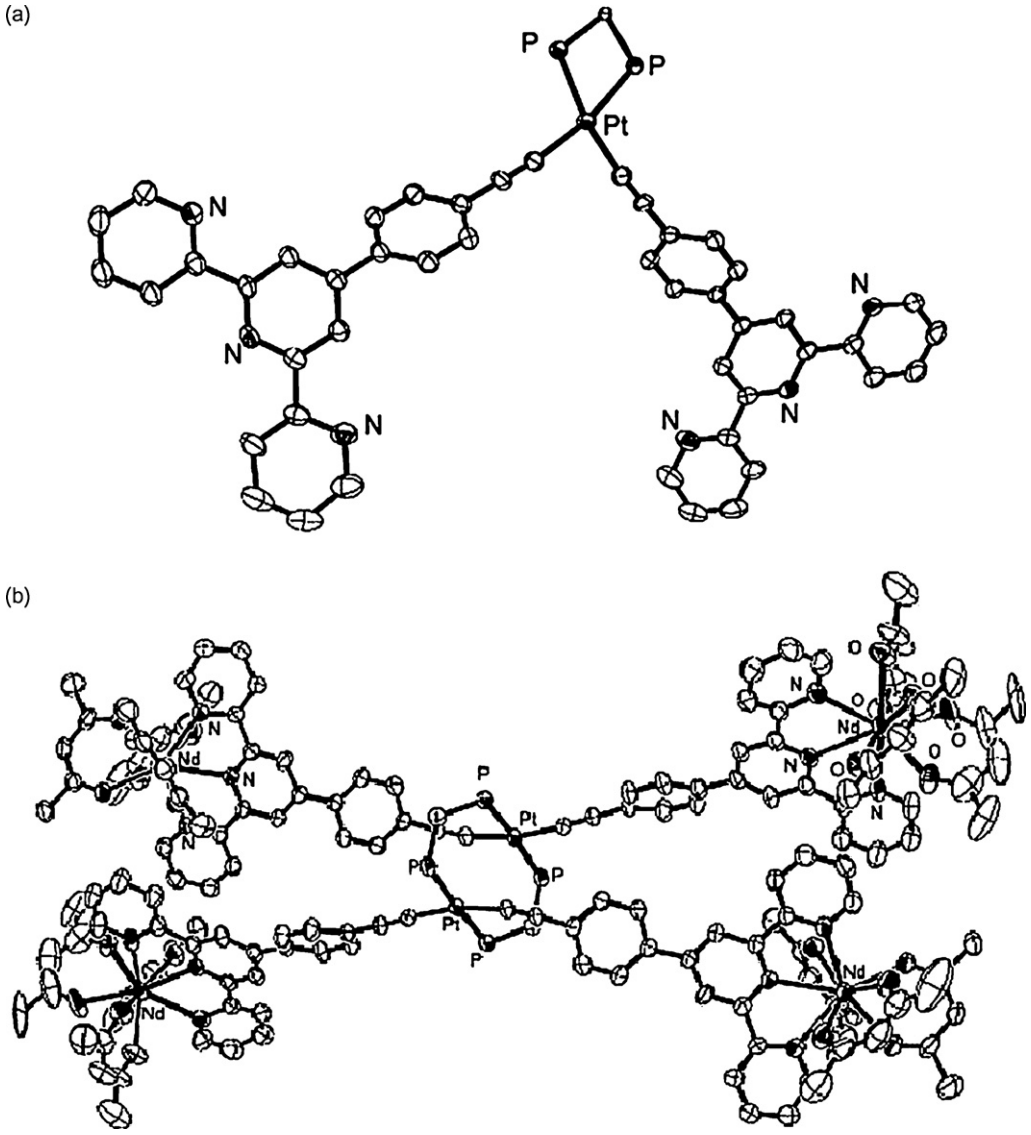

Fig. 50. Structures of *cis*-[Pt(μ-dppm)(C≡CC_6H_4terpy)$_2$] (a) and *trans*-[Pt_2Nd_4(μ-dppm)$_2$(C≡CC_6H_4terpy)$_4$(**10**)$_{12}$] (b) [155].

gives rise to [$PtLn_2$(dppm)(C≡CC_6H_4terpy)$_2$(**10**)$_6$] or [Pt_2Ln_4(dppm)$_2$(C≡CC_6H_4terpy)$_4$(**10**)$_{12}$], respectively [155].

The platinum(II) center in [Pt(dppm)(C≡CC_6H_4terpy)$_2$] adopts a distorted square planar geometry composed of *cis*-oriented C_2P_2 donors from σ-coordinated acetylides and chelated dppm. Intermolecular Pt–Pt contact is absent since the shortest Pt···Pt distance is 10.88 Å between adjacent platinum(II) ions in the crystal lattice (Fig. 50a). For [Pt_2Ln_4(dppm)$_2$(C≡CC_6H_4terpy)$_4$(**10**)$_{12}$] (Ln = Nd, Eu, Yb), the {Pt_2(μ-dppm)$_2$(C≡CC_6H_4terpy)$_4$} subunit exhibits a face-to-face conformation, in which the two platinum(II) coordination planes are in parallel orientation. The diplatinum(II) ions, doubly linked by two μ-dppm to give a eight-membered ring consisting of $Pt_2P_4C_2$ atoms, are in distorted square planar environments built by *trans*-arranged C_2P_2 donors with intramolecular Pt···Pt distances of 3.41, 3.30, 3.31 Å in Pt_2Nd_4, Pt_2Eu_4 and Pt_2Yb_4 respectively. The lanthanide(III) ions are nine coordinated in a N_3O_6 distorted capped square antiprism. The intramolecular Pt···Ln distances across the bridging {C≡CC_6H_4terpy} groups are in the range from 14.01 to 14.15 Å (Fig. 50b). Both *cis*-[Pt(dppm)(C≡CC_6H_4terpy)$_2$] or *trans*-[Pt_2(dppm)$_2$(C≡CC_6H_4terpy)$_4$] exhibit intense, long-lived room-temperature phosphorescence originating from an admixture of ^{3}ILCT [π → π(C≡CC_6H_4terpy)] and ^{3}MLCT [d(Pt)π*(C≡CC_6H_4terpy)]/^{3}MMLCT [dσ*(Pt_2) → pσ(Pt_2)/π*(C≡CC_6H_4terpy)] triplet states. The phosphorescent character qualifies these platinum(II) precursors as favourable energy donors to facilitate Pt → Ln energy transfer in the $PtLn_2$ and Pt_2Ln_4 adducts. Upon excitation at 360–450 nm for the $PtLn_2$ complexes and at 360–500 nm for the Pt_2Ln_4 (Ln = Nd, Eu, Yb) complexes, where only the platinum(II) alkynyl antenna chromophores absorb strongly, the $PtLn_2$ and Pt_2Ln_4 species exhibit bandlike lanthanide luminescence that is typical of the corresponding lanthanide(III) ions, demonstrating unambiguously that efficient Pt → Ln energy transfer occurs indeed from the platinum(II) alkynyl antenna chromophores to the lanthanide(III) centers across the bridging {C≡CC_6H_4terpy} group with intramolecular Pt···Ln distances being ca. 14.2 Å. The Pt → Ln energy transfer rate (K_{ET}) is 6.07×10^7 s^{-1} for Pt_2Nd_4 and 2.12×10^5 s^{-1} for Pt_2Yb_4 species [155].

The complexes *cis*-[Pt(P–P)(C≡CC_6H_4terpy)$_2$] (P–P = $Ph_2P(CH_2)_n$ PPh_2; *n* = 2, 3), prepared by *cis*-[Pt(P–P)$(Cl)_2$] and HC(CC_6H_4terpy, react with an excess of [Ln(**10**)$(H_2O)_2$] in CH_2Cl_2 to form *cis*-[$PtLn_2$(P–P)(C≡CC_6H_4terpy)$_2$(**10**)$_6$] (Ln = Eu, Nd, Tb), where the square planar platinum(II) and the distorted square antipris-

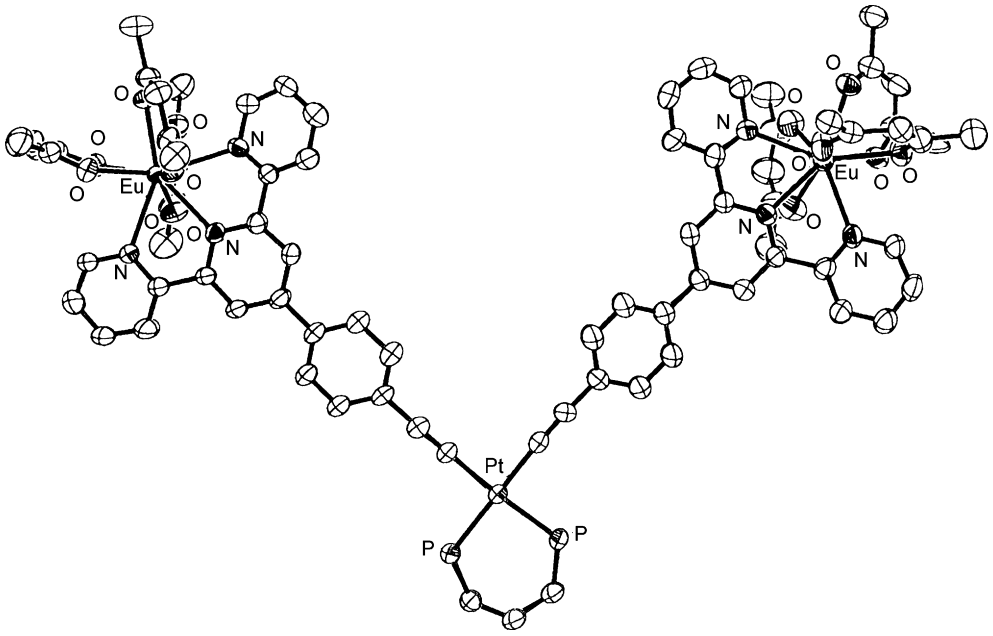

Fig. 51. Structure of *cis*-[$PtEu_2$(μ-P-P)(C≡CC_6H_4terpy)$_2$(**10**)$_6$] [156].

matic lanthanide(III) ions are at Pt···Ln distances in the range 14.23–14.46 Å (Fig. 51) [156].

Upon excitation at 250–450 nm, these $PtLn_2$ complexes show characteristic emissions of the corresponding lanthanide(III) ions with microsecond to millisecond (for europium(III) species) ranges of lifetimes in both the solid state and dichloromethane. The observation of characteristic emissions from the corresponding lanthanide(III) centers by excitation of platinum(II)-based absorption (λ_{ex} = 350–450 nm) demonstrate that the sensitized lanthanide luminescence is indeed achieved by Pt → Ln energy transfer from the platinum(II)-based antenna triple states. As expected, give emission bands were observed for europium(III) species at 581, 596, 616, 652, and 687 nm, three for the PtNd species at 877, 1066, and 1339 nm, and one for the PtYb species at 981 nm. In dichloromethane solutions of the $PtLn_2$ complexes, ILCT fluorescence from the $^1\pi \rightarrow \pi^*$ excited state of C≡CC_6H_4terpy is observed with a maximum at 420–460 nm, whereas low-energy phosphorescence emission from ^{3}ILCT ($\pi \rightarrow \pi^*$(C≡CC_6H_4terpy))/^{3}MLCT(dπ(Pt) → π^*(C≡CC_6H_4terpy)) triplet states is quenched. Since the tail of the ILCT fluorescence emission may overlap with the phosphorescence region of the Pt(C≡CC_6H_4terpy)$_2$ moiety, it is uncertain whether the phosphorescence of the platinum(II) alkynyl chromophore is entirely quenched. Thus, the [Pt(P–P)(C(CC_6H_4terpy)$_2$] precursors exhibit intense, long-lived room-temperature phosphorescence, originating probably from an admixture of ^{3}ILCT ($\pi \rightarrow \pi^*$(C≡CC_6H_4terpy)) and ^{3}MLCT(d(Pt) → π^*(C≡CC_6H_4terpy) triplet states, which qualifies them as favourable energy donors to facilitate Pt → Ln energy transfer in the corresponding $PtLn_2$ heterotrinuclear complexes. As above anticipated, sensitized lanthanide luminescence in $PtLn_2$ heterotrinuclear complexes is attained through efficient energy transfer from the platinum(II) alkynyl chromophore based ^{3}MLCT and ^{3}ILCT triplet states [156].

Heterodi- and heteropolynuclear d, f complexes with peculiar magnetic properties have been prepared by using single binucleating ligands as 1,1′-dipyridyloxime (H-pdk). For instance, [$CuDy_2$(**10**)$_6$(dpk)$_2$], prepared from [Cu(dpk)$_2$] and [Dy(**10**)$_3$(H_2O)$_2$], contains a linear DyCuDy trinuclear core, where each oximate N–O^- group bridges one O_8 eight coordinate, lateral dysprosium(III) ion, with three [**10**]$^-$ ligands completing its coordination environment, and the central N_4 square planar copper(II) ion (Fig. 52). The similar trinuclear core was found also in [$NiDy_2$(**10**)$_6$(dpk)$_2$(py)$_2$] or [$NiLn_2$(**10**)$_6$(dpk)$_2$(phen)], which coordinate additional nitrogen-containing ligands. Magnetic susceptibility measurements revealed that the Ln_2Ni complexes do not posses appreciable intramolecular ferromagnetic or ferrimagnetic interaction. The frequency dependence of out-of-phase ac susceptibility, observed only for the Dy_2Cu complex, is an indication of its behaviour as single-molecule magnet

Equimolar amounts of [M(L^a)] (M = Cu^{II}, Ni^{II}; H_2–L^a = N,N′-bis(salicylidene)-2-iminobenzylamine) and [Ln(**10**)$_3$(H_2O)$_2$] (Ln = Gd, Lu) furnish [MLn(**10**)$_3$(L^a)], where the shortest intermolecular M···M, M···Ln and Ln···Ln distances, 6.002, 7.522, and 8.507 Å for the CuGd complex, 5.945, 7.510 and 8.555 Å for the NiGd complex and 5.972, 7.455, 8.635 Å for the NiLu complex, respectively, attest that discrete dinuclear entities take place. The two metal ions, 3.248, 3.214 and 3.151 Å apart for the CuGd, NiGd and NiLu complex, respectively, are bridged by the two phenolate oxygen atoms. The transition metal(II) ion is bound to the two imine nitrogen atoms and the two phenolate oxygen atoms of [L^a]$^{2-}$, while the lanthanide(III) ion is eight coordinate with six oxygen atoms of three [**10**]$^-$ and two phenolate oxygen atoms

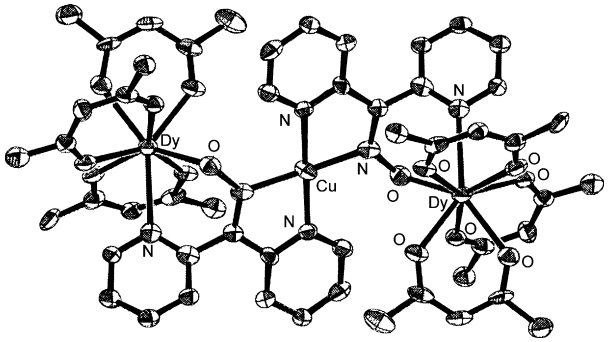

Fig. 52. Structure of [$CuDy_2$(**10**)$_6$(dpk)$_2$] [157].

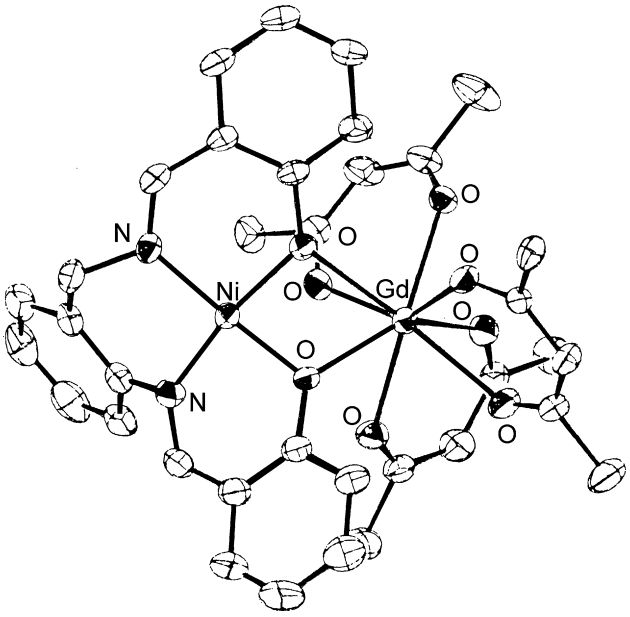

Fig. 53. Structure of [NiGd(**10**)$_3$(L^a)] [158].

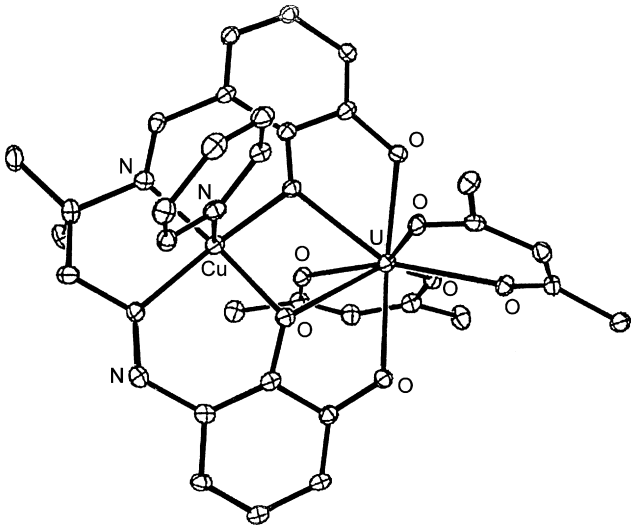

Fig. 54. Structure of [CuU(**5**)$_2$(L^c)(py)] [159].

of [L^a]$^{2-}$ (Fig. 53). Magnetic data indicate a ferromagnetic spin coupling between the gadolinium(III) and copper(II) ions [158].

Furthermore, the mononuclear complexes, derived from symmetric or asymmetric acyclic compartmental ligands with the transition metal ion in the inner N_2O_2 coordination chamber and the outer O_2O_2 chamber ready for further metal ion complexation, form heterodi- and -polynuclear lanthanide complexes whose magnetic properties strongly depend upon the resulting supramolecular assembly. Several of these systems have widely been discussed in previous reviews [9,10]; we report here some explanatory examples, published in the most recent literature. H_4–L^b and H_4–L^c, derived from the [2 + 1] condensation of 2,3-dihydroxybenzaldehyde with 1,3-diaminopropane or *N*,*N*′-dimethylethylenediamine, respectively, form with the appropriate metal(II) salt [M(H_2-L^b)] and [M(H_2-L^c)] (M = Co^{II}, Ni^{II}, Cu^{II}, Zn^{II}), which react with [M′(**5**)$_4$] (M′ = U^{IV}, Th^{IV}, Zr^{IV}) in a 2:1 molar ratio in pyridine at 110 °C to afford [M_2M′(L^b)$_2$]·npy and [M_2M′(L^c)$_2$]·npy. By lowering the temperature to 20 °C and to 60 °C, [CuU(**5**)$_2$(L^b)(py)] together with [Cu_2U(L^b)$_2$(py)] and [CuU(**5**)$_2$(L^c)(py)] were formed, respectively, this last complex identical to that synthesized from [M(**5**)$_2$] and [U(**5**)$_2$(H_2-L^c)]. Noticeably, similar treatment of [Cu(**5**)$_2$] with [U(**5**)$_2$(H_2-L^b)] gives mixtures of the CuU and Cu_2U complexes [159].In [MU(**5**)$_2$(L^c)(py)] (M = Cu^{II}, Zn^{II}) the transition metal(II) and the uranium(IV) ions in the inner N_2O_2 and outer O_2O_2 cavity of [L^c]$^{4-}$, respectively, are bridged by the two oxygen atoms of the salicylidene fragments. Four oxygen atoms from [L^c]$^{4-}$ and four from [**5**]$^-$ complete the dodecahedron around the uranium(IV) ion (Fig. 54). The Cu···U distance in [CuU(**5**)$_2$(L^c)(py)] is 3.574 Å and the shortest intermetallic Cu···Cu distance is 8.783 Å. Antiferromagnetic coupling occurs in [CuU(**5**)$_2$(L^c)(py)].

The tetranuclear M_2Ln_2 complexes [M_2Ln_2(**10**)$_4$(L^d)$_2$] (M = Cu, Ni; Ln = La···Lu except Pm; H_3–L^d = 1-(2-hydroxybenzamido)-2-(2-hydroxy-3-methoxybenzylideneaminoethylene)) were prepared by simple mixing equimolar methanolic solutions of K[M(L^d)]·nH_2O and [Ln(**10**)$_3$(H_2O)$_2$], in order to investigate the nature of the Cu^{II}–Ln^{III} magnetic interactions and to try to understand why some complexes, i.e. the $Cu_2^{II}Tb_2^{III}$ and $Cu_2^{II}Dy_2^{III}$ complexes, are single molecule magnets while the other complexes are not. The powder X-ray diffraction patterns showed that the Cu_2Ln_2 complexes are isomorphous to each other. All the Cu_2Ln_2 complexes possess a similar cyclic tetranuclear structure, in which the copper(II) and lanthanide(III) ions are arrayed alternately via bridges of the {Cu(L^d)} unit as found in the Cu_2Gd_2 complex. The two phenoxo and the methoxy groups at one side of the planar copper(II) complex coordinate to a gadolinium(III) ion as a tridentate ligand with a Cu···Gd distance of 3.432 Å. The amido

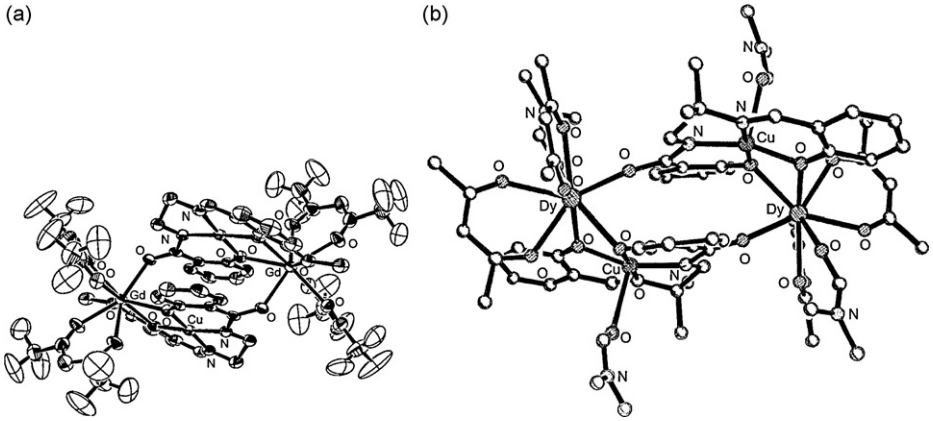

Fig. 55. Structures of [Cu_2Gd_2(**10**)$_4$(L^d)$_2$] (a) [160] and [Cu_2Dy_2(**10**)$_4$(L^e)$_2$(DMF)$_4$] (b) [162].

oxygen atom on the opposite side of the copper(II) complex coordinates to another gadolinium(III) ion as a monodentate ligand with the Cu···Gd distance of 5.620 Å. Including the coordination of the two [**10**]$^-$ ions as a bidentate chelate ligand, the gadolinium(III) ion reaches an O_8 eight coordinate geometry (Fig. 55a) [160,161,137].

Also the Ni_2Ln_2 complexes are isomorphous to each other but are not isomorphous to the Cu_2Ln_2 analogues. FAB–MS of the Ni_2Ln_2 complexes shows a molecular ion peak corresponding to the tetranuclear species $[Ni_2Ln_2(\mathbf{10})_3(L^d)_2]^+$, indicating that the Ni_2Ln_2 complexes assume a tetranuclear structure similar to that of the Cu_2Gd_2 complex [160,161,137].

The temperature-dependent magnetic susceptibilities from 2 to 300 K and the field-dependent magnetizations from 0 to 5 T at 2 K, measured for the Cu_2Ln_2 and Ni_2Ln_2 complexes with the Ni_2Ln_2 complex containing diamagnetic nickel(II) ions being used as a reference for the evaluation of the Cu–Ln magnetic interactions, have revealed that the interactions between the copper(II) and lanthanide(III) ions are very weakly antiferromagnetic for Ln = Ce, Nd, Sm, Yb, ferromagnetic for Ln = Gd, Tb, Dy, Ho, Er, Tm, and negligible for Ln = La, Eu, Pr, Lu. The magnetic properties examined down to 0.1 K reveal the unusual slow setting-up of a 3D order below 0.6 K.

Among the Cu_2Ln_2 complexes exhibiting ferromagnetic interaction, only the terbium(III) and dysprosium(III) complexes showed a frequency dependence of χ'_M and χ''_2, and were therefore expected to be SMMs, while the gadolinium(III), holmium(III), erbium(III) and thulium(III) complexes showed no frequency dependence under the same experimental conditions. With the goal of better understanding the evolution of the intramolecular magnetic interactions, X-ray magnetic circular dichroism has also been measured on $Cu^{II}_2Tb^{III}_2$, $Cu^{II}_2Dy^{III}_2$, and $Ni_2{}^{II}Tb_2{}^{III}$ complexes, both at the L- and M-edge of the metal ions and at the K-edge of the nitrogen and oxygen atoms. It was observed that the moment on the 4f ions is lower than that is predicted by Hund's rule, the orbital moment on the copper ions is almost completely quenched and the moments on the 3d and 4f ions are parallel, which confirms the ferromagnetic coupling deduced from SQUID observations. While no magnetic polarization could be measured on the nitrogen atoms, some amount has been detected on the oxygen. This is relevant, since the magnetic intramolecular coupling within these SMMs usually pass through light elements such as oxygen. Unfortunately, it was not possible to perform these measurements below 2 K, where a more intense signal below the blocking temperature could probably be observed. A closer examination of the low temperature magnetic properties down to 0.1 K. of the Cu_2Tb_2 complex exhibiting SMM behaviour have revealed an unexpected behaviour, ascribed to the very slow setting-up of a 3D order below 0.6 K [160,161,137].

Furthermore, 2-hydroxy-*N*-(2-{[2-hydroxyphenyl)methylene] amino}-2-methylpropyl)benzamide (H_3–L^e), containing an inner N_2O_2 coordination site and an oxygen atom coming from an amide function not involved in this site, by treatment with copper(II) acetate in the presence of piperidine (pip) affords [H-pip][Cu(L^e)] which reacts with the appropriate Ln(**10**)$_3$·$n$$H_2O$ (Ln = Gd,Dy,Tb) in methanol to yield $[Cu_2Ln_2(\mathbf{10})_4(L^e)_2(CH_3OH)_2]$; slow diffusion of acetone into a dimethylformamide solution of these complexes gives $[Cu_2Ln_2(\mathbf{10})_4\ (L^e)_2(DMF)_4]$. In $[Cu_2Dy_2(\mathbf{10})_4(L^e)_2(DMF)_4]$ each distorted square pyramidal copper(II) ion is surrounded by the N_2O_2 atoms of a $[L^e]^{3-}$ ligand in the basal plane and a dimethylformamide oxygen atom in apical position while each eight coordinate dysprosium(III) ion is surrounded by two [**10**]$^-$ ligands and linked to the anionic $[L^e]^{3-}$ entity by the two phenoxo oxygen atoms that make a double bridge between the two metal ions with a Cu···Dy separation of 3.297 Å. The coordination sphere is completed by a dimethylformamide oxygen atom and the amide functions not involved in the copper coordination. Thus, two heteronuclear CuDy entities are assembled through the oxygen atoms of the amido groups to form a double (Cu–N–C–O–Dy) bridge. The shortest metal···metal separations not related by a material link are equal to 5.900 Å for Cu···Cu, 6.087 Cu···Dy and 7.813 Å and Dy···Dy. The intermolecular metal···metal separations, larger than 10.4 Å, preclude any significant magnetic interaction between these tetranuclear units (Fig. 55b) [162].

Ferromagnetic interactions are active in the Cu_2Gd_2 entities, through the double phenoxo bridge ($J = 3.2\ cm^{-1}$) and through the single amide bridge ($J = 9.54\ cm^{-1}$), these interactions are still present in the Cu_2–Tb_2 and Cu_2–Dy_2 complexes which behave as single molecule magnets (SMMs), due to the introduction of anisotropic lanthanide(III) ions in place of gadolinium(III) ions [162].

Compartmental ligands and β-diketones were jointly used for the recognition of alkaline earth ions. [Cu(L)], where H_2–L^f is the Schiff base derived from the [2 + 1] condensation of 3-methoxy-2-hydroxy-benzaldehyde with 1,2-diaminoethane, reacts with related metal(II) hydroxide in the presence of H–**7** to yield $[CuM(\mathbf{7})_2(L^f)]$, (M = Ca^{II}, Sr^{II}, Ba^{II}). In $[CuCa(\mathbf{7})_2(L^f)(CH_3OH)]$ the copper(II) and calcium(II) cations, 3.460 Å apart, are doubly bridged by phenoxo oxygen atoms. The five coordinate copper(II) ion is equatorially bound to the nearly coplanar N_2O_2 donors afforded by the inner chamber of $[L^f]^{2-}$ while the axial position is occupied by the methanol oxygen atom. The eight coordinate calcium cation is surrounded by the O_2O_2 donors of the outer chamber of $[L^f]^{2-}$ and by four oxygen atoms from two chelating [**7**]$^-$ anions. π–π• stacking interactions between the aromatic rings induce short intermolecular Cu···Cu (3.819 Å) and large Ca···Ca (8.951 Å) distances (Fig. 56) [163].

The copper(II) oximato complexes [Cu(H-dmg)$_2$] and [Cu(H-emg)$_2$] (H_2-dmg = dimethylglyoxime, H-emg = methylethylglyoxime) act as templates in the synthesis of heteropolynuclear complexes, mediating the magnetic interaction between the metal ions through the N–O bridges [9,10]; consequently, they have been chosen as precursors for the preparation of 3d, 4f-ferri- or -ferromagnetic molecular materials. They, after deprotonation in basic media, form discrete tetranuclear, pentanuclear or one dimensional polymeric species by reaction with [Ln(**10**)$_3$(H_2O)$_2$] (Ln = Gd, Dy). Introduction of ethyl groups ion place of methyl groups leads to a remarkable steric effect: the same procedures using [Cu(H-dmg)$_2$] or [Cu(H-emg)$_2$] gives $[Cu_2Gd_2(\mathbf{10})_4(dmg)_2$(H-dmg)$_2(CH_3OH)_2]_n$ and $[Cu_2Gd_2(\mathbf{10})_4(emg)_2$(H-emg)$_2(CH_3OH)_4]$,

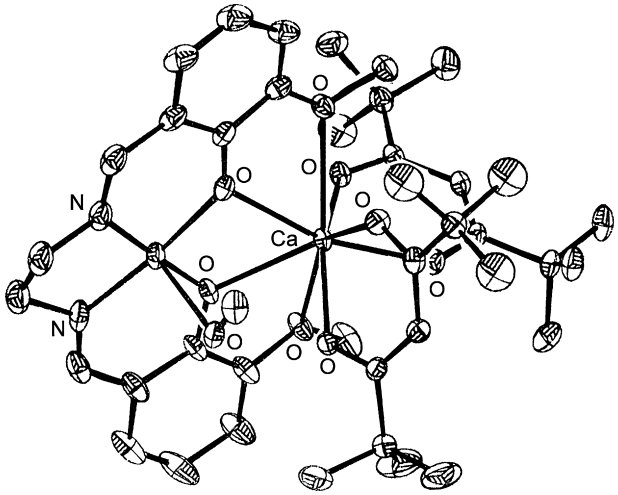

Fig. 56. Structure of $[CuCa(\mathbf{7})_2(L^f)(CH_3OH)]$ [163].

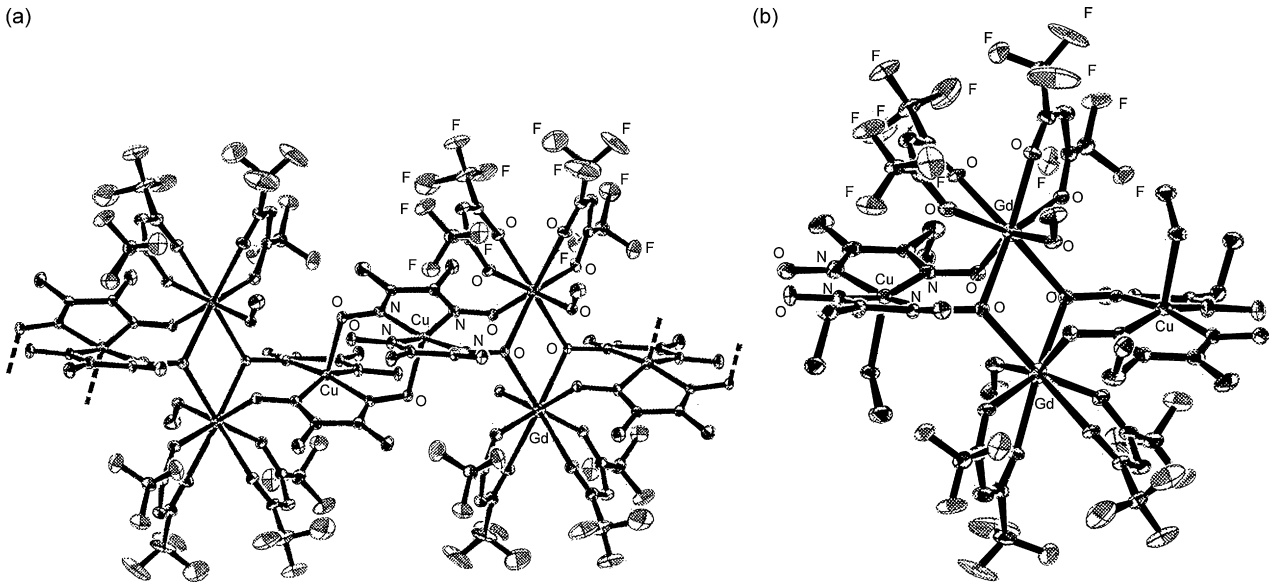

Fig. 57. Structures of $[Cu_2Gd_2(\mathbf{10})_4(dmg)_2(H\text{-}dmg)_2(CH_3OH)_2]_n$ (a) and $[Cu_2Gd_2(\mathbf{10})_4(emg)_2(H\text{-}emg)_2(CH_3OH)_4]$ (b) [165].

respectively [164,165]. In the chain structure of the $\{Gd_2Cu_2\}_n$ complex, the gadolinium(III) ions are eight coordinate with a methanol molecule coordinated in place of a $[\mathbf{10}]^-$ ligand while the copper(II) ions are five coordinate with a neighbouring oximate oxygen atom located in the axial position. The gadolinium and copper ions, 4.044 Å apart, are doubly bridged by the oximate N–O groups. Also the two gadolinium(III) ions are doubly bridged by oximate oxygen atoms. The interatomic Gd···Gd and Cu···Cu distances are 4.023 Å and 3.889 Å, respectively. The {Cu(dmg)(H-dmg)} moieties form a sandwich dimer, correlated with an inversion of symmetry. The core structure of the tetranuclear Cu_2Gd_2 complex is the same as that of $\{Gd_2Cu_2\}_n$. The Gd···Gd and Gd···Cu separations are 3.985, 3.939 and 4.784 Å, respectively, within a molecule. The presence of bent ethyl groups in {Cu(emg)(H-emg)} prevents dimerization of this moiety. Instead, a methanol ligand occupies the axial position (Fig. 57a and b) [164,165].

Using the same procedure, $[Dy(\mathbf{10})_3(H_2O)_2]$ gives $[Cu_2Dy_2(\mathbf{10})_4(emg)_2(H\text{-}emg)_2(ROH)_4]$ (R = CH_3, C_2H_5) and $[Cu_2Dy_2(\mathbf{10})_4(dmg)_2(H\text{-}dmg)_2(CH_3OH)_2]_n$. The Cu_2Gd_2 and Cu_2Dy_2 complexes are isomorphous. Solely the *cis*-isomer of the [Cu(emg)(H-emg)] moiety in the Dy_2Cu_2 complex (R = C_2H_5) was observed, in contrast to the case of $[Cu_2Dy_2(\mathbf{11})_4(emg)_2(H\text{-}emg)_2(CH_3OH)_4]$, where only the *trans*-isomer was found. Also in the absence of the X-ray structure of $\{Cu_2Dy_2\}_n$, the cell parameters strongly support that $\{Cu_2Dy_2\}_n$ and $\{Cu_2Gd_2\}_n$ are isomorphous [164,165].

In $[P(C_6H_5)_4]_2[CuGd_4(\mathbf{10})_8(dmg)_2(CH_3COO)_4]$, prepared by mixing $Gd(CH_3COO)_3{\cdot}4H_2O$ and $[Gd(\mathbf{10})_3(H_2O)_2]$ in a 2:1 molar ratio to $[Cu(dmg)_2]^{2-}$ followed by addition of $[P(C_6H_5)_4](Cl)$, there are two crystallographically independent $\{Gd(\mathbf{10})_2\}$ units: one with an eight coordinate gadolinium(III) ion and the other with a nine coordinate gadolinium(III) ion. The $\{Cu(dmg)_2\}^{2+}$ ion is surrounded by four $\{Gd(\mathbf{10})_2\}^{2+}$ units, giving rise to Cu···Gd distances of 3.183 and 3.853 Å. The four gadolinium(III) ions are at the corners of a rectangle while the copper(II) ion sits at the center. For the shorter edge of the rectangular gadolinium array, the oximato oxygen atoms doubly bridge two gadolinium ions, giving rise to a butterfly-like structure in the Gd_2O_2 moiety. An acetate oxygen atom also bridges two gadolinium(III) ions, 3.713 Å, apart. For the longer edge, an acetate anion bridges two gadolinium(III) ions, 6.713 Å, apart, in a $\mu_{1,3}$-manner (Fig. 58) [164,165].

The $\{Cu_2Dy_2\}_n$ one-dimensional polymeric complexes, consisting of alternating dicopper(II) and digadolinium(III) units, exhibit ferrimagnetic behaviour, ascribable to antiferromagnetic coupling across the oximate N–O bridges between the high-spin homodinuclear units. Although ferromagnetic coupling between gadolinium (III) and copper (II) ions has often been observed, the $\{Cu_2Gd_2\}_n$ and Cu_2Gd_2 complexes were reported to have antiferromagnetic coupling due to their bent Cu–N–O–Gd structure. As a result, the $\{Cu(dmg)_2\}$ core plays the role of ferrimagnetic coupler between the gadolinium(III) spins. $\{Cu_2Gd_2\}_n$ is A_2B_2-type ferromagnetic chain. Also in $[Cu_2Dy_2(\mathbf{10})_4(emg)_2(H\text{-}emg)_2(ROH)_4]$ (R = CH_3, C_2H_5), as in $[Cu_2Dy_2(\mathbf{10})_4(dmg)_2(H\text{-}dmg)_2(CH_3OH)_2]_n$, the *M–H* curves clarified antiferromagnetic coupling between the dysprosium(III) and the copper(II) ions in the Dy_2Cu_2 motif, leading to the dysprosium(III) magnetic moments alignes parallel ({Cu(↓)Dy(↑)Cu(↓)Dy(↑)]). Ac magnetic susceptibility measurements on $[Cu_2Dy_2(\mathbf{10})_4(emg)_2(H\text{-}emg)_2(CH_3OH)_4]$ and $[Cu_2Dy_2(\mathbf{10})_4(dmg)_2(H\text{-}dmg)_2(CH_3OH)_2]_n$ show a χ_{ac} (in-phase) decrease and a concomitant χ''_{ac} (out-of-phase) increase with a frequency increase. Low temperature magnetization measurements on $\{Cu_2Dy_2\}_n$ exhibit magnetic hysteresis, characteristic of single-chain magnets. Finally magnetic measurements on $[P(C_6H_5)_4]_2[Cu_2Gd_2(\mathbf{10})_8(dmg)_2(CH_3COO)_4]$ reveal high ground spin multiplicity, as expected regardless of the sign of magnetic Cu···Gd coupling through N–O bridges. The ground state was suggested to be $S_{tot} = 27/2$ with the exchange parameter $2J/K_B = -2.9$ K between the gadolinium and copper ions. The antiferromagnetic coupling is operative owing to the largely distorted Gd–O–N–Cu bridges [164,165].

10. 1,3,5-Triketonato complexes

The β,δ-tricarbonyl compounds, the higher analogues of the β-dicarbonyl compounds, can take triketo-, monoenol- and bisenol-forms in their tautomeric equilibrium, deeply studied by IR and ^1H NMR spectroscopy, the percentage of the different tautomeric forms depending on the solvent polarity the temperature and the different substituents at the periphery of the coordinating moiety [6,9,12,166,167].

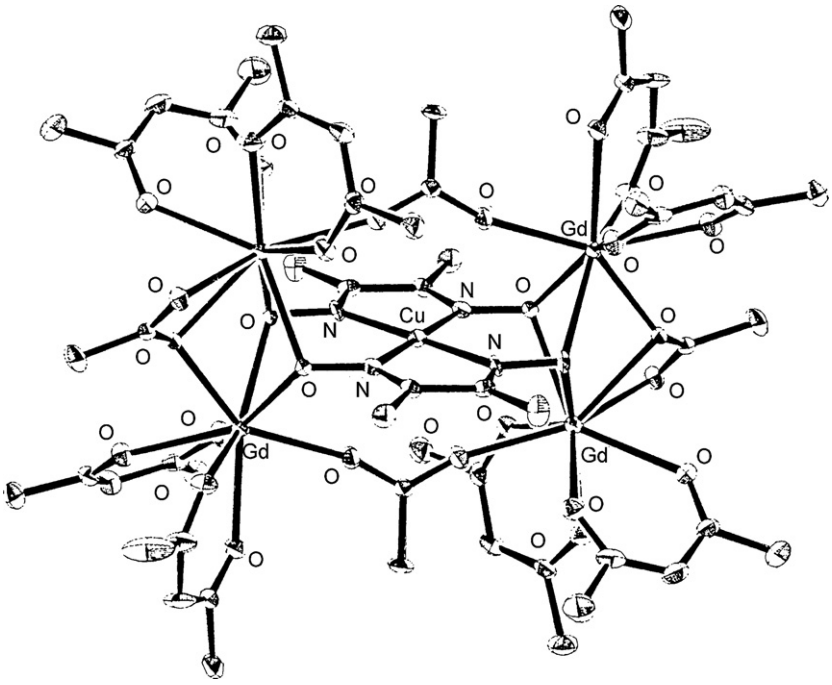

Fig. 58. Structure of $[CuGd_4(\mathbf{10})_8(dmg)_2(CH_3COO)_4]^{2-}$ [165].

The well developed π-system, present in the potentially dinegative, tridentate ligands H_2–**54a**···H_2–**54f**, confers them a planar structure. Mononuclear or dinuclear complexation occurs when these ligands are reacted with the appropriate metal salt, the dinuclear complexes being favoured over the mononuclear one at higher temperatures. For instance, $[Cu(H\text{-}\mathbf{54a})_2]\cdot 2H_2O$ or $[Cu_2(\mathbf{54a})_2]$ occur when copper(II) acetate is added to H_2–**54a** in water/methanol at about 0 °C or 30 °C, respectively. The mononuclear blue complex transforms into the dinuclear green one at about 80 °C under reduced pressure or when dissolved in boiling methanol. On the other hand the green complex changes into the blue one in pyridine in the presence of a large excess of H_2–**54a**, once the solvent is removed at 0 °C. These transformations indicate that $[Cu_2(\mathbf{54a})_2]$ is stable at elevated temperature, while $[Cu(H\text{-}\mathbf{54a})_2]$ prefers a lower temperature and that the conversion from one to the other is reversible [168].

While H_2–**54a**···H_2–**54f** give rise to homodinuclear vanadyl(IV) complexes, they are not suitable for the formation of dinuclear uranyl(VI) complexes as the seven coordinated pentagonal bipyramidal geometry around this ion imposes constraints on these chelating ligands [169,170]. On the contrary, no problem arises for the preparation of mononuclear complexes as ascertained for $[UO_2(H\text{-}\mathbf{54b})_2(CH_3OH)]$, where the seven coordinate pentagonal bipyramidal uranium(VI) ion is equatorially surrounded by two $[H\text{-}\mathbf{54b}]^-$ ligands in a *cis*-configuration and one methanolic oxygen atom. In the presence of $N(C_2H_5)_3$, the trinuclear complexes occur as found for $[NH(C_2H_5)_3]_2[(UO_2)_3(\mathbf{54c})_3(\mu_3\text{-}O)]$ which contains a nearly equilateral triangle of uranyl(VI) ions with a central $\{\mu_3\text{-}O\}^{2-}$ ion, trigonally bonded to the three uranium ions and additionally linked by two bridging $[\mathbf{54c}]^{2-}$ ligands resulting in a seven coordination about each uranium ion in a nearly pentagonal bipyramidal geometry (Fig. 59) [169].

In $[Cu_2(\mathbf{L})_2(py)_2]$ (H_2–**L** = H_2–**54a**, H_2–**54d**, H_2–**54e**–H_2–**54f**) the copper(II) ions are square pyramidal with the four oxygen atoms from two $[\mathbf{L}]^{2-}$ ligands attached to each copper ion coplanar and two axial pyridine molecules *trans* to each other, this precluding any dimerization (Fig. 60)

Dimerization occurs in $[Cu_2(\mathbf{55})_2(H_2O)_2]$, as the sixth axial coordination site of one dinuclear unit is occupied by a ketone oxygen of another symmetry-related dinuclear unit at a distance of 3.01 Å. The copper ions are distorted octahedral with the two coordinated water molecules on the same side of the plane described by the two copper ions and two triketonates [171].

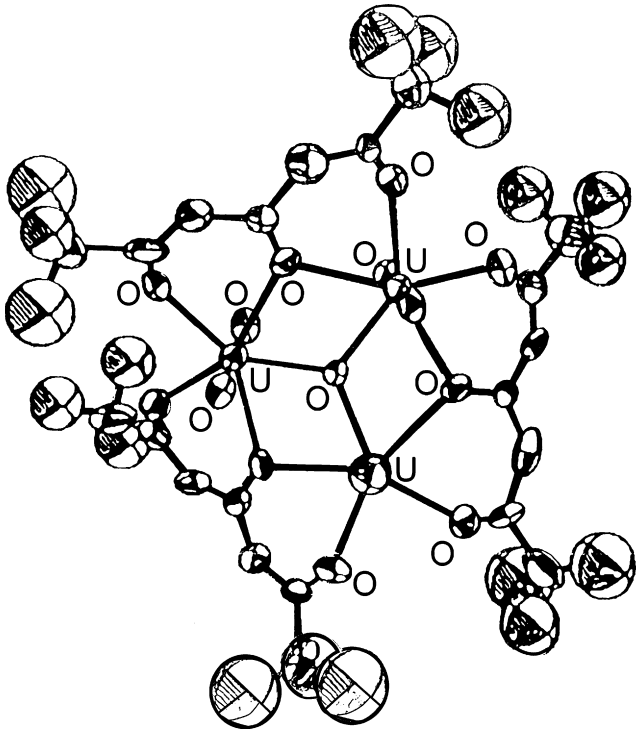

Fig. 59. Structure of $[(UO_2)_3(\mathbf{54c})_3(\mu_3\text{-}O)]^{2-}$ [169].

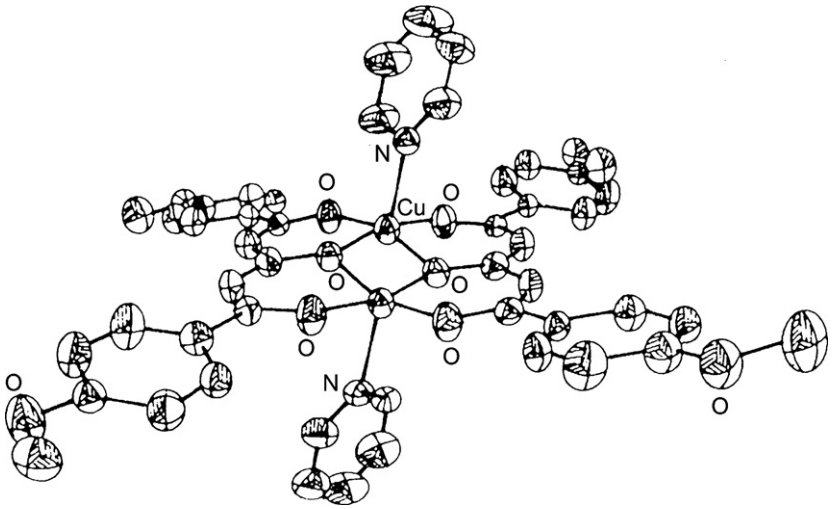

Fig. 60. Structure of $[Cu_2(\mathbf{54d})_2(py)_2]$ [170].

A comparable strong antiferromagnetic interaction, with no EPR signals at room temperature and often diamagnetism, was found in these dicopper(II) complexes indicating that changes of substituent groups produce a small perturbation on a very large exchange interaction [172], while $-2J$ value of 160 cm^{-1} occurs in $[(VO)_2(\mathbf{54a})_2(py)_2]$ [170].

$[M_2(\mathbf{54a})_2(H_2O)_4]$ ($M = Ni^{II}, Co^{II}$) have been isolated by a synthetic procedure similar to that of the copper(II) analogues, while the corresponding mononuclear ones could not be obtained by the procedure employed in the synthesis of $[Cu(H\text{-}\mathbf{54a})_2]$. Nickel(II) or cobalt(II) acetate, allowed to react with an excess of H_2–**54a** with the purpose of obtaining the related mononuclear chelates, always produce the dinuclear complexes and byproducts (1-hydroxy-2,6-diacetyl-3-acetomethyl-5-methylbenzene and/or 1,8-dihydroxy-3,6-dimethyl-7-acetylnaphtalene) derived from the bimolecular condensation of H_2–**54a**. $[M(H\text{-}\mathbf{54a})_2]$ was prepared by the ligand exchange reaction between $[M(\mathbf{5})_2]$ and H_2–**54a** in anhydrous diethylether or by the reaction of $[M_2(\mathbf{54a})_2]$ and molten H_2–**54a** [173,174].

Coordinated water in $[M_2(\mathbf{54b})_2(H_2O)_4]$ ($M = Ni^{II}, Co^{II}$) can easily be replaced by pyridine to afford $[M_2(\mathbf{54b})_2(py)_4]$, where each octahedral metal(II) ion is surrounded by to the four coplanar carbonyl oxygen atoms of two $[\mathbf{54b}]^-$ ligands and two axial pyridine nitrogen atoms. The Ni···Ni distance of (3.166 Å) is 0.106 Å shorter than the Co···Co one. While the magnetic moments of dinickel(II) chelates are typical of magnetically dilute complexes at room temperature although there is evidence for spin coupling at lower temperatures, the occurrence of an antiferromagnetic interaction between the two cobalt(II) ions in $[Co_2(\mathbf{54b})_2(py)_4]$ was found (Fig. 61) [174,175].

$[Ni_3(\mathbf{54f})_2(OH)_2(CH_3OH)_4]$, obtained under conditions that favour $[Ni_2(\mathbf{54f})_2(CH_3OH)]$, shows a magnetic susceptibility behaviour in the 4–296 K temperature range typical of linear array of three nickel(II) ions with the adjacent metal(II) ions ferromagnetically coupled ($J_{12} = 10\ cm^{-1}$), and the terminal nickel(II) ions antiferromagnetically coupled ($J_{13} = -6\ cm^{-1}$). Dissolution of $[Ni_3(\mathbf{54f})_2(OH)_2(CH_3OH)_4]$ in pyridine, followed by slow evaporation at room temperature in air, causes a ligand oxidation and migration of the *tert*-butyl group from the terminal carbonyl 3-carbon to the adjacent 4-carbon. In addition, a hydroxyl group resides on the same carbon in the final product. The entire process has converted the original ligand, $[\mathbf{54f}]^{2-}$ to $[\mathbf{56}]^{3-}$ through a chemical pathway involving an oxidation of the 4-carbon of $[\mathbf{54f}]^{2-}$ and an attack of OH^- on the carbonyl 3-carbon, followed by a benzylic acid type rearrangement. The final coordination environment of each nickel(II) ion in the final complex $[Ni_2(H\text{-}\mathbf{56})_2(py)_4]$ consists of one β-diketonate chelate ring, one carboxylate oxygen and one hydroxo oxygen, forming together a 5-membered σ-hydroxy carboxylate chelate ring, and two pyridine nitrogen atoms (Fig. 62) [176].

11. 1,3,5,7-Tetraketonato complexes

Tetraketones, containing two (H_2–**57**, H_2–**58a**···H_2–**58b**) or three enolisable protons (H_3–**59a**, H_3–**59b**), have been prepared so far; they give rise to different structures when reacted with the appropriate metal salt. The first ligand type quite easily forms polynuclear complexes; dinuclear entities can be obtained only when additional charged or neutral ligands are inserted in order to prevent oligomerization. The second tetraketone type forms homotrinuclear complexes, with the metal ions close together and strongly interacting each other, in addition to homodinuclear ones with the two metal ions occupying the external O_2O_2 chambers and very weakly magnetically interacting each other.

H_2–**57**, obtained by reaction of $[Na(\mathbf{5})]$ with I_2 [177], affords $[Ni_2(\mathbf{57})(tmeda)_2(H_2O)_2](ClO_4)_2{\cdot}H_2O$ or $[Ni_2(\mathbf{57})(NO_3)_2(tmeda)_2]$ when mixed with stoichiometric amounts of the appropriate

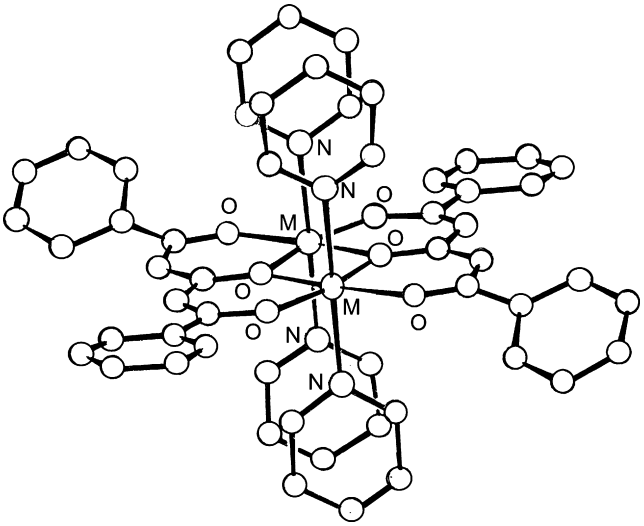

Fig. 61. Structure of $[M_2(\mathbf{54b})_2(py)_4]$ ($M = Ni^{II}, Co^{II}$) [174].

nickel(II) salt and *N*,*N*,*N*′,*N*′-tetramethylenediamine (tmeda) in ethanol. In $[Ni_2(\mathbf{57})(tmeda)_2(H_2O)_2](ClO_4)_2{\cdot}H_2O$ one nickel(II) ion is square planar and the other one is octahedral, being coordinated also to the two water molecules, while two octahedral nickel(II) ions occur in $[Ni_2(\mathbf{57})(NO_3)_2(tmeda)_2]$ where two coordination site of each metal ion being filled by a chelating nitrate group. Two square planar nickel(II) ions occur also in $[Ni_2(\mathbf{57})(tmeda)_2](BPh_4)_2$, prepared by the addition of sodium tetraphenylborate to $[Ni_2(\mathbf{57})(NO_3)_2\ (tmeda)_2]$ in 1,2-dichloroethane [178].

The *meso* (Δ–Λ) isomer and the *racemic* isomer (a mixture of Δ–Λ and Λ–Λ) of $[Ru_2(\mathbf{57})(\mathbf{5})_4]$ originate from the reaction of $[Ru(\mathbf{5})_2(CH_3CN)](PF_6)$ and H_2–**57** in toluene. The reaction of H_2–**57** with $[Ru(\mathbf{7})_2(CH_3CN)_2](PF_6)$ forms $[Ru(H\text{-}\mathbf{57})(\mathbf{7})_2]$, in addition to $[Ru_2(\mathbf{57})(\mathbf{7})_4]$, the latter being a mixture of *meso* and *racemic* isomers, as above described for $[Ru_2(\mathbf{57})(\mathbf{5})_4]$. Mixtures of the *meso* (Λ–Δ and Δ–Λ) and *racemic* (Δ–Δ and Λ–Λ) isomers of $[Ru_2(\mathbf{57})(\mathbf{5})_2(\mathbf{7})_2]$ were obtained from the reaction of $[Ru_2(\mathbf{57})(\mathbf{5})_4]$ and $[Ru(\mathbf{7})_2(CH_3CN)_2](PF_6)$, while a mixture of *meso* and *racemic* isomers of $[Ru_2(\mathbf{57})(bipy)_4](PF_6)_2$ was synthesized by reaction of $[Ru(Cl)_2(bipy)_2](Cl){\cdot}2H_2O$ with H_2–**57** in water/ethanol followed by the addition of $KHCO_3$ [179].

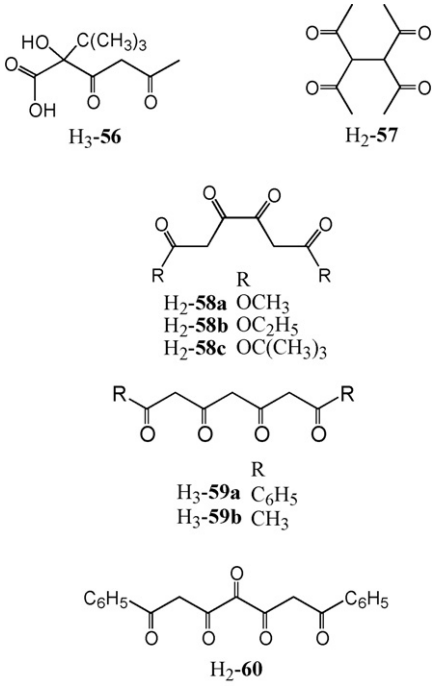

In the *meso* isomer of $[Ru_2(\mathbf{57})(\mathbf{5})_4]$ the two β-diketonato groups of the bridging $[\mathbf{57}]^{2-}$ ligand are almost perpendicular to one another. The octahedral coordination about each ruthenium(II) ion is completed by two chelating $[\mathbf{5}]^-$ ligands (Fig. 63a). A similar structure has been proposed for the other complexes. Voltammetric and electrospectroscopic measurements show that the comproportionation constant values K_c and K_c' of the mixed-valence $Ru^{III}Ru^{IV}$ and $Ru^{II}Ru^{III}$ complexes, respectively, are low because of the non-coplanarity of the two β-diketonato units of $[\mathbf{57}]^{2-}$ as revealed by the structure of $[Ru_2(\mathbf{57})(\mathbf{5})_4]$. Such a structure weakens the electron interaction between the two ruthenium(III) ions in $[Ru_2(\mathbf{57})(bipy)_4](PF_6)_2$, and this influences the conproportional constant values, slightly smaller than those of $[Ru_2(\mathbf{57})(\mathbf{5})_4]$ and $[Ru_2(\mathbf{57})(\mathbf{7})_4]$. The K_c of the oxidation process $Ru^{III}Ru^{III} \rightleftharpoons Ru^{III}Ru^{IV} \rightleftharpoons Ru^{IV}Ru^{IV}$, and the K_c' of the reduction process $Ru^{III}Ru^{III} \rightleftharpoons Ru^{II}Ru^{III} \rightleftharpoons Ru^{II}Ru^{II}$ of $[Ru_2(\mathbf{57})(\mathbf{7})_4]$ were larger than those of $[Ru_2(\mathbf{57})(\mathbf{5})_4]$. This would be due to the electron donating properties of the *tert*-butyl groups in the $[\mathbf{7}]^-$ ligand. Furthermore, the K_c values were larger than those of the K_c' in both the $[Ru_2(\mathbf{57})(\mathbf{5})_4]$ and $[Ru_2(\mathbf{57})(\mathbf{7})_4]$ [179].

$[Ru(\mathbf{5})_2(CH_3CN)_2](PF_6)$ and H_2–**57** in toluene afford $[Ru(\mathbf{5})_2(H\text{-}\mathbf{57})]$, whose Δ and Λ isomers can be separated by chromatography. The *racemic* complex reacts with the appropriate metal perchlorate in methanol to afford $[Ru_2Pd(\mathbf{5})_4(\mathbf{57})_2]$ or $[Ru_3M(\mathbf{5})_6(\mathbf{57})_3]$ ($M = Fe^{III}$, Al^{III}). The analogous chiral complexes are similarly obtained by Δ-$[Ru^{III}(\mathbf{5})_2(H\text{-}\mathbf{57})]$. For $[\{\Delta\text{-}Ru(\mathbf{5})_2(\mathbf{57})\}_2Pd]$, identical NMR spectra were recorded as for the *racemic* complex, this implying that the diastereomeric properties of peripheral ruthenium(III) groups has little effect on the configuration of a central palladium(II) core, because the two ruthenium(III) moieties are remote from each other so that their Δ/Λ configurations do not affect the stereochemistry of the central core. The same behaviour is observed for $[\{D\text{-}Ru(\mathbf{5})_2(\mathbf{57})\}_3Fe]$; on the contrary, NMR and CD data show that the central labile core of the aluminum(III) ion in $[\{\Delta\text{-}Ru(\mathbf{5})_2(\mathbf{57})\}_3Al]$ takes initially the coordination structure analogous to Λ-$[Al(\mathbf{5})_3]$ or Λ-$[\{\Delta\text{-}Ru(\mathbf{5})_2(\mathbf{57})\}_3Al]$, which slowly epimerizes to a diastereomeric mixture of Λ- and Δ-$[\{\Delta\text{-}Ru(\mathbf{5})_2(\mathbf{57})\}_3Al]$. This agrees with the low energy differences of 1.2 KJ mol^{-1} between Δ and Λ-$[\{\Delta\text{-}Ru(\mathbf{5})_2(\mathbf{57})_6\}_3Al]$. The molecular stacking in a crystalline state represents a main factor in locking the chiral configuration around the aluminum(III) core. According to the structure obtained by XRD data, the chiral configuration of the central aluminum(III) core is stabilized by intermolecular interactions with the three branches ejected from the neighbouring molecules (Fig. 63b). This locks the Ru_2Al complex as a Λ-form in the solid state [179].

A mixture of (ΔΔ/ΛΛ)-*rac*- and (ΔΛ)-*meso*-$[Ru_2^{III}(\mathbf{5})_4(L)]$ (H_2–L = 1,4-dihydroxy-9,10-anthraquinone) was synthesized by the reaction of H_2–L and $[Ru(\mathbf{5})_2(CH_3CN)_2]$ in the presence of CH_3COONa under aerobic conditions. The two diastereomers have been separated by chromatography. The structure of the (ΔΛ)-*meso* isomer shows that each ruthenium ion is bonded to the bridge via two oxygen donor centers in a β-diketonate chelate fashion. The ruthenium centers lie virtually in the same plane as the $[L]^{2-}$ bridging ligand. Each RuO_6 configuration is in a slightly distorted octahedral arrangement. The Ru···Ru distance is 8.158 Å. It contains two antiferromagnetically coupled ruthenium(III) ions. The potential of both the ligand ($L^0 \rightarrow L^{4-}$) and the metal complex fragment combination $[Ru^{II}(\mathbf{5})_2]_2 \rightarrow \{[Ru^{IV}(\mathbf{5})_2]_2\}^{4+}$ to exist in five different redox states creates a large variety of combinations, which was assessed for the electrochemically reversibly accessible 2+, 1+, 0, 1−, 2− forms using cyclic voltammetry as well as EPR and UV–vis–NIR spectroelectrochemistry. The results for the two isomers are similar: oxidation to $[Ru_2(\mathbf{5})_4(L)]^+$ causes the emergence of a near-infrared band at 1390 nm, without revealing an EPR response even at 4 K. Reduction to $[Ru_2(\mathbf{5})_4(L)]^-$ produces an EPR signal, signifying metal-centered spin but no near-infrared absorption. The metal-based oxidation of $[Ru^{III}{}_2(\mu\text{-}L^{2-})(\mathbf{5})_4]$ was tentatively assumed to a mixed-valent intermediate $[Ru^{III}Ru^{IV}(\mathbf{5})_4(\mu\text{-}L^{2-})]^+$ and ligand-centered reduction to a radical complex $[Ru^{III}{}_2(\mathbf{5})_4(\mu\text{-}L^{3-})]^-$ with antiferromagnetic three-spin interaction [180].

Equimolar amounts of $Co(CH_3COO)_4{\cdot}4H_2O$, di-2-pyridylamine (dpa) and H_2–**57** in CH_2Cl_2/CH_3OH produce the chiral square complex $[Co_4(\mathbf{57})_4(dpa)_4]$, with the four octahedral cobalt(II) centers in the identical chirality, i.e, either all in a Δ or Λ optical geometry. Each edge of the square, i.e. each pair of cobalt (II) ions, has a helical structure similar to that observed in $[Co_2(\mathbf{57})(dpa)_4(CH_3COO)_2(H_2O)_2]$, with $[\mathbf{57}]^-$ bridging two cobalt(II) ions. The Co···Co distances along the edge of the square are essentially identical (8.009 and 8.000 Å) while the diagonal Co···Co separation distance is 11.306 Å. The dpa ligand is chelated to each cobalt(II) ion via the two pyridyl nitrogen atoms (Fig. 64). In

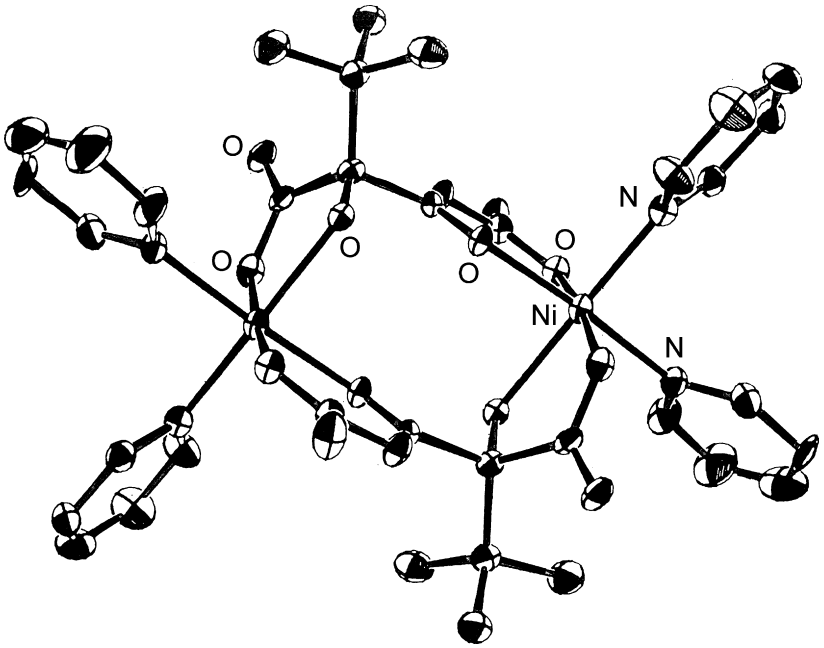

Fig. 62. Structure of $[Ni_2(H\text{-}\mathbf{56})_2(py)_4]$ [176].

the tetracobalt(II) and dicobalt(II) complexes ferromagnetic interactions occur [181].

Claisen condensation of alkyl acetates or methyl ketones with dialkyl oxalates, followed by acid workup, yields H_2–**58a**···H_2–**58c**. Deprotonation of H_2–**58b** with aqueous ammonia in ethanol, followed by the addition of the appropriate metal(II) dichloride, affords $[M_8(\mathbf{58b})_8]\cdot 4H_2O$ ($M = Ca^{II}$, Cd^{II}, Mn^{II}) which leads to the isostructural $[M_8(\mathbf{58b})_8(S)_4]$ ($S = C_2H_5OH$, C_3H_7OH, $(CH_3)_2CHOH$, $(CH_3)_3COH$). In $[Mn_8(\mathbf{58b})_8(C_3H_7OH)_4]$ (Fig. 65) the eight manganese ions are seven coordinate and at the corners of two differently sized concentric squares, turned 45° relative to each other. The four outer manganese ions are linked in a μ_1-fashion through the two ester carbonyl oxygen atoms of a set of four ketipinic acid diester dianions, which lie almost in a plane. The two keto oxygen atoms of these four ligands are μ_2-bound and bridge inner and outer manganese ions. Furthermore, a propanol molecule is coordinated to each of the four outer manganese ions. Four ketipinic acid diester dianions are each bound in a μ_1-fashion through the ester carbonyl oxygen atoms to one outer and one inner manganese ion. One of the keto oxygen atoms forms a μ_2 bridge between two inner manganese ions, and the other forms a μ_3 bridge to two inner and an outer manganese ion [181].

Tetranuclear adamantanoid chelate complexes are formed in a one-pot reaction from dimethyl malonate, methyllithium, the desired metal(II) chloride and oxalylchloride at −78 °C in tetrahydrofuran (THF) and subsequent workup with aqueous ammonium chloride. However, this methodology does not work in the case of ethyl acetate and oxalylchloride. Instead, double deprotonation of H_2–**58b** with methyllithium at −78 °C in tetrahydrofuran and addition of magnesium chloride, followed by workup with aqueous ammonium chloride, furnishes $[NH_4]_4[(Mg_4(\mathbf{58b})_6)]$ where, on each face of the tetrahedron constituted by the four magnesium ions, three oxygen atoms bind an ammonium ion through three hydrogen bonds [181].

Double deprotonation of H_2–**58b** with sodium hydroxide in a methanol sodium tetrafluoroborate solution and subsequent treatment with $CuCl_2\cdot 2H_2O$ lead to $[Cu_3Na(\mathbf{58b})_3](BF_4)$, which crystallizes from tetrahydrofuran to give the double-decker metalla-coronate complex $[Cu_6Na_2(\mathbf{58b})_6(BF_4)_2(THF)_2(H_2O)_2]$ and the triple decker metalla-crown ether complex $[Cu_9Na_3(\mathbf{58b})_9(BF_4)_2(THF)_2](BF_4)$ (Fig. 66a and b). A common feature of $[Cu_6Na_2(\mathbf{58b})_6(BF_4)_2(THF)_2(H_2O)_2]$ and $[Cu_9Na_3(\mathbf{58b})_9(BF_4)_2(THF)_2](BF_4)$ is the neutral, [15]-membered trimetalla-crown-6(15-MC-6) building block. Formal replacement of the three

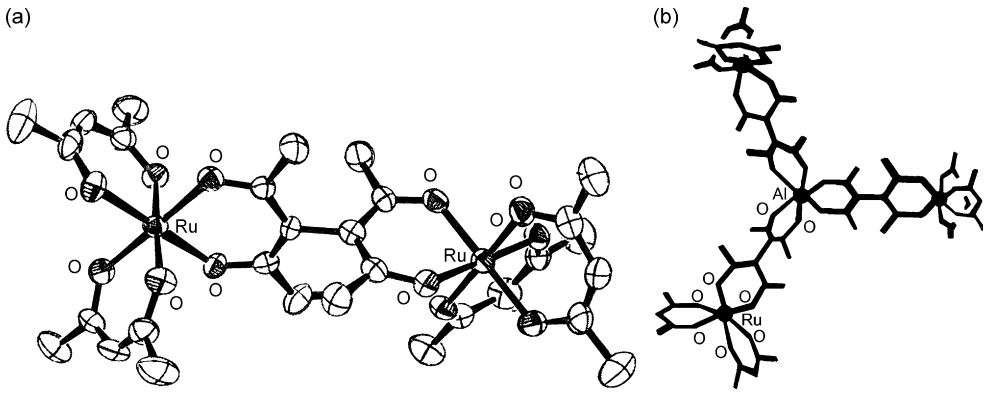

Fig. 63. Structures of $[Ru_2(\mathbf{57})(\mathbf{5})_4]$ (a) [179] and Λ-[{Δ-$Ru_3(\mathbf{5})_6(\mathbf{57})_3$}Al] (b) [179].

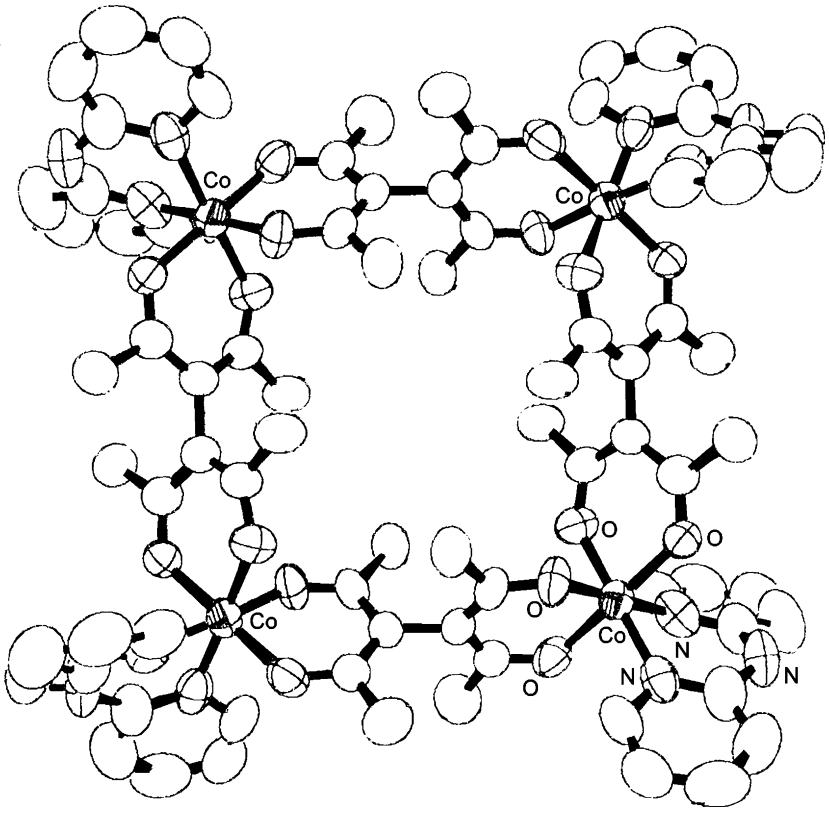

Fig. 64. Structure of $[Co_4(\mathbf{57})_4(dpa)_4]$ [181].

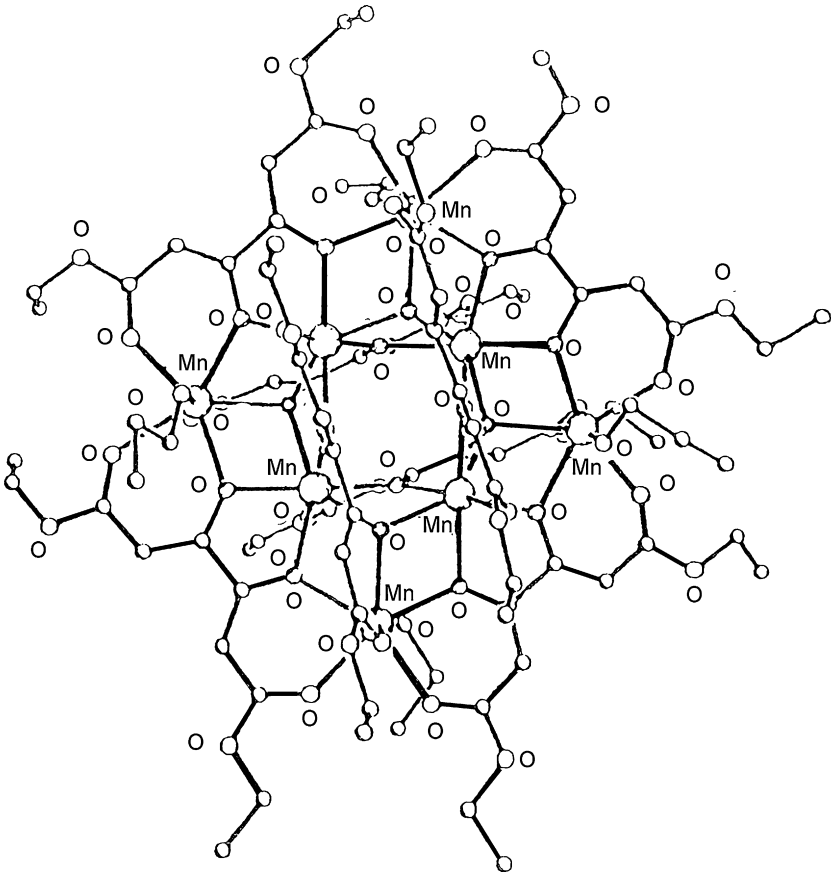

Fig. 65. Structure of $[Mn_8(\mathbf{58b})_8(C_3H_7OH)_4]$ [181].

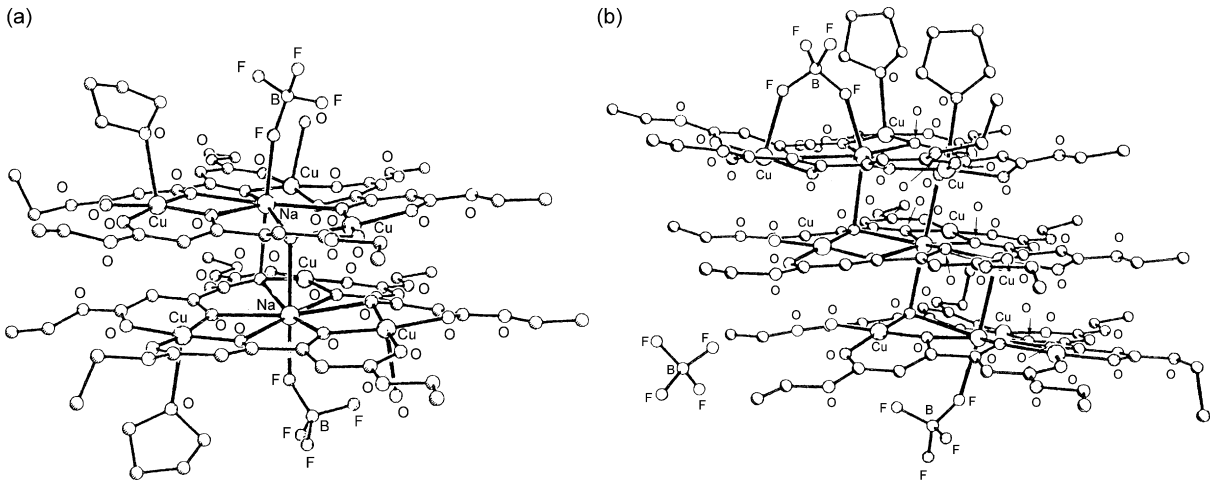

Fig. 66. Structures of $[Cu_6Na_2(\mathbf{58b})_6(BF_4)_2(THF)_2(H_2O)_2]$ (a) and $\{[Cu_9Na_3(\mathbf{58b})_9(BF_4)_2(THF)_2](BF_4)$ (b) [181].

copper(II) centers in the 15-MC-6 fragments of $[Cu_6Na_2(\mathbf{58b})_6(BF_4)_2(THF)(H_2O)_2]$ or $[Cu_9Na_3(\mathbf{58b})_9(BF_4)_2(THF)_2](BF_4)$ by C_2H_5O bridges leads to the topologically equivalent crown ether 18-crown-6. The three copper(II) ions in the 15-MC-6 fragments are linked across the triangular edges by bis(bidentate)diethyl ketipinate dianions. A sodium ion is encapsulated in the center of the 15-MC-6 fragment. In order to accomplish eight coordination of the sodium ions, aggregation of the $\{Cu_3Na(\mathbf{58b})_3\}^+$ monomers furnishes double- and triple-decker metalla-coronates $[Cu_6Na_2(\mathbf{58b})_6(BF_4)_2(THF)_2(H_2O)_2]$ and $[Cu_9Na_3(\mathbf{58b})_9(BF_4)_2(THF)_2](BF_4)$. The stacking features are governed by the coordination of water molecules, which lead to the formation $[Cu_6Na_2(\mathbf{58b})_6(BF_4)_2(THF)_2(H_2O)_2]$ where both sides of the stack are totally coordinatively blocked by solvent molecules (tetrahydrofuran or water) or the counterions. However, without water coordination, the most suitable ligation around the copper(II) and the sodium ions is achieved by the formation of $[Cu_9Na_3(\mathbf{58b})_9(BF_4)_2(THF)_2](BF_4)$ [181].

H_3–**59a** and H_3–**59b**, prepared by benzoylation or acetylation of 1-phenyl 1,3,5-hexanetrione or 2,4,6-heptanetrione using NaH as the base and monoglyme as solvent, form homotrinuclear or homodinuclear copper(II), nickel(II) and cobalt(II) complexes by reaction with the appropriate metal salt in methanol/water or acetone/water and in the presence of base. Isolation of complexes with two or three metal ions appears to depend on preparative details such as the solvent, temperature and base used [181]. The infrared spectra of these complexes are very similar, none of them exhibiting absorption due to free unchelated carbonyl groups. The low magnetic moment of $[Cu_3(\mathbf{59a})_3(H_2O)_3]$ indicates intramolecular antiferromagnetic interactions, while the high magnetic moment of $[Ni_3(\mathbf{59a})_2(H_2O)_6]$ and $[Co_3(\mathbf{59a})_2(H_2O)_6]$ has been assumed to be indicative of ferromagnetic interactions, suggesting a configuration with the three metal(II) ions close each other and bridged by the carbonyl oxygen atoms. The magnetic behaviour, typical of isolated metal(II) ions, and the lack of free carbonyl absorptions in the IR spectra of the binuclear complexes support a coordination of the two metal ions in the two external chambers as found in $[Co_2(H\text{-}\mathbf{59a})_2(py)_4]$, prepared by H_3–**59a** and $CoCl_2{\cdot}6H_2O$ in the presence of $N(C_2H_5)_3$ in refluxing acetone under nitrogen followed by crystallization from pyridine, where the cobalt(II) ions reside at the 1,3- and 5,7-enolate positions with the potential third central coordination site vacant [182].

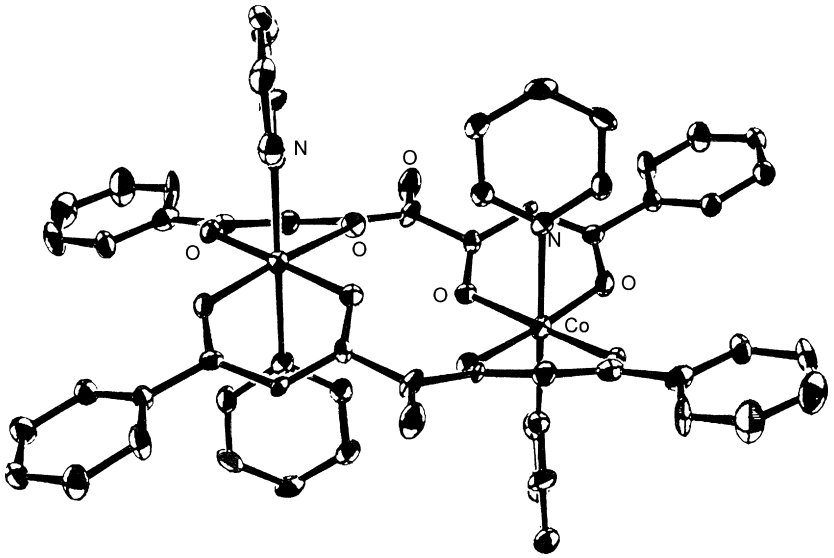

Fig. 67. Structure of $[Co_2(\mathbf{60})_2(py)_4]$ [182].

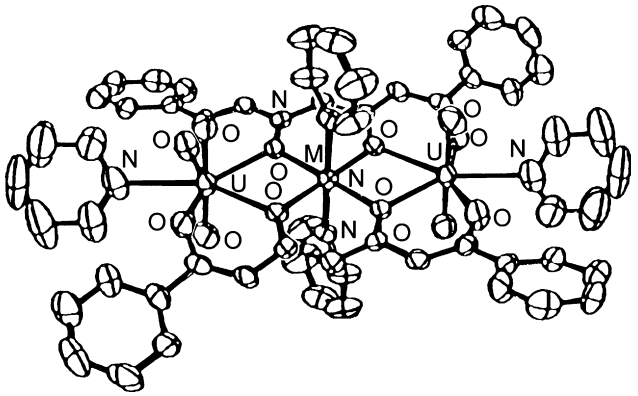

Fig. 68. Structure of $[(UO_2)_2M(\mathbf{59a})_2(py)_4]$ (M = Co^{II}, Ni^{II}) [183].

Crystallization of this dicobalt(II) complex from benzene/pyridine in the air causes oxidation of the 4-carbon of both ligands to carbonyls and the consequent formation of $[Co_2(\mathbf{60})_2(py)_4]\cdot 4py$ where the two six coordinate cobalt(II) ions, 5.37 Å apart, are bound to two 1,7-diphenyl-1,3,4,5,7-heptanepentaonato $[\mathbf{60}]^{2-}$ ligands at the 1,3- and 5,7-positions via four enolate oxygen atoms from two different $[\mathbf{60}]^{2-}$ ligands and two axial pyridine nitrogen atoms (Fig. 67). The oxidation of the 4-carbon atom to carbonyl does not destroy the dianionic character of the ligand and therefore the complex. No oxidation was observed in the dinuclear copper(II), nickel(II), zinc(II) and uranyl(VI) and several heterotrinuclear complexes of H_3–**59a**, indicating that the oxidation to the 1,3,4,5,7-pentaketonate $[\mathbf{60}]^{2-}$ ligand is metal ion dependent rather than due to unusual ligand reactivity. This assumption is corroborated by the chemical behaviour of $[Mn_2(H\text{-}\mathbf{59a})_2]$ which is also oxidized to $[Mn_2(\mathbf{60})_2]$, whose structure is similar to that of $[Co_2(\mathbf{60})_2]$ [182].

In the isomorphous heterotrinuclear complexes $[(UO_2)_2M(\mathbf{59a})_2(py)_4]$ (M = Zn^{II}, Cu^{II}, Ni^{II}, Co^{II}, Fe^{II}, Mn^{II}), two uranyl(VI) ions occupy the two terminal coordination positions in the molecules with four ketonate oxygen atoms and one pyridine nitrogen constituting the five equatorial donor atoms in a distorted pentagonal bipyrimidal coordination geometry; the divalent transition metal ion occupies the central position and is bound to four ketonate oxygen atoms, which all act as bridging atoms between the transition metal and uranium atom. In addition pyridine nitrogen atoms occupy the fifth and sixth coordination position above and below the plane of the tetraketonates (Fig. 68). It was suggested that a reasonable precursor to these trinuclear products is $[(UO_2)_2(H\text{-}\mathbf{59a})_2(S)_2]$, where the two uranyl(VI) ions are in the external O_2O_2 sites, a solvent molecule (S) completing the pentagonal equatorial coordination of each uranyl(VI) ion. This could explain the easy and specific preparation of the related heterotrinuclear complexes from solutions containing different UO_2^{2+}: M^{2+} ratios [183,184].

12. Dinuclear and polynuclear complexes derived from bis-β-diketones with a spacer without donor groups

The bis-β-diketones are tetraketones where two β-diketonato moieties are separated by a spacer which does not contain additional donor groups. The linkage between the two β-diketone moieties and the spacer occurs at the position 1 or 2 of the β-diketones. In these systems, the two β-diketonate moieties behave as two well separated coordinating moieties; hence they give rise to dinuclear complexation where the two metal ions do not interact each other, a possible interaction occurring only through the spacer group and/or through additional bridging groups, appropriately added during the synthesis of the related complexes. In these compounds two keto-enol equilibria can take place according to Scheme 11.

12.1. Complexes containing an aliphatic spacer

These tetraketones form dinuclear complexes $[M_2(\mathbf{L})_2]$ or $[M_2(\mathbf{L})_3]$ where each metal(II) or metal(III) ion lies in one of the two O_2O_2 or $O_2O_2O_2$ coordination chambers formed by two or three bis-β-diketonato ligands in consequence of metal ion encapsulation.

The branched H_2–**61a**···H_2–**61d** and linear H_2–**62a**···H_2–**62c** bis-β-diketones, linked through alkyl chains, were prepared by reaction of H–**5** and the appropriate α,ω-dibromoalkane. IR indicates that the shorter branched compounds (H_2–**61a** and H_2–**61b**) and the linear β-diketonates (H_2–**62a**···H_2–**62c**) are in a bis-enol form while the longer-branched analogues (H_2–**61c** and H_2–**61d**) are in the keto-form [185,186]. In general, both linear and branched β-diketones closely resemble the corresponding β-diketones, once the increase in molecular mass and the electronic effect of the connecting alkyl chain are taken into consideration. The effect of the alkyl chain depends markedly on the point of attachment: when this is a terminal carbon atom, only very minor changes in the ^1H NMR in $CDCl_3$ chemical shifts and in the keto-enol or acid–base equilibria are observed, compared to H–**5**. When the point of attachment is the central carbon atom, however, a marked downfield shift of the enolic —OH proton results, together with a drastic lowering of the enol percentage and of the acidity [187,188].

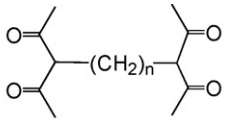

	n
H_2-**61a**	6
H_2-**61b**	8
H_2-**61c**	10
H_2-**61d**	12

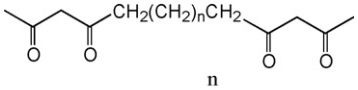

	n
H_2-**62a**	4
H_2-**62b**	6
H_2-**62c**	8

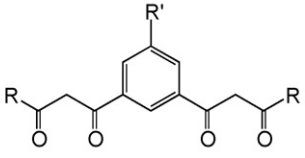

	R	R'
H_2-**63a**	CH_3	H
H_2-**63b**	C_2H_5	H
H_2-**63c**	C_3H_7	H
H_2-**63d**	$C(CH_3)_3$	H
H_2-**63e**	C_6H_5	H
H_2-**63f**	C_6H_5	OC_2H_5
H_2-**63g**	$(CH_2)_7CH_3$	H
H_2-**63h**	$(CH_2)_8CH_3$	H

These bis-β-diketones (H_2–**L**) react with $Cu(X)_2\cdot nH_2O$, (X = CH_3COO^-, NO_3^-, Cl^-) in anhydrous ethanol to form [Cu(**L**)]. The square planar copper(II) complexes with linear β-diketone coordinate pyridine to give rise to the five coordinate, square pyramidal complexes [Cu(**L**)(py)] which evolve in ethanol into

the insoluble square planar polymeric complexes $[Cu(\mathbf{L})]_n$. Partial depolymerisation of $[Cu\mathbf{L}]_n$ occurs upon prolonged heating in chloroform. Attempts to depolymerise $[Cu\mathbf{L}]_n$ by vacuum sublimation result only in decomposition [187,188].

The copper(II) complexes with the branched bis-β-diketonate ligands show similar physico-chemical properties but differ markedly in their solubility: the complexes of H_2–**61a** and H_2–**61b** are completely insoluble in chloroform while that of H_2–**61d** is very soluble and that of H_2–**61c** shows an intermediate behaviour. The UV–vis spectra of the chloroform solutions thus obtained are similar to those of the corresponding solids and nearly identical to that of the bis-(3-hexyl-2,4-pentanedionato) copper(II) complex. [Cu(**61c**)] was suggested to be a polymer–monomer mixture, [Cu(**61d**)] a bifurcated monomer both in the solid state and in solution and [Cu(**61a**)] and [Cu(**61b**)] polymers as supported by the occurrence of the parent peak of the monomeric species in the mass spectrum of [Cu(**61d**)] and only of fragments in the mass spectra of [Cu(**61a**)] and [Cu(**61b**)] [187,188].

12.2. Complexes containing a phenylene spacer

H_2–**63a**···H_2–**63h** have been prepared by Claisen condensation of a 1:2 mixture of dimethyl-isophthalate or dimethyl-5-ethoxyisophtalate and the appropriate ketone (acetone, butan-2-one, pentan-2-one, 3,3-dimethylbutan-2-one, acetophenone, 2-decanone or 2-undecanone) respectively, with an excess of sodium amide in dry diethyl ether/tetrahydrofuran at low temperature (0 °C) [189–191]. These β-diketones are in the enolic form in the solid state, as confirmed by the X-ray structure of H_2–**63d**, and in solution according to ^{1}H NMR spectra in $CDCl_3$ or DMF-d_7, where they are stabilized by the occurrence of O–H···O hydrogen bonds and by the conjugated nature of this tautomer with respect to its corresponding bis-keto form. H_2–**63e** adopts a planar structure as expected to maximize conjugation with the two diketonate units arranged asymmetrically about the 1,3-phenylene spacer, i.e. one diketonate is oriented in the opposite direction from the other, pointing toward different protons around the 1,3-central phenyl ring [189–191].

H_2–**63a** and the appropriate metal acetate in hot ethanol form $[M_2(\mathbf{63a})_2]\cdot nC_2H_5OH$ (M = Zn^{II}, Cu^{II}, Co^{II}, Ni^{II}, Mn^{II}; n = 0,1,2,4), which turns into $[(M_2(\mathbf{63a})]_2\cdot$npy, ($n$ = 1, 2, 4) in pyridine. Under similar conditions $UO_2(NO_3)_2\cdot 6H_2O$ and $VO_2(CH_3COO)_2\cdot 2H_2O$ afford $[(UO_2)_2(\mathbf{63a})_2(C_2H_5OH)_2]$ and $[(VO)_2(\mathbf{63a})_2]\cdot 2H_2O$. FAB mass spectra of $[(Cu)_2(\mathbf{63a})_2]$, $[(Ni)_2(\mathbf{63a})_2]\cdot 4H_2O$ and $[(Zn)_2(\mathbf{63a})_2]$ indicate the occurrence of dinuclear entities. Although too involatile for mass spectrometry measurements, also for the complexes with the other metal ions a homodinuclear structure was suggested. For the homodinuclear copper(II) complexes a small exchange coupling through the benzene ring was proposed while for the nickel(II) and cobalt(II) complexes the magnetic moments are comparable with those expected for magnetically diluted, octahedral species without no magnetic

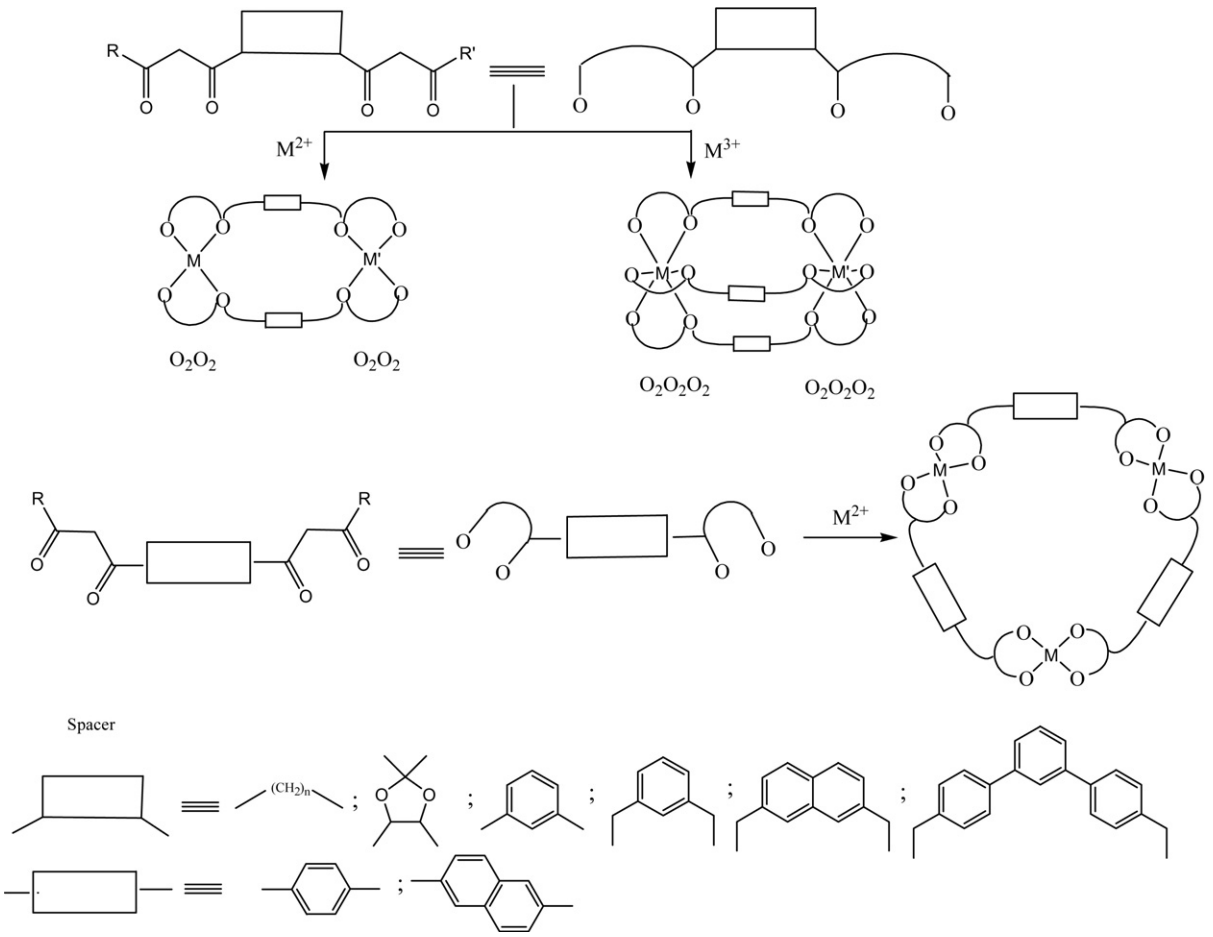

Scheme 11. Bis-β-diketones with a spacer without donor atoms, their schematic representation and the adjacent chambers and complex formation in consequence of metal complexation.

interaction between the two metal ions [189]. Attempts to produce the related mononuclear complexes were successful only for $[VO(H\text{-}\mathbf{63})_2]\cdot H_2O$, recovered from the mother liquor after precipitation of $[(VO)_2(\mathbf{63a})_2]\cdot 2H_2O$. According to mass spectrometry measurements, the subsequent reaction of $[VO(H\text{-}\mathbf{63a})_2]$ with copper acetate affords $[CuVO(\mathbf{63a})_2]$ [189]. $Th(NO_3)_4$ and H_2–**63a** in hot ethanol yield the insoluble and involatile complex $[Th(\mathbf{63a})_2]$, for which a dinuclear or an oligomeric structure was suggested.

Iron(III) salts and H_2–**63a** or H_2–**63d** under basic conditions yield $[Fe_2(\mathbf{L})_3]$ where the two iron(III) centres are bridged by three $[\mathbf{L}]^{2-}$ ligands to produce a triple helical arrangement with each metal ion surrounded by three β-diketonato fragments. Each dinuclear complex has homochiral iron(III) centres (either Λ–Λ or Δ–Δ) equally contained in each crystal (Fig. 69) [190].

$[Cu_2(\mathbf{63d})_2(THF)_2]$, synthesised by equimolar amounts of H_2–**63d** and copper(II) chloride in tetrahydrofuran and in the presence of base, has two five coordinate square pyramidal copper(II) ions bridged by two $[\mathbf{63d}]^{2-}$ ligands. The basal plane of each copper(II) ion is filled by four β-diketonato oxygen atoms while the apical position is occupied by a tetrahydrofuran molecule on opposite sides of the mean plane of the $\{Cu_2(\mathbf{63d})_2\}$ unit. The structures of $[Cu_2(\mathbf{63d})_2(py)_2]\cdot py$ and $[Cu_2(\mathbf{63d})_2(dmapy)_2]\cdot 3.25THF$, obtained by crystallization of $[Cu_2(\mathbf{63d})_2(THF)_2]$ from tetrahydrofuran/pyridine or tetrahydrofuran in the presence of 4-dimethylaminopyridine (dmapy), are similar to that of the starting tetrahydrofuran complex with two pyridine or 4-dimethylaminopyridine ligands replacing the bound tetrahydrofuran molecules (Fig. 70) [190].

$[Cu_2(\mathbf{63d})_2(THF)_2]$ and excess 4,4′-bipyridine produce $[Cu_2(\mathbf{63d})_2(bipy)_2]\cdot 2bipy$, which does not have an extended bridged structure, but the same stoichiometry, connectivity and general stereochemistry as the analogous dinuclear complexes incorporating tetrahydrofuran, pyridine or 4-dimethylaminopyridine. On the contrary, 4,4′-*trans*-azopyridine (azpy) gives rise to the one dimensional polymer $\{[Cu_2(\mathbf{63d})_2(azpy)]\cdot 2THF\}_n$, where the copper(II) ions are five coordinate, square pyramidal with 4,4′-*trans*-azopyridine ligands occupying apical positions such that they bridge adjacent copper(II) dimer units in a step-like fashion (Fig. 71) [190].

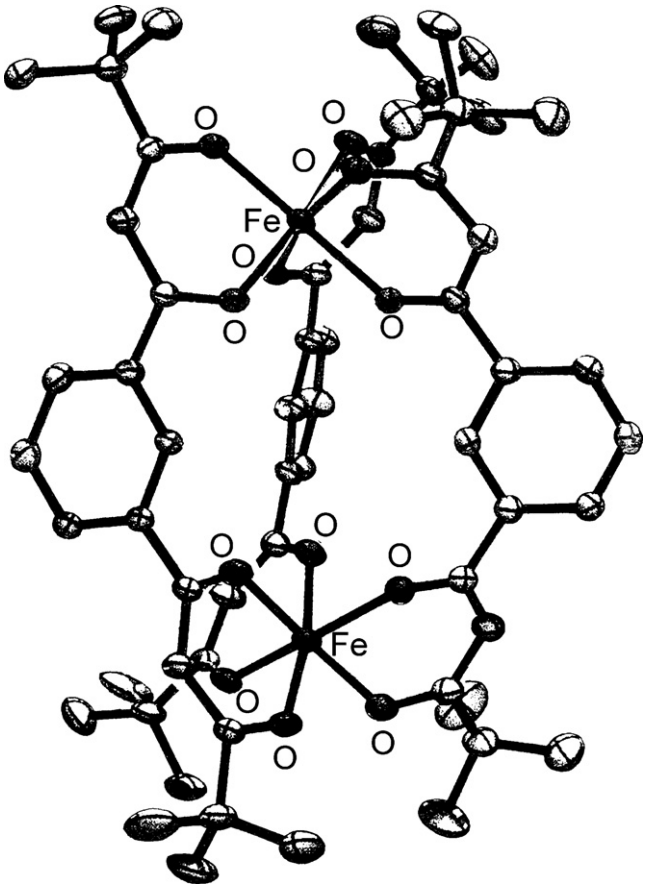

Fig. 69. Structure of $[Fe_2(\mathbf{63d})_3]$ [190].

In contrast to the above, $[Cu_2(\mathbf{63d})_2(THF)_2]$ and excess pyrazine (pyz) form $[Cu_4(\mathbf{63d})_4(pyz)_2]\cdot 4THF$, with the copper(II) ions again five coordinate square pyramidal but with the pyrazine ligands protruding on the same side of the mean plane of each dinuclear

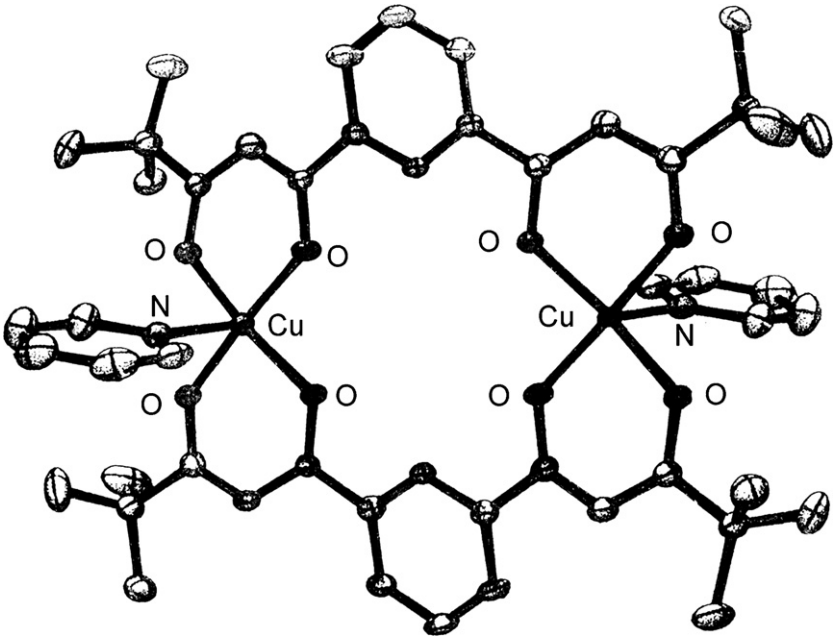

Fig. 70. Structure of $[Cu_2(\mathbf{63d})_2(py)_2]$ [190].

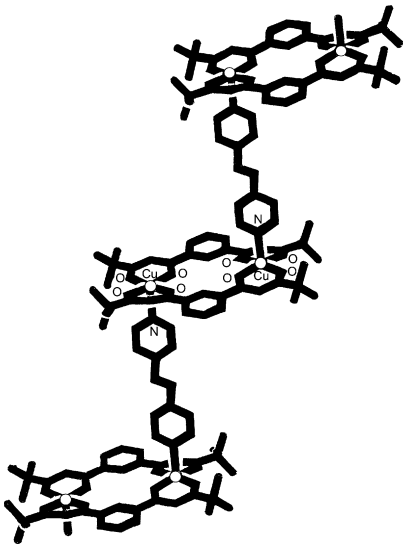

Fig. 71. Structure of $[Cu_2(\mathbf{63d})_2(azpy)]_n$ [190].

copper(II) entity such that bridging between copper centres on adjacent complexes takes place to produce a discrete tetranuclear dimer of dimers (Fig. 72) [190].

An analogous structure was found in $[Cu_4(\mathbf{63d})_4(apyz)_2]$, derived from equimolar amounts of aminopyrazine (apyz) and $[Cu_2(\mathbf{63d})_2]$ in tetrahydrofuran/diethyl ether. The copper(II) ions are weakly antiferromagnetically coupled, mediated by the aminopyrazine linker units, while no coupling occurs across the benzene rings in each dinuclear component [191].

Under the above conditions, 1,4-diazabicyclo[2,2,2]octane (dabco) affords $[Cu_4(\mathbf{63d})_4(dabco)_2]$, which contains a tetranuclear sandwich structure with two dinuclear units approximately planar and 7.26 Å apart, resulting in four, five coordinate copper(II) centres [191].

Equimolar amounts of $[Cu_2(\mathbf{63d})_2]$ and 2,2′-dipyridylamine (dpa) in tetrahydrofuran afford $[Cu_2(\mathbf{63d})_2(dpa)_2]$, where each copper(II) ion is square pyramidal and two 2,2′-dipyridylamine ligands coordinate *trans* with respect to each other. Only one of the 2,2′-dipyridylamine pyridyl nitrogen atoms coordinates to a copper centre [192].

$[Cu_2(\mathbf{63d})_2]$ and 4,4′-dipyridyl sulfide (dps) form $\{[Cu_2(\mathbf{63d})_2(dps)_2]\cdot 2THF\}_\infty$, consisting of one-dimensional chains incorporating alternate $\{Cu_2(\mathbf{63d})_2\}$ and dps units in a 1:1 ratio. Each dinuclear unit is attached to two adjacent units by bridging 4,4′-dipyridyl sulfide linkers which project on opposite sides of the dicopper(II) unit in a mutually *trans* fashion. The 4,4′-dipyridyl sulfide units are bound in the axial sites of each square pyramidal copper(II) ion (Fig. 73a) [191].

The same reaction, using 4,4′-(1,3-xylene)-bis(3,5-dimethylpyrazolo) (xbp) as linker, yields the polymeric product $\{[Cu_2(\mathbf{63d})_2(xbp)]\cdot 2.2THF\}_\infty$ with the bis-pyrazole units linking $\{Cu_2(\mathbf{63d})_2\}$ units in a stepwise manner through square pyramidal copper(II) centres (Fig. 73b) [191].

Hexamethylenetetramine (hmt) and $[Cu_2(\mathbf{63d})_2]$ in tetrahydrofuran in a 2:3 molar ratio afford $[Cu_6(\mathbf{63d})_6(hmt)_2]_n$, where a two-dimensional network takes place with the hexamethylenetetramine ligand acting as triply bridging unit. Each dinuclear component incorporates two, five coordinate copper(II) centres with one hexamethylenetetramine linker coordinated on either side of the mean plane of the platform. Each layer in the network may be viewed as being composed of fused chiral hexagons, each hexagon being defined by six dinuclear platforms and six hexamethylenetetramine linker units forming infinite two-dimensional sheets [191].

Crystals of $[Co_2(\mathbf{63c})_2(py)_4]\cdot 2.25CHCl_3\cdot 0.5H_2O$ (Fig. 74a), grown over three days at the interface of a chloroform/pyridine solution of H_2–**63c** and an aqueous solution of cobalt(II) acetate, contain two octahedral cobalt(II) centres with pyridine ligands occupying both axial positions and the oxygen donors from two essentially planar β-diketone fragments binding in the equatorial positions [192].

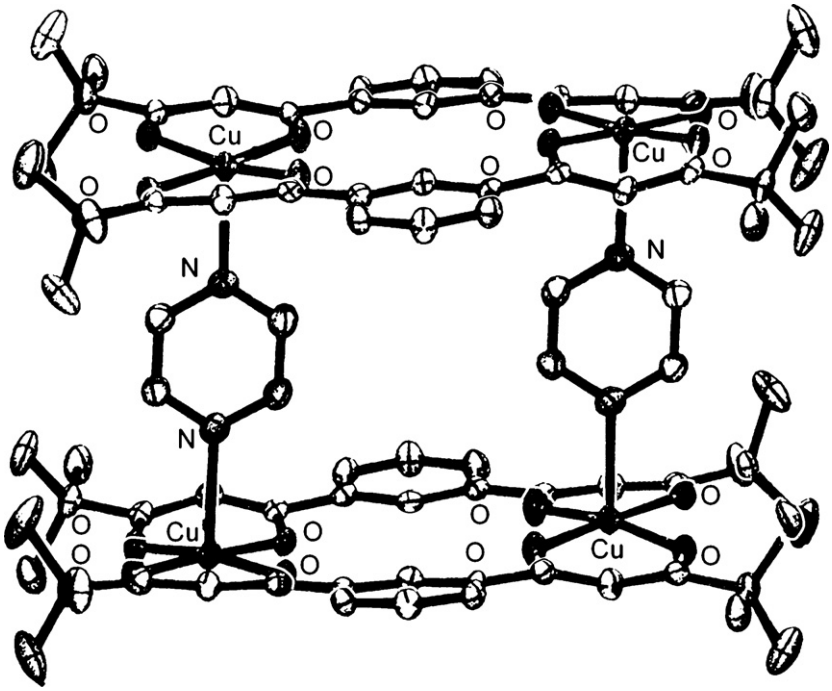

Fig. 72. Structure of $[Cu_4(\mathbf{63d})_4(pyz)_2]$ [190].

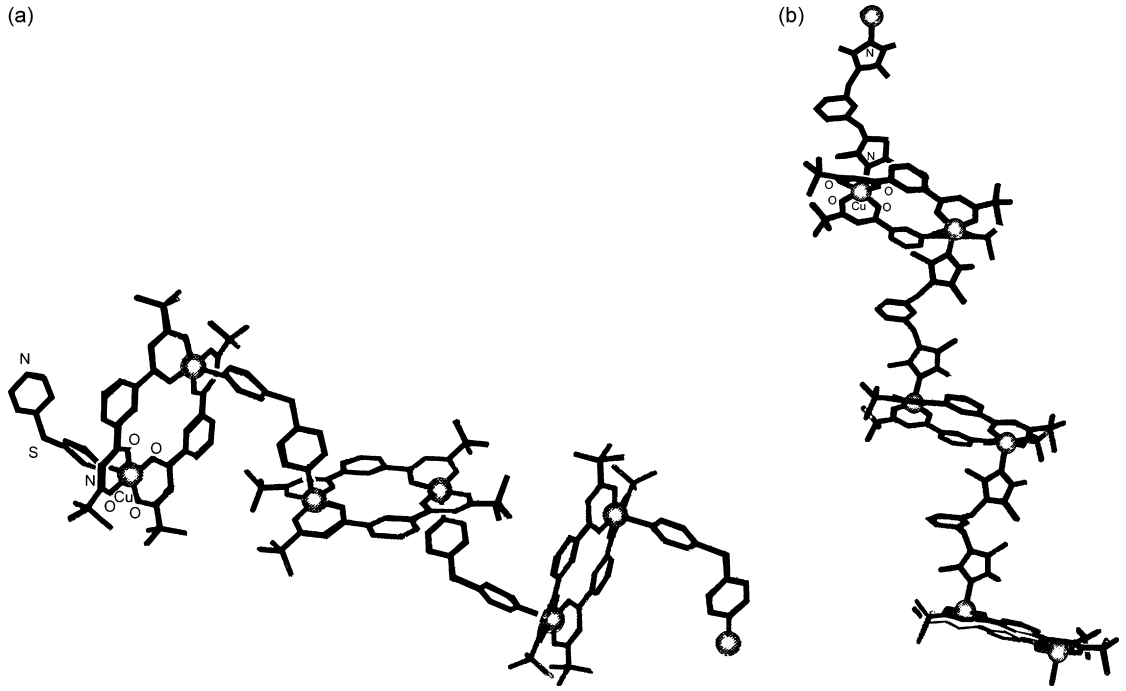

Fig. 73. Structures of $\{[Cu_2(\mathbf{63d})_2(dps)_2]\cdot 2THF\}_\infty$ (a) and $\{[Cu_2(\mathbf{63d})_2(xbp)]\cdot 2.2THF\}_\infty$ (b) [191].

In the isostructural complexes $[Co_2(\mathbf{63d})_2(Etpy)_4]\cdot 0.25H_2O$, $[Ni_2(\mathbf{63d})_2(Etpy)_4]$ and $[Zn_2(\mathbf{63d})_2(Etpy)_4]$, derived from H_2-**63d** and the appropriate metal(II) acetate in 4-ethylpyridine (Etpy), the bis-β-diketonato oxygen atoms again occupy the equatorial positions of the respective metal ions, with the 4-ethylpyridine ligands bound in each axial site, approximately orthogonal with respect to each other with π–π interactions between them [192].

On the contrary, in the similarly prepared $[Zn_2(\mathbf{63a})_2(Etpy)_2]$ (Fig. 74b) each metal ion is five coordinate in a distorted trigonal bipyramidal geometry with the axial 4-ethylpyridine groups on the zinc ions lying on opposite sides of the equatorial plane [192].

For $[Zn_2(\mathbf{63d})_2(py)_2]$ one irreversible ligand centred oxidation process at +1.465 V and another at −1.99 V with a shoulder at −2.16 V are observed (reference electrode Ag/AgCl). $[Co_2(\mathbf{63d})_2(py)_4]$ exhibits irreversible oxidation at +1.29 V assigned to the Co^{II}/Co^{III} metal-centered process and a metal-centered quasi reversible wave at −1.755 V (ΔE = 165 mV at 100 mV s^{-1} scan rate) together with additional irreversible reductions, presumably ligand centred, below −2.0 V. $[Ni_2(\mathbf{63d})_2(py)_4]$ displays

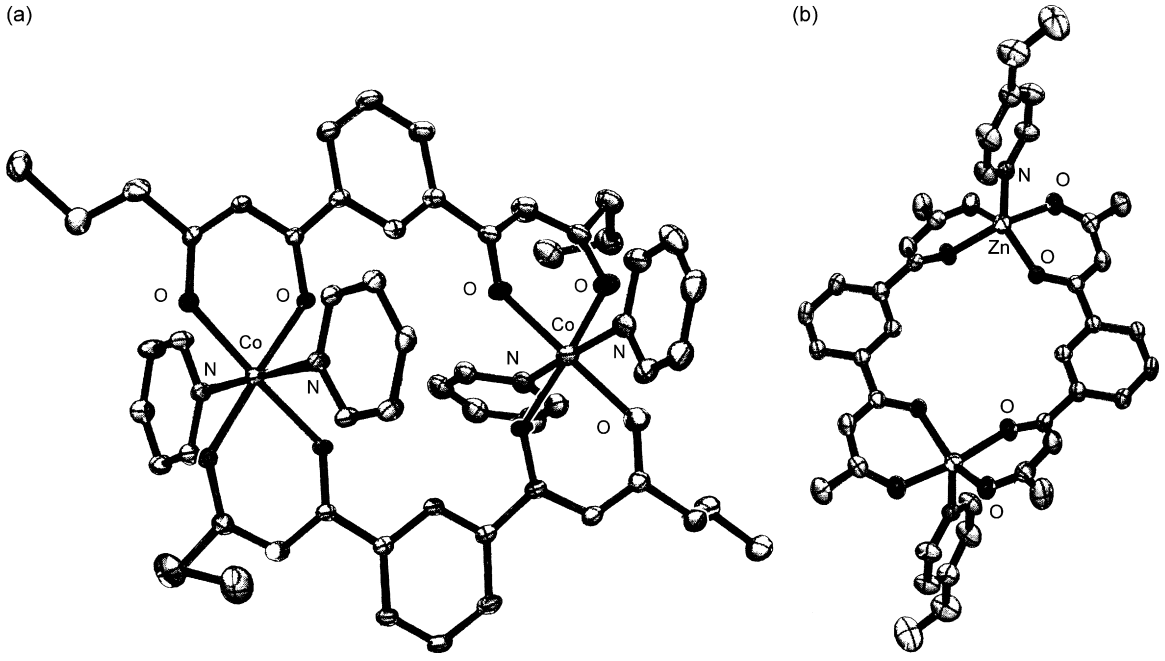

Fig. 74. Structures of $[Co_2(\mathbf{63c})_2(py)_4]$ (a) and $[Zn_2(\mathbf{63d})_2(Etpy)_4]$ (b) [192].

a quasi-reversible metal-centered Ni^{II}/Ni^{III} oxidation at +1.04 V (ΔE = 155 mV at 100 mV s^{-1} scan rate) and an irreversible reduction near −1.85 V, somewhat comparable to that reported for $[Ni(\mathbf{5})_2(H_2O)_2]$ of −1.70 V. $[Cu_2(\mathbf{63d})_2]$ exhibits an irreversible oxidation process at +1.64 V possibly associated to the Cu^{II}/Cu^{III} copper-centered process with a prior wave as a shoulder at +1.35 V and an irreversible wave at −1.26 V assigned to a Cu^{II}/Cu^{I} process. Other irreversible redox processes are seen below −1.6 V, possibly associated with sequential metal reduction. Oxidation for $[Fe_2(\mathbf{63d})_3]$ (+1.43 V) is shifted catodically slightly higher compared to the process reported for $[Fe(\mathbf{5})_3]$. No other processes are observed before approximately +2 V, where they occur in a similar position to oxidative processes for the free ligand. $[Fe_2(\mathbf{63d})_3]$ displays a metal-centered Fe^{III}/Fe^{II} reduction process near −0.7 V ($E_{1/2}$ = −0.745 V, ΔE = 150 mV at 100 mV s^{-1} scan rate) in agreement with the metal-centered reduction process occurring in [Fe(β-dike)$_3$] followed by further irreversible waves below −1.0 V presumably associated with other metal centres or the ligand itself. For $[Fe_2(\mathbf{63e})_3]$, two sequential reversible reductions were observed at −0.46 and −0.58 V. The absence of a second, closely following wave suggests a single-electron process; alternatively, the two metal-centered reduction processes are too close to resolve. In these complexes, assignment as sequential metal-centered processes was not made with certainty, given the redox behaviour of the ligand itself. Reduction processes are not substantially shifted from those found for the zinc(II) complexes, where the metal ion is electroinactive, suggesting these processes formally involve ligand-centered molecular orbitals [190,192].

Stoichiometric amounts of H_2–**63e** or H_2–**63f** and $LnCl_3{\cdot}6H_2O$ in the presence of $N(C_2H_5)_3$ form the triple stranded complexes $[Ln_2(\mathbf{L})_3]{\cdot}nH_2O$ (Ln = Eu, Sm, Nd, Y for H_2–**63e**, Ln = Eu, Nd for H_2–**63f**), while $[Hpip]_2[Eu_2(\mathbf{63e})_4]$ is prepared by altering the ligand-to-metal ratio to 2:1 and using piperidine as counterion [193]. The complexes display strong visible (red or pink) or NIR luminescence upon irradiation at the ligand band around 350 nm, depending on the choice of the lanthanide. The luminescence signals of the dinuclear complexes are up to 11 times more intense than the luminescence signals of similar mononuclear complexes. $[\mathbf{63e}]^{2-}$ is an efficient sensitizer, particularly for the samarium(III) and neodymium(III) ions. Photophysical studies of the europium complexes at room temperature and 77 K show the presence of a thermally activated deactivation pathway, attributed to ligand-to-metal charge transfer (LMCT). Quenching of the luminescence from this level seems to be operational for the europium(III) complex but not for the samarium(III) and neodymium(III) complexes, which exhibit long lifetimes. Compared with the triple-stranded solid state structure of $[Eu_2(\mathbf{63e})_3]$, the quadruple-stranded complex $[Eu_2(\mathbf{63e})_4]^{2-}$ displays a more intense emission signal with a distinct emission pattern indicating the higher symmetry of this complex. The sensitizing properties of the ligands, investigated by luminescence spectroscopy, show that their $^3\pi$–π^* state is well placed to allow energy transfer to europium(III), samarium(III) and neodymium(III) excited states, following UV absorption. The complexes have long luminescence lifetimes and high luminescence quantum yields, even in the case of the europium(III) complex where it is shown that the presence of a thermally activated LMCT pathway acts to deactivate the $^5D_0$ state. These results indicate that the energy transfer process is efficient [193].

Simple β-diketones were successfully used as extractant in liquid–liquid extraction studies [192]; analogously, the extraction behaviour of H_2–**63c**, H_2–**63d**, H_2–**63e**, H_2–**63g** and H_2–**63h** towards cobalt(II) and zinc(II) was studied using the radiotracer technique both in the absence and presence of 4-ethylpyridine. At pH 8.7 in the absence of 4-ethylpyridine, cobalt(II) extraction ranges from 2 to 13% for the above ligand series, while the range is 3–53% for zinc(II). The more lipophilic ligand derivatives H_2–**63g** and especially H_2–**63h** give rise to enhanced extraction. Furthermore, 4-ethylpyridine considerably enhances the percentage extraction and reduces the time required to reach equilibrium in the presence of stoichiometric amounts of extractants. With the

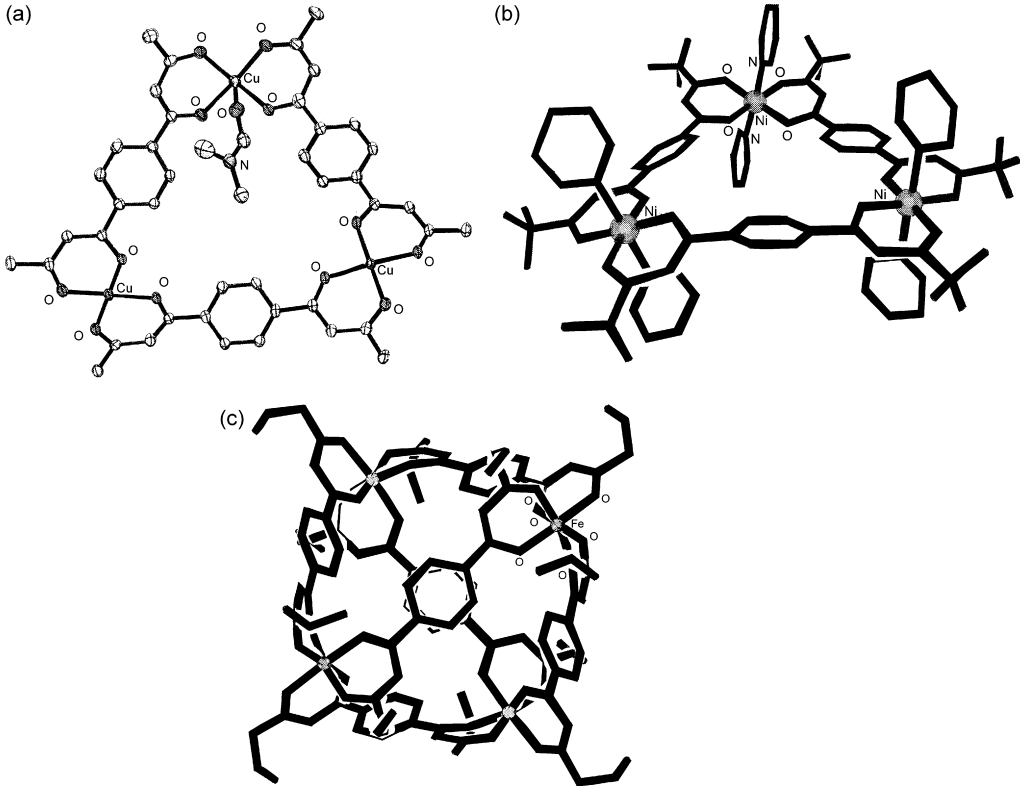

Fig. 75. Structures of $[Cu_3(\mathbf{64a})_3(DMF)]$ (a), $[Ni_3(\mathbf{64d})_3(py)_6]$ (b) and $[Fe_4(\mathbf{64c})_6]$ (c) [195].

addition of 2 equiv. (relative to the employed β-diketone) of 4-ethylpyridine the extraction of cobalt(II) and zinc(II), respectively, markedly increases from 13 to 70% and from 53 to 85% in the case of H_2–**63h**. The time required to reach equilibrium in the case of the cobalt(II) ion is also approximately reduced (from 3 to 1.5 hours). Using only 4-ethylpyridine at the same concentration the metal extraction is negligible (≤1%.). Both in the presence and absence of 4-ethylpyridine, these systems show no significant extraction of metal ions below approximately pH 6 and thus the extracted metal may be stripped by pH adjustment of the aqueous phase to pH < 6.

Furthermore, extraction of cobalt(II) and zinc(II) ions (1×10^{-4} M) at pH 8.7 under variable H_2–**63d** or H_2–**63h** concentration (5×10^{-4} to 1.5×10^{-3} M) in the presence of a fixed concentration (2×10^{-3} M) of 4-ethylpyridine, as well as in the absence of this coligand in the case of the zinc(II) ion, shows that mixed 1: 1 and 1: 2 (metal: ligand) species are extracted, their proportions differing somewhat from system to system. Variation of the 4-ethylpyridine concentration (2×10^{-4} to 2×10^{-3} M) while the other concentrations are held constant carried out to probe 4-ethylpyridine dependence, indicates that in the case of H_2–**63d** with both the zinc(II) and cobalt(II) ions, a metal: 4-ethylpyridine ratio of approximately 1: 1 occurs while for H_2–**63h** the ratio is somewhat lower at 0.7 for both the metal ions systems, indicating some involvement of extracted species where not all metal sites have an attached 4-ethylpyridine. A pH dependence study for the Zn^{II}/H_2–**63h** system, employing a pH variation from 7.0–8.8, indicates that a mixture of singly and doubly deprotonated ligands are involved in the extraction process. Similar experiments, carried out in the presence of 4-ethylpyridine (2×10^{-3} M) for both the cobalt(II) and zinc(II) ions over the pH range 7.5–8.7, prove that 4-ethylpyridine influences the stoichiometry of the extracted species for the zinc ion [192].

Experiments, using H_2–**63d** and H_2–**63h** at a concentration of 1×10^{-3} M in the chloroform phase and a zinc(II) concentration in the aqueous phase from 1×10^{-4} M to 5×10^{-3} M (at pH 8.7), show that, metal:ligand = 1:1 species are extracted with both ligands in the absence of added 4-ethylpyridine. This ratio, comparable to the corresponding X-ray structure, suggests that, under the experimental conditions employed, related solid state and organic phase solution structures occur. The symmetric ^{1}H NMR spectrum observed for the zinc(II) complex of H_2–**63d** also agrees with this assumption. The same experimental conditions, but also in the presence of 4-ethylpyridine (2×10^{-3} M), lead to the approximately formation of [M(H-**L**)$_2$] species. Thus, in the absence of 4-ethylpyridine only a 1:1 (M: **L**) complex, most likely of type [M_2(**L**)$_2$], occurs while in the presence of 4-ethylpyridine the dominant complex in each case corresponds to a 1: 2 (M: **L**) species, most likely of type [M(H-**L**)$_2$(4-ethylpyridine)]. These results agree those obtained in the ligand dependence studies where, under different conditions, mixtures of 1:1 and 1:2 species are proposed to occur in both the presence and absence of added 4-ethylpyridine. Overall, the solvent extraction experiments point to three complex species being formed in the respective organic phases, with the mix of each species depending on the conditions employed. In the absence of 4-ethylpyridine both 1:1 and 1:2 (M:**L**) complexes are proposed to occur while in the presence of 4-ethylpyridine a 1:2 (M:**L**) complex appears to be the dominant extracted species in all cases [192].

Complete extraction of the copper ion and high selectivity for copper(II) over the other four metal(II) ions occur when equal amounts of water solutions of cobalt(II), nickel(II), copper(II), zinc(II), cadmium(II) perchlorate (1×10^{-4} M) are shaken for 24 h at pH 7.8 with H_2–**63d**, H_2–**63g** and H_2–**63h** (1×10^{-3} M) in chloroform. Similar experiments in the presence of 4-ethylpyridine (2×10^{-3} M, pH 7.4) again show a clear selectivity for the copper(II) ion, although the extraction of other metal ions is enhanced significantly increasing from 0 to 24% in the case of the zinc(II) ion with H_2–**63d** and from 0 to 35% in the case of the nickel(II) ion with H_2–**63h** [192].

Stoichiometric amounts of $HOOCCH_2N[CH_2CH_2N(CH_2COOH)CH_2CONHC_3H_7]_2$ (H_3–L), $LnCl_3{\cdot}6H_2O$ (Ln = Eu, La, Y) and $[NH(C_2H_5)_3]_2$[**63e**], derived from the deprotonation of H_2–**63e** with excess $N(C_2H_5)_3$ in dimethylformamide with 1% H_2O, lead to $[NH(C_2H_5)_3]_2[Ln_2(\mathbf{63e})(L)_2]$, synthesized also by stepwise assembly of [Ln(L)] and $[NH(C_2H_5)_3]_2$ [**63e**] in 2:1 molar ratio as confirmed by ESI–MS and NMR spectra in DMF-d_7/D_2O. [Eu(L)], upon excitation at 350 nm, shows a very weak luminescence, due to the lack of any sensitising groups in the complex. Addition of the sensitizer $[\mathbf{63e}]^{2-}$ leads to an approximately ≈200-fold signal increase. Titration experiments confirm the 2:1 stoichiometry of [Eu(L)] to $[\mathbf{63e}]^{2-}$; a similar control experiment, performed by addition of dibenzoylmethane to [Eu(L)] under the same conditions indicate a 1:1 ratio of dibenzoylmethide to [Eu(L)]. The luminescence spectrum of the complex from the one-pot assembly was identical in shape and peak intensities with the spectrum of the step-wise assembly. The same luminescence signal output demonstrates that the sensitisation of both the europium(III) ions takes place via the bound bis-didentate ligand by energy transfer from $[\mathbf{63e}]^{2-}$ to the europium(III) ion [194].

^{1}H NMR spectra in $CDCl_3$ of H_2–**64a**···H_2–**64h** and H_2–**65**, derived from Claisen condensation of dimethylterephthalate or 2,6-dimethylnaphthlalene-2,6-dicarboxylate with the appropriate ketone in dry diethylether in the presence of sodium amide, indicate that all these ligands exist almost entirely in their bis-enol tautomeric form, proved by the X-ray structure of H_2–**64d** where the two β-diketone fragments are in opposite direction each other. These ligands react with the desired metal chloride in tetrahydrofuran or tetrahydrofuran/pyridine and in the presence of excess Na_2CO_3 or $NaHCO_3$ to form [Cu_3(**L**)$_3$], [Fe_4(**L**)$_6$] and [Ga_4(**64a**)$_6$] or [M_3(**L**)$_3$(py)$_6$] (M = Co^{II}, Ni^{II}, Zn^{II}), respectively [195].

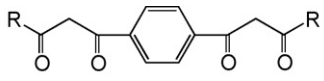

	R
H_2-**64a**	CH_3
H_2-**64b**	C_2H_5
H_2-**64c**	C_3H_7
H_2-**64d**	$C(CH_3)_3$
H_2-**64e**	C_6H_5
H_2-**64f**	C_6H_{13}
H_2-**64g**	C_8H_{17}
H_2-**64h**	C_9H_{19}

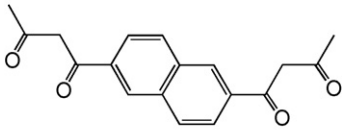

H_2-**65**

The similar essentially planar structures of [Cu_3(**64a**)$_3$(DMF)]·DMF and of [Cu_3(**64a**)$_3$]·0.3CH_3CN contain three copper(II) ions at the corners of an equilateral triangle and three dianionic $[\mathbf{64a}]^-$ ligands comprising the sides in the latter complex. While in the latter complex the three copper(II) ions are square planar, in the former one two copper(II) ions are approximately square planar and the third one is square pyramidal, due to coordination of a dimethylformamide molecule (Fig. 75a) [195].

All the solvate complexes $[M_3(\mathbf{L})_3(py)_6]$ ($M = Co^{II}$, Zn^{II}, Ni^{II}; H_2–**L** = H_2–**64a**···H_2**64e**) have the same triangular structure somewhat distorted from an ideal equilateral triangle, where each metal(II) ion is in an octahedral arrangement with the pyridine ligands occupying the axial sites. In the Ni_3 complex the Ni···Ni distances range from 10.56 to 10.77 Å (Fig. 75b) [195].

Cobalt(II) extraction by H_2–**64e**···H_2-**64h** (H_2–**L**) at pH 8.7 and in the absence of 4-ethylpyridine is negligible (1–2%) for each member of the above ligand series, while zinc(II) extraction ranges from 2 to 35%; H_2–**64h** gives rise to enhanced extraction. On addition of 2 equiv. of 4-ethylpyridine relative to H_2–**64h**, the cobalt(II) and zinc(II) extraction is markedly enhanced from ~2 to 26% and from 35 to 61%, respectively. Further, the time for equilibrium to be reached in the case of cobalt(II) ion is also approximately halved (from 3 to 1.5 h). Parallel control experiments in the absence H_2–**64h** but at the same concentration of 4-ethylpyridine indicate a negligible metal extraction at ≤1%. Both in the presence and absence of 4-ethylpyridine, these systems show no significant extraction of metal below approximately pH 6 and thus stripping may be achieved by pH adjustment of the aqueous phase to pH < 6 [195].

Cobalt(II) and zinc(II) extraction (at a fixed concentration of 1×10^{-4} M) under variable H_2–**L** concentration from 5×10^{-4} to 1.5×10^{-3} M in the presence of a fixed concentration (2×10^{-3} M) of 4-ethylpyridine indicates the presence of $[M(H\text{-}\mathbf{L})_2]$ predominantly. 4-Ethylpyridine dependence studies, using a variation of the 4-ethylpyridine concentration over the range 2×10^{-4} M to 2×10^{-3} M while the other concentrations are held constant, suggest that the predominant species extracted approximates one 4-ethylpyridine coordinated per each metal centre.

When H_2–**64h** for cobalt(II) and nickel(II) ions or H_2–**64d** for zinc(II) ion (1×10^{-3} M) in $CHCl_3$ are treated with an excess metal(II) ion in water, the species occurring in the organic phase have a 1:1 = Zn:H_2–**L** ratio compatible with the formation of a complex formulated as $[M_3(\mathbf{L})_3]$. The presence of 4-ethylpyridine leads to extracted species with a 1:2 = M:**L** ratio likely of type $[M(\mathbf{L})_2$(4-

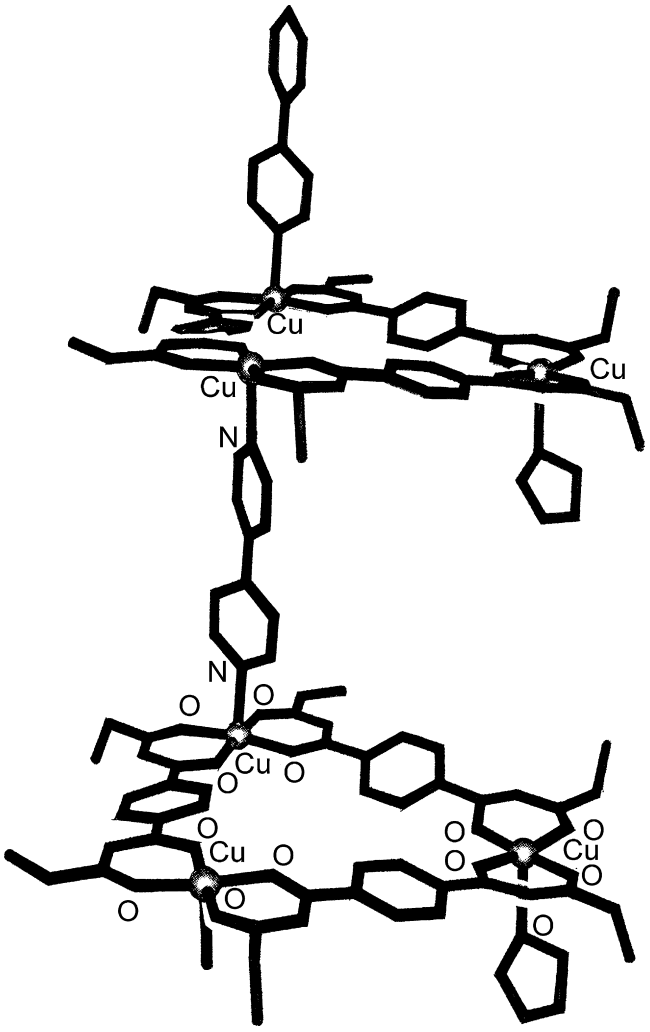

Fig. 76. Structure of $[Cu_3(\mathbf{64b})_3(4,4'\text{-bipy})(THF)]_\infty$ [196].

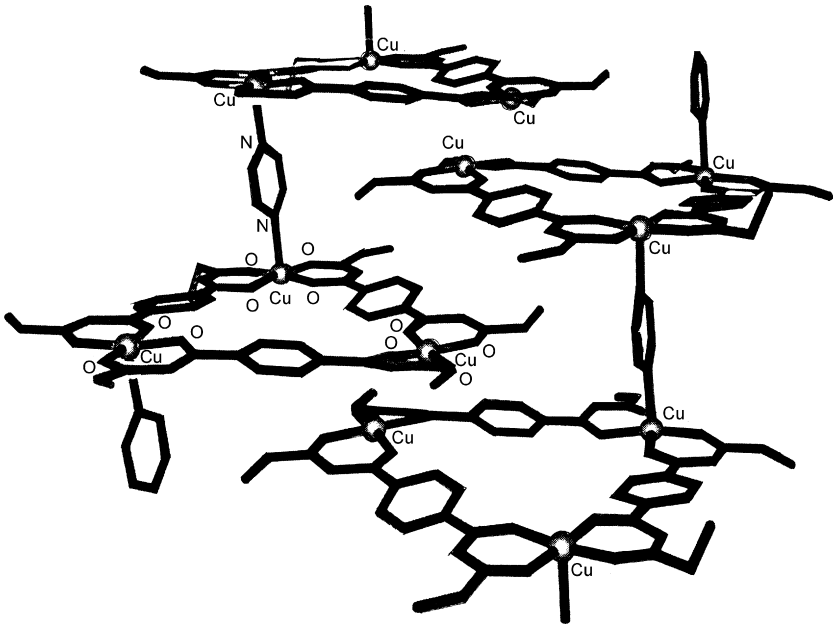

Fig. 77. Structure of $[Cu_3(\mathbf{64b})_3(pyz)]_\infty$ [196].

ethylpyridine)]. Competitive extractions, carried out at pH 7.8 in the absence of 4-ethylpyridine using equal concentrations (1×10^{-4} M) of cobalt(II), nickel(II), copper(II), zinc(II) and cadmium(II) perchlorates in water with chloroform solution of the appropriate H_2–**L** ligand (1×10^{-3} M), show quantitative (100%) extraction of the copper ion with zero extraction of for the remaining four metal ions. Similar competitive extraction experiment, carried out in the presence of 4-ethylpyridine (2×10^{-3} M) at pH 7.4, show effectively quantitative extraction of copper(II) across all ligand derivatives. In contrast, extraction of cobalt(II), nickel(II), zinc(II) and cadmium(II) was found to be zero in all cases apart from nickel(II) with H_2–**64h**, where a marked nickel(II) extraction enhancement occurs (from ~0 to 63%) [196].

$[Fe_4(\mathbf{64c})_6]\cdot 6THF$, $[Fe_4(\mathbf{64b})_6]\cdot H_2O$, $[Fe_4(\mathbf{64c})_6]\cdot 6THF$, $[Ga_4(\mathbf{64a})_6]\cdot 8.5THF$ have a similar tetranuclear assembly. In $[Fe_4(\mathbf{64c})_6]\cdot 6THF$ (Fig. 75c) the four iron(III) ions are at the vertices of tetrahedron with the six ligands bridging the metal ions defining the edges. The structure is maintained in solution. The six coordinate, approximately octahedral iron(III) ions are very weakly antiferromagnetically coupled [195].

$[Cu_3(\mathbf{64b})_3]0.5H_2O$, whose structure resembles that of the above similar complexes, reacts with 1.5 equiv. of 4,4-bipyridine in tetrahydrofuran to form the one-dimensional step-like complex $\{[Cu_3(\mathbf{64b})_3(4,4'bipy)(THF)]\cdot 2.75THF\}_\infty$. One copper(II) ion of each trinuclear unit is not axially bound to a 4,4′-bipiridine linker but to a tetrahydrofuran molecule. The same reaction in the presence of an excess of 4,4′-bipyridine again originates the same one dimensional step-like polymeric complex, showing the same structures (Fig. 76) [196].

The smaller pyrazine gives rise to $\{[Cu_3(\mathbf{64b})_3(pyz)]\cdot THF\}_\infty$, whose stepped polymeric structure resembles that with 4,4'-bipyridine. However, in this complex no tetrahydrofuran molecules are bound to individual copper(II) centres; thus, two copper(II) sites in each triangle are formally five coordinate, while the third copper(II) site is square planar (Fig. 77) [196].

The addition of excess 1,4-diazobicyclo-[2,2,2]-octane (dabco) to a tetrahydrofuran solution of $[Cu_3(\mathbf{64d})_3]$ forms $\{[Cu_3(\mathbf{64d})_3(dabco)_3]\cdot(C_2H_5)_2O\}_n$, where each copper ion is six coordinate with three dabco units per triangular complex bridging axial positions to produce an infinite one-dimensional triangular prismatic arrangement (Fig. 78) [196].

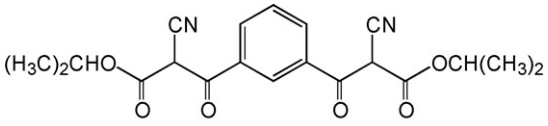

H_2-**66**

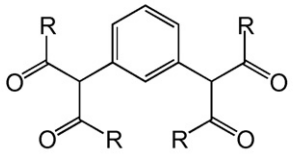

R
H_2-**67a** CH_3
H_2-**67b** CH_2CH_3

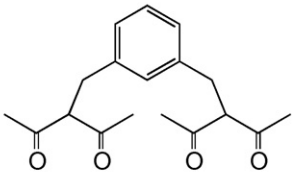

H_2-**68**

Equimolar amounts of hexamethylenetetramine (hmt) and $[Cu_3(\mathbf{64c})_3]\cdot 2H_2O$ in tetrahydrofuran afford $[Cu_3(\mathbf{64c})_3(hmt)]_n$, whose structure reveals neutral three-dimensional network with both hexamethylenetetramine and $\{Cu_3(\mathbf{64c})_3\}$ acting as triply-bridging units. Each triangle incorporates three five coordinate copper(II) centres, with three hexamethylenetetramine linkers coordinated on one side of the mean plane of the triangle. The structure was ascribed as a network arrangement with an anti-clockwise helical twist where the crystals are optically active (Fig. 79) [196].

Cyanoacetic diisopropyl ester, triethylamine, dry magnesium chloride and isophthaloylchloride in acetonitrile at −15 °C for 16 h

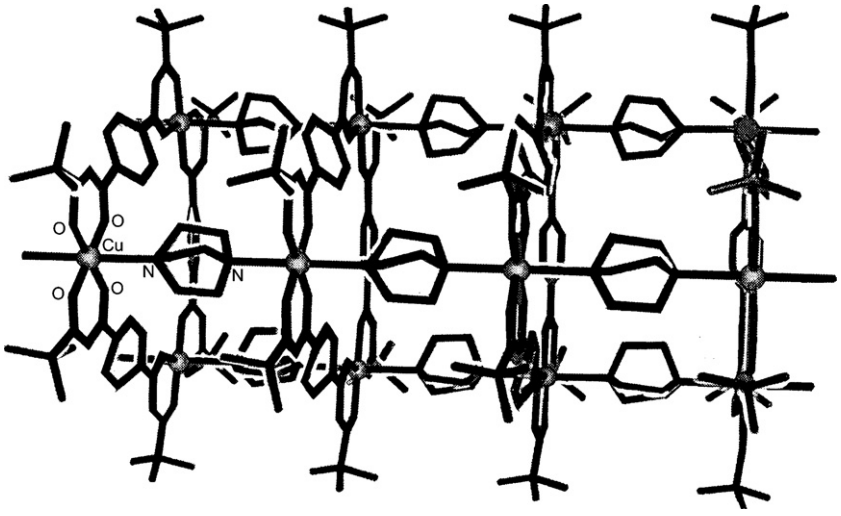

Fig. 78. Structure of $[Cu_3(\mathbf{64d})_3(dabco)_3]_n$ [196].

and work up in 1N HCl afford H_2–**66**, capable to self assemble in one pot to the triple helicate $[Fe_2(\mathbf{66})_3]$ when treated with $FeCl_3$ and $N(C_2H_5)_3$ in CH_2Cl_2 (Fig. 80). Each of the two iron(III) centres, 7.09 Å apart, is octahedrally surrounded by six oxygen atoms. The interior of the metallacryptand is not suitable for alkali metal cations complexation. Cyclic voltammograms of $[Fe_2(\mathbf{66})_3]$ display a quasireversible, one-potential, two-electron transfer process at $E_{1/2} = -430$ mV (reference electrode Fc^+/Fc), corresponding to the redox process $[Fe^{III}_2(\mathbf{66})_3] \rightleftharpoons [Fe^{II}_2(\mathbf{66})_3]^{2-}$ [197].

Reaction of isophthalaldehyde with 2,2,2-trimethoxy-4,5-dimethyl-1,3,2-dioxaphospholene or 2,2,2-trimethoxy-4,5-diethyl-1,3,2-dioxaphospholene at room temperature and heating of the resulting intermediate in methanol under nitrogen, afford H_2–**67a** and H_2–**67b**, respectively, which reacts with a CH_2Cl_2/H_2O solution of $[Cu(NH_3)_4]^{2+}$ to produce the molecular squares $[Cu_4(\mathbf{67a})_4]$ and $[Cu_4(\mathbf{67b})_4]$, with an edge of 14 Å, the organic bridging groups are at the corners all bent away from coplanarity while the metal ions are in the center of the sides (Fig. 81a). The $\{Cu_4(\mathbf{L})_4\}$ squares are parallel and create channels, filled by solvent whose removal causes a crystallinity loss; the resulting non-crystalline materials adsorb at room temperature under hydrogen pressure (75 atm) approximately 4.3 and 4.4 molecules of H_2 per molecule of complex, respectively. Greater adsorption was observed at 77 K under lower hydrogen pressure (43 atm) 4.3% for $[Cu_4(\mathbf{67a})_4]$ and 4.2% w/w for $[Cu_4(\mathbf{67b})_4]$. These values, among the best recorded for porous metal-organic compounds, demonstrate that non-crystalline, molecular hosts can function effectively in H_2 adsorption [198].

$[Cu_4(\mathbf{67a})_4]$ and 4,4′-bipy produce the polymeric complex $[Cu_4(\mathbf{67a})_4(4,4'\text{-bipy})_2]_n$ (Fig. 81b), with the 4,4′-bipy molecules intra- and intermolecularly bonded to the molecular square. The Cu···Cu distances in $[Cu_4(\mathbf{67a})_4]$ are longer than those normally observed in the 4,4′-bipy-bridged complex (ca. 10 Å). However, in $[Cu_4(\mathbf{67a})_4(4,4'\text{-bipy})_2]_n$ the 4,4′-bipy molecules are accommodated by means of smaller distortions at the two copper(II) ions and larger distortions at the other two copper(II) ions. The square pyramidal environment of the copper(II) ions favours both changes, bringing the endo-coordinated copper ions closer together, and the exo-coordinated ones farther apart [197].

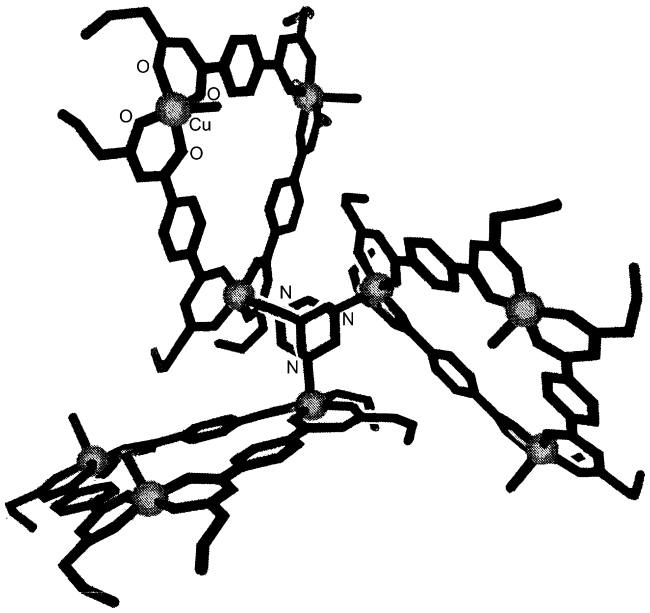

Fig. 79. Structure of $[Cu_3(\mathbf{64c})_3(hmt)]_n$ [196].

$[Cu_4(\mathbf{67a})_4]$ and $[Cu_4(\mathbf{67b})_4]$ readily incorporate C_{60} or C_{70} in chlorobenzene, as confirmed by the X-ray structure of $\{[Cu_4(\mathbf{67b})_4 \cdot (C_{60})]\}$, where the ethyl groups of the $[\mathbf{67b}]^{2-}$ ligands are all oriented toward the C_{60} guest; the Cu···Cu distances (13.96 and 14.06 Å) are slightly smaller than in $[Cu_4(\mathbf{67b})_4]$. Weak interactions stabilize the host–guest adduct.

The condensation of benzene-1,3-dicarboxaldehyde with 2,4-pentanedione and subsequent catalytic hydrogenation of the resulting product affords H_2–**68** which, on treatment with aqueous $[Cu(NH_3)_4]^{2+}$, gives rise to $[Cu_2(\mathbf{68})_2]$ whose structure consists of a dinuclear assembly with a Cu···Cu distance of 4.908 Å and essentially planar $\{Cu(\beta\text{-diketonato})_2\}$ moieties (Fig. 82). The addition of pyridine to $[Cu_2(\mathbf{68})_2]$ gives rise to $[Cu_2(\mathbf{68})_2(py)_2]$ with the two pyridine in the external axial positions [199].

Equimolar amounts of $[V(X)_3(THF)_3]$ ($X = Cl^-$, Br^-) or $[V(Cl)_2(tmeda)_2]$ (tmeda = *N*,*N*′,*N*′-tetramethylethylenediamine) and $[Na_2(\mathbf{68})]$, generated in tetrahydrofuran from H_2–**68** and 2 equiv. of NaH, produce $[V_2(\mathbf{68})_2(X)_2(THF)_2]$ (Fig. 83) or $[V_2(\mathbf{68})_2(Cl)_2(tmeda)_2]$, which have analogous dinuclear entities with a V···V distance just over 11.66 Å for the former and 11.444 Å for the latter. The $[\mathbf{68}]^{2-}$ ligand orientation again is in an extended conformation while the remaining sites are occupied by tmeda [200].

12.3. Complexes containing other aromatic spacers

Claisen condensation of the appropriate precursors in dry diethylether and in the presence of $NaOCH_3$ affords H_2–**69a**···H_2–**69d**, H_2–**70**, H_2–**71** and H_2–**72a**···H_2–**72c**. An acetone/petroleum ether solution of $N(C_2H_5)_3$ and $\{H_2[Eu_2(\mathbf{72a})_4] \cdot C_2H_5OH\}$, obtained from equimolar amounts of H_2–**72a** and $EuCl_3$ in ethanol, affords $[NH(C_2H_5)_3]_2[Eu_2(\mathbf{72a})_4].C_2H_5OH$, where four $[\mathbf{72a}]^{2-}$ ligands bridge the two O_8 eight coordinate, square antiprismatic europium(III) ions with bidentate coordination to each metal ion, thus surrounded by eight oxygen atoms of the four $[\mathbf{72a}]^{2-}$ ligands (Fig. 84). The europium(III) complexes with H_2–**72a** have stronger luminescence and luminescence lifetime when compared with β-diketonato (i.e. H–**17**) and other similar bis β-diketonate complexes. In the complexes with H_2–**69a** and H_2–**72b**, substitution of CF_3 with C_2F_5 causes noticeable increase in the luminescence intensity [201].

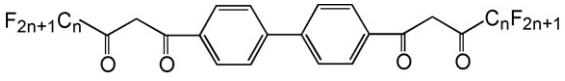

n
H_2-**69a** 1
H_2-**69b** 2
H_2-**69c** 3
H_2-**69d** 4

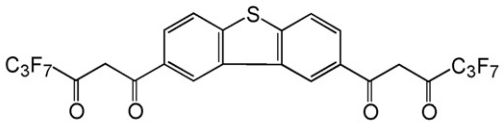

H_2-**70**

The similar larger ligand H_2–**73**, derived from alkylation of H–**5** by 2,7-bromo(methyl)naphthalene, in the presence of an aqueous solution of $[Cu(NH_3)_4]^{2+}$ rapidly turns into $[Cu_2(\mathbf{73})_2]$ with a Cu···Cu distance of 7.349 Å and two almost parallel $\{Cu(\beta\text{-diketonato})_2\}$ moieties which favour π-stacking between adjacent molecules. $[Cu_2(\mathbf{73})_2]$ changes in solution from olive green to turquoise on addition of a nitrogen containing coordinating base,

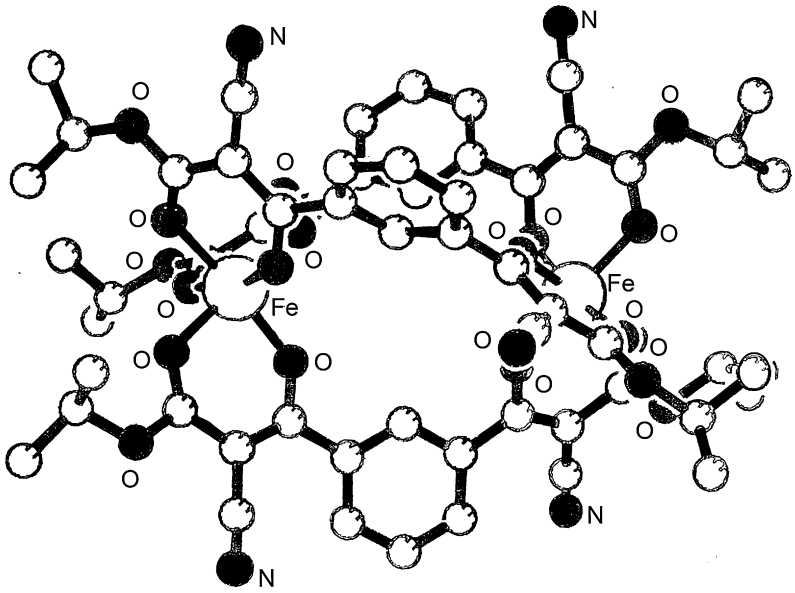

Fig. 80. Structure of $[Fe_2(\mathbf{66})_3]$ [197].

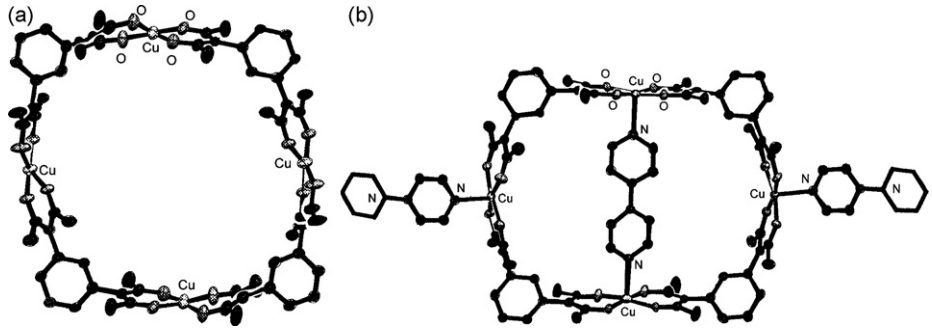

Fig. 81. Structures of $[Cu_4(\mathbf{67a})_4]$ (a) and $[Cu_4(\mathbf{67a})_4(4,4'\text{-bipy})_2]_n$ (b) [198].

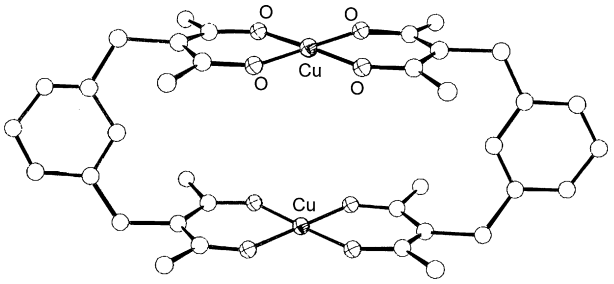

Fig. 82. Structure of $[Cu_2(\mathbf{68})_2]$ [199].

in consequence of the formation of the related complex: pyridine and quinoline act as monodentate ligands while the larger binding constants for pyrazine, 2-aminopyrazine and 1,4-diazabicyclo-[2,2,2]-octane (dabco) are consistent with endo-coordination, proved by the structures of $[Cu_2(\mathbf{73})_2(\mu\text{-dabco})]$ (Fig. 85) containing two square pyramidal copper (II) ions, 7.403 Å apart, and of the 2,5-dimethylpyrazine (2,5-CH_3-pyz) adduct $[Cu_2(\mathbf{73})_2(2,5\text{-}CH_3\text{-pyz})]\cdot 4CH_2Cl_2$ where the square pyramidal copper(II) ions, 7.554 Å apart, are slightly displaced toward the axial nitrogen atoms. Hydrogen bonding between the NH_2 group of 2-aminopyrazine and the oxygen atoms of the $[Cu_2(\mathbf{73})_2]$ host is probably responsible for its unusually large binding constant [202,203].

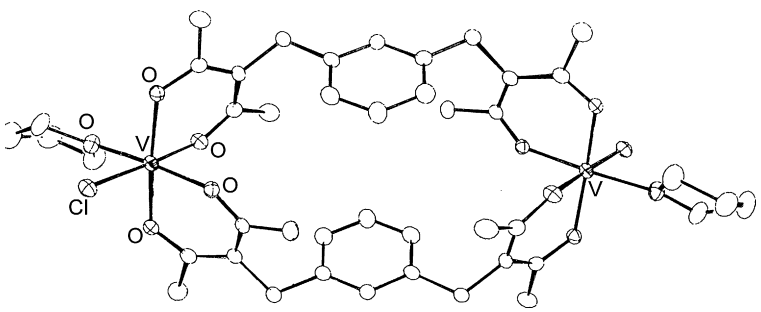

Fig. 83. Structure of $[V_2(\mathbf{68})_2(Cl)_2(THF)_2]$ [200].

4,4′-Bis(bromomethyl)-1,1′:3′,1″-terphenyl, synthesized from 4,4′-dimethyl-1,1′:3′,1″-terphenyl by radical bromination with $[N(CH_3)_4](Br)_3$, allowed to react with 2 equiv. of potassium acetylacetonate in *tert*-butanol, affords H_2–**74**, which reacts with $[Cu(NH_3)_4](SO_4)$ in $H_2O/CHCl_3$ to form the macrocycle $[Cu_2(\mathbf{74})]$, large enough to encapsulate and coordinate 4,4′-bipyridine giving rise to $[Cu_2(\mathbf{74})_2(4,4'\text{-bipy})]$, where the two nitrogen donors occupy the internal axial positions of the two square pyramidal copper(II) ions 11.8 Å apart (Fig. 86) [204].

12.4. Complexes with related ligands bearing an aromatic or an aliphatic spacer

Equimolar amounts of H_2–**75** or H_2–**76**, and $[Pt(Cl)_4]^{2-}$ lead to *cis*-$[Pt_3(\mathbf{75})_3]$ (Fig. 87a) or *cis*-$[Pt_2(\mathbf{76})_2]$ (Fig. 87b) metallomacrocyclic assemblies, where the aromatic rings of the isophthaloyl and terephthaloyl moieties are essentially coplanar with the coordination environment of the platinum(II) ions. A distorted square planar geometry about each platinum(II) ion occurs in both *cis*-$[Pt_3(\mathbf{75})_3]$ and *cis*-$[Pt_2(\mathbf{75})_2]$ [205].

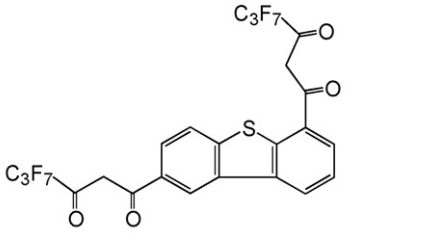

H_2-**71**

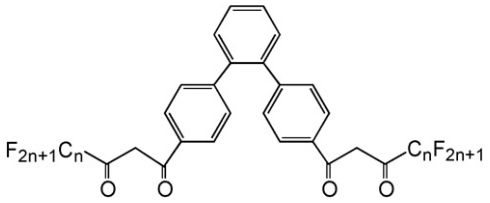

	n
H_2-**72a**	1
H_2-**72b**	2
H_2-**72c**	3

^{195}Pt NMR studies reveal that I_2 react with the *cis*-$[Pt_3(\mathbf{75})_3]$ in chloroform at room temperature to yield, by stepwise oxidative addition to each platinum(II) centre, the mixed valence species *cis*-$[Pt^{II}_2Pt^{IV}(\mathbf{75})_3(I)_2]$ and *cis*-$[Pt^{II}Pt^{IV}_2(\mathbf{75})_3(I)_4]$, and the fully oxidised *cis*-$[Pt^{IV}_3(\mathbf{75})_3(I)_6]$, depending on the I_2:*cis*-$[Pt^{II}_3(\mathbf{75})_3]$ molar ratio. Treatment of *cis*-$[Pt^{II}_2(\mathbf{76})_2]$ with iodine results in facile oxidative addition to yield *cis*-$[Pt^{IV}_2(\mathbf{76})_2(I)_4]$, where the $[\mathbf{76}]^{2-}$ ligands remain *cis*-S,O-coordinated to the platinum(IV) centres, with the halides in *trans* axial positions. The molecules in the crystal structure of *cis*-$[Pt^{IV}_2(\mathbf{76})_2(I)_4]$, have their *trans*-platinum(IV)–iodo axes essentially aligned, with very close intermolecular iodide contacts resulting in chains of weakly bound metallamacrocycles in the solid (Fig. 88) [206].

An alternative electrolytic synthesis method, using a simple two-compartment glass cell containing *cis*-$[Pt_2(\mathbf{76})_2]$ and a chosen halide salt in dichloromethane, leads to the formation of *cis*-$[Pt^{IV}_2(\mathbf{76})_2(X)_4]$ (X = Cl^-, Br^-) in consequence of the Br_2 or Cl_2 *in situ* release at the anode. In these complexes the $[\mathbf{76}]^{2-}$ ligands remain coordinated in a *cis*-S,O-fashion, and halide ions occupy the *trans* axial sites of octahedral platinum(IV) ions [205,206].

^{1}H NMR spectra in $CDCl_3$ of the chiral ligand H_2–**77**, prepared by Claisen condensation of the acetone ketal of L-tartaric acid diethyl ester with 2 equiv. of 4-bromoacetophenone in the presence of sodium amide, reveal that the ligand adopts the bis-enol rather than the tetraketo form. In methanol H_2–**77** forms the structurally very similar dinuclear complexes $[M_2(\mathbf{77})_3]$ with iron(III) chloride or gallium(III) nitrate. Three $[\mathbf{77}]^{2-}$ ligands bridge the two octahedral metal(III) centers, with a Fe···Fe separation of 5.343 Å and a Ga···Ga separation of 5.448 Å, giving rise to a right-handed Δ,Δ-helix (Fig. 89a) [207].

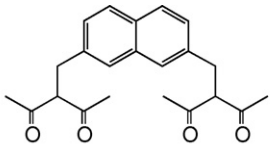

H_2-**73**

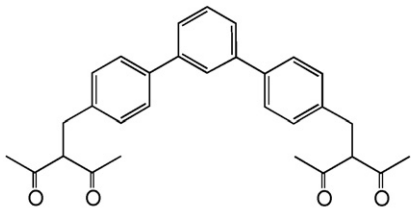

H_2-**74**

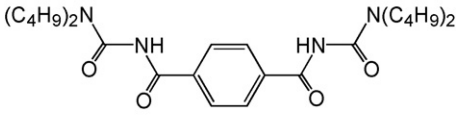

H_2-**75**

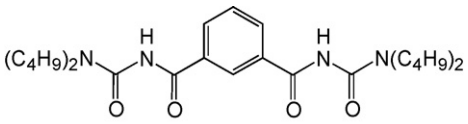

H_2-**76**

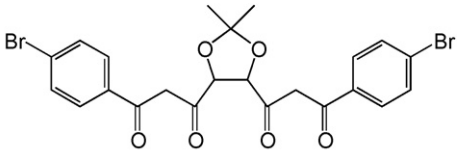

H_2-**77**

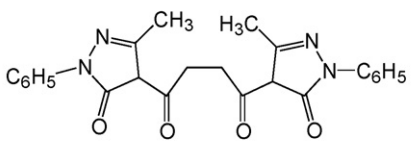

H_2-**77a**

The size of the internal cryptand-type cavity is capable to bind lithium cations, but is too small for sodium or potassium cations. Mass and NMR spectra in $CDCl_3$ show that uptake of $LiClO_4$, but not of $NaClO_4$ or $KClO_4$ by $[M_2(\mathbf{77})_3]$ (M = Ga^{III}, Fe^{III}) occurs with the consequent formation of $[M_2Li(\mathbf{77})_3](ClO_4)$ [207].

H_2–**77** and 0.3 equiv. $Ni(CH_3COO)_2{\cdot}4H_2O$ in refluxing pyridine for 3.5 h afford $[H\text{-}py]_2[Ni_2(\mathbf{77})_3]$ with $[Ni_2(\mathbf{77})_3]^{2-}$ presumably adopting a right-handed (ΔΔ) triple-stranded dinuclear helicate as

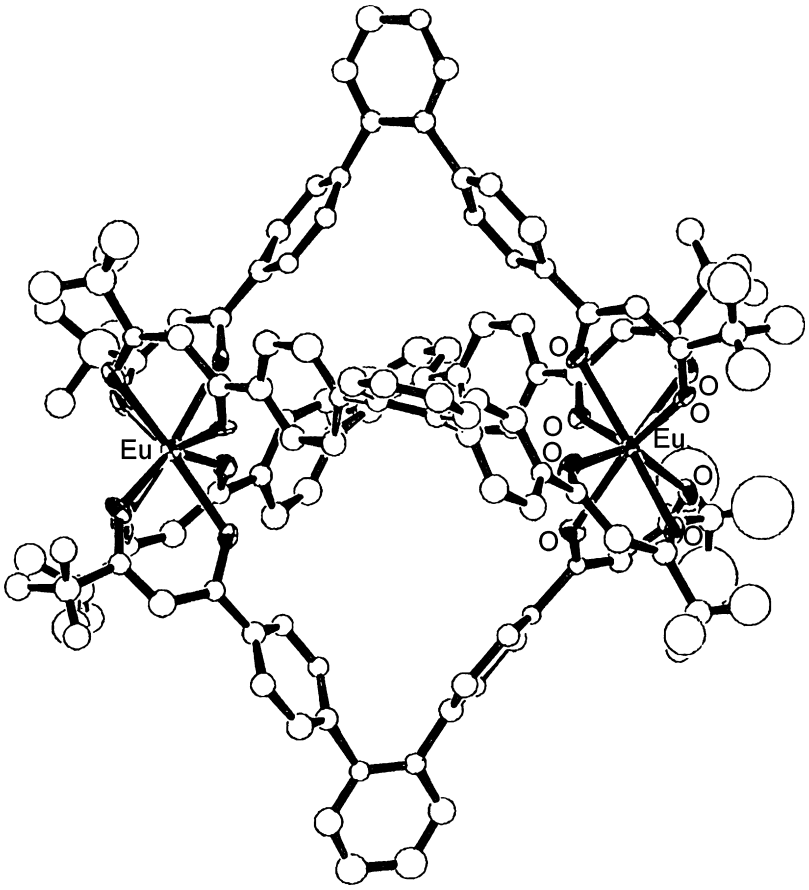

Fig. 84. Structure of $[Eu_2(\mathbf{72a})_4]^{2-}$ [201].

found for the corresponding neutral complexes $[M_2(\mathbf{77})_3]$ ($M = Ga^{III}$, Fe^{III}). When H_2–**77** is reacted with 1.5 equiv. of $Ni(CH_3COO)_2{\cdot}4H_2O$ in pyridine, $[Ni_3(\mathbf{77})_2(CH_3COO)_2(py)_2]$ takes place (Fig. 89b). The nickel ions possess a distorted octahedral coordination geometry with the $[\mathbf{77}]^{2-}$ ligands occupying the equatorial positions. The two external metal ions are coordinating to the β-diketonate units of the $[\mathbf{77}]^{2-}$ ligands, while the third one is included in the centre of the molecule binding to the internal carbonyl oxygen atoms of the β-diketonates which bridge the central and the terminal nickel ions. Also the acetate groups bridge the central and the terminal nickel(II) ions. The terminal metal centres are saturated by coordination of a pyridine each. In this arrangement

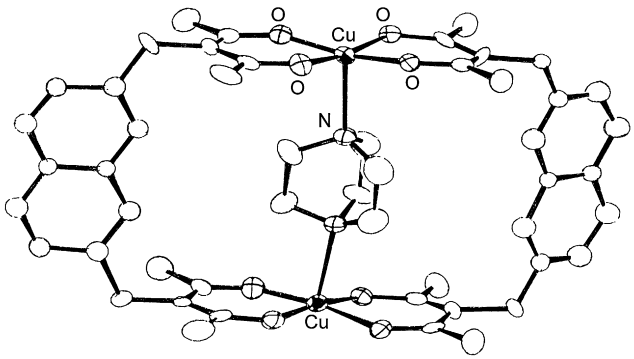

Fig. 85. Structure of $[Cu_2(\mathbf{73})_2(dabco)]$ [202].

the Ni–Ni–Ni axis is close to linear and separations of 3.060 and 3.065 Å are observed between the central and the terminal nickel ions and. While UV–vis spectra of H_2–**77**, $[py\text{-}H]_2[Ni_2(\mathbf{77})_3]$ and $[Ni_3(\mathbf{77})_2(CH_3COO)_2\ (py)_2]$ in dichloromethane are very similar, circular dichroism indicates significant difference in the geometry of the coordinated ligands. The conformational differences of the ligands in $[Ni_3(\mathbf{77})_2(CH_3COO)_2(py)_2]$ and $[H\text{-}py]_2[Ni_2(\mathbf{77})_3]$ causes fluorescence in the former complex in dichloromethane at room temperature, while the latter one is nonemissive under similar conditions [208].

H_2–**77a** reacts with $Tb(NO_3)_3{\cdot}6H_2O$ in ethanol and in the presence of $N(C_2H_5)_3$ to afford the triple-stranded helicate $[Tb_2(\mathbf{77a})_3(H_2O)_2]$ which evolves into $[Tb_2(\mathbf{77a})_3(DMF)_2]$ when recrystallized from dimethylformamide. The slow substitution of dimethylformamide by $OP(C_6H_5)_2CH_2CH_2(C_6H_5)_2PO$ (L) gives rise to the polymeric complex $[Tb_2(\mathbf{77a})_3(L)]_n$ which results also by direct assembly of a mixture of the ligand and the terbium(III) salt at 78 °C in ethanol. The dinuclear helical complexes consist of a $\{Tb_2(\mathbf{77a})_3\}$ fragment, capped by two monodentate water or dimethylformamide ligand, respectively. Both the seven coordinate terbium(III) ions are in a monocapped octahedral environment completed by six oxygen atoms of three β-diketonate moieties from the $[\mathbf{77a}]^-$ ligands (Fig. 90a). The polymeric complex $[Tb_2(\mathbf{77a})_3(L)]_n$ consists of infinite parallel chains, formed by helical $\{Tb_2(\mathbf{77a})_3\}$ units bridged by L ligands, the structure of each $\{Tb_2(\mathbf{77a})_3(L)\}_n$ fragment resembling those of the related dinuclear complexes (Fig. 90b) [208].

13. Dinuclear and polynuclear complexes derived from bis-β-diketones with a spacer bearing additional donor atoms

These tetraketones contain two β-diketonato moieties, linked at the 1 or 2 positions of a spacer bearing additional donor atoms. They can for the homo-$[M_3^{II}(\mathbf{L})_2]^{2+}$ or-$[M_3^{III}(\mathbf{L})_3]^{3+}$ and especially the heterotrinuclear $[M_2M'(\mathbf{L})_2]^{2+}$ or $[M_2M'(\mathbf{L})_3]^{3+}$ complexes, where the two equal metal(II) or metal(III) ions lie in the two external O_2O_2 or $O_2O_2O_2$ sites and the hetero metal ion M′ in the inner $O_2X_nO_2$ or $O_3X_nO_3$ (X = N, O, n = 1, 2) site with the metal ions close enough to interact each other. Of

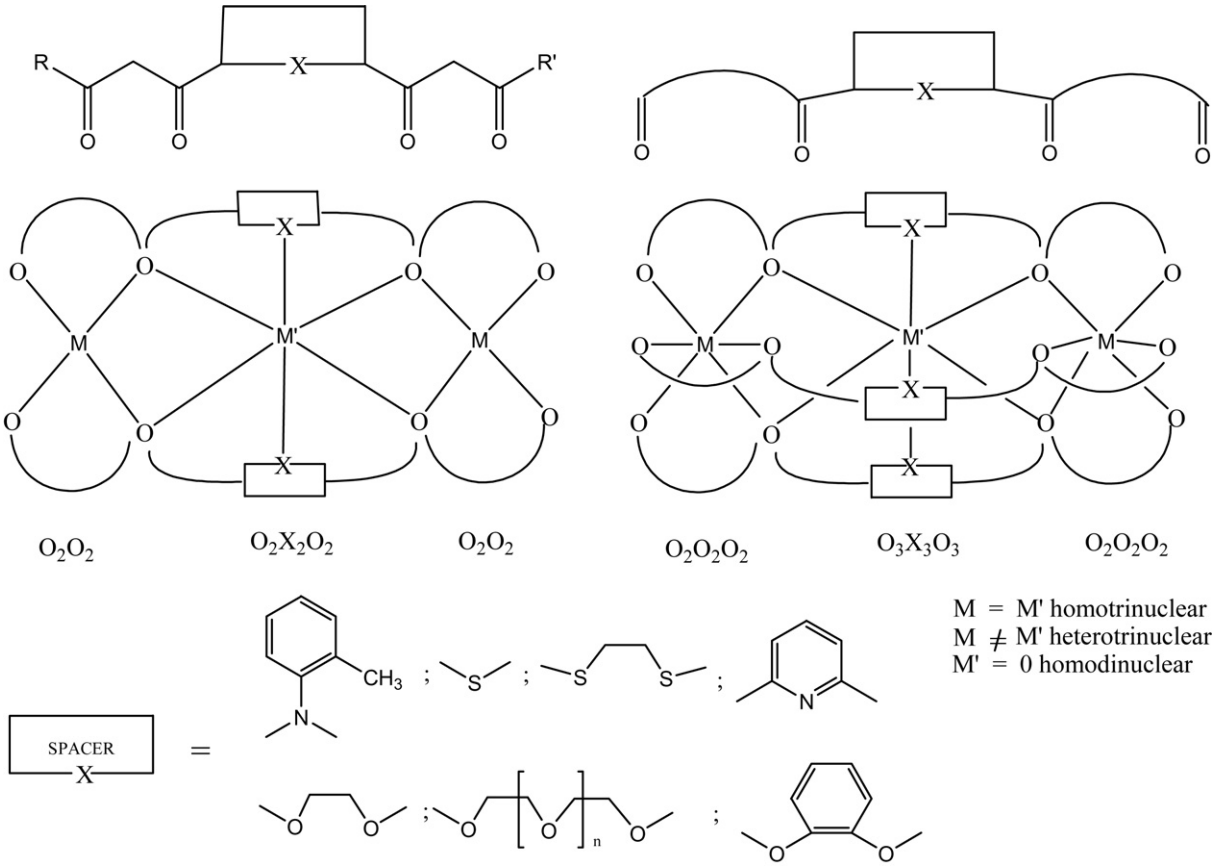

Scheme 12. Bis-β-diketones with a spacer bearing donor atoms, their schematic representation and the adjacent chambers and complex formation in consequence of homo- or heteronuclear complexation.

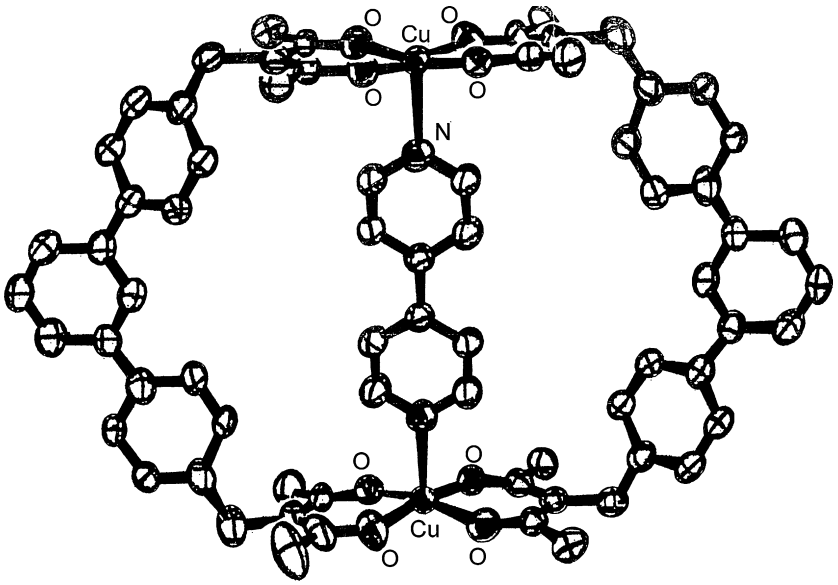

Fig. 86. Structure of $[Cu_2(\mathbf{74})_2(4,4'\text{-bipy})]$ [204].

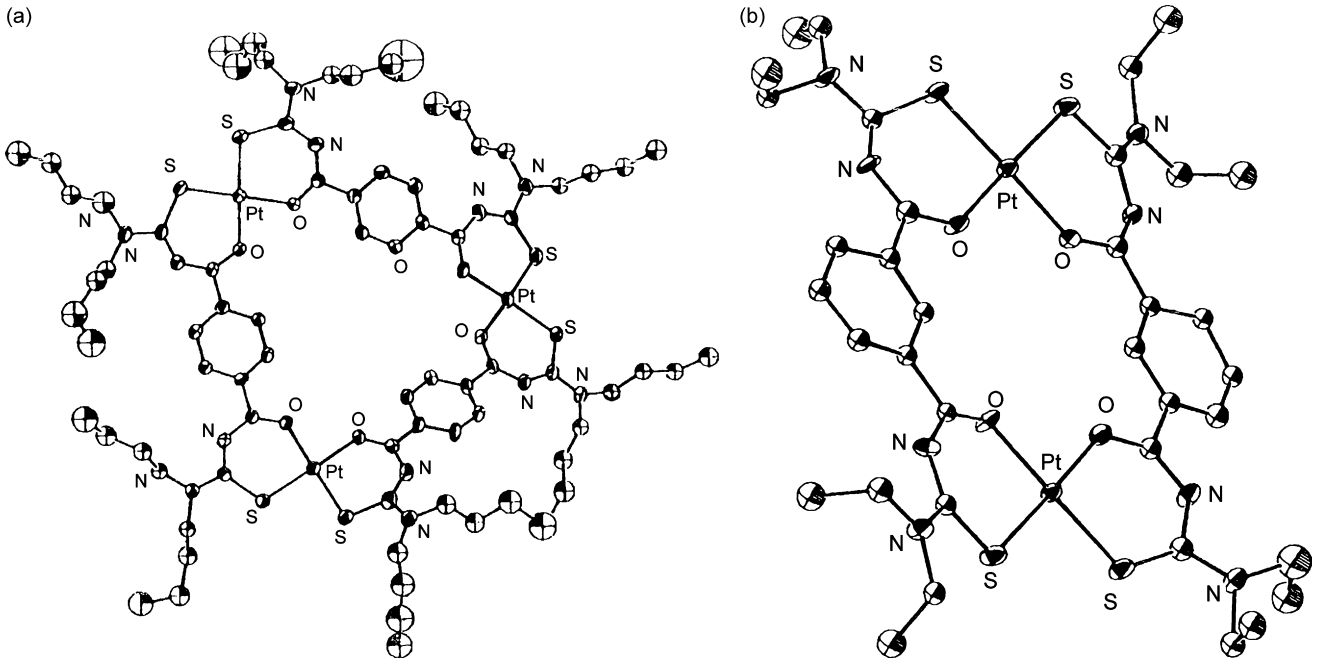

Fig. 87. Structures of *cis*-[Pt_3(**75**)$_3$] (a) and *cis*-[Pt_2(**76**)$_2$] (b) [205].

course homodinuclear complexation at the two external chamber is feasible, giving rise to [M_2^{II}(**L**)$_2$] or]M_2^{III}(**L**)$_3$] structural arrangements comparable to those observed with the related bis-β-diketones linked to a spacer without additional donor groups (Scheme 12).

13.1. Complexes with a spacer containing thioether or aliphatic amine donors

H_2–**78a**···H_2–**78c** react with [Ru(H)(Cl)(CO)(PPh_3)$_3$], [Ru(H)(Cl)(CO)(PPh_3)$_2$(py)] [Ru(H)(Cl)(CO)(PPh_3)$_2$(pip)] or [Ru(H)(Cl)

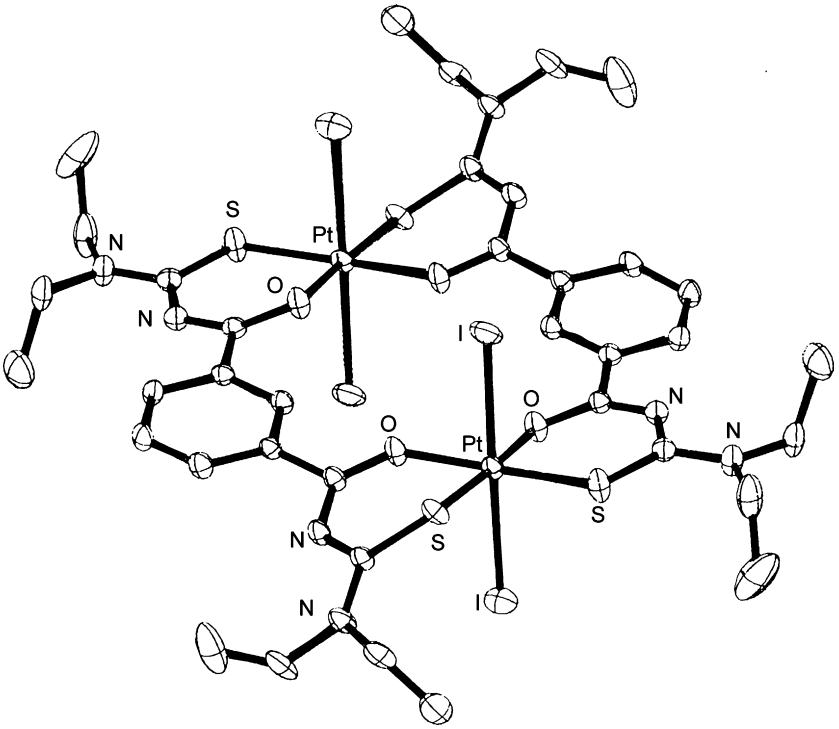

Fig. 88. Structure of *cis*-[Pt_2(**76**)$_2$(I)$_4$] [206].

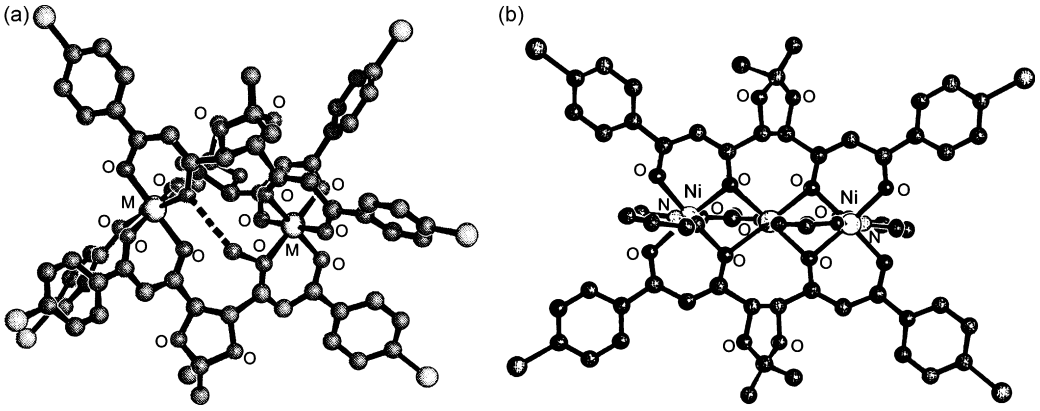

Fig. 89. Structures of $[M_2(\mathbf{77})_3]$ ($M = Ga^{III}$, Fe^{III}) (a) [207] and $[Ni_3(\mathbf{77})_2(CH_3COO)_2(py)_2]$ (b) [208].

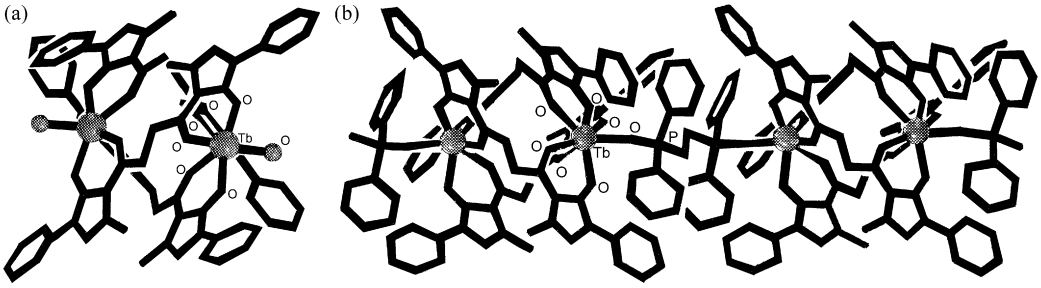

Fig. 90. Structure of $[Tb_2(\mathbf{77a})_3(H_2O)_2]$ (a) and $[Tb_2(\mathbf{77a})_3\{OP(C_6H_5)_2CH_2CH_2(C_6H_5)_2PO\}]_\infty$ (b) [208].

$(CO)(PPh_3)_2(mor)]$ in a 2:1 molar ratio in benzene to form $[Ru_2(\mathbf{L})_2(Cl)_2(CO)_2(PPh_3)_2(L)_2]$ (L = triphenylphosphine (PPh_3), pyridine (py), piperidine (pip), morpholine (mor)), where the $[\mathbf{L}]^{2-}$ ligands act as bridging groups with the thioether donor not coordinated to the octahedral ruthenium(III) ions [209].

Cyclic voltammetry of the octahedral complexes $[Ru_2(\mathbf{L})_2(X)_2(L)_4]$ ($X = Cl^-$, Br^-; L = PPh_3, $AsPh_3$), derived from H_2–**78a**···H_2–**78c** and $[Ru(X)_3(PPh_3)_3]$, $[Ru(X)_3(AsPh_3)_3]$, and $[Ru(Br)_3(PPh_3)_2(CH_3OH)]$ in benzene and in a 2:1 ratio in acetonitrile at a glassy carbon working electrode, using s.c.e. as reference, exhibits two successive quasi reversible or irreversible couples at positive potential due to the oxidations: $Ru^{III}Ru^{III} \leftrightarrows Ru^{III}Ru^{IV} \leftrightarrows Ru^{IV}Ru^{IV}$. The irreversible oxidation was assumed to be due to oxidative dissociation of the ligands, occurring at the ruthenium(IV) centre. These ruthenium(III) complexes catalyse the oxidation of $C_6H_5CH_2OH$ and cyclohexanol to C_6H_5CHO and cyclohexanone respectively

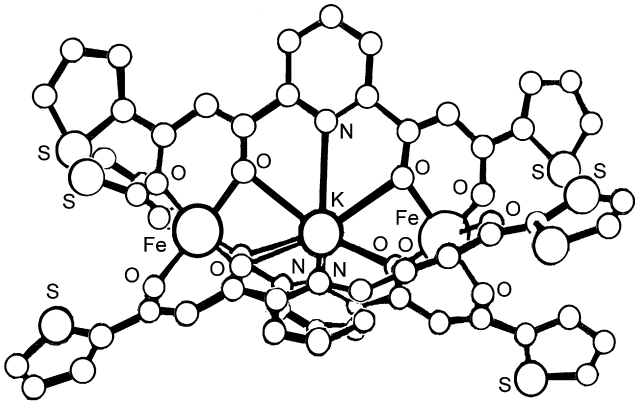

Fig. 91. Structure of $[Fe_2K(\mathbf{82c})_3]^+$ [216].

using *N*-methylmorpholine-*N*-oxide as cooxidant. Furthermore, the ligands and the majority of the complexes have antifungal activity; in particular they show growth inhibitory activity against the bacteria *Escherichia coli*, *Bacillus* sp. and *Pseudomonas* sp. [210,211].

H_2–**79**, prepared by reaction of H–**5** and S_2Cl_2, breaks down in the presence of $[Ru(\mathbf{5})_2(CH_3CN)_2]$ in acetone at 25 °C under argon forming $[Ru(\mathbf{5})_2(\mathbf{79a})]$, where $[\mathbf{79a}]^-$ behaves as an O,S chelating ligand. However, when the same reaction is carried out under reflux, two isomers of sulfur-bridged binuclear $[Ru_2(\mathbf{5})_4(\mu\text{–}\mathbf{79b})]$ are obtained, where $[\mathbf{79b}]^-$ behaves as a O,S,O-bridging and chelating ligand. In addition, an orange fraction occurs, identified according to mass spectrometry as the $[\mathbf{79}]^{2-}$-bridged di-ruthenium(III) complex $[Ru_2(\mathbf{79})(\mathbf{5})_4]$. A similar reaction of $[Ru(\mathbf{7})_2(CH_3CN)_2]$ with H_2-**79** under refluxing conditions in acetone yields two isomeric binuclear complexes, identified as the *racemic* and *meso* forms of $[Ru_2^{II}(\mathbf{7})_4(\mathbf{79b})]$. The X-ray structure of *racemic* (Δ, Δ and Λ, Λ) and the *meso* (Δ, Λ) forms of $[Ru_2(\mathbf{5})_4(\mu\text{–}\mathbf{79b})]$ confirm the above reported structure: in both complexes the sulfur atom of the $[\mathbf{79b}]^{2-}$ ligand bridges two octahedral ruthenium(III) ions. There is no difference in the electronic spectra of the *meso* and *racemic* isomers of the dinuclear complexes. The X-ray photoelectron spectra (XPS) and cyclic voltammetric studies of the mononuclear complex indicate the presence of the ruthenium(III) ion whereas the spectra of all of the binuclear complexes indicate the presence of both ruthenium(III) and ruthenium(II) species. Electrochemical data show that the binuclear complexes do not have distinct Ru^{II} and Ru^{III} ions, whereas the valence averaged of the oxidation state is 2.5 on each ruthenium ion, thus an extensive electron delocalization takes place in the {Ru–S–Ru} core in all of the binuclear complexes [212].

Mass spectra indicate a trimeric structure for [VO(**79**)(py)] and [VO(**79**)(DMSO)], prepared by reaction of equimolecular amounts of $[VO(\mathbf{5})_2]$ and the H_2–**79** in pyridine or dimethylsulfoxide, respec-

tively. No V···V magnetic interaction occurs in these complexes [213].

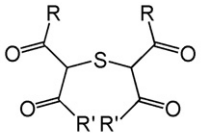

	R	R'
H_2-**78a**	CH_3	CH_3
H_2-**78b**	C_2H_5	CH_3
H_2-**78c**	C_6H_5	C_6H_5

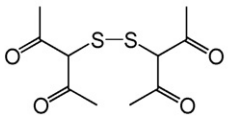

H_2-**79**

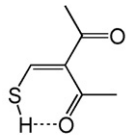

H-79a

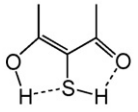

H_2-**79b**

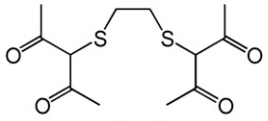

H_2-**80**

In the isomorphous high spin complexes $[M(\mathbf{80})(H_2O)_2]\cdot H_2O$ ($M = Co^{II}$, Ni^{II}), obtained by the related metal(II) acetate and H_2–**80** in methanol/acetone, $[\mathbf{80}]^{2-}$ coordinates via the two sulfur atoms but uses only two oxygen atoms for binding to the pseudo-octahedral metal(II) ion. The sulfur donors are mutually *cis* while the two bound β-diketone oxygen atoms are *trans*. The remaining two coordination sites are occupied by water molecules [214].

The four ketonic moieties of H_2–**81** are at the appropriate positions to form homo- or heterotrinuclear complexes in addition to homodinuclear ones. Equimolar amounts of H_2–**81** and the appropriate metal(II) acetate or uranyl(VI) nitrate hexahydrate in ethanol give $[Zn_2(\mathbf{81})_2]$, $[Cu_2(\mathbf{81})_2]\cdot 2H_2O$ and $[M_2(\mathbf{81})_2(H_2O)_4]\cdot 2H_2O$ ($M = Ni^{II}$, Mn^{II}) or $[(UO_2)_2(\mathbf{81})_2(C_2H_5OH)_2]$, sparingly soluble in non coordinating solvents and more soluble in dimethylsulfoxide or pyridine where they form the related adducts as found for $[(UO_2)_2(\mathbf{81})_2(py)_2]$ and $[(UO_2)_2(\mathbf{81})_2(dmso)_2]$. Furthermore, UV–vis spectra of the copper(II) and nickel(II) complexes in dimethylsulfoxide show the occurrence of a five coordinate copper(II) and a non-planar high spin nickel(II) species. For all these complexes a dinuclear structure was proposed , also taking into account that they are easily converted into the trinuclear ones $[M_3(\mathbf{81})_2(OH)(H_2O)_2](ClO_4)$ ($M = Cu^{II}$, Ni^{II}), when treated with equimolar amounts of the appropriate metal perchlorate. The same trinuclear complexes have been obtained by reaction of the ligand H_2–**81** with the appropriate metal salt in a 2:3 molar ratio. The dinuclear complexes exhibit physico-chemical properties typical of isolated β-diketonato compounds without magnetic coupling between the two metal(II) ions while in the trinuclear species (for instance in the trinuclear copper(II) complexes), antiferromagnetic interactions take place, indicating that the metal ions are close each other [215].

13.2. Complexes with a pyridine spacer

Equimolar alcohol solutions of H_2–**82a** and copper(II) or uranyl(IV) acetate or vanadyl(IV) sulfate precipitate $[M_2(\mathbf{82a})_2(solvent)_n]$ ($n = 0,2$), while the complexes $[M_2(\mathbf{82a})_2(py)_4]$ ($M = Co^{II}$, Ni^{II}) are conveniently prepared by refluxing equimolar quantities of the ligand and the appropriate metal(II) acetate in pyridine. UV–vis spectra indicate that in $[Cu_2(\mathbf{82a})_2]$ the copper(II) ions are square planar while in $[M_2(\mathbf{82a})_2(py)_4]$ ($M = Ni^{II}$, Co^{II}) the metal(II) ions are octahedral. The magnetic moments indicate the occurrence of a weak antiferromagnetic interaction in these dinuclear complexes [215].

A mixture of $[Cu_2(\mathbf{82a})_2]$ or $[Ni_2(\mathbf{82a})_2(py)_4]$ and a slight excess of $Ba(SCN)_2$ in hot ethanol gives $[Cu_2Ba(\mathbf{82a})_2(SCN)_2]$ and $[Ni_2Ba(\mathbf{82a})_2(SCN)_2]$, respectively, which presumably have a discrete trinuclear structure with the barium(II) ion in the inner coordination chamber. If KNCS is used, only the starting binuclear precursors are recovered. Furthermore, discrete homotrinuclear $[Zn_3(\mathbf{82a})(CH_3COO)_2]$ and heterotrinuclear complexes $[M_2M'(\mathbf{82a})_2]^{2+}$ ($M = Cu^{II}$, Ni^{II}; $M' = Zn^{II}$, Ba^{II}) or polynuclear manganese(II) complexes, particularly $[Mn_4(\mathbf{82a})_2]^{4+}$ and $[Mn_8(\mathbf{82a})_6(O)_2]$, have been suggested to occur [215].

H_2–**82a**···H_2–**82d** and iron(III) chloride in the presence of the appropriate metal salt yield $[Fe_2M(\mathbf{L})_3](X)_n$ ($M = K^I$ $n = 1$; Ba^{II}, Sr^{II} $n = 2$; La^{III} $n = 3$), where the guest cation M^{n+} is encapsulated in the cavity of the bicyclic dinuclear $\{Fe(\mathbf{L})_3\}$ host. In $[Fe_2K(\mathbf{82c})_3](PF_6)$ (Fig. 91) the potassium ion is nine coordinated by six oxygen and three nitrogen atoms of the three ligands. The ligands are coordinated in a helical fashion to the octahedral iron centers which are 7.01 Å apart. In the chiral complex $[Fe_2K(\mathbf{82c})_3]^+$ either a (Δ,Δ)-fac or (Λ,Λ)-fac {2}-iron cryptate occurs. Also in $[Fe_2K(\mathbf{82d})_3][Fe(Cl)_4]$ the cation is a *racemic* mixture of the helical (Δ,Δ)-fac or (Λ,Λ)-fac {2}-iron cryptates. In $[Fe_2Ba(\mathbf{82b})_3]^{2+}$ the barium ion is 11 coordinated by six oxygen and three nitrogen atoms of the three ligands and two additional tetrahydrofuran molecules, situated between each of the two ligand strands. $[Fe_2Ba(\mathbf{82b})_3]^{2+}$ is helical with either (Δ,Δ)-fac or (Λ,Λ)-fac coordinated iron centers, comparable to $[Fe_2La(\mathbf{82b})_3]^{3+}$ [216].

0.75 equiv. of H_2–**82b**···H_2–**82d** and 1 equiv. of the related metal(II) dichloride form the bis(triple-helical) complexes $[M_8(\mathbf{L})_6(O)_3]$ ($M = Mn^{II}$, Co^{II}, Cd^{II}) with a core of eight octahedral metal(II) ions, forming a twofold capped, slightly twisted trigonal prism with a μ_3-O^{2-} ion centered in each of the two inner faces. All the six $[\mathbf{L}]^{2-}$ ligands link to three metal(II) ions. The two antipodal metal(II) ions are coordinated by three μ_1- and three μ_2-oxygen chelate atoms of three ligands. However, the six metal centres, constituting the trigonal prism, are coordinated by one pyridylene nitrogen and two μ_2-chelate oxygen atoms. Two extra μ_3-O^{2-} ions complete the coordination of the metal(II) ions (Fig. 92) [216].

The one-pot reaction of H_2–**82a**, $Cu(NO_3)_2\cdot 3H_2O$, $Ln(NO_3)_3\cdot 6H_2O$ and $N(C_2H_5)_3$ gives rise to $[Cu_2Ln(\mathbf{82a})_2(NO_3)_3]$ (Ln = Y, La-Lu), where two $[\mathbf{82a}]^{2-}$ ligands sandwich two copper(II) ions via the 1,3-diketonate sites and one lanthanide(III) ion via the 2,6-diacetylpyridine site. Each five coordinate square pyramidal copper(II) ion has a water, methanol or dimethylformamide molecule at the axial site while the O_2O_2 equatorial coordination is formed by the four oxygen atoms of two diketonate moieties of two different $[\mathbf{82a}]^{2-}$ ligands and the 10 or 12 coordinate lanthanide(III) ion has an equatorial O_4N_2 hexagonal site formed by four oxygen and two nitrogen atoms of two diacetylpyridine entities and two or three nitrate ions bonded above and below the equatorial plane [217,218].

The structures of these complexes have been classified into three types (A, B, and C) with respect to the geometry about the central lanthanide(III) ion: in type A the three nitrate ions are bonded to the lanthanide ion; the type B (further subdivided in B1, B2 and B3) has two coordinate nitrate ions above and below the lanthanide ion; in the type C one dimethylformamide molecule is bonded to the lanthanide(III) ion along with two nitrate ions. The type A and B complexes were obtained by slow crystallization from methanol,

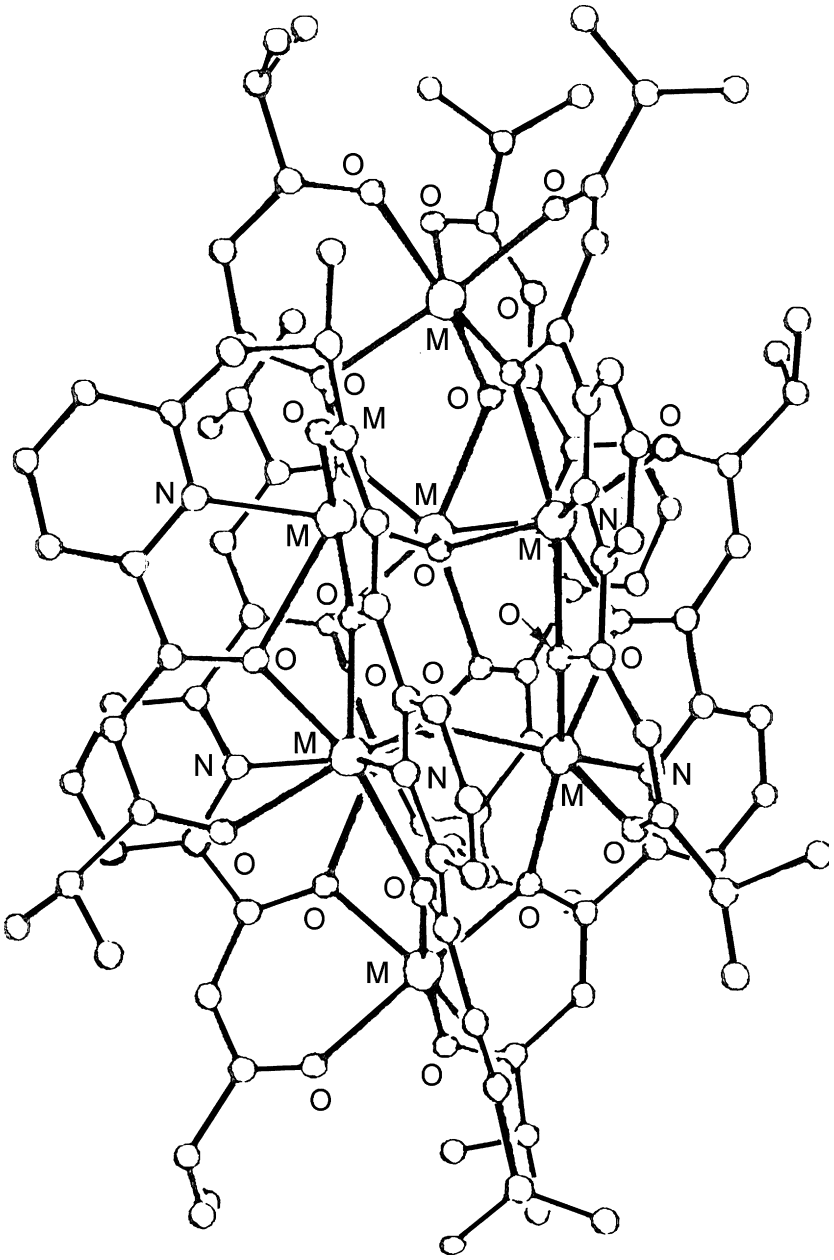

Fig. 92. Structures of $[M_8(\mathbf{82b})_6(O)_3]$ ($M = Mn^{II}$, Co^{II}, Cd^{II}) [216].

whereas the type C complexes were obtained by crystallization from dimethylformamide [217,218].

The type A structure, found only in $[Cu_2La(\mathbf{82a})_2(NO_3)_3(CH_3OH)_2]\cdot CH_3OH$ (Fig. 93), consists of 2 equiv. copper(II) ions with the methanol molecules on the same side with respect to the equatorial plane and a 12 coordinate lanthanum(III) ion axially bonded by three bidentate nitrate groups: two on one side and one on the other side with respect to the equatorial plane. The two $[\mathbf{82a}]^{2-}$ ligands of the $\{Cu_2La(\mathbf{82a})_2\}$ moiety are twisted at the lanthanide ion. The Cu···La and Cu···Cu separations of the trinuclear core are 3.648 and 7.153 Å, respectively. The shortest Cu···Cu, Cu···La, and La···La intermolecular separations are 7.152, 8.577, and 9.393 Å, respectively [217,218].

$[Cu_2Lu(\mathbf{82a})_2(NO_3)_2(CH_3OH)(H_2O)](NO_3)\cdot CH_3OH$ (Fig. 94) is an example of the B1 type: the two non-equivalent copper(II) ions have an axial methanol or water molecule, respectively, in opposite position with respect to the equatorial plane. The 10 coordinate lutetium(III) ion has two axial bidentate nitrate on opposite sides with respect to the equatorial coordination plane. Within the non coplanar trinuclear $\{Cu_2Ln(\mathbf{82a})_2\}$ moiety the intermetallic Cu···Lu distances are 3.625 and 3.629 Å, while the Cu···Cu separation is 7.252 Å. The shortest Cu···Cu, Cu···Lu, and Lu···Lu intermolecular separations are 7.168, 6.9621, and 7.305 Å, respectively [217,218].

The type B2 structure, observed in $[Cu_2Nd(\mathbf{82a})_2(NO_3)_2(CH_3OH)_2](NO_3)\cdot 3CH_3OH$ (Fig. 95), is essentially the same as that of the Cu_2Lu analogue. One methanol molecule coordinates each equivalent copper(II) ion and the Cu···Nd and Cu···Cu separations in the two molecules present in the unit cell are 3.650 and 7.301, 3.641 and 7.282 Å, respectively. The trinuclear $\{Cu_2Nd(\mathbf{82a})_2\}$ moiety is coplanar with respect to the two $[\mathbf{82a}]^{2-}$ ligands. The shortest Cu···Cu, Cu···Nd, and Nd···Nd intermolecular separations are 7.323, 7.177, and 7.341 Å, respectively [217,218].

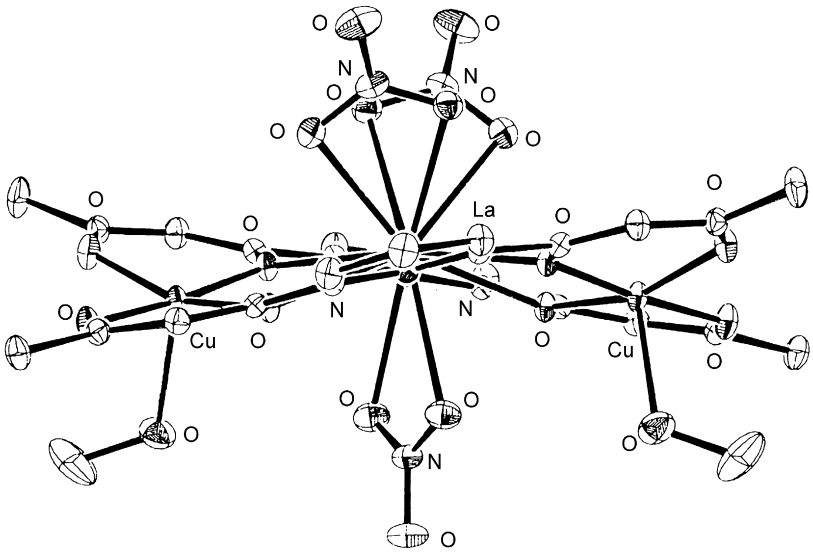

Fig. 93. The type A structure of $[Cu_2La(\mathbf{82a})_2(NO_3)_3(CH_3OH)_2]$ [217].

The Cu_2Gd and Cu_2Ho complexes (Fig. 96) have the B3 type structure. In $[Cu_2Gd(\mathbf{82a})_2(NO_3)_2(CH_3OH)_2](NO_3)\cdot CH_3OH$ one methanol molecule fills the axial site of each copper(II) ion while the 10 coordinate gadolinium(III) ion, located at an inversion center, has two bidentate nitrate ions. The trinuclear core forms a planar structure with intermetallic Cu···Gd and Cu···Cu separations of 3.469 and 7.298 Å, respectively [217,218]. In the similar complex $[Cu_2Ho(\mathbf{82a})_2(NO_3)_2(CH_3OH)(H_2O)](NO_3)\cdot CH_3OH$ each copper(II) ion has a methanol or water molecule at the apical position while the coordination about the holmium(III) ion parallels that of the gadolinium(III). The intermetallic Cu···Ho and Cu···Cu separations are 3.637 and 7.273 Å, respectively. The shortest Cu···Cu, Cu···Ho and Ho···Ho intermolecular separations are 7.520, 7.2283 and 7.5524 Å, respectively [217].

The Cu_2La, Cu_2Nd, Cu_2Sm, Cu_2Cu and Cu_2Gd complexes, obtained by crystallization of $[Cu_2Ln(\mathbf{82a})_2(NO_3)_3(CH_3OH)_2]$, $[Cu_2Ln(\mathbf{82a})_2(NO_3)_3(CH_3OH)_2]\ (NO_3)$, (Ln = Nd, Sm, Gd), and $[Cu_2Eu(\mathbf{82a})_2(NO_3)_2](NO_3)$, from dimethylformamide, show the type C structure of $[Cu_2Sm(\mathbf{82a})_2(NO_3)_3(DMF)_2]\cdot DMF.0.5(C_2H_5)_2O$ (Fig. 97), where the copper(II) ions have a dimethylformamide oxygen or an oxygen of a monodentate nitrate group at the apical position, respectively. The 10 coordinate samarium(III) ion is surrounded by one bidentate nitrate ion and one monodentate nitrate ion, located on the same side with respect to the equatorial plane, and one dimethylformamide molecule. The intermetallic Cu···Sm, Cu···Sm, and Cu···Cu separations are 3.616, 3.685, and 7.254 Å, respectively. The shortest Cu···Cu, Cu···Sm and Sm···Sm intermolecular separations are 7.410, 8.437 and 8.848 Å, respectively [217].

The similar one pot reaction of equimolar amounts of H_2–**82a**, $Ni(NO_3)_2{\cdot}6H_2O$ and $Ln(NO_3)_3{\cdot}nH_2O$ in methanol containing $N(C_2H_5)_3$ affords different crystalline types (A–D) of $[Ni_2Ln(\mathbf{82a})_2(NO_3)_2(H_2O)_4]$, with two $[\mathbf{82a}]^{2-}$ ligands sandwiching two six coordinate nickel(II) ions by the terminal 1,3-diketonate

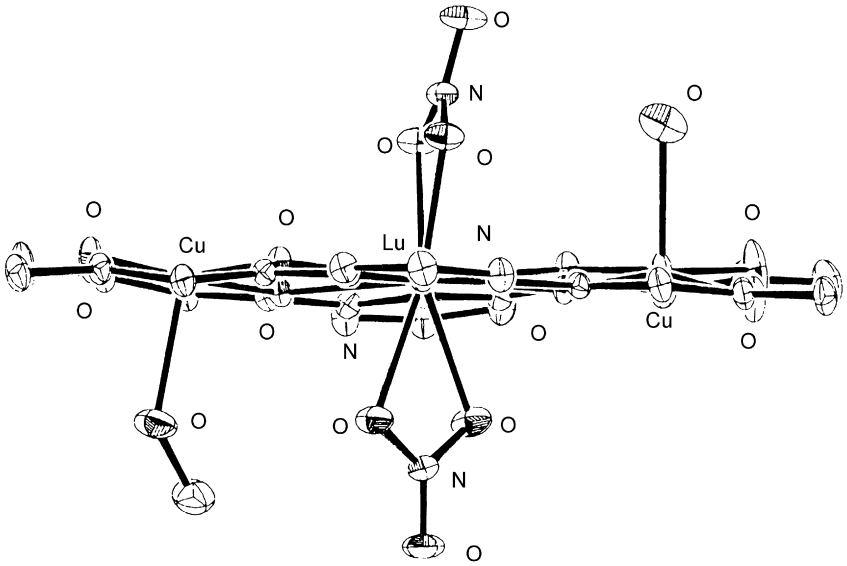

Fig. 94. The type B1 structure of $[Cu_2Lu(\mathbf{82a})_2(NO_3)_3(CH_3OH)(H_2O)]^+$ [217].

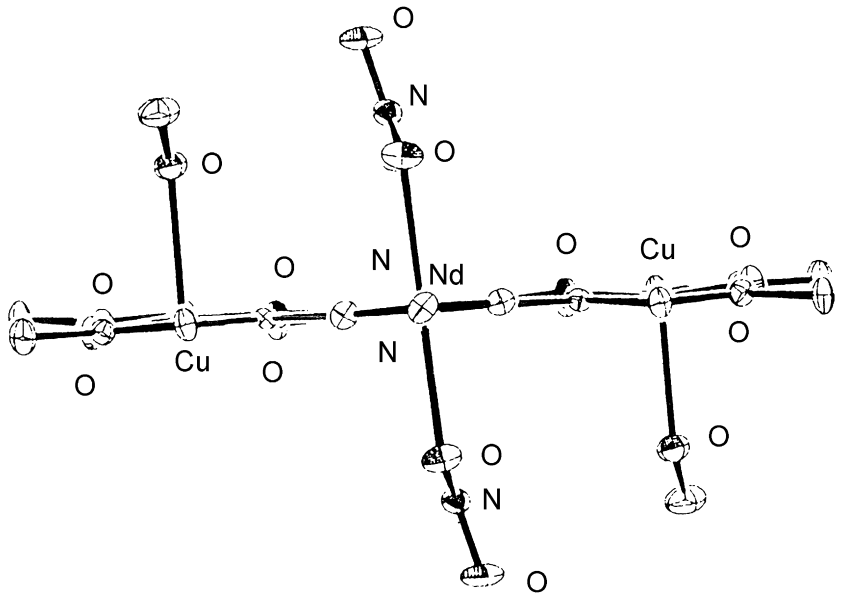

Fig. 95. The type B2 structure of $[Cu_2Nd(\mathbf{82a})_2(NO_3)_2(CH_3OH)_2]^+$ [217].

sites and one 10 coordinate lanthanide(III) ion by the central 2,6-diacylpyridine site to afford a $\{Ni_2Ln(\mathbf{82a})_2\}$ core of a linear NiLnNi structure [218].

In the type A $[Ni_2Ln(\mathbf{82a})_2(NO_3)_2(CH_3OH)_4](NO_3)\cdot CH_3OH$ (Ln = La, Ce, Pr, Nd, Sm, Eu, Gd), the $\{Ni_2Ln(\mathbf{82a})_2\}$ core affords a N_2O_4 hexagonal base for the lanthanide(III) ion together with two bidentate nitrate groups above and below this base and an O_4 tetragonal base for the nickel(II) ion each with two methanol molecules at the axial sites. In the Ni_2Gd complex the Ni···Gd and Ni···Ni separations are 3.692 and 7.383 Å, respectively. The other Ni···Ln and Ni···Ni distances are comparable (Fig. 98) [218].

In the type B $[Ni_2Ln(\mathbf{82a})_2(NO_3)_2(H_2O)_2(CH_3OH)_2](NO_3)2H_2O\cdot CH_3OH$ (Ln = Sm, Eu, Gd), the two non-equivalent nickel(II) ions have one water and one methanol molecule at the axial sites, *cis* with respect to the basal plane. The Ni···La distances are shorter than those occurring in the type A (Fig. 99) [218].

In the type C $[Ni_2Ln(\mathbf{82a})_2(NO_3)_3(CH_3OH)_4]$ (Ln = Gd, Tb, Dy) the 2 equiv. nickel(II) centres have two methanol molecules at the axial sites while the lanthanide(III) ion has two unidentate and one bidentate nitrate groups (Fig. 100) [218].

In the type D $[Ni_2Ln(\mathbf{82a})_2(NO_3)_2(H_2O)(CH_3OH)_3](NO_3)\cdot(C_2H_5)_2O\cdot CH_3OH$ (Ln = Ho–Lu), two bidentate nitrate groups link to the lanthanide(III) ion while the apical position of the two non-equivalent nickel(II) ions are filled by two methanol molecules or one water and one methanol molecule, respectively (Fig. 101) [218].

Obviously the size of the lanthanide(III) ion is a dominant factor determining the trinuclear core structure. Large La^{III}–Nd^{III} ions (ionic radius 1.06–0.99 Å) preferentially afford type A, and subsequent Sm^{III}–Gd^{III} ions (0.96–0.94 Å) afford both type A and type B. Type C is produced with Gd^{III}–Dy^{III} ions of medium size (0.94–0.91 Å), and type D is produced with small Ho^{III}–Lu^{III} ions (0.89–0.85 Å). The $\{Ni_2Ln(\mathbf{82a})_2\}$ core is essentially coplanar in

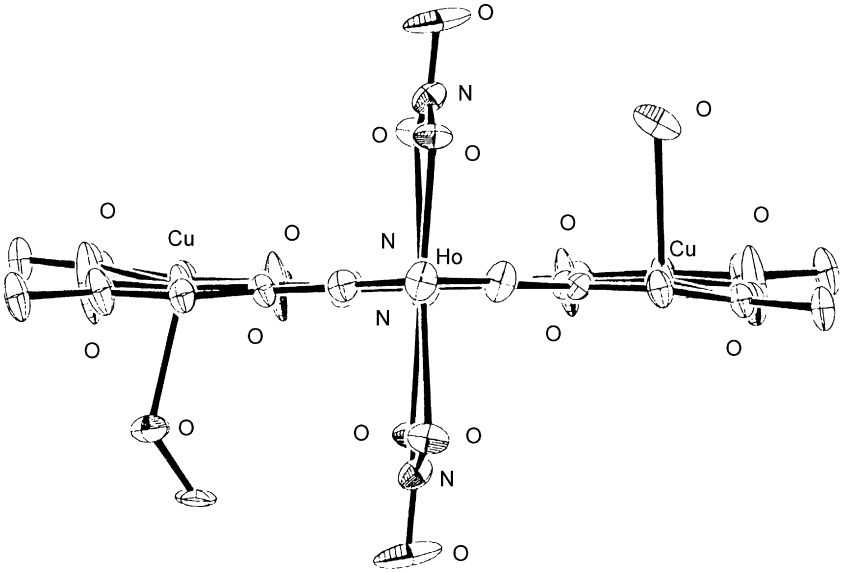

Fig. 96. The type B3 structure of $[Cu_2Ho(\mathbf{82a})_2(NO_3)_2(CH_3OH)(H_2O)]^+$ [217].

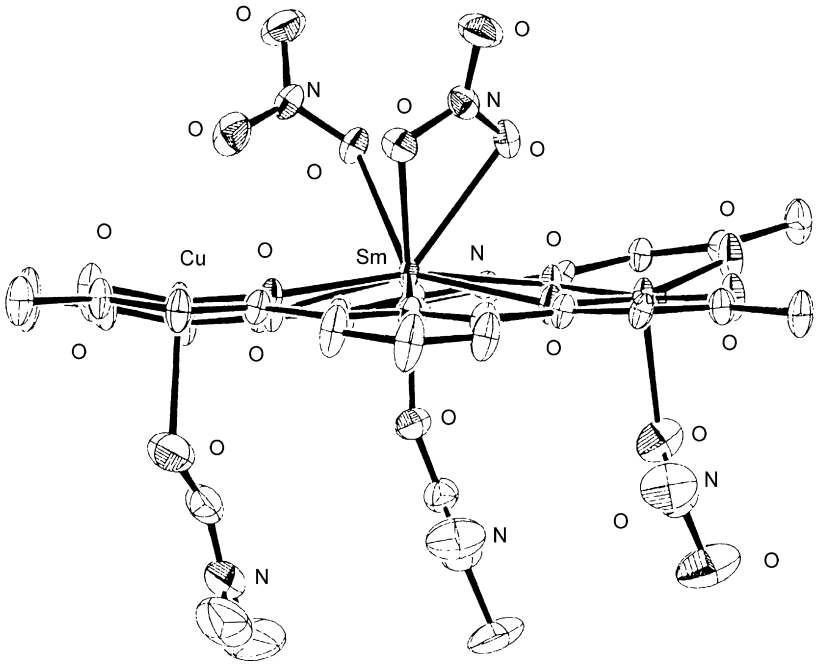

Fig. 97. The type C structure of $[Cu_2Sm(\mathbf{82a})_2(NO_3)_3(DMF)_2]$ [217].

type A, whereas it shows a distortion in types B, C and D in the increasing order B < C < D. This distortion is the necessary result when the central N_2O_4 cavity accommodates a small lanthanide(III) ion while maintaining the terminal nickel geometry with ordinary bond distances. The terminal nickel(II) ions keep their geometries while allowing an optimal coordination environment for the central lanthanide(III) ion. A comparison of the structures of the Ni_2Ln complexes with those of the analogous Cu_2Ln complexes shows that in the latter ones the $\{Cu^{II}$ bis(1,3-diketonato)$\}$ moiety prefers a planar geometry irrespective of the kind of lanthanide(III) ion [218].

The cryomagnetic properties of the Cu_2Ln trinuclear complexes, in the temperature range of 2–300 K under an applied field of 500 G, were analyzed also in comparison with the Cu_2La, Cu_2Ln, and Cu_2Y complexes with a diamagnetic lanthanide(III) or yttrium(III) ion or with the Zn_2Ln analogues, neglecting the magnetic interaction between adjacent trinuclear units because of significant metal–metal separations (>7.1 A). The Cu_2La, Cu_2Lu and Cu_2Y complexes show a weak antiferromagnetic coupling ($J = -0.51$, -0.39 and $-0.47\ cm^{-1}$ respectively), supported also by studies on the field dependence on magnetization for these complexes. The magnetic moment of the Cu_2Gd complex (8.30 μB) very close to the spin-only value (8.30 μ_B) increases with decreasing temperature up to 9.74 μ_B at 3 K: ferromagnetic interaction ($J = +1.4\ cm^{-1}$) was found between the copper(II) and gadolinium(III) ions corroborated also by the field dependence of the magnetization while the negative ϑ-value (−0.11 K) means an antiferromagnetic interaction between the two terminal copper(II) ions. The temperature variation of the magnetic moment and the field dependence of the magnetization suggest an antiferromagnetic interaction between the copper(II)

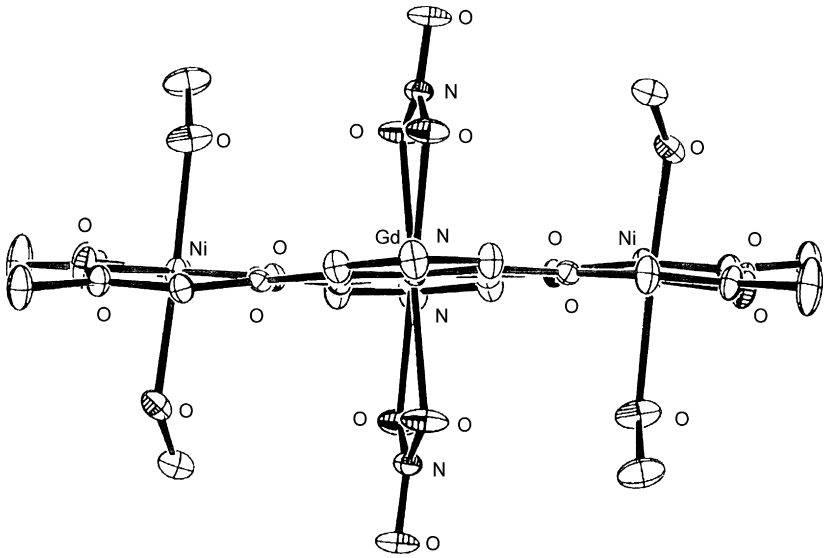

Fig. 98. The type A structure of $[Ni_2Gd(\mathbf{82a})_2(NO_3)_2(CH_3OH)_4]^+$ [218].

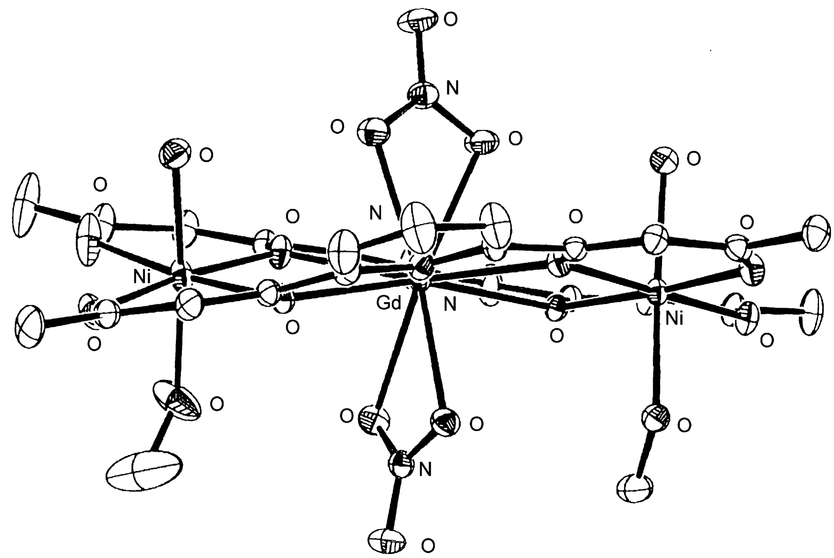

Fig. 99. The type B structure of $[Ni_2Gd(\mathbf{82a})_2(NO_3)_2(H_2O)_2(CH_3OH)_2]^+$ [218].

and lanthanide(III) ions for Cu_2Ce, Cu_2Pr, Cu_2Nd, and Cu_2Sm and a ferromagnetic one for Cu_2Tb, Cu_2Dy, Cu_2Ho and Cu_2Er [217].

Magnetic studies for the Ni_2La and Ni_2Lu complexes indicate an antiferromagnetic interaction between the terminal nickel(II) ions. A magnetic analysis of the Ni_2Gd complex indicates a ferromagnetic interaction between the adjacent nickel(II) and gadolinium(III) ions and an antiferromagnetic interaction between the terminal nickel(II) ions. For the other Ni_2Ln complexes, the Ni^{II}–Ln^{III} interaction is weakly antiferromagnetic for Ln = Ce, Pr, and Nd and ferromagnetic for Ln = Gd, Tb, Dy, Ho and Er [218].

H–**82b**, CaH_2 and $Cu(CH_3COO)_2$ in methanol afford $[Cu_2Ca(\mathbf{82b})_2(CH_3COO)_2(CH_3OH)_2]$, where the calcium(II) ion is encapsulated at the center of the $\{Cu_2(\mathbf{82b})_2\}$ moiety coordinated by two acetate anions. The two crystallographically equivalent copper(II) ions are tetragonal pyramidal, each with two pairs of oxygen donors and one molecule of methanol. In contrast, H_2–**82b**, copper(II) acetate and cesium carbonate in methanol form the one-dimensional polymer $\{[Cu_8Cs_6(\mathbf{82b})_8(CH_3COO)_4](CH_3COO)_2\}_n$ whose individual modules contain two concave $\{Cu_2(\mathbf{82b})_2\}$ metallacoronands linked by two bidentate acetate ions, resulting in a tetragonal pyramidal coordination of the four copper ions. Endohedral encapsulation of two cesium ions and two molecules of ethanol into the thus formed container $\{Cu_4(\mathbf{82b})_4(CH_3COO)_2\}$ then gives the cryptate $[Cu_4Cs_2(\mathbf{82b})_4(CH_3COO)_2(C_2H_5OH)_2]$. Exohedral coordination of a further cesium ion to the cryptate generates the self-complementary unit $\{Cu_4Cs_3(\mathbf{82b})_4(CH_3COO)_2(C_2H_5OH)_2\}^+$. Linkage of these building blocks alternately rotated by 90° finally affords the dicationic monomer $[Cu_8Cs_6(\mathbf{82b})_8(CH_3COO)_4(C_2H_5OH)_2]^{2+}$ of the one-dimensional coordination polymer. An interesting feature of this polymeric complex is the formal encapsulation of a cesium acetate dimer between the two concave $\{Cu_2(\mathbf{82b})_2\}$ metallacoronands with a very short Cs···Cs distance of 3.75 Å (Fig. 102) [219].

The isomorphous complexes $\{[Co_2Ln(\mathbf{82a})_2(H_2O)_4][Cr(CN)_6]\}\cdot nH_2O$ (La, $n = 3$; Gd, $n = 4$), derived from $[Co_2Ln(\mathbf{82a})_2(NO_3)_3]\cdot 4H_2O$ ($Ln = La^{III}$, Gd^{III}) and $K_3[Cr(CN)_6]$ in water, show a trinuclear $\{Co_2Ln(\mathbf{82a})_2(H_2O)_4\}^{3+}$ unit with a linear CoLnCo core, held by four enolate bridges between two $[\mathbf{82a}]^{2-}$ ligands. Each elon-

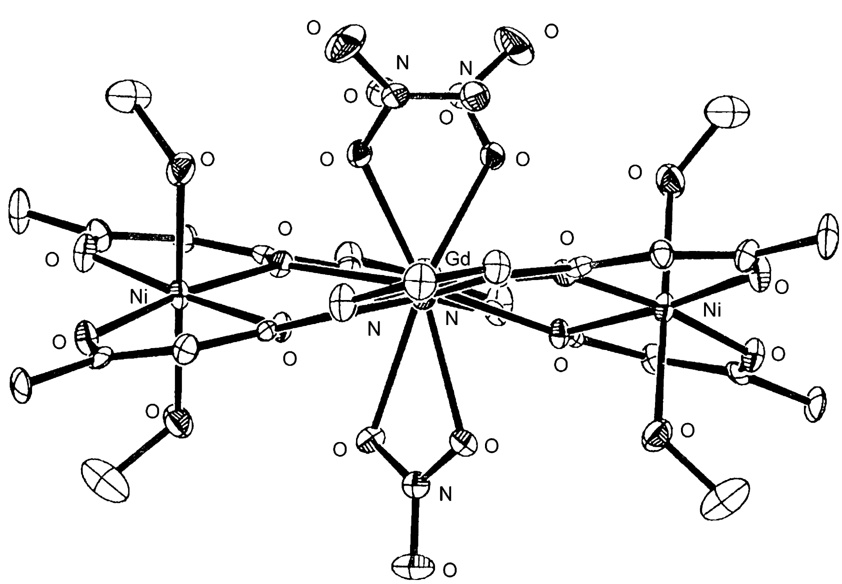

Fig. 100. The type C structure of $[Ni_2Gd(\mathbf{82a})_2(NO_3)_3(CH_3OH)_4]$ [218].

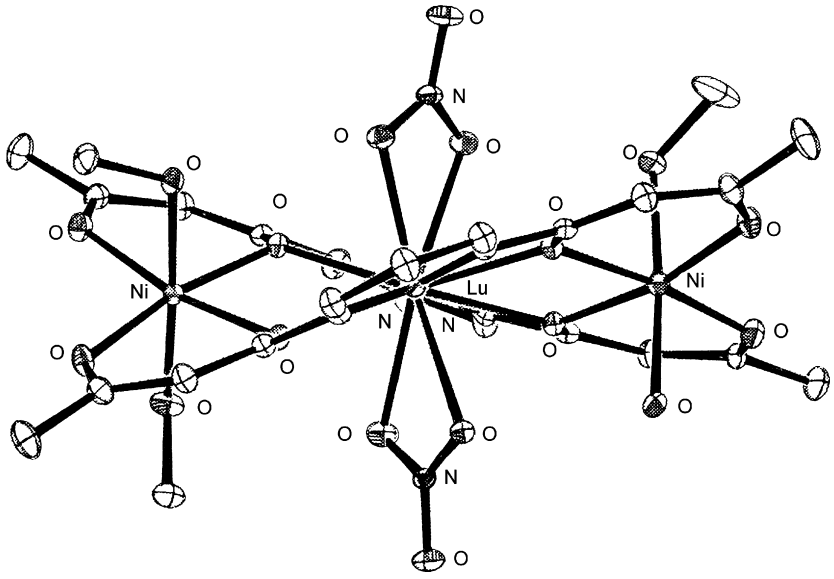

Fig. 101. The type D structure of $[Ni_2Lu(\mathbf{82a})_2(NO_3)_2(H_2O)(CH_3OH)_3]^+$ [218].

gated octahedral cobalt(II) ion is located at the β-diketone sites of $[\mathbf{82a}]^{2-}$ with two axial cyano nitrogen atoms. The 10 coordinate lanthanide(III) ion in the 2,6-diacetylpyridine site has four water molecules above and below the $\{Co_2Ln(\mathbf{82a})_2\}$ plane. Four equatorial cyano groups of $[Cr(CN)_6]^{3-}$ coordinate to adjacent cobalt(II) ions to form a 2D grid layer extended by Cr–CN–Co linkages. The $\{Co_2Ln(\mathbf{82a})_2\}$ moiety is not planar and the two ligands show a significant twist with respect to the central lanthanide(III) ion. Also the two $\{CoO_4\}$ planes in the trinuclear unit are not coplanar (Fig. 103). Magnetic susceptibility measurements indicate an onset tridimensional ferromagnetic ordering [220].

13.3. Complexes with a polyether spacer

H_2–**83a** and H_2–**84b**, bearing two β-diketones at both terminals of a polyethylene glycol framework, form [M(**L**)] (M = Cu^{II}, Zn^{II}) with the metal ion coordinated by two β-ketoenolate groups. These complexes have been used for the extraction of alkali metal picrates from water into chloroform [Cu(**83a**)] and [Cu(**83b**)] are selective in the extraction of the sodium and the potassium ion, respectively, exhibiting selectivity for ionic diameters based on cavity size. In these complexes contributions from two anionic oxygen atoms each from two β-ketoenolate units and three or four neutral oxygen atoms in the polyether linkage afford the most appropriate and selective binding site to these alkali metal ions. The partition coefficients of Na^+ and K^+ picrates were negligibly small when H_2–**83a** and H_2–**83b** were used in their free or K^+ salt forms [221].

H_2–**83c**, copper(II) acetate and a large excess of the desired alkali metal acetate in methanol give $[Cu_2M(\mathbf{83c})_2(CH_3COO)]\cdot 2CH_3OH$ (M = K^I, Rb^I, Cs^I). In the potassium complex the two square pyramidal copper(II) centres are linked to four oxygen atoms of the $[\mathbf{83c}]^{2-}$ ligands and to the oxygen of a methanol molecule, affording a [22]-metallacrown-[8]-system wrapped around the central potassium ion which is coordinated by four carbonyl oxygen and four ethyleneglycol oxygen donors. Coordination of an acetate group completes the coordination about the potassium ion. Thus, this complex can be described as a double-stranded helicate encapsulating a potassium ion (Fig. 104) [222].

A methanol solution of H_2–**84a** and nickel(II) acetate in the presence of a large excess of template cesium acetate separates $\{Cs[Ni_2Cs(\mathbf{84a})_3]\}$ with a $[Ni_2(\mathbf{84a})_3]^{2-}$ core composed of two O_6 octahedral nickel(II) centres linked by three $[\mathbf{84a}]^{2-}$ dianions. The resulting {2}-metallacryptands are homochiral with either (Δ,Δ)-fac or (Λ,Λ)-fac configuration at the nickel centres. They hold a cesium ion in the void, coordinated by six carbonyl oxygen and six catecholate oxygen donors. Charge compensation of the {2}-metallacryptates $[Ni_2Cs(\mathbf{84a})_3]^-$ is achieved through external cesium ions to give $Cs[(\Delta,\Delta)/(\Lambda,\Lambda)Ni_2Cs(\mathbf{84a})_3]$ which self-aggregate alternating across the external cesium ions to give the one-dimensional *meso*-$\{Cs[Ni_2Cs(\mathbf{84a})_3]\}\cdot 2CH_3OH]_n$, where the external cesium ions are coordinated to two sets of three peripheral carbonyl oxygen donors and two methanol molecules (Fig. 105) [222].

The one-dimensional polymer rac-$\{Cs[Mg_2Cs(\mathbf{84a})_3]\}_n$, originating from H_2–**84a**, $Mg(CH_3COO)_2$ and $Cs(CH_3COO)$, contains two octahedral magnesium(II) ions are linked through three $[\mathbf{84a}]^{2-}$ ligands by six diketo oxygen donors. The resulting {2}-metallacryptands are homochiral with either (Δ,Δ)-fac or (Λ,Λ)-fac stereochemistry at the magnesium centres and capable to host a cesium ion in the cavity, which is coordinated by six carbonyl and six catecholate oxygen donors each. Charge compensation of the thus formed enantiomers $[(\Delta,\Delta)/(\Lambda,\Lambda)Mg_2Cs(\mathbf{84a})_3]^-$ is achieved through external cesium ions which aggregate to give $\{Cs[(\Delta,\Delta)\text{-}Mg_2Cs(\mathbf{84a})_3]\}_n$ and $\{Cs[(\Lambda,\Lambda)\text{-}Mg_2Cs(\mathbf{84a})_3]\}_n$, packed in the crystals in alternating homochiral layers (Scheme 13). In $\{Cs[(\Delta,\Delta)\text{-}Mg_2Cs(\mathbf{84a})_3]\}_n$, the coupling external cesium ions are coordinated by two sets of three peripheral carbonyl oxygen donors and two acetonitrile molecules (Fig. 106) [223].

The bulkier H_2–**84b**,cesium or rubidium acetate and magnesium, cobalt or zinc acetate in a 3.2:1 ratio yield the meandering polymer *meso*-$\{[(\Delta,\Delta)\text{-}M^2{}_2M^1(\mathbf{84b})_3]M_{end}{}^1)(\{[(\Lambda,\Lambda)\text{-}M^{II}{}_2M^I(\mathbf{84b})_3]\}M_{side}{}^1)][([(\Lambda,\Lambda)\text{-}M^{II}{}_2M^I(\mathbf{84b})_3]\}M_{end}{}^1)(\{[(\Delta,\Delta)\text{-}M^{II}{}_2M^1(\mathbf{84b})_3]M_{side}{}^1)\}]_n$ (M^I = Cs^I, Rb^I; M^{II} = Mg^{II}, Co^{II}, Zn^{II}), where the {2}-metallacryptates $\{[(\Delta,\Delta/\Lambda,\Lambda)\text{-}M^2{}_2\ M^1(\mathbf{84b})_3]\}^-$ are linked by only one cesium ion end-on to give the fragments *meso*-$\{[(\Delta,\Delta)\text{-}M^{II}{}_2M^I(\mathbf{84b})_3]M_{end}{}^I)([(\Lambda,\Lambda)\text{-}M^{II}{}_2M^I(\mathbf{84b})_3]M_{side}{}^I\}$, which are connected by the second cesium ions side-on (Scheme 14) [223]. On the contrary, zinc(II) acetate, cesium or rubidium acetate and H_2–**84b** in a 4:2:1 molar ratio afford $[Zn_2M(\mathbf{84b})_2(CH_3COO)]$ (M = Cs^I, Rb^I). In the Zn_2Cs complex two $[\mathbf{84b}]^{2-}$ ligands together with an encapsulated cesium ion

create a {2}-metallacoronate, folded by an acetate bridge. In the heteroleptic cryptate, one acetate oxygen atom functions as a μ_1-donor to one zinc ion and the other as a μ_2-donor to the other zinc ion and to the cesium ion. The cesium ion at one side is coordinatively unsaturated and, therefore, two molecules of [Zn_2Cs(**84b**)$_2$(CH_3COO)] form a dimer, due to cation–π interaction of neighbouring phenyl groups (Fig. 107) [223].

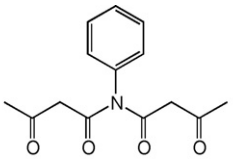

H_2-**81**

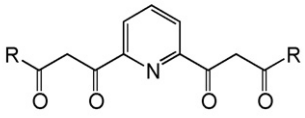

	R
H_2-**82a**	CH_3
H_2-**82b**	$C(CH_3)_3$
H_2-**82c**	C_4H_3S
H_2-**82d**	$C_{10}H_8$

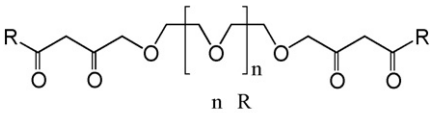

	n	R
H_2-**83a**	1	CH_3
H_2-**83b**	2	CH_3
H_2-**83c**	1	C_6H_5
H_2-**83d**	0	C_6H_5

Esterification of (2*S*,3*S*)-1,4-dimethoxy-2,3-butanediol, derived from L-tartaric acid, and ethyl bromoacetate in the presence of sodium hydride, affords (2*S*,3*S*)-1,4-dimethoxy(2,3-ethylacetoxy)butane which, by subsequent Claisen condensation with acetophenone and sodium amide, leads to the enantiomerically pure ligand H_2–**85a**. H_2–**85b** is similarly prepared using D-tartaric acid. Reaction of 1 equiv. of H_2–**85a** and copper(II) acetate and 0.5 equiv. of cesium acetate in methanol yields [Cu_2Cs(**85a**)$_2$(CH_3OH)$_2$](CH_3COO) which evolves in the copper cubane (CCCC) [Cu_4(**85a**)$_2$(OCH_3)$_4$]. The same synthetic pathway using H_2–**85b** affords the single enantiomeric cubane (A,A,A,A)-[Cu_4(**85b**)$_2$(OCH_3)$_4$]. [Cu_4(**85a**)$_2$(OCH_3)$_4$] exists as a single enantiomer with a [$Cu_4(\mu_3\text{-}O)_4$] cubane core, consisting of two interpenetrating tetrahedra: one made up of four copper ions and one of four μ_3-OCH_3 ligands. The Cu···Cu separations are 2.98 Å and 3.25 Å. The approximate square pyramidal coordination about each copper(II) ion is reached by two μ_1-O ions from the ligand and three μ_3-OCH_3 donors. Consequently, the two bisbidentate ligands bridge opposite edges of the copper tetrahedron (Fig. 108a). Whereas in other complexes above reported, for instance in [Cu_2Cs(**83c**)$_2$(CH_3OH)$_2$](CH_3COO), the role of the cesium(I) ion in determining the reaction pathway and hence the resulting structures via encapsulation in the coordination moiety is clear, its role in the formation of both the cubane (C,C,C,C)-[Cu_4(**85a**)$_2$(OCH_3)$_4$] and (A,A,A,A)-[Cu_4(**85b**)$_2$(OCH_3)$_4$] enantiomers is not yet clear; however, in the absence of cesium ions only polymeric materials are isolated [224].

The reaction of H_2–**85a** or H_2–**85d** (H_2–**L**) with potassium acetate and copper(II) acetate monohydrate in a 1:2:2 molar ratio results in the formation of (C,C,C,C)-[Cu_4(**L**)$_2$(OCH_3)$_4$], with the same of structure of (C,C,C,C)-[Cu_4(**85a**)$_2$(OCH_3)$_4$]. Unexpectedly, H_2-**85c** reacts with 5 equiv. of potassium acetate and 1 equiv. of copper(II) acetate monohydrate to yield the double-stranded helicate (P)-[Cu_2(**85c**)$_2$], where each copper(II) ion has approximate square planar coordination, formed by the chelating 1,3-diketo units of the ligands. The Cu···Cu distances ($D_{intra} = D_{inter} = 3.55$ Å) are rather short. In the absence of alkali ions, only polymeric material is isolated, insoluble in standard solvents [224].

When H_2–**85a**, lithium hydroxide monohydrate and nickel(II) acetate tetrahydrate react in methanol at room temperature, the heterochiral complex (Δ,Λ)-[Ni_2Li_2(**85a**)$_2$(OCH_3)$_2$(CH_3OH)$_2$] is isolated, where each approximately octahedral nickel(III) ion coordinates to two μ_1-oxygen atoms and two μ_2-oxygen atoms from each ligand and two μ_2-(OCH_3) donors. One nickel(II) ion has Λ- and the other one has Δ-configuration with a Ni···Ni distances of 3.08 Å. However, because of the stereogenic centres of [**85a**]$^{2-}$, the complex is not a mesocate, but rather exists as a single enantiomer with idealized C_2 molecule symmetry. Each halve of the nickel(II) coronate backbone hosts an approximately square pyramidal lithium cation with a Li···Li distance of 6.14 Å, coordinated by two carbonyl μ_2-oxygen donors and two ether μ_2-oxygen donors of one ligand [**85a**]$^{2-}$ and a μ_1-oxygen donor of methanol (Fig. 108b) [224].

Equimolar amounts of H_2–**85a** or H_2–**85d** and palladium(II) acetate in the presence of pyridine afford the helicates (P)-[Pd_2(**L**)$_2$], isostructural with (P)-[Cu_2(**85c**)$_2$]. In the solid-state the helicates self-organize into polymeric superstructures with linear threading of the transition-metal ions, as exemplarily presented for (P)-[Pd_2(**85d**)$_2$]$_\infty$ (Fig. 109). Solution CD measurements

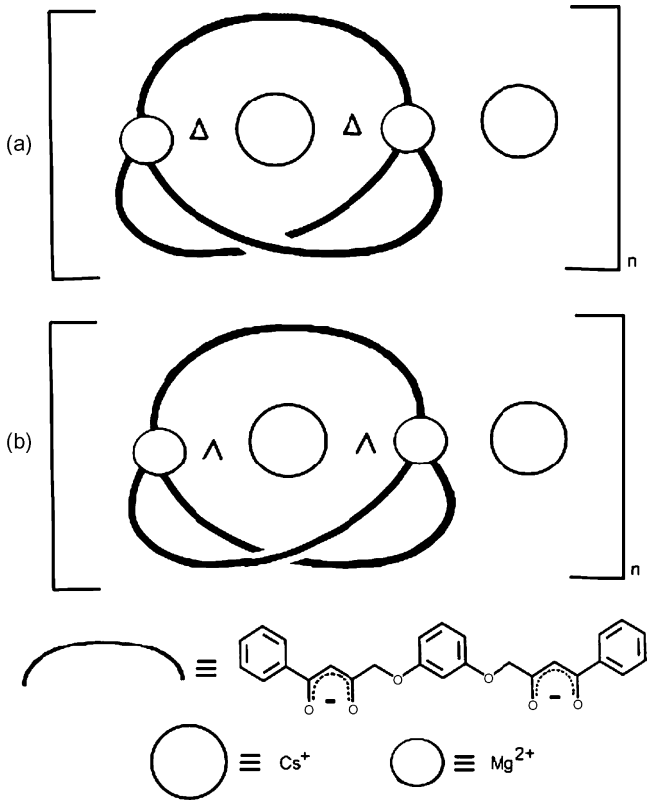

Scheme 13. Schematic representation of {Cs[(Δ,Δ)-Mg_2Cs(**84a**)$_3$]}$_n$ (a) and {Cs[(Λ,Λ)-Mg_2Cs(**84a**)$_3$]}$_n$ (b).

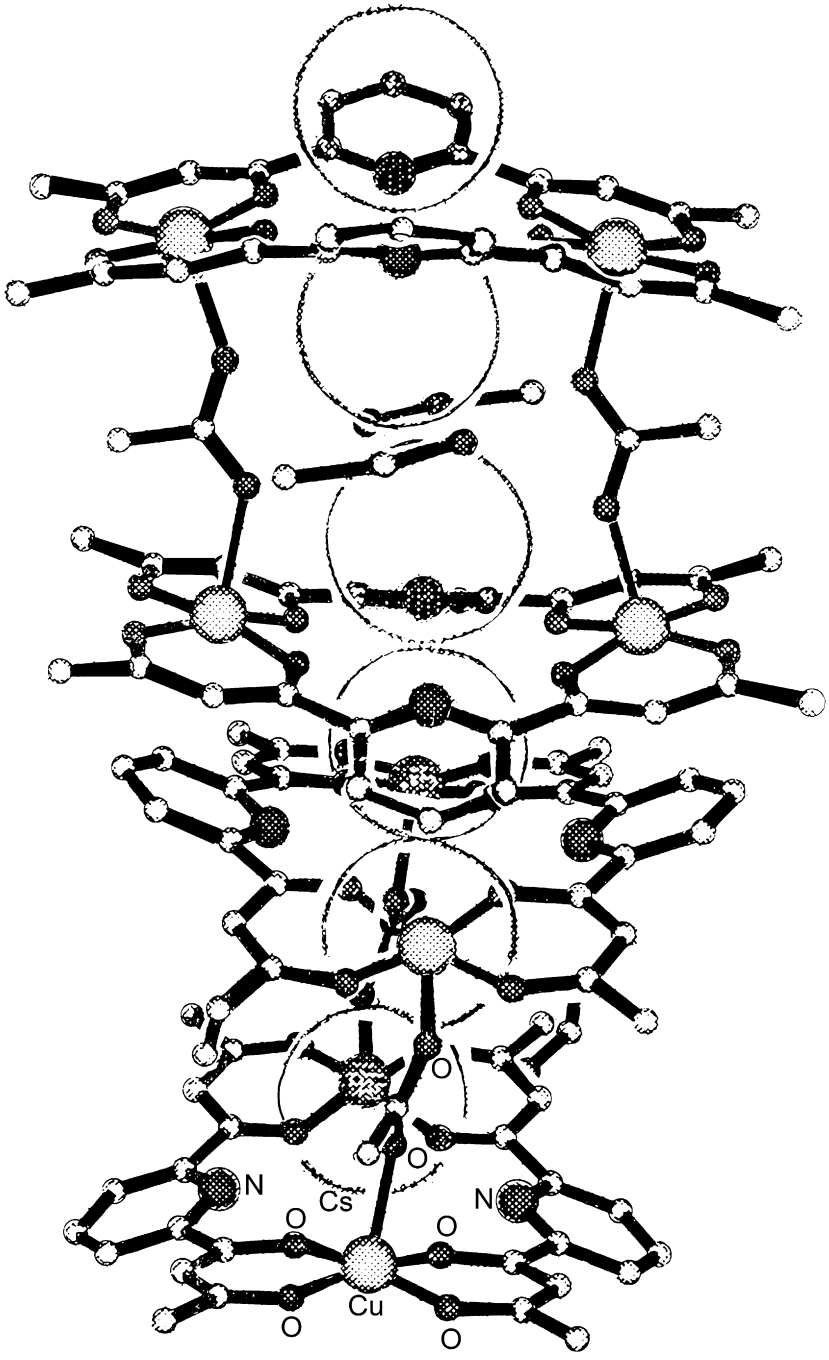

Fig. 102. Structure of $\{[Cu_8Cs_8(\mathbf{82b})_8(CH_3COO)_4(C_2H_5OH)_2]^{2+}\}_n$ [219].

of palladium(II) helicates $[Pd_2(\mathbf{85a})_2]$ and $[Pd_2(\mathbf{85b})_2]$, similarly synthesized from H_2-**85b** in CH_2Cl_2, display a perfect mirror image with an slightly bathochromic-shifted, enhanced absorption at 401 nm, compared to the free ligand at 367 nm, induced by the helicity of complexes (P)-$[Pd_2(\mathbf{85a})_2]$ and (M)-$[Pd_2(\mathbf{85b})_2]$ [224].

14. Hexaketonate complexes

H_3–**86a** and H_3–**86b**, which behaves as tris-(β-diketonate) systems, are formally accessible by the coupling of benzene-1,3,5-tricarboxylic acid trichloride with three monoanions of dialkyl- or diaryl malonate. Treatment of di-*tert*-butyl malonate with methyllithium, iron(II) dichloride and benzene-1,3,5-tricarboxylic acid trichloride at −78 °C in tetrahydrofuran, under aerobic conditions and subsequent thin-layer chromatography, affords $[Fe_4(\mathbf{86a})_4]$ where four O_6 octahedral iron(III) centres, at mean Fe···Fe distance of 8.57 Å are at the apices of a tetrahedron and the four tris-bidentate $[\mathbf{86a}]^{3-}$ ligands are located above the triangular faces of the tetrahedron. Hence, the complex has nearly T-molecular symmetry and the crystal is a *racemic* mixture of homoconfigurational (Δ,Δ,Δ,Δ)-fac and (Λ,Λ,Λ,Λ)-fac stereoisomers (Fig. 110a)

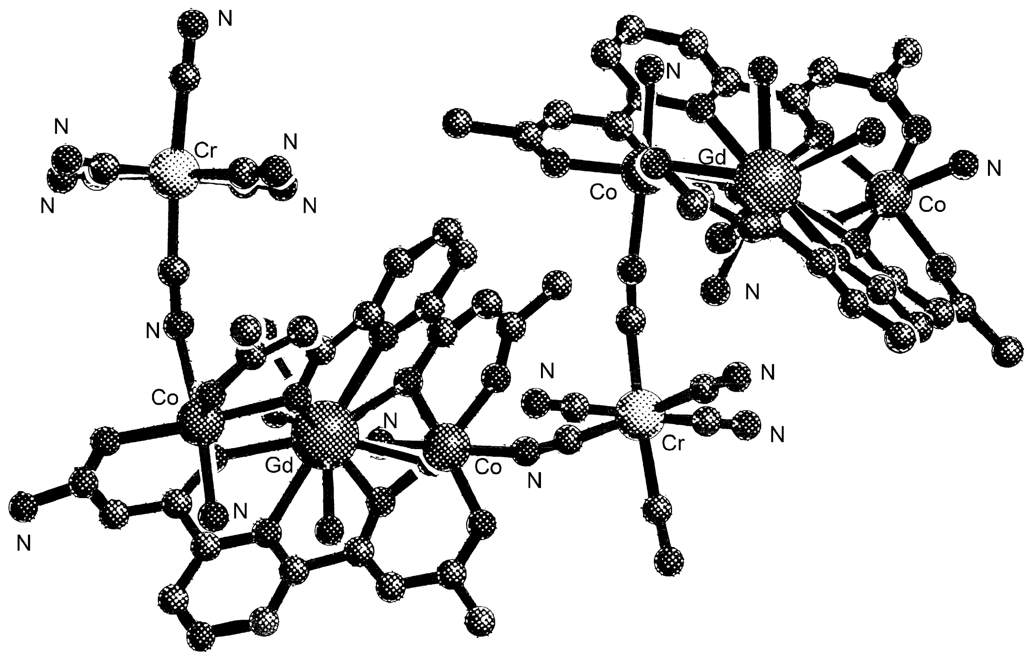

Fig. 103. Structure of $\{[Co_2Gd(\mathbf{82a})_2(H_2O)_4][Cr(CN)_6]\}_n$ [220].

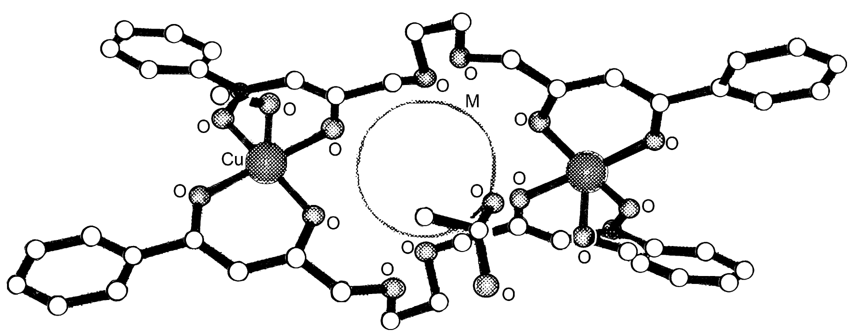

Fig. 104. Structure of $[Cu_2M(\mathbf{83c})_2(CH_3COO)]$ ($M = K^I, Rb^I, Cs^I$) [222].

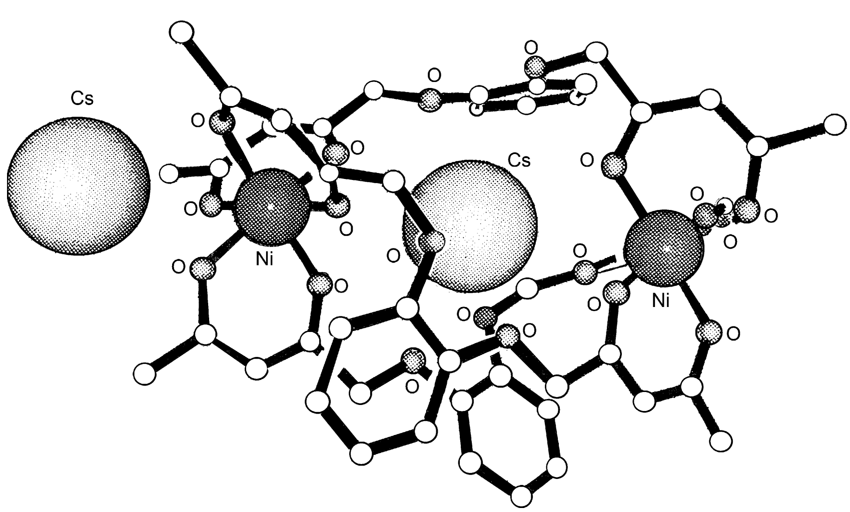

Fig. 105. Structure of $\{Cs[Ni_2Cs(\mathbf{84a})_3]\}$ [222].

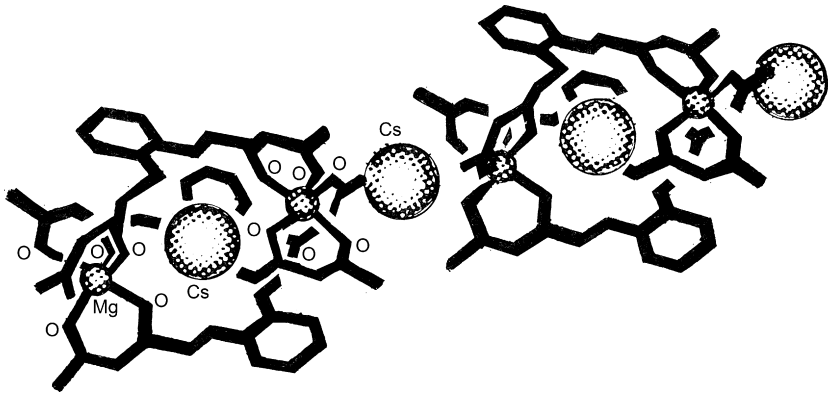

Fig. 106. Structure of $\{Cs[(\Delta,\Delta)\text{-}Mg_2Cs(\mathbf{84a})_3]\}_n$ [223].

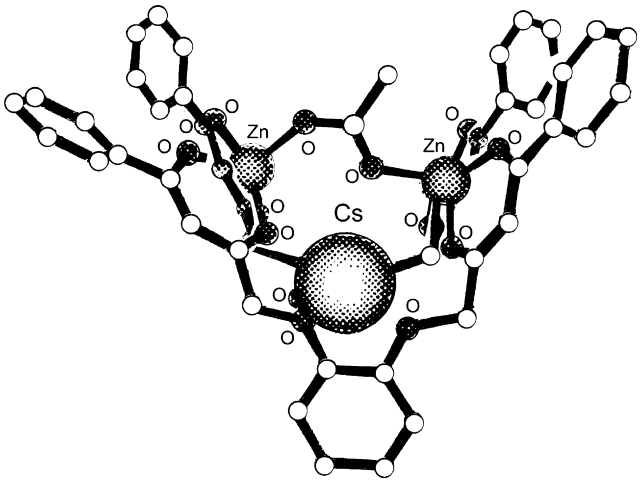

Fig. 107. Structure of $[Zn_2Cs(\mathbf{84b})_2(CH_3COO)]$ [223].

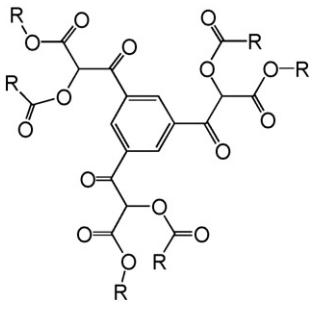

	R
H_3-**86a**	$C(CH_3)_3$
H_3-**86b**	p-$CH_3C_6H_4$

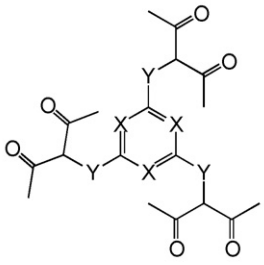

	X	Y
H_3-**86c**	CH	CH_2
H_3-**86d**	N	S

[225].

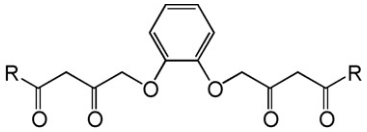

	R
H_2-**84a**	CH_3
H_2-**84b**	C_6H_5

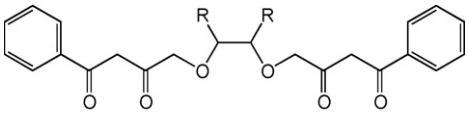

	R
H_2-**85a**	CH_2OCH_3 (S,S)
H_2-**85b**	CH_2OCH_3 (R,R)
H_2-**85c**	C_6H_5 (S,S)
H_2-**85d**	$C_{10}H_7$ (S,S)

On the contrary, *p*-tolylmalonate, methyllithium, iron(II) dichloride and benzene-1,3,5-tricarboxylic acid trichloride at −78 °C in tetrahydrofuran yield $[Fe_6(\mathbf{86b})_6]$, where the iron(III) centres define the apices of a distorted trigonal antiprism in which six tris-bidentate $[\mathbf{86b}]^{3-}$ ligands make up the equatorial faces leaving the top and the bottom triangles unoccupied. The iron(III) centres are identically octahedrally coordinated by six oxygen donors in a compressed antiprismatic arrangement with shorter (8.54 Å) and longer (9.69 Å) Fe···Fe distance. In the crystal $[Fe_6(\mathbf{86b})_6]$ exists as a *racemic* mixture of homoconfigurational $(\Delta,\Delta,\Delta,\Delta,\Delta,\Delta)$-fac and $(\Lambda,\Lambda,\Lambda,\Lambda,\Lambda,\Lambda)$-fac stereoisomers (Fig. 110b) [225].

The tris-β-diketone H_3–**86c** was prepared by reaction of 1,3,5-tris(bromomethylbenzene) with acetylacetone in the presence of $[K\{OC(CH_3)_3\}]$ in tetrahydrofuran. The structure of the similar tris-β-diketone H_3–**86d**, obtained by addition of 3-chloro-2,4-pentandione to an aqueous solution of Na_2CO_3 and trithiocyaminic

acid, indicates that the β-diketonate moieties are in the enol form. ESI-mass spectrometry shows that these ligands self-assemble, when reacted with $Cu(CH_3COO)_2{\cdot}2H_2O$ in pyridine to form $[Cu_3(\mathbf{L})_2]$. H_3–**86d** extracts the copper(II) ion from water into chloroform as $[Cu_3(\mathbf{86a})_2]$ with high efficiency [226].

The condensation of 6-methyl-2,4-heptanedione and dimethylisophtalate in tetrahydrofuran and in presence of NaH affords the bis-β-triketone H_4–**87** which contains a benzene spacer between the two coordinating moieties. In a one pot reaction with the appropriate metal salt it forms $[Cu_4(\mathbf{87})_2(py)_4]{\cdot}2py$ or $[(UO_2)_2(Zn)_2(\mathbf{87})_2(py)_6]$. In the tetracopper(II) complex, the four copper ions are grouped into two sets of two with a Cu···Cu distance of 6.9 Å across the plane of the phenyl groups and an intragroup Cu···Cu distance of 3.021 Å. The coordination sphere of the copper ions is composed of four ketonate oxygen atoms in the distorted tetragonal pyramid; within the molecule, the pyridine residues alternate above and below the plane of the ligand (Fig. 111). Strong magnetic exchange between the copper(II) ions in the binuclear units causes the molecule to be diamagnetic at room temperature. Cyclic voltammetry in pyridine in the range from 0 to −1.2 V yields one quasi reversible wave with $E_{1/2} = -0.8$ V versus SSCE. Chronoamperometric data reveal that this wave is a four-electron transfer process ascribed to two two-electron transfers in non-interacting binuclear centres [227].

15. Poly-β-diketophenolate complexes

The introduction of phenol groups at the periphery of the β-diketonato moieties or between them gives rise to the poly-β-ketophenolates H_2–**88a**···H_4–**94**, which progressively increase or modify their coordination properties and consequently the metal ion assembly and the related physico-chemical properties.

For H_2–**88a**···H_2–**88c**, synthesized by the Wittig reaction of *o*-hydroxyacetophenone with the appropriate alkylacetate in the presence of Na under nitrogen, one keto- and two enol-tautomeric forms can occur; the keto-form however was not observed in the solid state. The coordination properties of these ligands have been already reviewed. In $[Cu_2(\mathbf{L})_2{\cdot}H_2O]$, obtained by reaction of equimolar amounts of H–**L** and copper(II) acetate or synthesized by heating the mononuclear analogues $[Cu(H\text{-}\mathbf{L})_2]$ (H_2–L = H_2–**88a**, H_2–**88b**) which are stable only below 15 °C, strong antiferromagnetic interactions between the two copper(II) ions occur. Also, the complexes $[Ln_2(\mathbf{88c})_2(NO_3)(OH)]{\cdot}nH_2O$ (Ln = La, Eu, Pr; n = 2, 3, 6) have been prepared by reaction of H_2–**88c** with $Ln(NO_3)_3{\cdot}nH_2O$ in the presence of LiOH [9,10,12].

H_2–**88a** or H_2–**88b** and $UO_2(CH_3COO)_2{\cdot}2H_2O$ afford $[UO_2(H\text{-}\mathbf{88a})_2(C_2H_5OH)]$ or $[UO_2(H\text{-}\mathbf{88b})_2(C_2H_5OH)]$, containing a seven coordinate uranium(VI) ion in a pentagonal bipyramidal geometry with the uranyl oxygen atoms occupying the axial positions and four oxygen atoms from two bidentate β-diketophenolate ligands and the one ethanol oxygen forming the equatorial pentagon. The ligands $[H\text{-}\mathbf{88a}]^-$ are in a *trans* arrangement in $[UO_2(H\text{-}\mathbf{88a})_2(C_2H_5OH)]$ while the $[H\text{-}\mathbf{88b}]^-$ ones adopt the *cis* form in $[UO_2(H\text{-}\mathbf{88b})_2(C_2H_5OH)]$. In solution the two complexes have a fluxional behaviour: variable temperature ^1H NMR spectra indicate that the *cis* and *trans* isomers are in equilibrium for both complexes.

Transmetalation reaction occurs when copper(II) acetate is added to $[UO_2(H\text{-}\mathbf{88b})_2(C_2H_5OH)]$ in ethanol with the formation of $[Cu(H\text{-}\mathbf{88b})_2(H_2O)]$, whereas nickel(II) acetate produces a partial transmetalation, forming a mixture of the mononuclear uranyl(VI) and nickel(II) complexes. In contrast, mass spectrometry, magnetic and ESR data show that the addition of manganese(II) acetate to an ethanol solution of the appropriate mononuclear uranyl(VI) complex produces $[UO_2Mn(\mathbf{88a})_2(C_2H_5OH)]{\cdot}1.5H_2O$ and $[UO_2Mn(\mathbf{88b})_2(C_2H_5OH)]{\cdot}2H_2O$, respectively, where the high spin manganese(II) ion is in an O_6 octahedral environment. A dimeric structure for $[UO_2Mn(\mathbf{88a})_2(C_2H_5OH)]{\cdot}1.5H_2O$ and a monomeric one for $[UO_2Mn(\mathbf{88b})_2(C_2H_5OH)]{\cdot}2H_2O$ was proposed [228].

In $[M(H_2\text{-}\mathbf{89})_2]$ ($M = Ni^{II}$, Co^{II}, Zn^{II}), derived from H_3–**89** and the related metal(II) salt, the metal ion is surrounded by two β-diketonate moieties in non coordinating solvents and achieves a six coordination in coordinating solvents [229]. On the contrary a tetrahedral coordination occurs in $[Li(H_2\text{-}\mathbf{89})_2]^-$ [230] and an octahedral one in $[M(H_2\text{-}\mathbf{89})_3]$ ($M = Fe^{II}$, Cr^{II}) [231].

Hetero- or homotrinuclear complexes derive from the reaction of $[M(H_2\text{-}\mathbf{89})_2]$ ($M = Ni^{II}$, Co^{II}, Zn^{II}) with a different or alike metal salts under basic conditions. The synthetic conditions are critical to obtain the hetetrotrinuclear complexes, especially when the different metal ions have similar physico-chemical properties, because mixtures of the related homotrinuclear compounds, $[M_3(\mathbf{89})_2]$ and $[M'_3(\mathbf{89})_2]$, can be obtained. The boiling temperature used and the relatively long time required to dissolve the mononuclear complex in the presence of a large excess of $N(C_2H_5)_3$ favour reorganization to yield homotrinuclear complexes. The use of NaH in dry tetrahydrofuran at room temperature, to minimize this reorganization, does not give rise to analytically pure heterotrinuclear complexes. The use of pyridine gives rise to $[M_2(H\text{-}\mathbf{89})_2(py)_4]$, living a vacancy in the central position. On the contrary, using metal ions with different physico-chemical properties, the formation of heterotrinuclear species is easier as occurs for $[(UO_2)_2M(\mathbf{89})_2(py)_4]{\cdot}2py$, derived from the treatment of $[M(H_2\text{-}\mathbf{89})_2]$ ($M = Ni^{II}$, Co^{II}, Zn^{II}) and uranyl acetate in a strong basic medium. The isostructural complexes $[(UO_2)_2M(\mathbf{89})_2(py)_4]{\cdot}2py$ ($M = Co^{II}$, Ni^{II}) (Fig. 112) contain the octahedral transition metal(II) ion in the inner chamber, coordinated by two axially pyridine nitrogen atoms and four equatorial oxygen atoms of two β-diketonato moieties. The two distorted pentagonal bipyramidal uranyl(VI) ions occupy the outer chambers with two ketonate oxygen atoms, two phenolate oxygen atoms, and one pyridine nitrogen atom constituting the five equatorial donors. The $[\mathbf{89}]^{2-}$ ligands and the three metal ions are essentially coplanar. The specificity of this controlled synthesis is achieved because the outer positions are the only ones accessible to form the seven coordination of the uranium(VI) ions in these compounds [232].

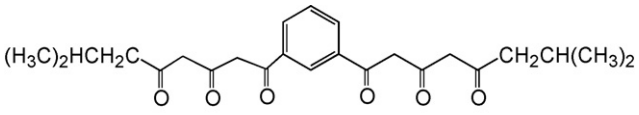

H_4-**87**

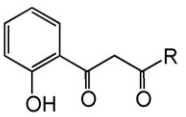

	R
H_2-**88a**	CH_3
H_2-**88b**	C_6H_5
H_2-**88c**	$C(CH_3)_3$

The β-diketone groups of H_3–**90** lie completely in the enolic form in the solid state and in solution, in an *anti–syn* conformation with respect to the phenol group [233]. Equimolar amounts of H_3–**90** and $M(CH_3COO)_2{\cdot}4\,H_2O$ ($M = Ni^{II}$, Mn^{II}) in pyridine produce $[M_2(H\text{-}\mathbf{90})_2(py)_4]$, where the two N_2O_4 octahedral metal(II) centres, 7.921 Å apart in the Ni_2 complex and 9.301 Å apart in the Mn_2 complex, are bridged and chelated by two $[H\text{-}\mathbf{90}]^{2-}$ ligands, while two axial pyridine ligands for each metal ion occupy *cis* and *trans* positions, respectively. The non-completely planar $[H\text{-}\mathbf{90}]^{2-}$ ligands are in the *syn–syn* conformation in the Ni_2 complex and

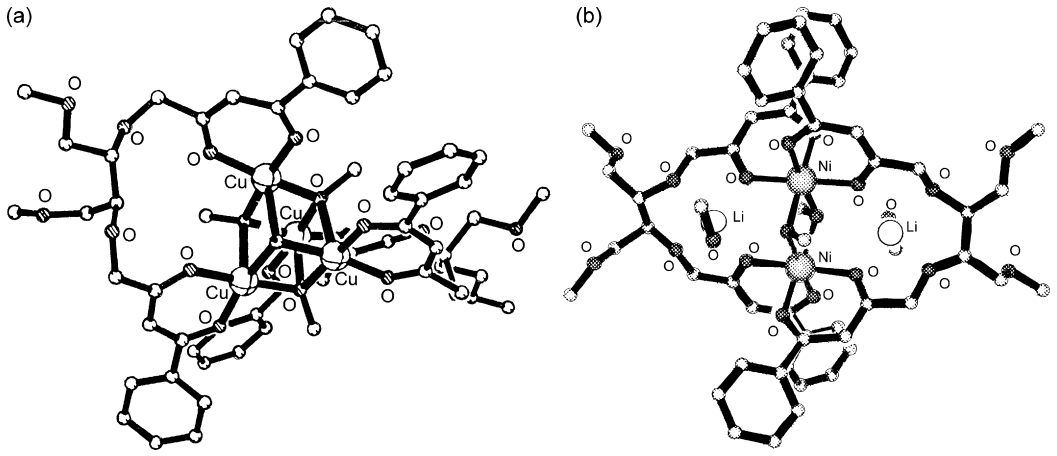

Fig. 108. Structures of $[Cu_4(\mathbf{85a})_2(OCH_3)_4]$ (a) and $\{(\Delta,\Lambda)$-$[Ni_2Li_2(\mathbf{85a})_2(OCH_3)_2(CH_3OH)_2]$ (b) [224].

in *anti–syn* conformation with respect to their β-diketonate units in the Mn_2 complex (Fig. 113). The phenolic proton atom remains on the ligand after complexation. $[Ni_2(H\text{-}\mathbf{90})_2(py)_2(THF)_2]$ shows the same structural features as $[Ni_2(H\text{-}\mathbf{90})_2(py)_4]$. In both complexes the magnetic susceptibility data indicate two noninteracting nickel(II) centres (Fig. 114) [233,234].

H_3–**90** and $Mn(CH_3COO)_2{\cdot}4H_2O$ in CH_3OH/C_5H_5N afford $[Mn_3(H\text{-}\mathbf{90})_3]$ (Fig. 115), where a quasi colinear trinuclear array of manganese(II) ions in a coordination environment intermediate between octahedral and trigonal prismatic is chelated and bridged by three $[H\text{-}\mathbf{90}]^{2-}$ ligands wrapped around the molecular axis in an irregular helical manner, with distances of 3.024 and 5.044 between the two neighbouring manganese(II) ions and 8.076 Å between the two peripheral metal ions. The peripheral metal(II) ions are chelated by the β-diketonate units of the ligands. The central metal(II) ion is bridged to one external manganese ion by the three inner oxygen donors of the corresponding diketonate groups, with the oxygen atoms from the phenol units completing the six coordination around this ion. The cavity between the central and one terminal manganese(II) ion most likely contains the three phenolic protons. In contrast with $[Mn_2(H\text{-}\mathbf{90})_2(py)_4]$, in $[M_3(H\text{-}\mathbf{90})_3]$ the $[H\text{-}\mathbf{90}]^{2-}$ ligands exhibit a *syn–syn* conformation of their β-diketonate groups [234].

H_3–**90** and basic manganese(III) acetate in dimethylformamide, generated in situ by mixing $Mn(CH_3COO)_2$ and $[N(C_4H_9)]_4[MnO_4]$ in a 4:1 molar ratio, lead, after workup with several solvents, to $[Mn_2(\mathbf{91})_2(py)_4]$, where $[\mathbf{91}]^{3-}$, resulting from the degradation of $[\mathbf{90}]^{3-}$, possesses a carboxylate residue in the place of a 3-oxo-3-phenylpropionyl group and can be viewed as the outcome of the oxidative cleavage of one of the 1,3-diketone units of H_3–**90**. If the mixtures yielding $[Mn_2(\mathbf{91})_2(py)_4]$ are allowed to stand unperturbed for a longer period of time, the formation of $[Mn_2(\mathbf{90})_2(py)_4]$ could be observed. A parallel reaction of H_3–**91**, obtained by the Claisen condensation of 5-methyl-3-acetylsalicylic acid and ethyl benzoate, with a manganese(III) salt in pyridine affords $[Mn_2(\mathbf{91})_2(py)_4]$, consisting of two octahedral manganese(III) ions, held at a distance of 5.261 Å by two $[\mathbf{91}]^{3-}$ ligands. Each metal(III)

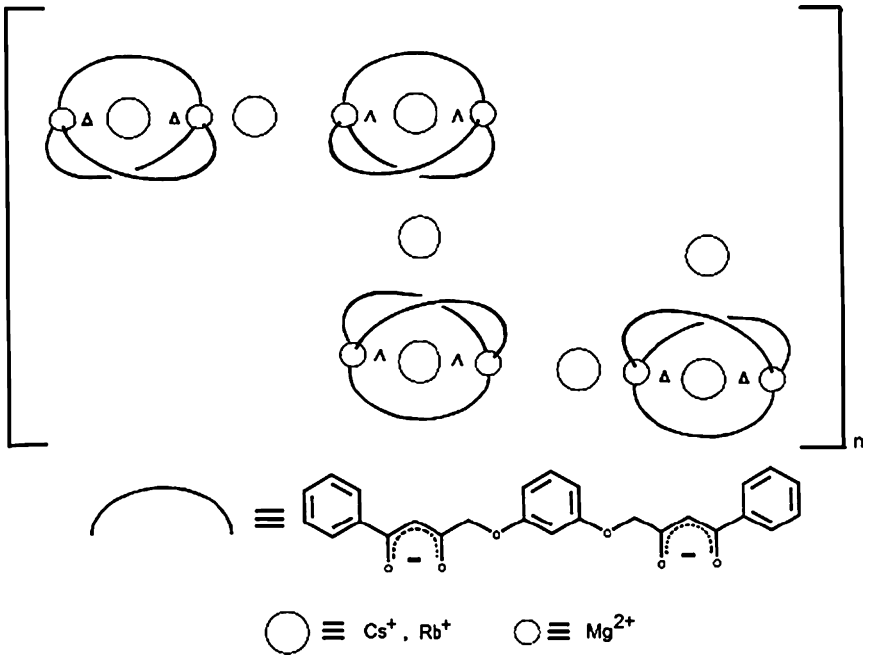

Scheme 14. Schematic representation of the polymer *meso*-$\{[(\Delta,\Delta)$-$M_2^{II}M^{I}(\mathbf{84b})_3]M^{I}_{end}\}([(\Lambda,\Lambda)$-$M_2^{II}M^{I}(\mathbf{84b})_3]\,M^{I}_{side}\}$.

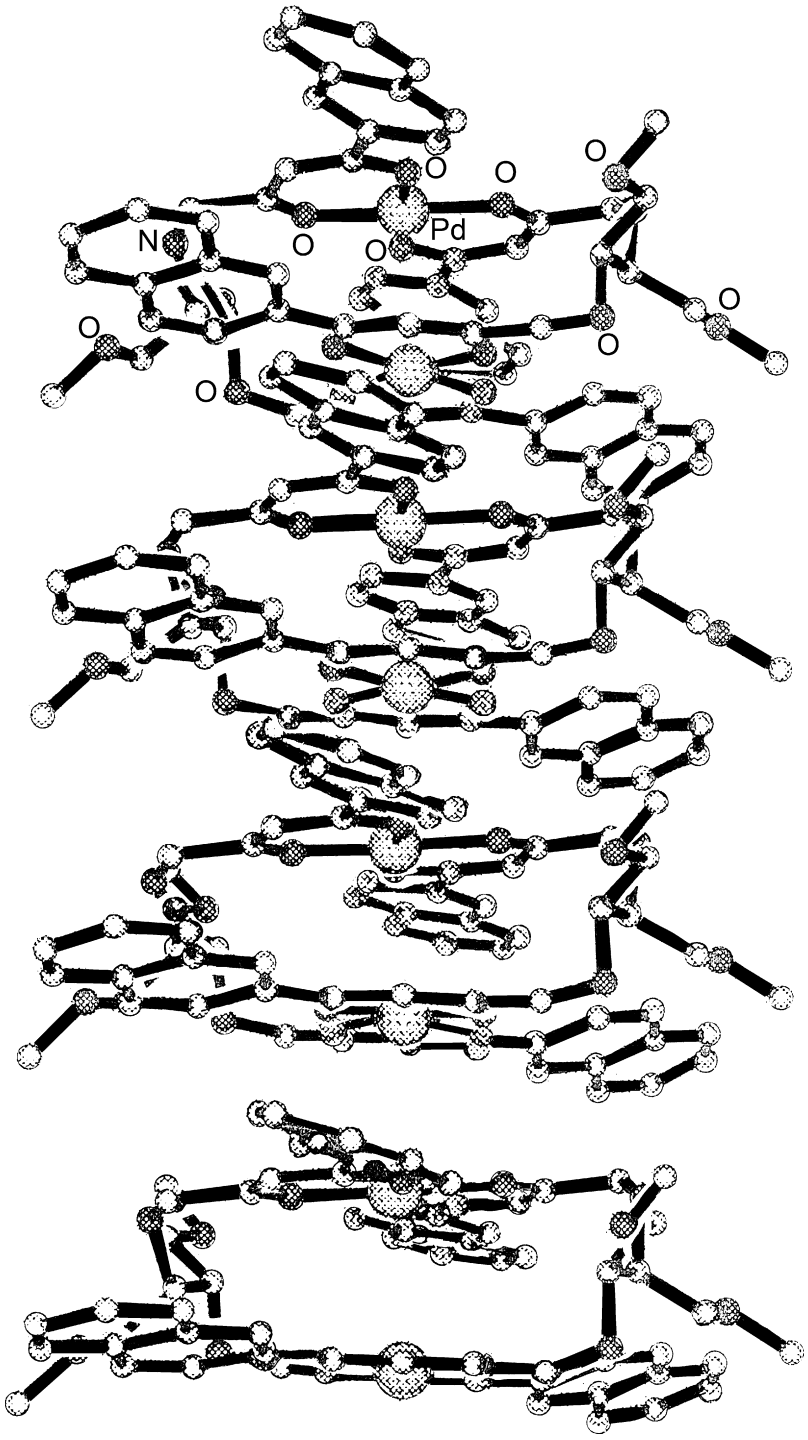

Fig. 109. Structure of P-$[Pd_2(\mathbf{85d})_2]_\infty$ [224].

ion is equatorially coordinated by four adjacent oxygen donors from two [**91**]$^-$ ligands and axially by two staggered pyridine nitrogen atoms (Fig. 116) [234].

Antiferromagnetic interactions occurs in $[Mn_3(H\text{-}\mathbf{90})_3]$; the experimental data fit with a model where an exchange-coupled $Mn^{II}\cdots Mn^{II}$ pair ($J = -2.75\,cm^{-1}$) is next to a third, magnetically isolated manganese(II) center. For $[Mn_2(\mathbf{91})_2(py)_4]$, a weak antiferromagnetic coupling within the molecule ($J = -1.48\,cm^{-1}$) and weaker intermolecular ferromagnetic interaction ($J = 0.39\,cm^{-1}$) occur [234].

The isolation and characterization of $[Mn_2(H\text{-}\mathbf{90})_2(py)_4]$ and $[Mn_3(H\text{-}\mathbf{90})_3]$ demonstrate the versatility of the $\{Mn^{II}(H\text{-}\mathbf{90})\}^{2-}$ system, whose molecular information can be expressed in the form of either of two discrete species with different topologies and magnetic properties, depending on the nature of the solvent used. The kinetic ability of the manganese(II) ion allows the reversible interconversion of these two complexes by using external stimuli. Thus, $[Mn_3(H\text{-}\mathbf{90})_3]$, in pyridine/diethylether forms $[Mn_2(H\text{-}\mathbf{90})_2(py)_4]$ in high yield after a few days, showing that the dinuclear complex is more stable than the trinuclear one in pyri-

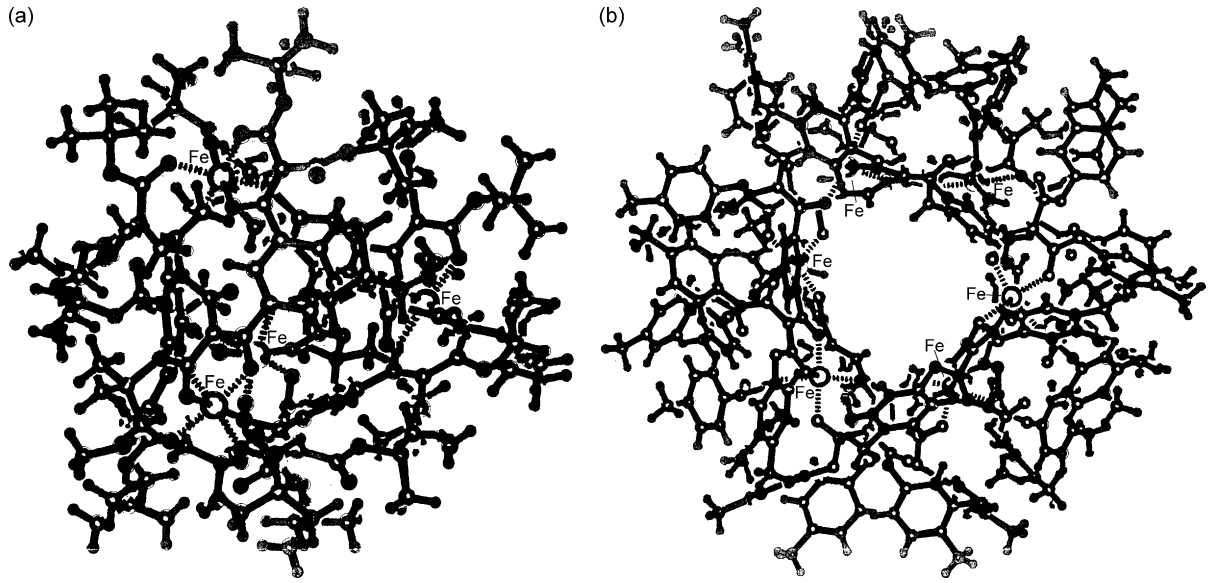

Fig. 110. Structures of $[Fe_4(\mathbf{86a})_4]$ (a) and $[Fe_6(\mathbf{86b})_6]$ (b) [225].

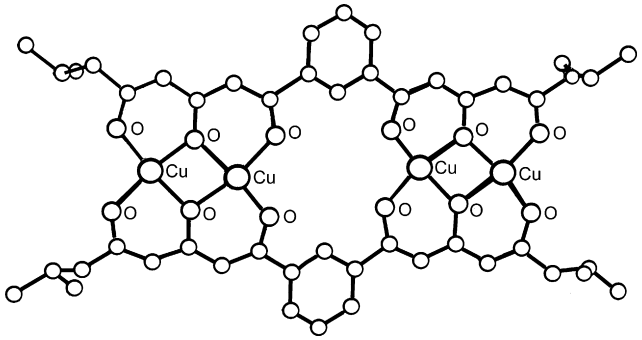

Fig. 111. Structure of $[Cu_4(\mathbf{87})_2(py)_4]$ [227].

dine and that the multiple dissociation and rearrangement steps necessary for this conversion are kinetically accessible under the reaction conditions. On the contrary, $[Mn_2(H\text{-}\mathbf{90})_2(py)_4]$ converts in dichloromethane/diethylether/hexane into $[Mn_3(H\text{-}\mathbf{90})_3]$, proving that if pyridine is not present in a large excess, the trinuclear complex is the most stable species and that its formation from the dinuclear analogue is also feasible kinetically. Thus, $[Mn_2(H\text{-}\mathbf{90})_2(py)_4]$ and $[Mn_3(H\text{-}\mathbf{90})_3]$ constitute a binary molecular switch that can be externally addressed by controlling the nature of the solvent medium. In addition of structurally distinct architectures, the two states of the switch are two magnetic entities displaying different properties. In one case the assembly possesses two uncoupled manganese(II) ions, and in the other it is formed by two exchange coupled manganese(II) centres next to a third, magnetically independent manganese(II) ion. This system represents an important contribution to the growing of adaptive chemistry, by which complex chemical systems are described, capable of delivering different responses to a variety of environmental stimuli [234].

Equimolar amounts of $Cu(CH_3COO)_2{\cdot}2H_2O$ and H_3–**90** in dimethylformamide produce $[Cu_2(H\text{-}\mathbf{90})_2(DMF)_2]$, while $Cu(NO_3)_2$, $CuCl_2$ or $CuBr_2$, H_3–**90** and $[N(C_4H_9)_4](OH)$ in a 8:1:16.4 molar ratio yield $[Cu_8(\mathbf{90})_2(OCH_3)_8(NO_3)_2]$, $[Cu_8(\mathbf{90})_2(OCH_3)_8(Cl)_2]$ or $[Cu(\mathbf{90})_2(OCH_3)_{7.86}(Br)_{2.14}]$, respectively. The same reaction in the presence of a lower amount of $[N(C_4H_9)_4](OH)$, affords catena-$[Cu_4(\mathbf{90})(OCH_3)_3(NO_3)_2(H_2O)_{0.36}]$. Similarly, when $Cu(ClO_4)_2$ is used, $[Cu_8(\mathbf{90})_2(OCH_3)_8)(ClO_4)_2(CH_3OH)_4]$ is obtained [235].

In $[Cu_2(H\text{-}\mathbf{90})_2(DMF)_2]$ (Fig. 117) the two square pyramidal copper(II) ions are chelated and bridged by the β-diketonate units of two $[H\text{-}\mathbf{90}]^{2-}$ groups. The apical position of each metal ion is occupied by the dimethylformamide oxygen atom. The phenol groups are not deprotonated and form hydrogen bonds with the oxygen atoms of neighbouring β-diketonate moieties [235].

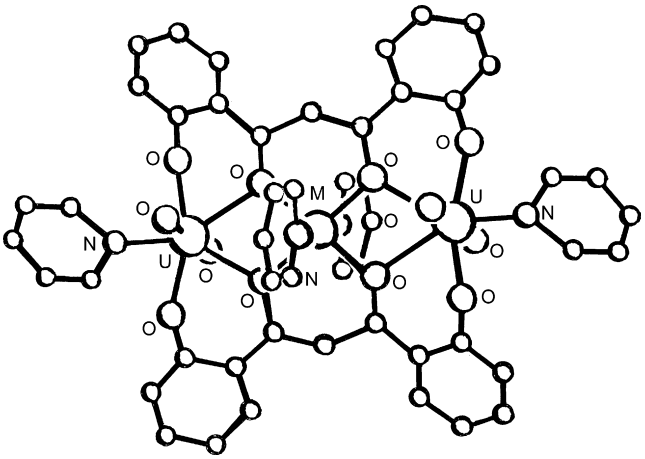

Fig. 112. Structure of $[(UO_2)_2M(\mathbf{89})_2(py)_4]$ ($M = Ni^{II}$, Co^{II}) [232].

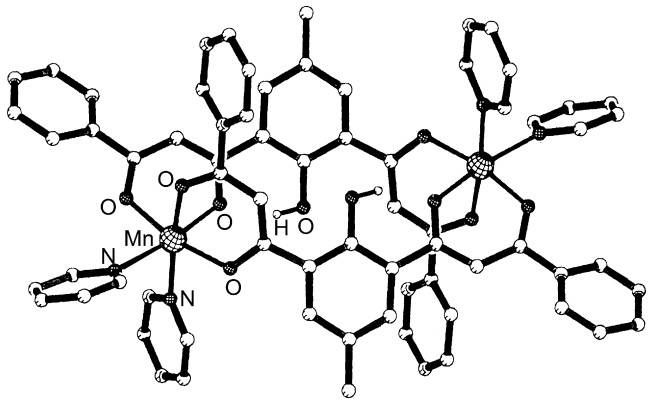

Fig. 113. Structure of $[Mn_2(H\text{-}\mathbf{90})_2(py)_4]$ [233].

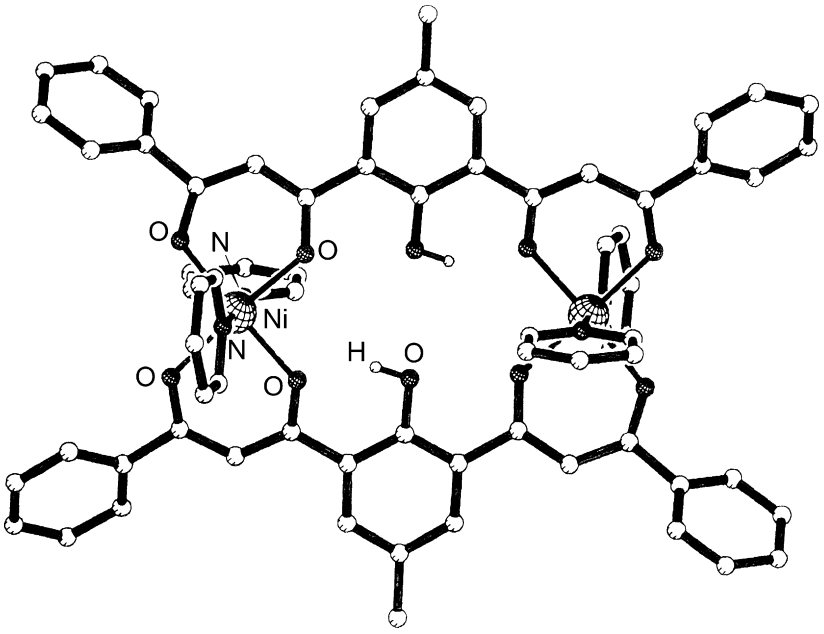

Fig. 114. Structure of $[Ni_2(H\text{-}\mathbf{90})_2(py)_4]$ [233].

$[Cu_8(\mathbf{90})_2(OCH_3)_8(NO_3)_2]$ (Fig. 118a) is a cluster of eight copper(II) centres arranged in two tetranuclear linear units, linked together by six μ_3-OCH_3 and two μ-OCH_3 groups. The asymmetric unit contains four, strictly linear metal ions, gathered by the template action of one $[\mathbf{90}]^{3-}$ ligand. The coordination around the copper ions is completed by nitrate ligands in an unusual μ_3-NO_3^- binding mode, which links each $\{Cu_8(\mathbf{90})_2(OCH_3)_8\}^{2+}$ aggregate to two other resulting in the formation of a 1D coordination polymer of clusters. Two of the four crystallographically independent copper(II) ions of $[Cu_8(\mathbf{90})_2(OCH_3)_8(NO_3)_2]$ are distorted octahedral, one is intermediate between trigonal bipyramidal and square pyramidal, and the last one is square pyramidal. The axial positions are taken by the six long bonds of the metal ions with μ_3-OCH_3 groups, which connect both the Cu_4 moieties to each other, or by the bonds with NO_3^- ligands. The average Cu···Cu distance within the tetranuclear arrays (2.883–2.999 Å) are shorter than between them (2.961-3.467 Å). The shortest intercluster Cu···Cu distance within the 1D chain is 5.231 Å [235].

In $[Cu_8(\mathbf{90})_2(OCH_3)_8(Cl)_2]$, structurally related to $[Cu_8(\mathbf{90})_2(OCH_3)_8(NO_3)_2]$ except that two coordinating positions of the copper(II) ions filled by NO_3^- in the latter complex are vacant in the former one, the connection between $\{Cu_8(\mathbf{90})_2(OCH_3)_8\}^{2+}$ clusters takes place with bridging chloride ligands. Thus, within the asymmetric unit of $[Cu_8(\mathbf{90})_2(OCH_3)_8(Cl)_2]$ there is one octahedral copper(II) ion, two square pyramidal copper(II) and the last one in a geometry that is intermediate between square pyramidal and trigonal bipyramidal. The Cu···Cu distances are in the range 2.904–2.990 Å within the tetranuclear arrays and 3.013–3.567 Å across the chains, only slightly longer than in the dinitrato complex. $[Cu_8(\mathbf{90})_2(OCH_3)_{7.86}(Br)_{2.14}]$ is isostructural with $[Cu_8(L)_2(OCH_3)_8(Cl)_2]$, the most relevant difference being the partially substitution of μ-OCH_3 with μ-Br [235].

$[Cu_8(\mathbf{90})_2(OCH_3)_8(ClO_4)_2(CH_3OH)_4]$ shows similar octanuclear unit not bridged, however, into infinite chains but in the form of discrete isolated clusters. Four vacant coordination sites are occupied by methanol molecules. Six copper(II) ions are in an elongated octahedron while the remaining two are close to a square pyramidal one (Fig. 118b) [235].

Catena-$[Cu_4(\mathbf{90})(OCH_3)_3(NO_3)_2(H_2O)_{0.36}]$ (Fig. 119) features four closely spaced copper(II) ions, assembled by the chelating effect of the five adjacent oxygen atoms of the ligand $[\mathbf{90}]^{3-}$. Each tetranuclear moiety is linked to two other equivalent fragments in a shifted manner, rather than face to face. There are two different ways in which the $\{Cu_4(\mathbf{90})\}^{5+}$ units are connected. The linkage of the largest contact involves a total of four μ_3-OCH_3 ligands and two μ_2-NO_3^- groups. The other connection mode occurs through the action of two μ_3-OCH_3 groups, one μ-NO_3^- ligand, and one μ_3-NO_3^- moiety. The asymmetric unit also contains one terminal ligand consisting of a partially occupied molecule of water. In the repeating unit of this polymer there are two octahedral copper(II) centres, one copper(II) ion in a coordination geometry distributed between octahedral and square pyramidal and a fourth copper(II) ion in a square pyramidal geometry with an additional, very long axial bond to a nitrate ligand. Within the catena-$[Cu_4(\mathbf{90})(OCH_3)_3(NO_3)_2(H_2O)_{0.36}]$ polymer there are eight unique Cu_2O_2 pairs with Cu···Cu distances of 2.850–2.964 Å within the $\{Cu_4(\mathbf{90})\}^{5+}$ unit, 3.325–3.376 Å within the short link, and 3.278–3.429 Å within the long link [235].

A very weak antiferromagnetic exchange between the copper(II) centres was found in $[Cu_2(H\text{-}\mathbf{90})_2(DMF)_2]$ ($J = -0.73\ cm^{-1}$) while strong antiferromagnetic coupling ($J = -113.8 - -177.3\ cm^{-1}$) occurs in $[Cu_8(\mathbf{90})_2(OCH_3)_8(NO_3)_2]$, $[Cu_8(\mathbf{90})_2(OCH_3)_8(ClO_4)_2(CH_3OH)_4]$, and catena-$[Cu_4(\mathbf{90})(OCH_3)_3(NO_3)_2(H_2O)_{0.36}]$ [235].

Again H_3–**90** shows its great potential for the aggregation of copper(II) spin carriers into structures with different degrees of aggregation and magnetic spin–spin interactions. The formed product can be chemically controlled by small changes in the reaction conditions, especially the molar ratio between the reactants or the used counteranions.

$Co(CH_3COO)_2{\cdot}4H_2O$ and H_3–**90** lead to $[Co_2(H\text{-}\mathbf{90})_2(py)_4]$ in pyridine and $[Co_2(H\text{-}\mathbf{90})_2(CH_3OH)_4]$ in methanol, while in dimethylformamide and in the presence of 2,2′-bipyridine (bipy), bipyridylamine (bipya), 4,4′-biphenyl-2,2′-bipyridine (Ph_2bipy) or phenanthroline (phen), capable to block two *cis* coordination positions of the metal ion and to force the polyketonate ligand $[H\text{-}\mathbf{90}]^{2-}$ to adopt a *syn*,*anti* mode in the formation of dinuclear

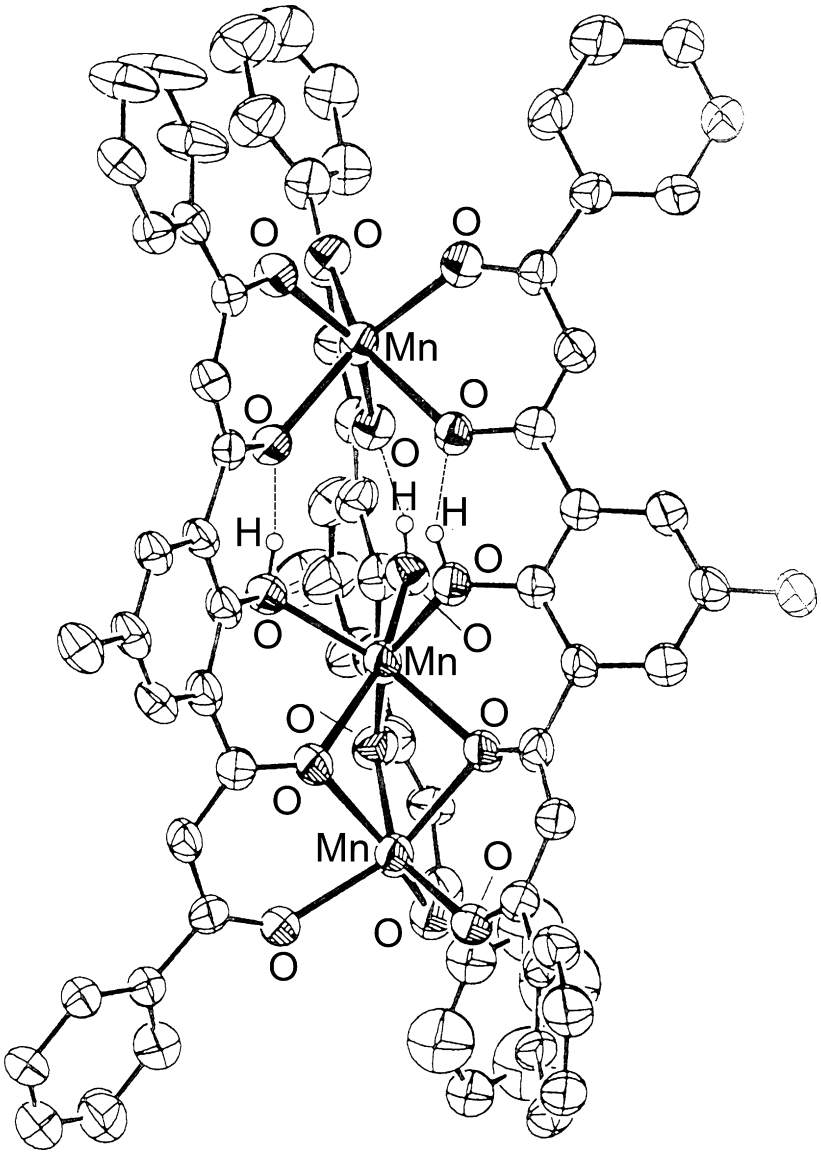

Fig. 115. Structure of $[Mn_3(H\text{-}\mathbf{90})_3]$ [234].

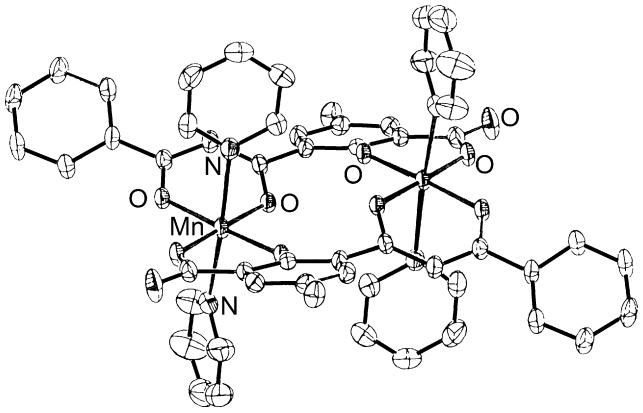

Fig. 116. Structure of $[Mn_2(\mathbf{91})_2(py)_4]$ [234].

complexes, they form $[Co_2(H\text{-}\mathbf{90})_2(bipy)_2]$, $[Co_2(H\text{-}\mathbf{90})_2(bpya)_2]$, $[Co_2(H\text{-}\mathbf{90})_2(Ph_2bipy)_2]$ and $[Co_2(H\text{-}\mathbf{90})_2(phen)_2]$, respectively. $Co(CH_3COO)_2{\cdot}4H_2O$, allowed to react with H_3–**90** for 24 h in CH_2Cl_2, produces $[Co_3(H\text{-}\mathbf{90})_3]$ which turns into $[Co_2(H\text{-}\mathbf{90})_2(py)_4]$ in pyridine/toluene. The reverse conversion of $[Co_2(H\text{-}\mathbf{90})_2(CH_3OH)_4]$ to $[Co_3(H\text{-}\mathbf{90})_3]$ was successfully achieved in CH_2Cl_2 [235].

$[Co_2(H\text{-}\mathbf{90})_2(py)_2]$ (Fig. 120a) contains two distorted octahedral cobalt(II) centres, 7.955 Å apart, equatorially chelated and bridged by two $[H\text{-}\mathbf{90}]^{2-}$ ligands in a *syn*,*syn* conformation by means of their deprotonated β-diketonate moieties and axially coordinated by two pyridine ligands [235].

In $[Co_2(H\text{-}\mathbf{90})_2(bipy)_2]$ (Fig. 120b) both cobalt(II) ions are gathered by two $[H\text{-}\mathbf{90}]^{2-}$ ligands which again use the chelating β-diketonate groups for coordination while maintaining the protons on their phenol groups. These protons are part of hydrogen bonds with one oxygen atom of a neighbouring diketonate. The distorted octahedral cobalt(II) centres are additionally coordinated by chelating bipyridyl ligands that occupy two *cis* coordination sites on each metal ion. This forces the $[H\text{-}\mathbf{90}]^{2-}$

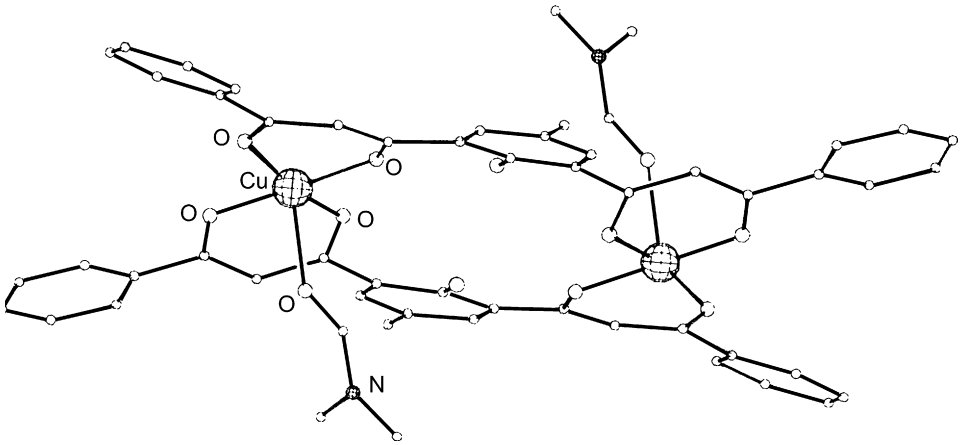

Fig. 117. Structure of $[Cu_2(H\text{-}\mathbf{90})_2(DMF)_2]$ [235].

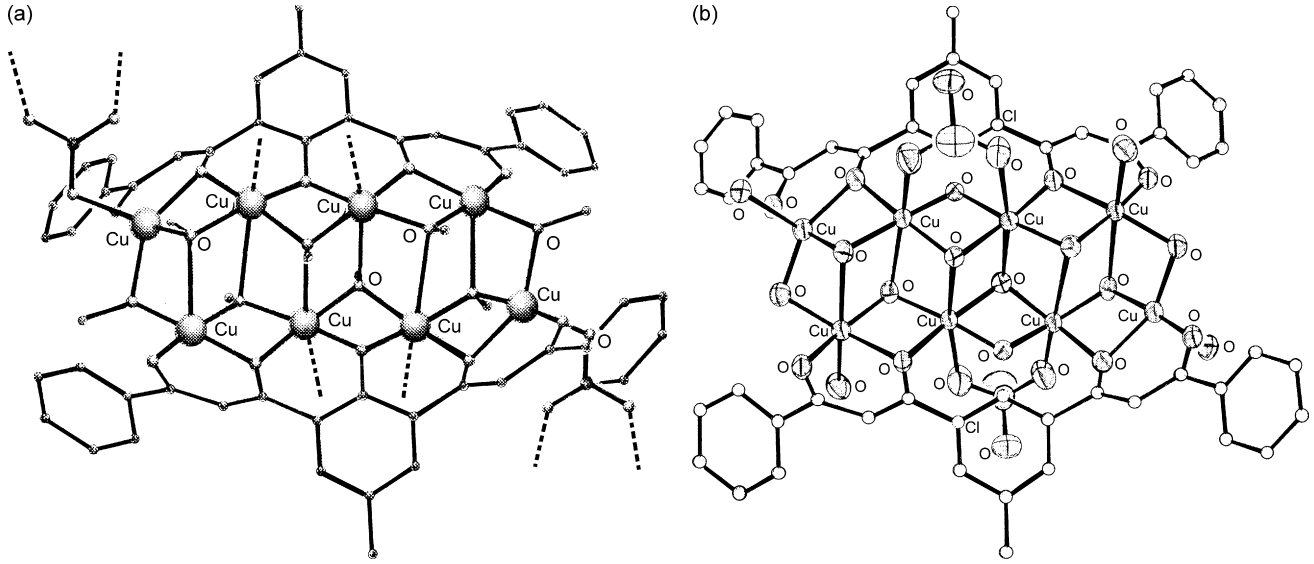

Fig. 118. Structures of $[Cu_8(\mathbf{90})_2(OCH_3)_8(NO_3)_2]$ (a) and $[Cu_8(\mathbf{90})_2(OCH_3)_8(ClO_4)_2(CH_3OH)_4]$ (b) [235].

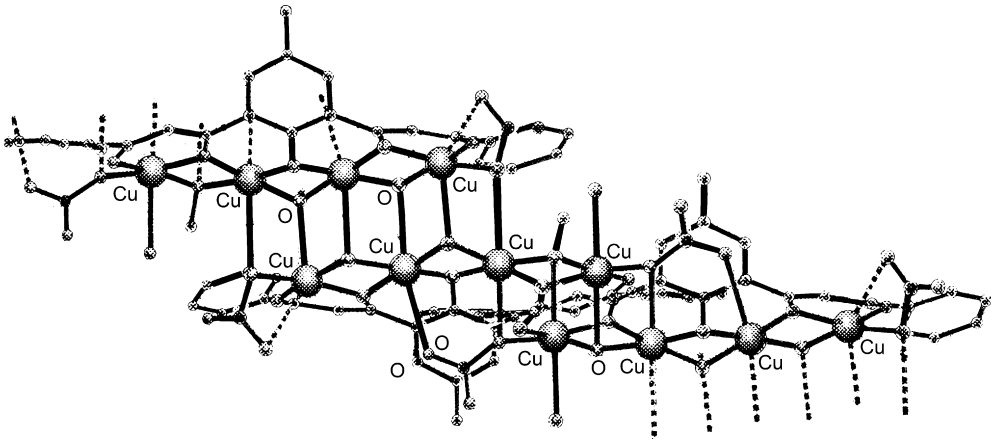

Fig. 119. Structure of catena-$[Cu_4(\mathbf{90})(OCH_3)_3(NO_3)_2(H_2O)_{0.36}]$ [235].

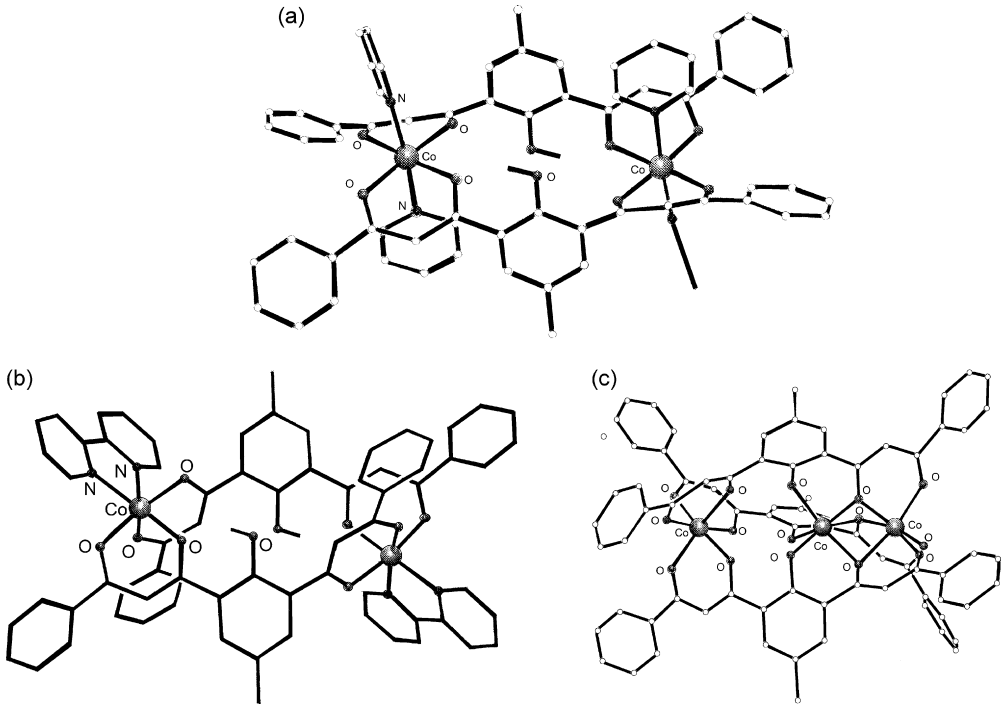

Fig. 120. Structures of $[Co_2(H\text{-}\mathbf{90})_2(py)_4]$ (a), $[Co_2(H\text{-}\mathbf{90})_2(bipy)_2]$ (b) and $[Co_3(H\text{-}\mathbf{90})_3]$ (c) [236].

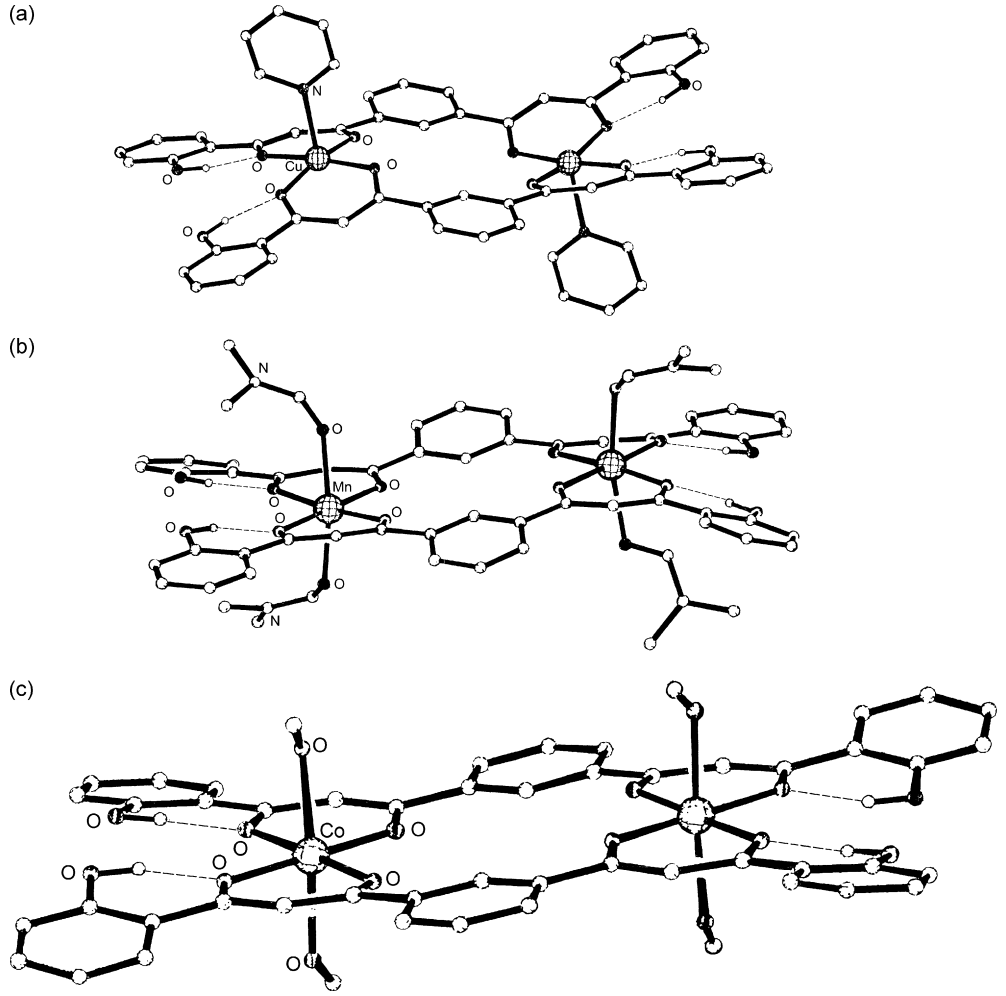

Fig. 121. Structures of $[Cu_2(H_2\text{-}\mathbf{92})_2(py)_2]$ (a), $[Mn_2(H_2\text{-}\mathbf{92})_2(DMF)_4]$ (b) and $[Co_2(H_2\text{-}\mathbf{92})_2(CH_3OH)_4]$ (c) [237].

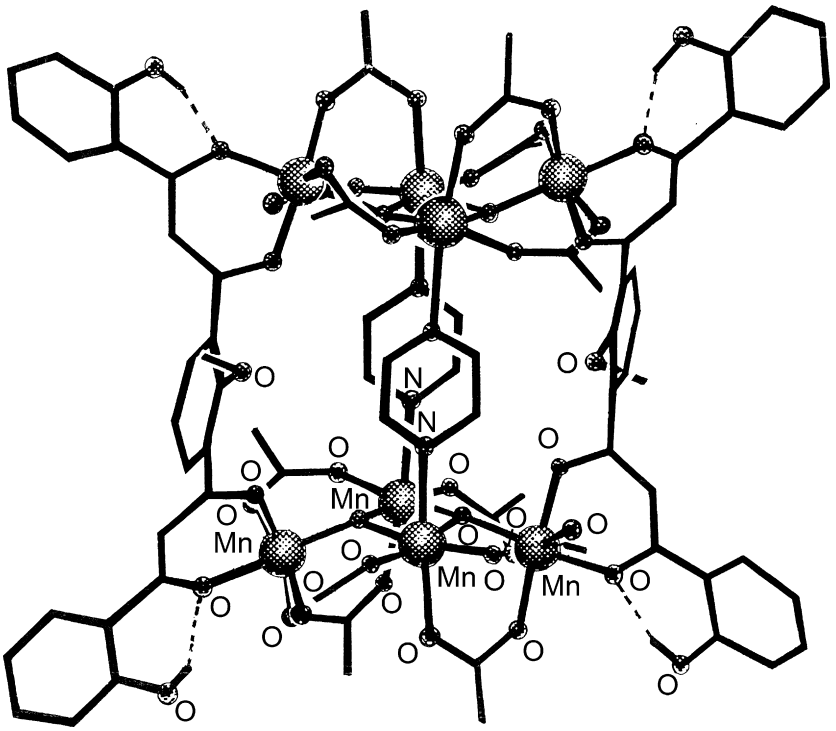

Fig. 122. Structure of $[Mn_4(H_2\text{-}\mathbf{93})(CH_3COO)_6(pyz)]_2$ [238].

ligands to adopt a conformation closer to the *syn,anti* mode in order to achieve the dinuclear assembly. The Co···Co distance (8.986 Å) significantly increase with respect to $[Co_2(H\text{-}\mathbf{90})_2(py)_2$ [236].

$[Co_3(H\text{-}\mathbf{90})_3]$ (Fig. 120c) consists of a quasi-linear array of three cobalt(II) ions, with intermetallic separations of 2.840 and 4.907 Å between the two closer cobalt(II) ions and 7.747 Å between the terminal cobalt(II) ions, held together by three $[H\text{-}\mathbf{90}]^{2-}$ ligands that retain the protons on the phenol groups. Each ligand chelates the three metal ions through two β-diketonate moieties and a third coordination pocket formed by the phenol oxygen and the inner oxygen of one β-diketonate, which then acts in a bridging mode. The fourth potential coordination pocket is most likely occupied by the phenol protons, which are presumably participating in hydrogen bridges, similar to those observed in $[Co_2(H\text{-}\mathbf{90})_2(py)_2]$ and $[Co_2(H\text{-}\mathbf{90})_2(bipy)_2]$. An octahedral geometry around the external cobalt(II) ions occurs while a trigonal prismatic coordination was observed for the inner cobalt(II) ion. Both β-diketonate units of each ligand are *cis* with respect to their respective phenol group [236].

Dimethylisophthaldehyde and 2′-hydroxyacetophenone in ethyleneglycol dimethylether containing activated molecular sieves followed by the addition of NaH at 4 °C produce H_4–**92**, which reacts with the appropriate metal(II) acetate in pyridine to form $[Cu_2(H_2\text{-}\mathbf{92})_2(py)_2]$ and $[M(H_2\text{-}\mathbf{92})_2(py)_4]$ ($M = Ni^{II}$, Mn^{II}). The same reaction with $Co(CH_3COO)_2{\cdot}4H_2O$ in

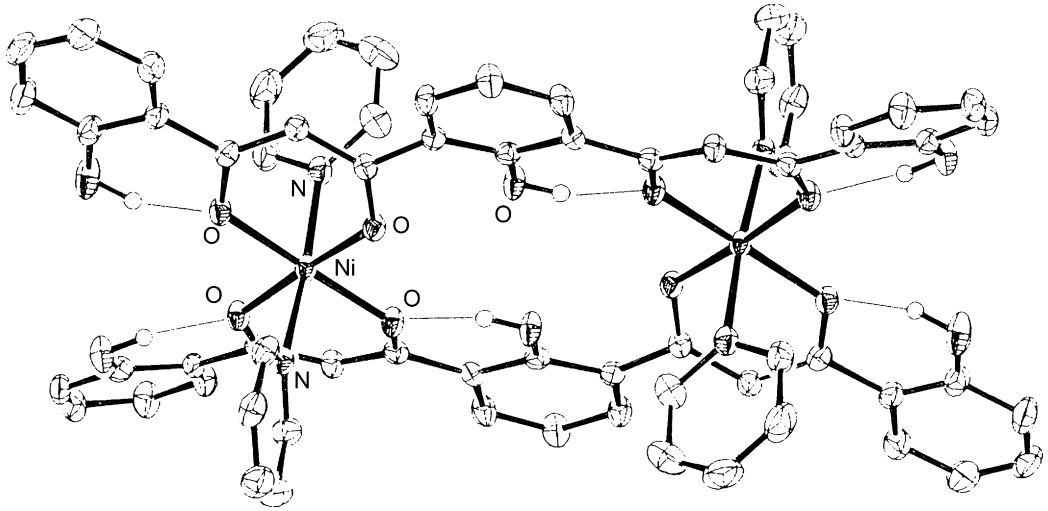

Fig. 123. Structure of $[Ni_2(H_3\text{-}\mathbf{94})_2(py)_4]$ [239].

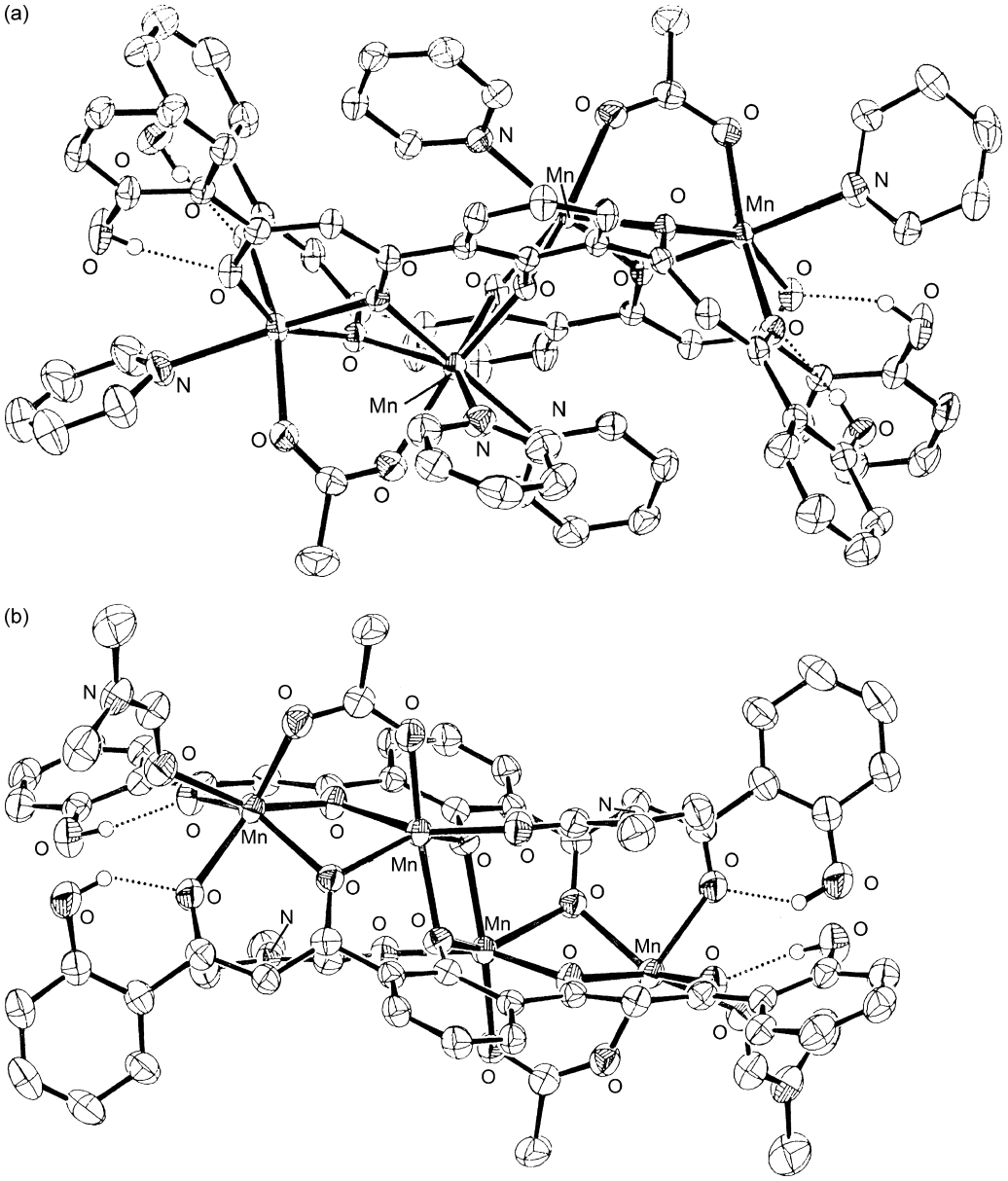

Fig. 124. Structures of $[Mn_4(H_2\text{-}\mathbf{94})_2(CH_3COO)_2(py)_5]$ (a) and $[Mn_4(H_2\text{-}\mathbf{94})_2(CH_3COO)_2(DMF)_4]$ (b) [239].

methanol affords $[Co_2(H_2\text{-}\mathbf{92})_2(CH_3OH)_4]$, while recrystallization of $[Mn_2(H_2\text{-}\mathbf{92})_2(py)_4]$ from dimethylformamide produces $[Mn_2(H_2\text{-}\mathbf{92})_2(DMF)_4]$ [237].

The two square pyramidal copper(II) ions in $[Cu_2(H_2\text{-}\mathbf{92})_2(py)_2]$, 7.539 Å apart, are bridged and chelated by two $[H_2\text{-}\mathbf{92}]^{2-}$ ligands through their β-diketonate moieties and by two axial pyridine ligands. H_4–**92** is preferentially deprotonated at the methylene positions between the carbonyl groups of the β-diketone fragments (Fig. 121a) [237].

In $[Ni_2(H_2\text{-}\mathbf{92})_2(py)_4]$, $[Mn_2(H_2\text{-}\mathbf{92})_2(DMF)_4]$ (Fig. 121b) and $[Co_2(H_2\text{-}\mathbf{92})_2(CH_3OH)_4]$ (Fig. 121c) two $[H_2\text{-}\mathbf{92}]^{2-}$ ligands bridge two distorted octahedral metal(II) ions, 7.322 Å, 7.609 Å and 7.410 Å apart, linked through chelation of both metal ions by each of two $[H_2\text{-}\mathbf{92}]^{2-}$ ligands displaying the same *cis–cis* conformation as in $[Cu_2(H_2\text{-}\mathbf{92})_2(py)_2]$, but is in contrast with $[Mn_2(H\text{-}\mathbf{90})_2(py)_4]$ where the ligand is found in the *syn–anti* conformation. Each metal ion is axially coordinated by two solvent molecules. Magnetic measurements show that the metal ions within these dinuclear complexes are maintained almost mutually independent [237].

H_4–**93**, synthesized through Claisen condensation of dimethyl-2-methoxyisophthalate with 2-hydroxyacetophenone followed by acidification of the resulting product and crystallization from acetone, has its two β-diketones in the enolic form both in the solid state and in $CHCl_3$. It reacts with $[Mn_3O(RCOO)_6(pyz)_3](ClO_4)$ (R = CH_3,C_6H_5,p$CH_3C_6H_4$) and pyrazine (pyz) in $CHCl_3$ to form $[Mn_4(H_2\text{-}\mathbf{93})(RCOO)_6(pyz)]_2$ whose structures, differing only in the nature of the R group of the carboxylate, consist of two tetranuclear manganese(III) clusters assembled into a centrosymmetric molecule by two $[H_2\text{-}\mathbf{93}]^{2-}$ and two pyrazine ligands. Each tetranuclear fragment features a Mn_4O_2 core of four octahedral manganese(III) ions bridged by two μ_3-oxides. Each pair of manganese(III) ions is also bridged by either one to two *syn*,*syn*-μ-CH_3COO^- groups. The terminal manganese(III) ions complete their coordination with a chelating diketonate group from the $[H_2\text{-}\mathbf{93}]^{2-}$ ligands, which thus subtend the clusters opposite to each

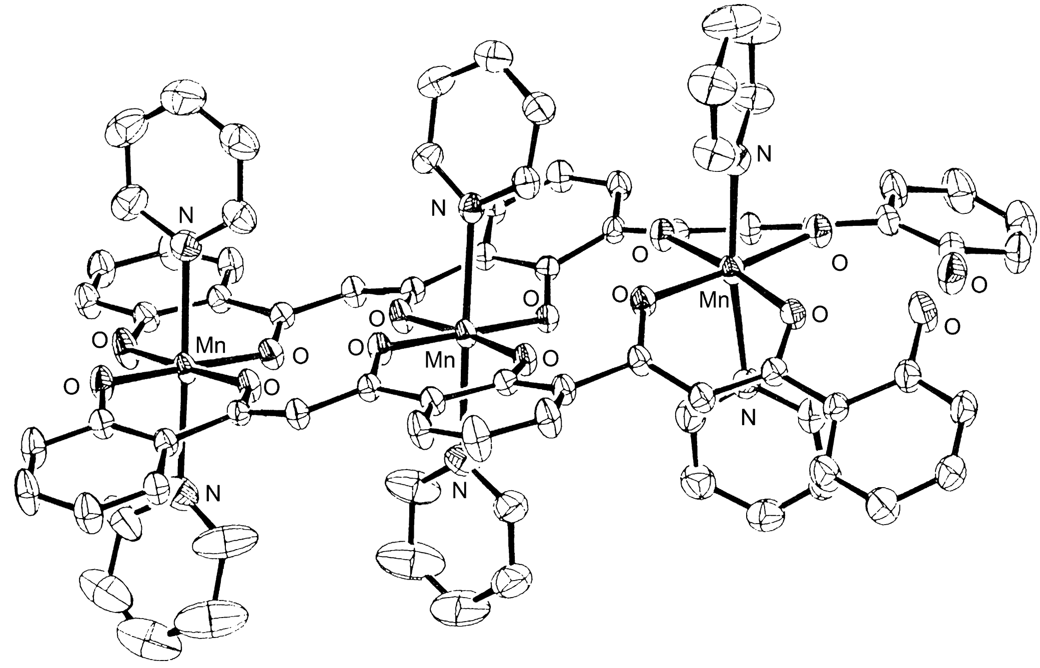

Fig. 125. Structure of $[Mn_3(H\text{-}\mathbf{94})_2(py)_6]$ [239].

other. Two pyrazine ligands bind the two central manganese(III) ions, thereby further linking the two Mn_4 units and leading to the shortest intercluster Mn···Mn distance of 7.443 Å (Fig. 122). The structure is maintained in CH_2Cl_2 [238].

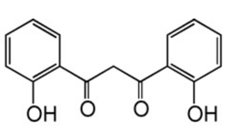

H_3-**89**

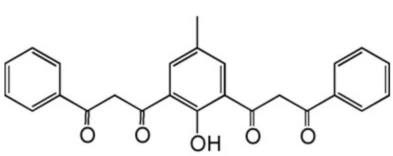

H_3-**90**

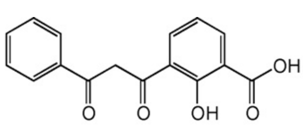

H_3-**91**

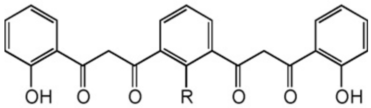

	R
H_4-**92**	H
H_4-**93**	OCH_3
H_4-**94**	OH

H_4–**93** and 1.5 equiv. of BBr_3 give H_5–**94** containing one β-diketone in the enolic form and the other in the biscarbonyl tautomer in the solid state. H_5–**94** and $M(CH_3COO)_2{\cdot}4H_2O$ (M = Ni^{II}, Co^{II}) in pyridine produce $[M_2(H_3\text{-}\mathbf{94})_2(py)_4]$ with the two pseudo-octahedral metal(II) ions, 7.714 Å apart in the nickel(II) complex and 7.807 Å apart in the cobalt(II) one, equatorially bridged by two $[H_3\text{-}\mathbf{94}]^{2-}$ ligands, their axial sites being occupied by pyridine ligands. The phenol protons remain at their original locations, being part of intramolecular hydrogen bonds as observed in the free ligand, although $[H_3\text{-}\mathbf{94}]^{2-}$ has varied its conformation upon coordination with respect to solid H_5–**94**. In the dicobalt(II) complex $[H_3\text{-}\mathbf{94}]^{2-}$ is more removed from planarity. The shortest intermolecular metal···metal separation is 8.929 Å for the nickel(II) complex and 9.038 Å for the cobalt(II) one (Fig. 123) [239].

H_5–**94** and $Mn(CH_3COO)_2{\cdot}4H_2O$ afford $[Mn_4(H_2\text{-}\mathbf{94})_2(CH_3COO)_2(py)_5]$ (Fig. 124a) in pyridine and $[Mn_4(H_2\text{-}\mathbf{94})_2(CH_3COO)_2(DMF)_4]$ (Fig. 124b) in dimethylformamide. In $[Mn_4(H_2\text{-}\mathbf{94})_2(CH_3COO)_2(py)_5]$ the Mn_4O_6 zigzag linear core is built up by the action of two $[H_2\text{-}\mathbf{94}]^{3-}$ ligands located opposite to each other and running along the chain, each engaging its central phenolate and both 1,3-diketonate moieties for coordination, thereby chelating and bridging the metal ions. The external phenol moieties of the ligands are not involved in coordination and retain their protons, which form intramolecular hydrogen bonds as in $[M_2(H_3\text{-}\mathbf{94})_2(py)_4]$ (M = Ni^{II}, Co^{II}). Additional bridging within the cluster is ensured by two *syn,syn*-CH_3COO^- ligands, supporting the two manganese(II) pairs, respectively. The central pair of metal ions is in turn bridged only by two alkoxide-type oxygen atoms. Terminal ligation is completed by five pyridine ligands, one on each metal except for one manganese(II) ions, which is bound to two such molecules and is therefore seven coordinate. The remaining manganese ions are pseudo-octahedral. The intramolecular Mn···Mn separations are 3.287, and 3.495 and 3.350 Å, between two adjacent metal ions, 5.752 and 5.898 Å between one external and one inner metal ion and 8.804 Å between the two external metal ions [239].

The structure of $[Mn_4(H_2\text{-}\mathbf{94})_2(CH_3COO)_2(DMF)_4]$**,** similar to that of $[Mn_4(H_2\text{-}\mathbf{94})_2(CH_3COO)_2(py)_5]$ with dimethylformamide terminal ligands instead of pyridine, contains octahedral man-

ganese(II) ions bound to one solvate ligand at intermetallic distances of 3.318, 3.387 5.861 and 8.903 Å [239].

The structure of $[Mn_3(H\text{-}\mathbf{94})_2(py)_6]$ (Fig. 125) comprises a mixed-valence trinuclear $Mn^{III}{}_2Mn^{II}$ array, supported by two $[H\text{-}\mathbf{94}]^{4-}$ ligands, one on each side of the chain. The oxygen donors of these ligands occupy all the equatorial positions of the metal ions as chelates, the axial sites being saturated by pyridine ligands. $[H\text{-}\mathbf{94}]^{4-}$ coordinates the metal ions in an asymmetric manner, by using three nonadjacent coordination pockets. This comes about through the involvement of two phenoxide groups and β-diketonate moieties per ligand. The third phenol moiety of each ligand retains its proton, and both groups are found in front of each other at the same end of the molecule. The central and one external metal ions are in a 3+ oxidation state. The Mn···Mn distances are 5.246 and 5.155 Å between neighbouring metal ions and 10.381 Å between the two external metal ions [239].

Antiferromagnetic interactions dominate the coupling within the $[Mn_4(H_2\text{-}\mathbf{93})(CO)_2(RCOO)_6(pyz)]_2$ clusters ($J_{bb} = -50.6\,cm^{-1}$, $J_{wb} = -22\,cm^{-1}$, $J_{ww} = 7.6\,cm^{-1}$) [238] while the manganese(II) ions weakly interact with coupling constants of $J_1 = 1.13\,cm^{-1}$ and $J_2 = -0.43\,cm^{-1}$ for $[Mn_4(H_2\text{-}\mathbf{94})_2(H_3COO)_2(py)_5]$ and $J_1 = -5.4\,cm^{-1}$ and $J_2 = -0.4\,cm^{-1}$ ($S = 5/2$) for $[Mn_3(H\text{-}\mathbf{94})_2(py)_6]$, these results are consistent with X-band EPR measurements [239].

16. Conclusion and perspectives

The well established coordinating properties of β-diketones and β-diphenols and related ligands have been widely used in the design of mononuclear and especially polynuclear complexes. The physico-chemical properties deriving from the resulting supramolecular assembly allowed for their employment as molecular components and precursors of novel materials. The growing of oxides on suitable surfaces via CVD technology using volatile β-diketonate was further tested. The growth of literature, dealing with new and promising aspects in basic research and possible applications of these systems, testifies that the field is far from being exhausted and appears quite rich and fruitful.

The recently undertaken synthetic routes, aimed at functionalising the β-diketones in order to magnify or modify the physico-chemical properties of the related complexes, have produced 1D, 2D or 3D metal organic frameworks (MOFs and M′MOFs) with well defined cavities capable of encapsulating specific molecules (i.e. H_2) or solvents.

The optical and magnetic properties of mononuclear and heteropolynuclear complexes, especially those containing d- and f-metal ions, and their ability to give rise to supramolecular architectures have been clarified in more detail. Furthermore, the large spin values of specific polynuclear clusters, combined with a large magnetic anisotropy, have led some of these species, for instance some polynuclear manganese complexes, to act as single molecule magnets, i.e. nanoscale magnetic particles of well defined size and structure. The development of appropriate syntheses of multinuclear metal systems, from building blocks possessing high spin ground states, is a stimulating and promising field to be pursued by supramolecular chemists.

Furthermore, the use of a wide range of radicals as nytrosyl-nitroxide ligands which act as magnetic modulators for 3d- or 4f-β-diketonates complexes and the properties of the resulting polymeric compounds which give rise to single chain magnets are better clarified. This opens new perspectives in storing information in a single magnet polymer.

The preparation of a large variety of mononuclear iridium(III) or lanthanide(III) complexes, containing functionalized β-diketonates and/or functionalized pyridine-based ligands, facilitated a better understanding of their optical properties and consequently, the set up of more efficient probes and devices, where they act as the necessary molecular components. Furthermore, the syntheses of the interesting series of bifunctional ligands and the related d- and f-heteronuclear complexes with a programmed variation of the d: f ratio was essential in producing systems capable of efficiently changing the d-block chromophores into f-block luminophores.

New biosensors, multi-redox and photoactive complexes for advanced photophysical studies are currently under scrutinity.

The non casual occurrence of oxo-hydroxo lanthanide(III) clusters is remarkable, owing to their role in catalytic processes. The possibility to adequately tune the stoichiometric complexity and the structure of these clusters (for instance using β-diketonates with different steric hindrance) will favour fast growing results and applications.

The formation of discrete, complexes and their evolution into the related oligomeric or polymeric species via the insertion of appropriate bridging groups (4,4′-bipyridine, pyrazine, 2,2′-dipyrimidine, etc.) was appropriately described by single crystal X-ray diffraction measurements, which elucidated the role of the different bridging spacers and of the different metal ions in the resulting molecular aggregation.

The insertion of spacers, containing coordinating or non coordinating donors between the β-diketonato and β-ketophenolato moieties, was successfully carried out and the role of different metal ions in addressing the synthetic pathway and toward a designed stoichiometry was checked.

The availability of binary molecular switches, belonging to two different magnetic entities with different properties, capable of delivering different responses to a variety of external stimuli, represent a major breakthrough in the growing of adaptative chemistry.

The use of the superior homologues of β-diketones (i.e. tri-, tetraketones, bis-β-diketones containing additional donor groups) in the selective separation of specific metal ions (i.e. Cu^{2+} with respect to Zn^{2+} and Cd^{2+}) was taken into consideration. The interesting results obtained offer new possibilities in the application of a new generation of β-diketones in separation science and technology.

Thus, the ligand design-metal ion role in complexation reaction was satisfactorily elucidated offering the chemists new opportunities for directing sophisticated synthesis.

All these results and those continuously appearing in the scientific literature show the vitality and the yet unexplored possibilities of these systems; there will continue to be a great interest shown in studies of basic and applied aspects, associated with progressively sophisticated β-diketonate and β-ketophenolate complexes.

Acknowledgements

We thank Mrs. Bonato Giuseppina and Mr. Antonio Aguiari for technical assistance in collecting date and in the manuscript preparation. We thank MIUR project FIRB-RBNE019H9K for financial support.

References

[1] A.C. Swallow, M.R. Truter, Proc. R. Soc. A 254 (1960) 205.
[2] F.P. Dwyer, D.P. Mellor, Chelating Agents and Metal Chelates, Academic Press, London, 1964.
[3] F. Bonati, Organomet. Chem. Rev. 1 (1966) 379.
[4] R.M. Pike, Coord. Chem. Rev. 2 (1967) 163.
[5] D. Gibson, Coord. Chem. Rev. 4 (1969) 225.
[6] U. Casellato, M. Vidali, P.A. Vigato, Inorg. Chim. Acta 18 (1976) 77.
[7] R.C. Mehrotra, Pure Appl. Chem. 60 (1988) 1349.

[8] (a) S. Kawaguchi, Coord. Chem. Rev. 70 (1986) 51;
(b) P.A. Vigato, S. Tamburini, Coord. Chem. Rev. 248 (2004) 1717.
[9] P. Guerriero, P.A. Vigato, M. Vidali, Coord. Chem. Rev. 139 (1995) 17.
[10] J.A. McCleverty, T.J. Meyer, Comprehen. Coord. Chem. II 1 (2004) 97.
[11] U. Casellato, M. Vidali, P.A. Vigato, Coord. Chem. Rev. 23 (1977) 31.
[12] D.J. Bray, J.K. Clegg, L.F. Lindoy, D. Schilter, Adv. Inorg. Chem. 59 (2007) 1.
[13] G. Aromí, P. Gamez, J. Reedijk, Coord. Chem. Rev. 252 (2008) 964.
[14] K. Makamoto, P.J. McCarthy, Spectroscopy and Structure of Metal Chelate Compounds, Wiley, New York, 1968.
[15] E.L. Muetterties, C.M. Wright, J. Am. Chem. Soc. 87 (1965) 4706.
[16] T. Jüstel, H. Nikol, Adv. Mater. 12 (2000) 527.
[17] S. Capecchi, O. Renault, D.-G. Moon, M. Halim, M. Etchells, P.J. Dobson, O.V. Salata, V. Christou, Adv. Mater. 12 (2000) 1591.
[18] (a) A.E. Merbach, E. Toth, The Chemistry of Contrast Agents in Medical Magnetic Resonance Imaging, Wiley, Chichester, 2001;
(b) P. Caravan, J.J. Ellison, T.J. McMurry, R.B. Lauffer, Chem. Rev. 99 (1999) 2293.
[19] (a) J. Ren, A.D. Sherry, Inorg. Chim. Acta 246 (1996) 331;
(b) M. Botta, U. Casellato, C. Scalco, S. Tamburini, P. Tomasin, P.A. Vigato, S. Aime, A. Barge, Chem. Eur. J. 8 (2002) 3917.
[20] (a) D. Parker, Coord. Chem. Rev. 205 (2000) 109;
(b) I. Hemmilä, V. Laitala, J. Fluorine Chem. 15 (2005) 529.
[21] V.W.W. Yam, K.K.W. Lo, Coord. Chem. Rev. 184 (1999) 157.
[22] (a) I. Hemmilä, T. Ståhlberg, P. Mottram, Bioanalytical Applications of Labeling Technologies, in: Wallac Oy (Ed.), Turku, (1995);
(b) G. Mathis, in: R. Saez Puche, P. Caro (Eds.), Rare Earths, Editorial Complutense S.A., Madrid, 1998, p. 285;
(c) I. Hemmilä, V.M. Mukkala, Crit. Rev. Clin. Lab. Sci. 38 (2001) 441.
[23] L.J. Charbonnière, R. Ziessel, J. Alloys Compd. 374 (2004) 283.
[24] (a) K. Binnemans, Y.G. Galyametdinov, R. Van Deun, D.W. Bruce, S.R. Collinson, A.P. Polishchuk, I. Bikchantaev, W. Haase, A.V. Prosvirin, L. Tinchurina, U. Litvinov, A. Gubajdullin, A. Rakhmatullin, K. Uytterhoeven, L. Van Meervelt, J. Am. Chem. Soc. 122 (2000) 4335;
(b) Y.G. Galyametdinov, L.V. Malykhina, W. Haase, K. Driesen, K. Binnemans, Liq. Cryst. 29 (2002) 1581.
[25] (a) V.K.L. Pecharsky, K.A. Gschneidner Jr., J. Magn. Magn. Mater. 200 (1999) 44;
(b) K. Ahn, A.O. Pecharsky, K.A. Gschneidner, V.K. Pecharsky, J. Appl. Phys. (2005) 97.
[26] (a) L.G. Hubert-Pfalzgraf, New J. Chem. 19 (1995) 727;
(b) F.A. Gleizes, M. Julve, N. Kuzmina, A. Alikhanyan, F. Lloret, I. Malkerova, J.L. Sanz, F. Senocq, Eur. J. Inorg. Chem. (1998) 1169.
[27] (a) G.A. Molander, Chem. Rev. 92 (1992) 29;
(b) G.A. Molander, C.R. Harris, Chem. Rev. 96 (1996) 307;
(c) P.G. Steel, J. Chem. Soc., Perkin Trans. 1 (2001) 2727.
[28] T. Gross, F. Chevalier, J.S. Lindsey, Inorg. Chem. 40 (2001) 4762.
[29] (a) J. Inanaga, Y. Sugimoto, T. Hanamoto, New J. Chem. 19 (1995) 707;
(b) S. Kobayashi, Top. Organomet. Chem. 2 (1999) 63.
[30] (a) H. Sasai, T. Suzuki, N. Itoh, K. Tanaka, T. Date, K. Okamura, M. Shibasaki, J. Am. Chem. Soc. 115 (1993) 10372;
(b) H. Sasai, M. Hiroi, Y.M.A. Yamada, M. Shibasaki, Tetrahedron Lett. 38 (1997) 6031;
(c) E. Emori, T. Arai, H. Sasai, M. Shibasaki, J. Am. Chem. Soc. 120 (1998) 4043;
(d) K. Yamakoshi, S.J. Harwood, M. Kanai, M. Shibasaki, Tetrahedron Lett. 40 (1999) 2565.
[31] D.M. Epstein, L.L. Chappell, H. Khalili, R.M. Supkowski, W. DeWitt Horrocks Jr., J.R. Morrow, Inorg. Chem. 39 (2000) 2130.
[32] C. Adachi, M. Baldo, M.E. Thompson, R.S. Forrester, J. Appl. Phys. 90 (2001) 5048.
[33] A. de Bettencourt-Dias, Dalton Trans. 22 (2007) 2229.
[34] E.L. Muetterties, H. Roesky, C.M. Wright, J. Am. Chem. Soc. 88 (1966) 4856.
[35] M. Hasegawa, Y. Inomaki, T. Inayoshi, T. Hoshi, M. Kobayashi, Inorg. Chim. Acta 257 (1997) 259.
[36] J.R. Chipperfield, S. Clark, J. Elliott, E. Sinn, Chem. Commun. 2 (1998) 195.
[37] A. Camard, Y. Ihara, F. Murata, K. Mereiter, Y. Fukuda, W. Linert, Inorg. Chim. Acta 358, 257 (2005) 409.
[38] S.I. Ahmed, J. Burgess, J. Fawcett, S.A. Parsons, D.R. Russell, S.H. Laurie, Polyhedron 19 (2000) 129.
[39] M.C. Barret, M.F. Mahon, K.C. Molloy, J.W. Steed, P. Wright, Inorg. Chem. 40 (2001) 4384.
[40] C.I.F. Denekamp, D.F. Evans, A.M.Z. Slawin, D.J. Williams, C.Y. Wong, J.D. Woollins, J. Chem. Soc., Dalton Trans. 15 (1992) 2375.
[41] A. Deák, P. Király, G. Tárkányi, Dalton Trans. (2007) 234.
[42] G. Bhalla, R.A. Periana, Angew. Chem. Int. Ed. 44 (2005) 1540.
[43] C.J. Weidenhaft, Inorg. Nucl. Chem. Lett. 7 (1971) 1023.
[44] (a) D. Brown, C.E.F. Rickard, J. Chem. Soc. (1970) 3373;
(b) V.W. Day, J.L. Hoard, J. Am. Chem. Soc. 92 (1970) 3626.
[45] G. Szigethy, J. Xu, A.E.V. Gorden, S.J. Teat, David K. Shuh, K.N. Raymond, Eur. J. Inorg. Chem. (2008) 2143.
[46] S.-I. Takekuma, K. Tomoda, M. Sasaki, T. Minematsu, H. Takekuma, Bull. Chem. Soc. Jpn. 77 (2004) 1935.
[47] M. Minato, J.-G. Ren, M. Kasai, K. Munakata, T. Ito, J. Organomet. Chem. 691 (2006) 282.
[48] G.E. Bono-Core, A.H. Klahn, R. Tejos, H. Manisol, H. Ross, Bol. Soc. Chil. Quim. 43 (1998) 339.
[49] (a) D.A. Clemente, G. Bandoli, M. Vidali, P.A. Vigato, R. Portanova, L. Magon, J. Cryst. Mol. Struct. 3 (1973) 221;
(b) G. Bombieri, S. Degetto, G. Marangoni, R. Graziani, E. Forsellini, Inorg. Nucl. Chem. Lett. 9 (1973) 233.
[50] (a) J. Zhang, P.D. Badger, S.J. Geib, S. Petoud, Angew. Chem. Int. Ed. 44 (2005) 2508;
(b) J. Zhang, P.D. Badger, S.J. Geib, S. Petoud, Inorg. Chem. 46 (2007) 6473.
[51] L. Bertolo, S. Tamburini, P.A. Vigato, W. Porzio, G. Macchi, F. Meinardi, Eur. J. Inorg. Chem. (2006) 2370.
[52] (a) N. Meyer, R. Rüttinger, P.W. Roesky, Eur. J. Inorg. Chem. 11 (2008) 1830;
(b) S. Dehner, M.R. Bürgstein, P.W. Roesky, Dalton Trans. 14 (1998) 2425;
(c) S. Datta, P.W. Roesky, S. Blechert, Organometallics 26 (2007) 4392;
(d) S. Datta, M.T. Gamer, P.W. Roesky, Dalton Trans. 21 (2008) 2839.
[53] C.-T. Yang, S.G. Sreerama, W.-Y. Hsieh, S. Liu, Inorg. Chem. 47 (2008) 2719.
[54] A.P. Ginsberg, R.L. Martin, R.C. Sherwood, Inorg. Chem. 7 (1968) 932.
[55] A. Cotton, G. Wilkinson, Advanced Inorganic Chemistry, Wiley, New York, 1980, p. 769.
[56] P.D.W. Boyd, R.L. Martin, J. Chem. Soc., Dalton Trans. 92 (1979) 92.
[57] (a) D.V. Soldatov, G.D. Enright, J.A. Ripmeester, Supramol. Chem. 11 (1999) 35;
(b) D.V. Soldatov, J.A. Ripmeester, Supramol. Chem. 12 (2001) 357;
(c) D.V. Soldatov, A.T. Henegouwen, G.D. Enright, C.I. Ratcliffe, J.A. Ripmeester, Inorg. Chem. 40 (2001) 1626.
[58] K. Lyczko, J. Narbutt, B. Paluchowska, J.K. Maurin, I. Persson, Dalton Trans. 33 (2006) 3972.
[59] J.M. Harrowfield, S. Maghaminia, A.A. Soudi, Inorg. Chem. 43 (2004) 1810.
[60] M.A. Malik, P. O'Brien, M. Motevalli, A.C. Jones, T. Leedham, Polyhedron 18 (1999) 1641.
[61] I.S. Tidmarsh, E. Scales, P.R. Brearley, J. Wolowska, L. Sorace, A. Caneschi, R.H. Laye, E.J.L. McInnes, Inorg. Chem. 46 (2007) 9743.
[62] N. Yu Kozitsyna, A.E. Gekhman, S.E. Nefedov, M.N. Vargaftik, I.I. Moiseev, Inorg. Chem. Commun. 10 (2007) 956.
[63] A. Hori, A. Shinohe, M. Yamasaki, E. Mishihori, S. Aoyagi, M. Sakata, Angew. Chem. Int. Ed. 46 (2007) 7617.
[64] (a) M.J. Bennett, F.A. Cotton, P. Legzdins, S.J. Lippard, Inorg. Chem. 7 (1968) 1770;
(b) H. Burns, M.D. Danford, Inorg. Chem. 8 (1969) 1780.
[65] F. Bai, H. Su, F. Chang, Chem. Lett. 36 (2007) 1104.
[66] M. Becht, K.H. Dahmen, V. Gramlich, A. Marteletti, Inorg. Chim. Acta 248 (1996) 27.
[67] T. Behrsing, A.M. Bond, G.B. Deacon, C.M. Forsyth, M. Forsyth, K.J. Kamble, B.W. Skelton, A.H. White, Inorg. Chim. Acta 352 (2003) 229.
[68] J. Gottfriedsen, R. Hagner, M. Spoida, Y. Suchorsky, Eur. J. Inorg. Chem. (2007) 2288.
[69] K.A. Fleeting, H.O. Hywell, O. Davies, A.C. Jones, P. O'Brien, T. Leedham, M.J. Crosbie, P.J. Wright, D.J. Williams, Chem. Vap. Depos. 5 (1999) 261.
[70] (a) K.J. Eisentraut, R.E. Sievers, J. Am. Chem. Soc. 87 (1965) 5254;
(b) A. Cotton, P. Legzdins, Inorg. Chem. 7 (1968) 1777.
[71] T. Phillips, D.E. Sands, W.F. Wagner, Inorg. Chem. 7 (1968) 2295.
[72] S.R. Drake, A. Lyons, D.J. Otway, D.J. Williams, Inorg. Chem. 33 (1994) 1230.
[73] J.C. Plakatouras, I. Baxter, M.B. Hursthouse, K.M.A. Malik, J. McAleese, S.R. Drake, J. Chem. Soc., Chem. Commun. (1994) 2455.
[74] S.R. Drake, A. Lyons, D.J. Otway, A.M.Z. Slawin, D.J. Williams, J. Chem. Soc., Dalton Trans. (1993) 2379.
[75] P.C. Junk, M.K. Smith, Polyhedron 22 (2003) 331.
[76] (a) A. Moller, P. Kögerler, Coord. Chem. Rev. 182 (1999) 3;
(b) R.E.P. Winpenny, Chem. Soc. Rev. 27 (1998) 447.
[77] C. Benelli, D. Gatteschi, Chem. Rev. 102 (2002) 2369.
[78] (a) Z. Zheng, Chem. Commun. (2001) 2521;
R. Anwander, Angew. Chem. Int. Ed. 37 (1998) 599.
[79] (a) B.C. Gates, L. Gucsi, H. Knözinger, Metal Clusters in Catalysis, Elsevier, Amsterdam, 1986;
(b) G. Schmid (Ed.), Clusters and Colloids. From Theory to Applications, VCH, Weinheim, 1994.
[80] R.-G. Xiong, J.-L. Zuo, Z. You, X.-Z. You, W. Chen, Inorg. Chem. Commun. (1999) 490.
[81] (a) M.T. Gamer, Y. Lan, P.W. Roesky, A.K. Powell, R. Clérac, Inorg. Chem. 47 (2008) 6581;
(b) P.W. Roesky, G. Canseco-Melchor, A. Zulys, Chem. Commun. (2004) 738.
[82] L.G. Hubert-Pfalzgraf, N. Miele-Pajot, R. Papiernik, J. Vaissermann, J. Chem. Soc., Dalton Trans. (1999) 4127.
[83] G. Xu, Z.-M. Wang, Z. He, Z. Lu, C.-S. Liao, C.-H. Yan, Inorg. Chem. 41 (2002) 6802.
[84] S. Datta, V. Baskar, H. Li, P.W. Roesky, Eur. J. Inorg. Chem. (2007) 4216.
[85] P.C. Andrews, T. Beck, C.M. Forsyth, B.H. Fraser, P.C. Junk, M. Massi, P.W. Roesky, Dalton Trans. (2007) 5651.
[86] R. Van Deun, P. Nockemann, P. Fias, K. Van Hecke, L. Van Meervelt, K. Binnemans, Chem. Commun. (2005) 590.
[87] (a) C.-P. Wong, R.F. Venteicher, W.DeW. Horrocks Jr., J. Am. Chem. Soc. 96 (1974) 7149;
(b) J.H. Agondanou, I. Nicolis, E. Curis, J. Purans, G.A. Spyroulias, A.G. Coutsolelos, S. Benazeth, Inorg. Chem. 46 (2007) 6871.
[88] H.-S. He, Z.-X. Zhao, W.-K. Wong, K.-F. Li, J.-X. Meng, K.-W. Cheah, Dalton Trans. (2003) 980.
[89] R.E. Cramer, K. Seff, J.C.S. Chem. Commun. (1972) 400.

[90] D.R. van Staveren, G.A. van Albada, J.G. Haasnoot, H. Kooijman, A.M. Manotti Lanfredi, P.J. Nieuwenhuizen, A.L. Spek, F. Ugozzoli, T. Weyhermüller, J. Reedijk, Inorg. Chim. Acta 315 (2001) 163.
[91] A. Bellusci, G. Barberio, A. Crispini, M. Ghedini, M. La Deda, D. Pucci, Inorg. Chem. 44 (2005) 1818.
[92] C.R. De Silva, J.R. Maeyer, R. Wang, G.S. Nichol, Z. Zheng, Inorg. Chim. Acta 360 (2007) 3543.
[93] (a) T. Lazarides, M.A.H. Alamiry, H. Adams, S.J.A. Pope, S. Faulkner, J.A. Weinstein, M.D. Ward, Dalton Trans. 15 (2007) 1484;
(b) B.-L. Li, Z.-T. Liu, G.-J. Deng, Q.-H. Fan, Eur. J. Org. Chem. 3 (2007) 508;
(c) H.S. Joshi, R. Jamshidi, Y. Tor, Angew. Chem. Int. Ed. 38 (1999) 2722.
[94] (a) N.M. Shavaleev, R. Scopelliti, F. Gumy, J.-C.G. Bünzli, Eur. J. Inorg. Chem. 9 (2008) 1523;
(b) A.A. Knyazev, Y.G. Galyametdinov, B. Goderis, K. Driesen, K. Goossens, C. Görller-Walrand, K. Binnemans, T. Cardinaels, Eur. J. Inorg. Chem. (2008) 756.
[95] (a) H. Jang, C.-H. Shin, B.-J. Jung, D.-H. Kim, H.-K. Shim, Y. Do, Eur. J. Inorg. Chem. (2006) 718;
(b) H. Jang, C.-H. n Shin, B.-J. Jung, D.-h. Kim, H.-K. Shim, Y. Do, Eur. J. Inorg. Chem (2006) 718;
(c) R. Sultan, K. Gadamsetti, S. Swavey, Inorg. Chim. Acta 359 (2006) 1233;
(c) A. Fratini, S. Swavey, Inorg. Chem. Commun. 10 (2007) 636;
(d) A. Fratini, G. Richards, E. Larder, S. Swavey, Inorg. Chem. 47 (2008) 1030.
[96] (a) B. Sarkar, M. Sinha Ray, M.G.B. Drew, A. Figuerola, C. Diaz, A. Ghosh, Polyhedron 25 (2006) 3084;
(b) C. Biswas, S. Chattopadhyay, M.G.B. Drew, A. Ghosh, Polyhedron 26 (2007) 4411.
[97] L. Han, Y. Zhou, Inorg. Chem. Commun. 11 (2008) 385.
[98] (a) K. Kukiri, Y. Koike, Y. Okamoto, Chem. Rev. 102 (2002) 2347;
(b) J. Kido, Y. Okamoto, Chem. Rev. 102 (2002) 2357;
(c) P.P. Sun, J.P. Duan, J.J. Lih, C.H. Chen, Adv. Funct. Mater. 13 (2003) 683;
(d) Q.M. Wang, B.J. Yan, Photochem. Photobiol. A: Chem. 177 (2006) 1;
(e) J. Pei, X.L. Liu, W.L. Yu, Y.H. Lai, Y.H. Niu, Y. Cao, Macromolecules 35 (2002) 7274.
[99] (a) G.F. de Sa, O.L. Malta, D.C. de Mello, A.M. Simas, R.L. Longo, P.A. Santa-Cruz, E.F.J. da Silva, Coord. Chem. Rev. 196 (2000) 165;
(b) H. Tsukube, S. Shinoda, Chem. Rev. 102 (2002) 2389;
(c) M. Elhabiri, J. Hamacek, N. Humbert, J.C.G. Bünzlib, A.M. Albrecht-Gary, New J. Chem. 28 (2004) 1096;
(d) M. Tan, G. Wang, X. Hai, Z. Ye, J. Yuan, J. Mater. Chem. 14 (2004) 2896.
[100] (a) S. Li, W. Zhu, Z. Xu, J. Pan, H. Tian, Tetrahedron 62 (2006) 5035;
(b) Y. Zheng, F. Cardinali, N. Armaroli, G. Accorsi, Eur. J. Inorg. Chem. 12 (2008) 2075.
[101] B.-L. Li, Z.-T. Liu, G.-J. Deng, Q.-H. Fan, Eur. J. Org. Chem. (2007) 508.
[102] (a) S. Lamansky, P. Djurovich, D. Murphy, F. Abdel-Razzaq, H.-E. Lee, C. Adachi, P.E. Burrows, S.R. Forrest, M.E. Thompson, J. Am. Chem. Soc. 123 (2001) 4304;
(b) S. Lamansky, P. Djurovich, D. Murphy, F. Abdel-Razzaq, R. Kwong, I. Tsyba, M. Bortz, B. Mui, R. Bau, M.E. Thompson, Inorg. Chem. 40 (2001) 1704.
[103] B.-L. Li, L. Wu, Y.-M. He, Q.-H. Fan, Dalton Trans. (2007) 2048.
[104] (a) R.H. Friend, R.W. Gymer, A.B. Holmes, J.H. Burrougnes, R.N. Marks, C. Taliani, D.D.C. Bradley, D.A. Dos Santos, J.L. Bredas, W.R. Salaneck, Nature 397 (1999) 121;
(b) I.S. Millard, Synth. Met. 111–112 (2000) 119;
(c) M. Wohlegenannt, K. Tandon, S. Mazumdar, S. Ramashesha, Z.V. Vardeny, Nature 409 (2001) 494.
[105] (a) X. Chen, J.-L. Liao, Y. Liang, M.O. Ahmed, H.-E. Tseng, S.-A. Chen, J. Am. Chem. Soc. 125 (2003) 636;
(b) X. Li, Z. Chen, Q. Zhao, L. Shen, F. Li, T. Yi, Y. Cao, C. Huang, Inorg. Chem. 46 (2007) 5518.
[106] F.-F. Chen, Z.Q. Bian, Z.-W. Liu, D.-B. Nie, Z.-Q. Chen, C.-H. Huang, Inorg. Chem. 47 (2008) 2507.
[107] (a) C.R. Hauser, J.K. Lindsay, J. Org. Chem. 22 (1957) 482;
(b) C.R. Hauser, C.E. Cain, J. Org. Chem. 23 (1958) 1142;
(c) C.E. Cain, I.A. Mashburn, C.R. Hauser, J. Org. Chem. 26 (1961) 1030.
[108] (a) P.D.W. Boyd, P.M. Johns, C.E.F. Rickard, Acta Cryst. C62 (2006) 590;
(b) P. Zanello, F. Fabrizi de Biani, C. Glidewell, J. Koenig, S.J. Marsch, Polyhedron 17 (1998) 1795.
[109] (a) C.-G. Yan, L. Liu, J. Han, Acta Cryst. E63 (2007) 683;
(b) G. Li, H. Hou, Y. Zhu, X. Meng, L. Mi, Y. Fan, Inorg. Chem. Commun. 5 (2002) 929.
[110] P.A. Vigato, U. Casellato, D.A. Clemente, G. Bandoli, J. Inorg. Nucl. Chem 35 (1973) 4131.
[111] W.C. du Plessis, T.G. Vosloo, J.C. Swarts, J. Chem. Soc., Dalton Trans. (1998) 2507.
[112] J. Conradie, T.S. Cameron, M.A.S. Aquino, G.J. Lamprecht, J.C. Swarts, Inorg. Chim. Acta 358 (2005) 2530.
[113] Y.-F. Yuan, T. Cardinaels, K. Lunstroot, K. Van Hecke, L. Van Meervelt, C. Gorller-Walrand, K. Binnemans, P. Nockemann, Inorg. Chem. 46 (2007) 5302.
[114] V. Baskar, P.W. Roesky, Dalton Trans. (2006) 676.
[115] N. Bellec, D. Lorcy, Tetrahedron Lett. 42 (2001) 3189.
[116] J. Massue, N. Bellec, S. Chopin, E. Levillain, T. Roisnel, R. Clerac, D. Lorcy, Inorg. Chem. 44 (2005) 8740.
[117] N. Bellec, J. Massue, T. Roisnel, D. Lorcy, Inorg. Chem. Commun. 10 (2007) 1172.
[118] P. Wang, J.E. Miller, L.M. Henling, C.L. Stern, N.L. Frank, A.L. Eckermann, T.J. Meade, Inorg. Chem. 46 (2007) 9853.
[119] (a) T.J. Meade, J.F. Kayyem, Angew. Chem. Int. Ed. 34 (1995) 352;
(b) S.O. Kelley, J.K. Barton, Science 283 (1999) 375;
(c) D.J. Hurley, Y. Tor, J. Am. Chem. Soc. 120 (1998) 2194;
D.J. Hurley, Y. Tor, J. Am. Chem. Soc. 124 (2002) 13231;
(d) S.C. Weatherly, I.V. Yang, H.H. Thorp, J. Am. Chem. Soc. 123 (2001) 1236;
(e) F.D. Lewis, R.L. Letsinger, M.R. Wasielewski, Acc. Chem. Res. 34 (2001) 159;
D.F. Lewis, M.R. Wasielewski, Top. Curr. Chem. 236 (2004) 45.
[120] (a) A.M. Brun, A. Harriman, J. Am. Chem. Soc. 114 (1992) 3656;
A. Harriman, Angew. Chem. Int. Ed. 38 (1999) 945;
(b) E.J.C. Olson, D. Hu, A. Hoermann, P.F.J. Barbara, Phys. Chem. B 101 (1997) 299;
(c) B. Giese, Annu. Rev. Biochem. 71 (2002) 51;
(d) M.A. O'Neill, J.K. Barton, Top. Curr. Chem. 236 (2004) 67.
[121] (a) C.J. Yu, Y. Wan, H. Yowanto, J. Li, C. Tao, M.D. James, C.L. Tan, G.F. Blackburn, T.J.J. Meade, J. Am. Chem. Soc. 123 (2001) 11155;
(b) P.M. Armistead, H.H. Thorp, Anal. Chem. 72 (2000) 3764;
(c) J.P. Knemeyer, N. Marme, M. Sauer, Anal. Chem. 72 (2000) 3717;
(d) J. Wang, Anal. Chim. Acta 469 (2002) 63;
(e) K.J. Odenthal, J.J. Gooding, Analyst 132 (2007) 603.
[122] (a) C. Benelli, A. Caneschi, D. Gatteschi, L. Pardi, P. Rey, Inorg. Chem. 29 (1990) 4223;
(b) C. Benelli, A. Caneschi, D. Gatteschi, R. Sessoli, Inorg. Chem. 32 (1993) 4797.
[123] K. Bernot, L. Bogani, R. Sessoli, D. Gatteschi, Inorg. Chim. Acta 360 (2007) 3807.
[124] A. Caneschi, D. Gatteschi, N. Lalioti, C. Sangregorio, R. Sessoli, G. Venturi, A. Vindigni, A. Rettori, M.G. Pini, M.A. Novak, Angew. Chem. Int. Ed. 40 (2001) 1760.
[125] L. Bogani, C. Sangregorio, R. Sessoli, D. Gatteschi, Angew. Chem. Int. Ed. 44 (2005) 5817.
[126] D. Luneau, C. Stroh, J. Cano, R. Ziessel, Inorg. Chem. 44 (2005) 633.
[127] C. Hirel, L. Li, P. Brough, K. Vostrikova, J. Pecaut, B. Mehdaoui, M. Bernard, P. Turek, P. Rey, Inorg. Chem. 46 (2007) 7545.
[128] A.D. Burrows, K. Cassar, M.F. Mahon, J.E. Warren, Dalton Trans. (2007) 2499.
[129] L.G. Mackay, H.L. Anderson, J.K.M. Sanders, J. Chem. Soc., Perkin Trans. 1 (18) (1995) 2269.
[130] S.S. Turner, D. Collison, F.E. Mabbs, M. Halliwell, J. Chem. Soc., Dalton Trans. (1997) 1117.
[131] B. Chen, F.R. Fronczek, A.W. Maverick, Chem. Commun. (2003) 2166.
[132] B. Chen, F.R. Fronczek, A.W. Maverick, Inorg. Chem. 43 (2004) 8209.
[133] (a) V.D. Vreshch, A.N. Chernega, J.A.K. Howard, J. Sieler, K.V. Domasevitch, Dalton Trans. (2003) 1707;
(b) V.D. Vreshch, A.B. Lysenko, A.N. Chernega, J.A.K. Howard, H. Krautscheid, J. Sieler, K.V. Domasevitch, Dalton Trans. (2004) 2899.
[134] Y. Zhang, B. Chen, F.R. Fronczek, A.W. Maverick, Inorg. Chem. 47 (2008) 4433.
[135] (a) F. Lloret, R. Ruiz, B. Cervera, I. Castro, M. Julve, J. Faus, J.A. Real, F. Sapiña, Y. Journaux, J.C. Colin, M. Verdaguer, J. Chem. Soc., Chem. Commun. (1994) 2615;
(b) R. Clerac, H. Miyasaka, M. Yamashita, C. Coulon, J. Am. Chem. Soc. 124 (2002) 12837.
[136] F. Mori, T. Nyui, T. Ishida, T. Nogami, K.-Y. Choi, H. Nojiri, J. Am. Chem. Soc. 128 (2006) 1440.
[137] S. Osa, T. Kido, N. Matsumoto, N. Re, A. Pochaba, J. Mrozinski, J. Am. Chem. Soc. 126 (2004) 420.
[138] C.M. Zaleski, E.C. Depperman, J.W. Kampf, M.L. Lirk, V.L. Pecoraro, Angew. Chem. Int. Ed. 43 (2004) 3912.
[139] (a) A. Mishra, W. Wernsdorfer, K.A. Abboud, G. Christou, J. Am. Chem. Soc. 126 (2004) 15648;
(b) A. Mishra, W. Wernsdorfer, S. Parsons, G. Christou, E.K. Brechin, Chem. Commun. (2005) 2086.
[140] (a) N. Ishikawa, M. Sugita, T. Ishikawa, S.-y. Koshihara, Y. Kaizu, J. Am. Chem. Soc. 125 (2003) 8694;
(b) N. Ishikawa, M. Sugita, W. Wernsdorfer, J. Am. Chem. Soc. 127 (2005) 3650;
(c) M. Sugita, N. Ishikawa, T. Ishikawa, S.-y. Koshihara, Y. Kaizu, Inorg. Chem. 45 (2006) 1299.
[141] J.-P. Costes, M. Auchel, F. Dahan, V. Peyrou, S. Shova, W. Wernsdorfer, Inorg. Chem. 45 (2006) 1924.
[142] J. Tang, I. Hewitt, N.T. Madhu, G. Chastanet, W. Wernsdorfer, C.E. Ansen, C. Benelli, R. Sessoli, A.K. Powell, Angew. Chem. Int. Ed. 45 (2006) 1924.
[143] K. Bernot, L. Bogani, A. Caneschi, D. Gatteschi, R. Sessoli, J. Am. Chem. Soc. 128 (2006) 7947.
[144] (a) C. Aronica, G. Pilet, G. Chastanet, W. Wernsdorfer, G.F. Jacquot, D. Luneau, Angew. Chem. Int. Ed. 45 (2006) 4659;
(b) F. He, M.-L. Tong, X.-M. Chen, Inorg. Chem. 44 (2005) 8285.
[145] S. Ueki, T. Ishida, T. Nogami, M. Tamura, Mol. Cryst. Liq. Cryst. 455 (2006) 129.
[146] (a) C.-I. Yang, Y.-J. Tsai, G. Chung, T.-S. Kuo, M. Shieh, H.-L. Tsai, Polyhedron 26 (2007) 1805;
(b) C.-I. Yang, W. Wernsdorfer, Y.-J. Tsai, G. Chung, T.-S. Kuo, G.-H. Lee, M. Shieh, H.-L. Tsai, Inorg. Chem. 47 (2008) 1925.
[147] S. Brück, M. Hilder, P.C. Junk, U.H. Kynast, Inorg. Chem. Commun. 3 (2000) 666.
[148] R. Wang, D. Song, C. Seward, Y. Tao, S. Wang, Inorg. Chem. 41 (2002) 5187.
[149] J.A.P. Nash, S.C. Thompson, D.F. Foster, D.J. Cole-Hamilton, J.C. Barnes, J. Chem. Soc., Dalton Trans. (1995) 269.

[150] D. Guo, C.-y. Duan, F. Lu, Y. Hasegawa, Q.-j. Meng, S. Yanagida, Chem. Commun. 13 (2004) 1486.
[151] T. Lazarides, H. Adams, D. Sykes, S. Faulkner, G. Calogero, M.D. Ward, Dalton Trans. (2008) 691.
[152] R. Ziessel, S. Diring, P. Kadjane, L. Charbonniere, P. Retailleau, C. Philouze, Chem. Asian J. 2 (2007) 975.
[153] T.K. Ronson, T. Lazarides, H. Adams, S.J.A. Pope, D. Sykes, S. Faulkner, S.J. Coles, M.B. Hursthouse, W. Clegg, R.W. Harrington, M.D. Ward, Chem. Eur. J. 12 (2006) 9299.
[154] (a) H.-B. Xu, L.-X. Shi, E. Ma, L.-Y. Zhang, Q.-H. Wei, Z.-N. Chen, Chem. Commun. (2006) 1601;
(b) H.-B. Xu, L.-Y. Zhang, Z.-L. Xie, E. Ma, Z.-N. Chen, Chem. Commun. (2007) 2744.
[155] X.-L. Li, L.-X. Shi, L.-Y. Zhang, H.-M. Wen, Z.-N. Chen, Inorg. Chem. 46 (2007) 10892.
[156] X.-L. Li, F.-R. Dai, L.-Y. Zhang, Y.-M. Zhu, Q. Peng, Z.-N. Chen, Organometallics 26 (2007) 4483.
[157] F. Mori, T. Ishida, T. Nogami, Polyhedron 24 (2005) 2588.
[158] (a) M. Sasaki, H. Horinuchi, M. Kumagai, M. Sakamoto, H. Sakiyama, Y. Nishida, Y. Sadaoka, M. Ohba, H. Okawa, Chem. Lett. (1998) 911;
(b) N. Kondoh, Y. Shimizu, M. Kurihara, H. Sakiyama, M. Sakamoto, Y. Nishida, Y. Sadaoka, M. Ohba, H. Okawa, Bull. Chem. Soc. Jpn. 76 (2003) 1007.
[159] L. l Salmon, P. Thuéry, E. Rivière, J.-J. Girerd, M. Ephritikhine, Dalton Trans. (2003) 2872.
[160] T. Hamamatsu, K. Yabe, M. Towatari, S. Osa, N. Matsumoto, N. Re, A. Pochaba, J. Mrozinski, J.-L. Gallani, A. Barla, P. Imperia, C. Paulsen, J.-P. Kappler, Inorg. Chem. 46 (2007) 4458.
[161] J.-P. Costes, F. Dahan, W. Wernsdorfer, Inorg. Chem. 45 (2006) 5.
[162] J.P. Costes, S. Shova, W. Wernsdorfer, Dalton Trans. 14 (2008) 1843.
[163] C. Fellah, F. Zohra, J.-P. Costes, F. Dahan, C. Duhayon, J.-P. Tuchagues, Polyhedron 26 (2007) 4209.
[164] Y. Kobayashi, S. Ueki, T. Ishida, T. Nogami, Chem. Phys. Lett. 378 (2003) 337.
[165] (a) S. Ueki, Y. Kobayashi, T. Ishida, T. Nogami, Chem. Commun. (2005) 5223;
(b) S. Ueki, A. Okazawa, T. Ishida, T. Nogami, H. Nojiri, Polyhedron 26 (2007) 1970.
[166] C.W. Dudley, T.N. Huckerby, C. Oldham, J. Chem. Soc. A (1970) 2606.
[167] F. Sagara, H. Kobayashi, K. Ueno, Bull. Chem. Soc. Jpn. 45 (1972) 900.
[168] F. Sagara, H. Kobayashi, K. Ueno, Bull. Chem. Soc. Jpn. 41 (1968) 266.
[169] R.L. Lintvedt, M.J. Heeg, N. Ahmad, M.D. Glick, Inorg. Chem. 21 (1982) 2350.
[170] R.W. Hay, in: E. Kimura (Ed.), Current Topics in Macrocyclic Chemistry in Japan, Hiroshima University, 1978, p. 56.
[171] N.W. Alcock, K.P. Balakrishnan, P. Moore, G.A. Pike, J. Chem. Soc., Dalton Trans. (1987) 889.
[172] K.A. Arnold, L. Echegoyen, F.R. Fronczek, R.D. Gandour, V.J. Gatto, B.D. White, G.W. Gokel, J. Am. Chem. Soc. 109 (1987) 3716.
[173] M. Kuszaj, B. Tomlonovic, D.P. Murtha, R.L. Lintvedt, M.D. Glick, Inorg. Chem. 12 (1973) 1297.
[174] R.L. Lintvedt, L.L. Borer, D.P. Murtha, J.M. Kuszaj, M.D. Glick, Inorg. Chem. 13 (1974) 18.
[175] (a) F.A. Cotton, R.C. Elder, Inorg. Chem. 5 (1966) 423;
(b) R.C. Elder, Inorg. Chem. 7 (1968) 1117;
(c) A.B. Blake, L.R. Fraser, J. Chem. Soc., Dalton Trans. (1974) 2554;
(d) F.A. Cotton, R.C. Elder, Inorg. Chem. 4 (1965) 1145.
[176] R.L. Lintvedt, G. Ranger, C. Ceccarelli, Inorg. Chem. 24 (1985) 2359.
[177] R.G. Charles, Org. Synth. 4 (1963) 869.
[178] Y. Fukuda, K. Mafune, Chem. Lett. (1988) 697.
[179] (a) T. Koiwa, Y. Masuda, J. Shono, Y. Kawamoto, Y. Hoshino, T. Hashimoto, K. Natarajan, K. Shimizu, Inorg. Chem. 43 (2004) 6215;
(b) N. Sato, Y. Furuno, Y. Fukuda, K. Okamoto, A. Yamagishi, Dalton Trans. (2008) 1283.
[180] S. Maji, B. Sarkar, S.M. Mobin, J. Fiedler, F.A. Urbanos, R. Jimenez-Aparicio, W. Kaim, G.K. Lahiri, Inorg. Chem. 47 (2008) 5204.
[181] Y. Zhang, Z. Wang, G.D. Enright, S.R. Breeze, J. Am. Chem. Soc. 120 (1998) 9398.
[182] (a) B. Andrelczyk, R.L. Lintvedt, M.R. Glick, J. Am. Chem. Soc. 94 (1972) 8633;
(b) R.L. Lintvedt, G. Ranger, C. Ceccarelli, Inorg. Chem. 24 (1985) 456.
[183] R.L. Lintvedt, B.A. Schoenfelner, C. Ceccarelli, M.D. Glick, Inorg. Chem. 21 (1982) 2113.
[184] R.L. Lintvedt, B.A. Schoenfelner, C. Ceccarelli, M.D. Glick, Inorg. Chem. 23 (1984) 2867.
[185] K.G. Hampton, R.J. Light, C.R. Hauser, J. Org. Chem. 30 (1965) 1413.
[186] D.F. Martin, W.C. Fernelius, M. Shamma, J. Am. Chem. Soc. 81 (1959) 130.
[187] M. Bassetti, L.M. Vallarino, Inorg. Chim. Acta 105 (1985) 135.
[188] M. Bassetti, L. De Cola, L.M. Vallarino, Inorg. Chim. Acta 105 (1985) 141.
[189] D.E. Fenton, C.M. Reagan, U. Casellato, P.A. Vigato, M. Vidali, Inorg. Chim. Acta 58 (1982) 83.
[190] J.K. Clegg, L.F. Lindoy, J.C. McMurtrie, D. Schilter, J. Chem. Soc., Dalton Trans. (2005) 857.
[191] J.K. Clegg, K. Gloe, M.J. Hayter, O. Kataeva, L.F. Lindoy, B. Moubaraki, J.C. McMurtrie, K.S. Murray, D. Schilter, Dalton Trans. (2006) 3977.
[192] J.K. Clegg, D.J. Bray, K. Gloe, K. Gloe, M.J. Hayter, K.A. Jolliffe, G.A. Lawrance, G.V. Meehan, J.C. McMurtrie, L.F. Lindoy, M. Wenzel, Dalton Trans. 17 (2007) 1719.
[193] A.P. Bassett, S.W. Magennis, P.B. Glover, D.J. Lewis, N. Spencer, S. Parsons, R.M. Williams, L. De Cola, Z. Pikramenou, J. Am. Chem. Soc. 126 (2004) 9413.
[194] M.M. Castaño-Briones, A.P. Bassett, L.L. Meason, P.R. Ashton, Z. Pikramenou, Chem. Commun. (2004) 2832.
[195] (a) J.K. Clegg, L.F. Lindoy, B. Moubaraki, K.S. Murray, J.C. McMurtrie, Dalton Trans. (2004) 2417;
(b) J.K. Clegg, D.J. Bray, K. Gloe, K. Gloe, K.A. Jolliffe, G.A. Lawrance, L.F. Lindoy, G.V. Meehan, M. Wenzel, Dalton Trans. (2008) 1331.
[196] J.K. Clegg, L.F. Lindoy, J.C. McMurtrie, D. Schilter, Dalton Trans. (2006) 3114.
[197] R.W. Saalfrank, A. Dresel, V. Seitz, S. Trummer, F. Hampel, M. Teichert, D. Stalke, C. Stadler, J. Daub, V. Schünemann, A.X. Trautwein, Chem. Eur. J. 3 (1997) 2058.
[198] C. Pariya, C.R. Sparrow, C.K. Back, G. Sandì, F.R. Fronczek, A.W. Maverick, Angew. Chem. Int. Ed. 46 (2007) 1.
[199] A.W. Maverick, F.E. Klavetter, Inorg. Chem. 23 (1984) 4129.
[200] P.J. Bonitatebus Jr., S.K. Mandal, W.H. Armstrong, Chem. Commun. 8 (1998) 939.
[201] S. Yuan, R. Sueda, K. Somazawa, K. Matsumoto, Matsumoto, Chem. Lett. 32 (2003).
[202] A.W. Maverick, S.C. Buckingham, Q. Yao, J.R. Bradbury, G.G. Stanley, J. Am. Chem. Soc. 108 (1986) 7430.
[203] A.W. Maverick, M.L. Ivie, J.H. Waggenspack, F.R. Fronczek, Inorg. Chem. 29 (1990) 2403.
[204] G.J.E. Davidson, A.J. Baer, A.P. Cotè, M.J. Taylor, G.S. Hanan, Y. Tanaka, M. Watanabe, Can. J. Chem. 80 (2002) 496.
[205] K.R. Koch, S.A. Bourne, A. Coetzee, J. Miller, J. Chem. Soc., Dalton Trans. (1999) 3157.
[206] A.N. Westra, S.A. Bourne, K.R. Koch, J. Chem. Soc., Dalton Trans. (2005) 2916.
[207] (a) M. Albrecht, S. Schmid, M. deGroot, P. Weis, R. Fröhlich, Chem. Commun. (2003) 2526;
(b) M. Albrecht, S. Dehn, G. Raabe, R. Fröhlich, Chem. Commun. (2005) 5690.
[208] S.N. Semenov, A.Y. Rogachev, S.V. Eliseeva, C. Pettinari, F. Marchetti, A.A. Drozdov, S.I. Troyanov, Chem. Commun. (2008) 1992.
[209] R.D.J. Jones, L.F. Power, Aust. J. Chem. 24 (1971) 735.
[210] R. Karvembu, K. Natarajan, Polyhedron 21 (2002) 1721.
[211] R. Karvembu, C. Jayabalakrishnan, K. Natarajan, Transit. Metal Chem. 27 (2002) 574.
[212] T. Hashimoto, A. Endo, N. Nagao, G.P. Satô, K. Natarajan, K. Shimizu, Inorg. Chem. 37 (1998) 5211.
[213] R. Grybos, W. Paw, Polyhedron 9 (1990) 1397.
[214] B.-S. Zheng, X.-Y. Zhang, H.-W. Zhua, S.-X. Luoa, L.F. Lindoy, J.C. McMurtrie, P. Turner, G. Wei, Dalton Trans. (2005) 1349.
[215] D.E. Fenton, J.R. Tate, U. Casellato, M. Vidali, S. Tamburini, P.A. Vigato, Inorg. Chim. Acta 83 (1984) 23.
[216] R. Saalfrank, N. Low, S. Trummer, G.M. Sheldrick, M. Teichert, D. Stalke, Eur. J. Inorg. Chem. (1998) 559.
[217] R.W. Saalfrank, V. Seitz, F.W. Heinemann, C. Göbel, R. Herbst-Irmer, J. Chem. Soc., Dalton Trans. (2001) 599.
[218] (a) T. Shiga, M. Ohba, H. Okawa, Inorg. Chem. Commun. 6 (2003) 15;
(b) T. Shiga, N. Ito, A. Hidaka, H. Okawa, S. Kitagawa, M. Ohba, Inorg. Chem. 46 (2007) 3492.
[219] R.W. Saalfrank, A. Scheurer, R. Puchta, F. Hampel, H. Maid, F.W. Heinemann, Angew. Chem. Int. Ed. 46 (2007) 265.
[220] T. Shiga, H. Okawa, S. Kitagawa, M. Ohba, J. Am. Chem. Soc 128 (2006) 16426.
[221] M.P. Hogerheide, S.N. Ringelberg, D.M. Grove, J.T.B.H. Jastrzebski, J. Boersma, W.J.J. Smeets, A.L. Spek, G. van Koten, Inorg. Chem. 35 (1996) 1185.
[222] R.W. Saalfrank, H. Maid, N. Mooren, F. Hampel, Eur. J. Inorg. Chem. 41 (2002) 304.
[223] R.W. Saalfrank, N. Mooren, A. Scheurer, H. Maid, F.W. Heinemann, F. Hampel, W. Bauer, Eur. J. Inorg. Chem. 30 (2007) 4815.
[224] (a) R.W. Saalfrank, C. Schmidt, H. Maid, F. Hampel, W. Bauer, A. Scheurer, Angew. Chem. Int. Ed. 45 (2007) 315;
(b) R.W. Saalfrank, C. Spitzlei, A. Scheurer, H. Maid, F.W. Heinemann, F. Hampel, Chem. Eur. J. 14 (2008) 1472.
[225] R.W. Saalfrank, H. Glaser, B. Demleitner, F. Hampel, M.M. Chowdhry, V. Schünemann, A.X. Trautwein, G.B.M. Vaughan, R. Yeh, A.V. Davis, K.N. Raymond, Chem. Eur. J. 8 (2002) 493.
[226] (a) S.-Y. Yu, Q. Jian, S.H. Li, H.-P. Huang, Y.-Z. Li, Y.-J. Pan, Y. Sei, K. Yamagauchi, Org. Lett. 9 (2007) 1379;
(b) D. Bray, B. Antonioli, J.C. Clegg, K. Gloe, K. Gloe, K.A. Jolliffe, L.F. Lindoy, G. Wei, M. Wenzel, Dalton Trans. (2008) 1683.
[227] R.L. Lintvedt, J.K. Zehetmair, Inorg. Chem. 29 (1990) 2204.
[228] E.W. Ainscough, A.M. Brodie, R.J. Cresswell, J.M. Waters, Inorg. Chim. Acta 227 (1998) 37.
[229] (a) F. Teixidor, A. Llobet, L. Escriche, J. Casabò, Polyhedron 4 (1985) 215;
(b) F. Teixidor, A. Llobet, J. Casabò, S. Bordas, Termochim. Acta 79 (1984) 315.
[230] F. Teixidor, A. Llobet, J. Casabò, X. Solans, M. Font-Altaba, M. Aguilò, Inorg. Chem. 24 (1985) 2315.
[231] F. Teixidor, J. Colomer, A. Llobet, J. Casabò, X. Solans, M. Font-Altaba, Inorg. Chim. Acta 128 (1987) 15.
[232] F. Teixidor, J. Colomer, J. Casabò, J. Rius, E. Molins, C. Miravittles, Inorg. Chem. 28 (1989) 678.
[233] (a) G. Aromí, P. Gamez, O. Roubeau, P. Carrero-Berzal, H. Kooijman, A.L. Spek, W.L. Driessen, J. Reedijk, Eur. J. Inorg. Chem. 5 (2002) 1046;
(b) G. Aromí, P. Carrero-Berzal, P. Gamez, O. Roubeau, H. Kooijman, A.L. Spek, W.L. Driessen, J. Reedijk, Angew. Chem. Int. Ed. 40 (2001) 3444.

[234] G. Aromí, P. Gamez, O. Roubeau, P. Carrero-Berzal, H. Kooijman, A.L. Spek, W.L. Driessen, J. Reedijk, Inorg. Chem. 41 (2002) 3673.
[235] G. Aromí, J. Ribas, P. Gamez, O. Roubeau, H. Kooijman, A.L. Spek, S.J. Teat, E. MacLean, H. Stoeckli-Evans, J. Reedijk, Chem. Eur. J. 10 (2004) 6476.
[236] G. Aromí, H. Stoeckli-Evans, S.J. Teat, J. Cano, J. Ribas, J. Mater. Chem. 16 (2006) 2635.
[237] G. Aromí, C. Boldron, P. Gamez, O. Roubeau, H. Kooijman, A.L. Spek, H. Stoeckli-Evans, J. Ribas, J. Reedijk, Dalton Trans. (2004) 3586.
[238] E.C. Sañudo, T. Cauchy, E. Ruiz, R.H. Laye, O. Roubeau, S.J. Teat, G. Aromi, Inorg. Chem. 46 (2007) 9045.
[239] G. Aromí, P. Gamez, J. Krzystek, H. Kooijman, A.L. Spek, E. MacLean, S.J. Teat, H. Nowell, Inorg. Chem. 46 (2007) 2519.